THE UNIVERSITY OF
SYDNEY

P53 RESPONSES TO FLUDARABINE IN HUMAN B-LYMPHOID CANCERS

Juhura G. Almazi

A thesis submitted in fulfilment of the requirements for the degree of

Doctor of Philosophy

School of Molecular Bioscience

The University of Sydney

Sydney, NSW, Australia

February, 2014

TABLE OF CONTENTS

DECLARATION

With the following exceptions, the experimental data presented in this thesis were obtained by the author alone. Cell cycle analysis and intercellular flow cytometry analysis was conducted in collaboration with Dr. Giles Best from the Kolling Institute, Royal North Shore Hospital (RNSH). Mass spectometry experiments on the Orbitrap Velos were conducted in collaboration with Dr. Mark Graham from the Children's Medical Research Unit (CMRI). Dr Pauline Huang and Medsaic Pty. Ltd is to be credited for the manufacture of the Dotscan antibody microarray. Experiments on the QSTAR were conducted at the Sydney University Proteomics Research Unit (SUPRU) with the technical aid of Mr Munther Alomari and Ms Erin Sykes.

Juhura G. Almazi

19th AUGUST 2013

ACKNOWLEDGEMENTS

I have been blessed with help and support or many individuals throughout my PhD research. First of all I would like to express my sincere gratitude to my supervisor Professor Richard Christopherson for his mentoring and support, thank you for allowing me study/research in your laboratory and for always having faith in me.

To Dr Giles Best, for your constant supervision, technical and theoretical discussions support through the difficult times and for always knowing the right thing to say at stressful moments. I hope that I may one day become a mentor like you.

To Dr Larissa Belov, for listening to my problems and providing very helpful advice.
To Drs Ben Crossett, Swetlana Mactier and Kim Kaufman for your expertise in proteomics.

To Dr. Pauline Huang for showing me that it is possible to achieve anything with hard work and dedication, and for being able to predict the future. To Jerry Zhou, for being my honours and PhD buddy, and a great 'co-worker' for the last five years. It's been a long haul and it wouldn't have been the same without you. To Munther Alomari for being like a brother to me and for all the help with the 'Death Star'.

To all the past and present members of the RICLAB particularly Philippa Kohnke, Sandra Wissmueller, Zoe Che, Duthika Mallawaaratchy, Meng Hsu and Erin Sykes who have been a part of my PhD journey. Thank you for all the memories. To the very new members Kieran and Rose, I hope your experience in the RICLAB will be as memorable, enjoyable and enriching as mine has been.

Lastly and most importantly, my heartfelt thanks to my parents Abul Almazi and Wafee Ara and my little brother Ishan for your love, understanding, support and faith in me. Thank you, for making me feel better when things were difficult and sharing the joys of my successes. Having a supportive family has been the most important factor in the completion of my PhD.

PUBLICATIONS & PRESENTATIONS

Manuscripts:

1. **Almazi, J. G**., Mactier, S., Best, O. G., Crossett, B., Mulligan, S. P. & Christopherson, R. I. 2012. Fludarabine nucleoside induces accumulations of p53, p63 and p73 in the nuclei of human B-lymphoid cell lines, with cytosolic and mitochondrial increases in p53. *Proteomics Clin Appl,* 6, 279-90 **(IF: 2.92).**
2. Kohnke, P. L., Mactier, S., **Almazi, J. G**., Crossett, B. & Christopherson, R. I. 2012. Fludarabine and cladribine induce changes in surface proteins on human B-lymphoid cell lines involved with apoptosis, cell survival, and antitumor immunity. *J Proteome Res,* 11, 4436-48 **(IF: 5.05)**.
3. Huang, P. Y, Best, O. G., **Almazi, J. G.,** Davis, Z. A.; Majid, A., Dyer, M., Pascovici, D., Mulligan, S. P. & Christopherson, R. I. 2014. Cell surface profiles distinguish stable and progressive chronic lymphocytic leukaemias. *Leukemia and Lymphoma*, in press **(IF: 2.30).**
4. **Almazi, J. G.,** Best, O. G., Graham, M., Alomari, M., Christopherson, R. I, 2013. Phosphorylation of HSP90 at Ser 254 aids in dissociation from p53 interactome in response to fludarabine treatment in B-lymphoid cancers. *Journal of Proteome Research*, manuscript in preparation.

Oral presentations:

5. **Almazi, J. G**. P53 responses to Fludarabine induced apoptosis in haematological malignancies. *School of Molecular Bioscience PhD Seminar*, University of Sydney, Sydney NSW Australia, 15th March 2013.

6. **Almazi, J. G.** P53 family proteins and mechanisms of drug induced apoptosis in B-cell Lymphoma. Requested speaker at *Pannell Laboratory Meeting*, Mitchell Cancer Institute, Mobile AL United States of America, 4th November 2011.

Selected conference abstracts:

7. **Almazi, J. G.**, Best. O. G., Alomari, M., Mulligan, S. P. & Christopherson, R. I. Fludarabine induced changes in p63 and p73 expression and TP53 protein binding partners. *24th Lorne Cancer Conference,* Mantra Beach Resort**,** Lorne VIC Australia, 8 – 10th Feb 2012.
8. **Almazi, J. G**., Best. O. G., Alomari, M., Mulligan, S. P. & Christopherson, R. I. Fludarabine-Induced changes in p63 and p73 expression and TP53 protein binding in *TP53* wild-type and mutated cell lines. *14th International Workshop on Chronic Lymphocytic Leukaemia***,** The Westin Galleria & The Westin Oaks, Houston TX United States of America, 28-30th October 2011
9. **Almazi, J. G.**, Kohnke, P. & Christopherson, R. I. Proteomic approach to study binding partners of p53 in Raji cells, *9th HUPO World Congress,* Sydney Exhibition Centre, Sydney NSW Australia, 19-23 September 2010.
10. **Almazi, J. G.**, Best. O. G., Mulligan, S. P. & Christopherson, R. I. Fludarabine induces changes in phosphorylation and levels of p53, p63 and p73 in chronic lymphocytic leukaemia (CLL). *13th International Workshop on Chronic Lymphocytic Leukaemia*, Barcelona, Spain, 16-18 October 2009

ABBREVIATIONS

1D	One-dimensional
2D	Two-dimensional
2D-PAGE	Two-dimensional polyacrylamide gel electrophoresis
5'-NT	5'-Nucleotidase
7-AAD	7-Amino-actomycin
ACN	Acetonitrile
AK	Adenylate kinase
AML	Acute Myeloid Leukaemia
APAF-1	Apoptotic Protease Activating Factor-1
ATM	Ataxia Telangectasia
ATR	Ataxia Telangectasia and RAD3-related Protein
ATCC	American type culture collection
ATP	Adenosine triphosphate
BSA	Bovine serum albumin
CD	Cluster of differentiation
CDK	Cyclin-dependent Kinase
CHAPS	3- ((3-Cholamidopropyl)dimethylammonio)-1-propanesulfonic acid
CID	Collision Induced Dissociation
CK	Casein Kinase
CLL	Chronic lymphocytic leukemia
DBD	DNA Binding domain
dCK	Deoxycytidine kinase
DMF	Dimethylformamide

DMSO	Dimethyl sulphoxide
DNA	Deoxyribonucleic acid
DTT	Dithiothreitol
EBV	Epstein–Barr virus
ECL	Enhanced chemiluminescence
ESI	Electrospray ionization
FGFR3	Fibroblast growth factor receptor 3
FCS	Foetal calf serum
GAPDH	Glyceraldehyde-3-phosphate dehydrogenase
hENT	Human equilibrative nucleoside-specific membrane transporters
hCNT	Human concentrative nucleoside-specific membrane transporters
HCL	Hairy cell leukemia
HPLC	High-performance liquid chromatography
HPRD	Human Protein Reference Database
HRP	Horseradish peroxidise
IAA	Iodoacetamide
IDA	Information dependent acquisition
IEF	Isoelectric Focussing
IPG	Immobilised pH Gradient
iTRAQ	Isobaric tag for relative and absolute quantitation
IWCLL	International workshop on CLL
kDa	Kilo Dalton
LC	Liquid chromatography
MALDI	Matrix-assisted Laser Desorption Ionisation

MCL	Mantle cell lymphoma
MDM2	Mouse Double Minute 2 protein
MMSET	Multiple myeloma SET-domain protein
MOMP	Mitochondrial Outer Membrane Permeabilisation
MQ-water	MilliQ water
mRNA	Messenger RNA
MS	Mass Spectrometry
MS/MS	andem Mass Spectrometry
NDK	Nucleoside diphosphate kinase
NHL	Non-Hodgkin's lymphoma
NK	Natural killer (cell)
NP-40	Nonidet P-40
p14ARF	p14 alternate reading frame
p53RE	p53 responsive element
p63RE	p63 responsive element
PBS	Phosphate-buffered saline
pI	Isoelectric Point
PKC	Protein Kinase C
PMSF	Phenylmethylsufonyl Fluoride
PRD	Proline rich domain
PTM	Post-translational modification
PVDF	Polyvinylidene difluoride
RNA	Ribonucleic acid
RT	Room temperature
SAM	Sterile alpha motif

SCX	Strong cation exchange
SDS	Sodium dodecyl sulphate
SDS-PAGE	SDS-polyacrylamide gel electrophoresis
TA	Transcription activating
TAD	transcription activation domain
TBP	Tributylphosphine
TBS-T	Tris-buffered saline Tween-20
TCA	Trichloroacetic acid
TCEP	Tris-(2-carboxyethyl) phosphine
TEAB	Triethylammonium bicarbonate
TEMED	N,N,N',N'-Tetramethylethyl-ethylenediamine
TFA	Trifluoroacetic acid
TiO2	Ttitanium dioxide
TOF	Time-of-flight
TRAIL	TNF-related Apoptosis-Inducing Ligand
UV	Ultraviolet
VRK1	Vaccinia-related Kinase 1
WBC	White Blood Count
WHO	World health organisation
WM	Walddenström's macroglobulinemia

SUMMARY

The tumour suppressor protein p53, is a transcription factor responsible for regulating the cell cycle and/or apoptosis in proliferating cells subjected to a variety of stressful events, including DNA damage. Mutations of p53 occur in >50% of human tumours, the most frequently altered gene in cancers. This thesis looks at the responses of the p53 interactome in B-lymphoid cancers after fludarabine (2-FaraA) induced DNA damage. The overall purpose was to contribute to our understanding of B-lymphoid cancers by 1) looking at the response of p53 and family proteins p63 and p73, after 2-FaraA induced DNA-damage, 2) compare the p53 interactome following DNA damage in cells with and without mutations in p53, 3) study the DNA-damage phosphorylation cascades in the p53 interactome and 4) analyse the effects of p53 knock-down on fludarabine responsive cells.

Analysis using 1D and 2D Western blotting and quantitative PCR has demonstrated that in the 2-FaraA-sensitive cell lines, Raji and IM9, p53 accumulates in nuclei, mitochondria and cytosol. Raji cells accumulate p53 in mitochondria earlier than in the nucleus suggesting that initiation of apoptosis in these cells is dependent on the roles of p53 at mitochondria, prior to effects on gene expression in the nucleus. In Raji, accumulation of p53 is likely to result from increased mRNA levels, and from inhibition of p53 degradation due to phosphorylation. 2-FaraA also induces phosphorylation and accumulation of lower molecular weight derivatives of p53, p63 and p73 in the nuclei of Raji cells that may have roles in inducing apoptosis.

Qualitative analysis of the p53 interactome in Raji, IM9 and MEC1 cell lines using mass spectrometry indicated that MEC1 may have a gain of function p53 mutation that may contribute to 2-FaraA resistance. In 2-FaraA responsive cells, treatment dissociates HSP90

from the p53 interactome. This suggests that HSP90 binding to p53 may play a role in regulating p53 activity and sensitivity to 2-FaraA treatment.

Quantitative phospho-proteomics of the p53 interactome showed that in response to 2-FaraA, HSP90 is phosphorylated at serine 254 by casein kinase, that may be associated with its dissociation from p53. 2-FaraA may also dysregulate ribosome biogenesis, essential for cell survival. p53 knockdown in Raji and IM9 with siRNA induced up-regulation of transcription the factor YY1, and the surface antigen ICAM1, that may have roles in altering the biochemistry of the cells and allow them to become resistant to 2-FaraA-induced apoptosis in p53 knock-down cells

Taken together the novel findings of this thesis provide greater insight into the p53-centric mechanism of 2-FaraA against B-lymphoid cancers and suggest new treatment strategies for drug resistant chronic lymphocytic leukaemia and lymphoma.

CHAPTER ONE

General Introduction

1.1 B-LYMPHOID CANCERS

The biological process of haematopoiesis describes the formation of leukocytes in the bone marrow and their differentiation into the different white blood cells from the original stem cells. The common lymphoid progenitors eventually differentiate into T- or B-lymphocytes (Figure 1.1) and the cancers of these cells are referred to as T- or B-lymphoid cancers. The latter arise when B-cell differentiation and activation are disrupted, resulting in lymphomas and leukaemias [1]. This thesis uses 4 immortalised cell lines that represent different B-lymphoid cancers.

The Raji cell line was derived from Burkitt 's lymphoma (non-Hodgkin's lymphoma), an aggressive B-cell lymphoma of children and young adults that is associated with translocations of the gene encoding the transcription factor c-MYC to immunoglobulin loci [2]. Burkitt's lymphomas can also accumulate somatic mutations of c-MYC that might alter its function as a transcription factor [3, 4]. These mutations of c-MYC could promote tumour-cell proliferation [5].The endemic form of Burkitt's lymphoma involves Epstein–Barr virus (EBV) infection of B-lymphoid cells, whereas the sporadic form is EBV independent. These lymphomas can be cured in more than 80% of cases [1].

The human IM9 and U266 cell lines are derived from myeloma, an incurable malignancy of plasma cells with a median survival of three years. Multiple myeloma constitutes ~10% of all haematological malignancies, with a median age at diagnosis of ~65. Neoplastic cells are located in the bone marrow, and osteolytic bone lesions are characteristic [6]. Reciprocal chromosomal translocations between one of the immunoglobulin loci and various other genes, including those that encode cyclin D1, cyclin D3, c-MAF, MMSET (multiple myeloma SET-domain protein) or fibroblast growth factor receptor 3 (FGFR3), are considered to be primary oncogenic events [7].

The MEC1 cell line was derived from chronic lymphocytic leukemia (CLL); the most common leukaemia, with a median age of onset of 65. CLL is molecularly and clinically related to a nodal lymphoma known as small lymphocytic lymphoma. Current therapies can remove CLL cells from the blood , but is not curative and does not prolong survival [1].

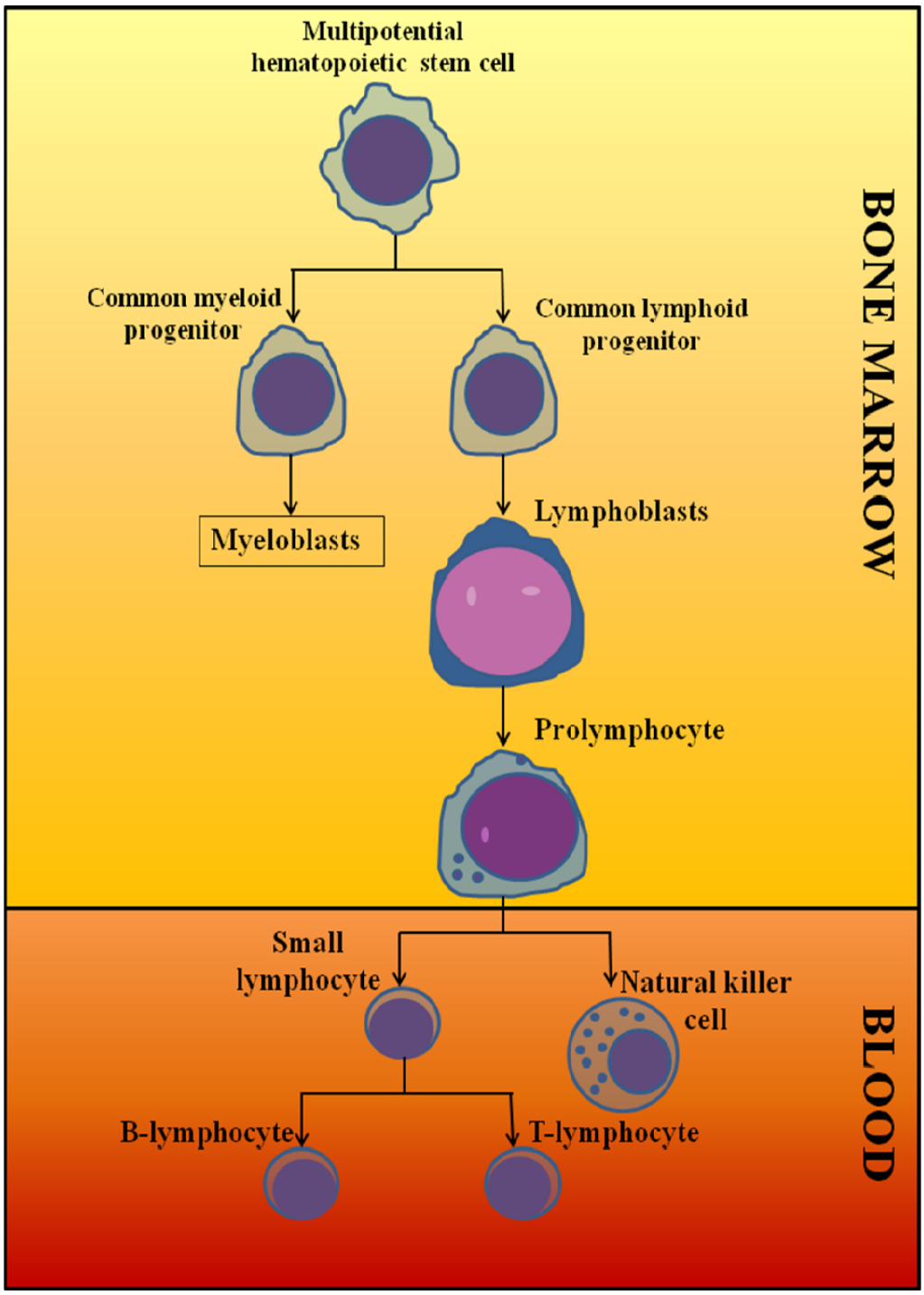

Figure 1.1 Hematopoiesis of B-lymphocytes from which Raji, IM9, MEC1 and U266 cell lines are derived.

1.1.1 Raji cell line (non-Hodgkin's lymphoma)

The Raji cell line (ACC319) was established from the left maxilla of a 12-year-old African boy with Burkitt's lymphoma in 1963 and is the first continuous human hematopoietic cell line. In suspension, Raji are round cells that partly grow in clusters and double in 24-36 h. The immunophenotype is positive for CD10, CD19, CD20, HLA-DR, CD37, CD79a, CD80 and IgM; and negative for CD3, CD13, CD34, and CD138 [8]. Raji cells have a p53 point mutation Arg(213)-Gln, but it retains the functional properties of wild-type p53 [9].

1.1.2 IM9 cell line (EBV-transformed B-lymphoblastoid)

The IM9 cell line (ACC117) was isolated from the bone marrow of a woman with multiple myeloma in 1967. Cells synthesize IgG, have receptors for insulin and calcitonin, and express BCL2 mRNA. IM9 are Epstein Barr Virus positive and B-lymphoblastoid derived cells. In suspension, IM9 are lymphoblastoid shaped, as single cells or clusters. The cells are positive for CD19, CD20, cyCD79a, CD80, CD138, and HLA-DR and negative for CD3, CD10, CD13, CD34, and CD37 [10, 11]. IM9 cells are p53 wild-type [12].

1.1.3 MEC1 cell line (chronic lymphocytic leukemia)

The MEC1 cell line (ACC497) was established in 1993 from the peripheral blood of a 61-year-old Caucasian man with chronic B-cell leukemia (B-CLL in prolymphocytoid transformation to B-PLL); a serial sister cell line MEC-2 (DSM ACC 500) was also isolated. In suspension, they appear as round to polymorphic cells growing singly or in clusters, a few cells are slightly adherent. The cells are positive for CD19, CD20, CD37, CD79a, CD80 and HLA-DR. They are negative for CD3, CD10, CD13, CD34 and CD138 [13]. For MEC1 and

MEC2, p53 is mutated with a deletion of 40 amino acids at the N-terminus of the protein [14].

1.1.4 U266 cell line (myeloma)

The U266 cell line (ACC9) was established from the peripheral blood of a 53-year-old man with IgE-secreting myeloma (refractory, terminal) in 1968. In suspension, they are round to polygonal, and grow singly or as clusters, some are loosely adherent. They are positive for CD33, CD38, CD79a, CD138 and HLA-DR. They are negative for CD3, CD4, CD5, CD10, CD13, CD14, CD15, CD19, CD20, CD21, CD22, CD34, CD37 and CD80. The U266 cell line has a single mutant p53 allele [15] in codon 161 [16].

1.2 FLUDARABINE (2-FaraA)

The anticancer drug fludarabine, was synthesized in 1969 by Montgomery and Hewson [17]. The chemical name for fludarabine is 9-β-D-arabinofuranosyl-2-fluoroadenine 5'-monophosphate, FdAMP (2-FaraAMP). It consists of an adenine base linked to a deoxyribose through a glycosidic bond, with a fluorine atom attached at carbon 2 of the purine ring and a phosphate group attached at carbon 5 of the deoxyribose group (Figure 1.2). The phosphate group aids in drug solubility.

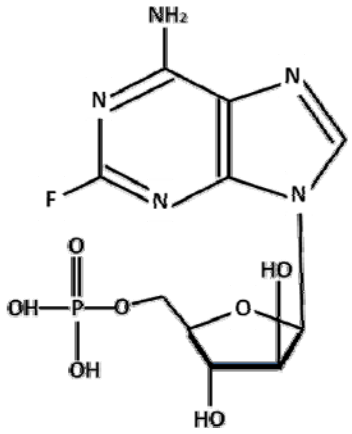

Figure 1.2 Chemical structure of 2-FaraAMP

1.2.1 Uptake and metabolism

Administered as a 2-FaraAMP, fludarabine is de-phosphorylated by the plasma membrane phosphatase CD73 to 2-FaraA [18]. 2-FaraA enters the cell through both (human) equilibrative nucleoside-specific membrane transporters (hENT1 and hENT2) and (human) concentrative nucleoside-specific membrane transporter (hCNT3) [18-20]. After 2-FaraA uptake, it is converted to the triphosphate form by deoxycytidine kinase (dCK), adenylate kinase (AK) and nucleoside diphosphate kinase (NDK) to produce 2-FaraATP [21]. In proliferating and resting cells 2-FaraATP accumulation is dependent on a high ratio of dCK/CD73 activity [22].

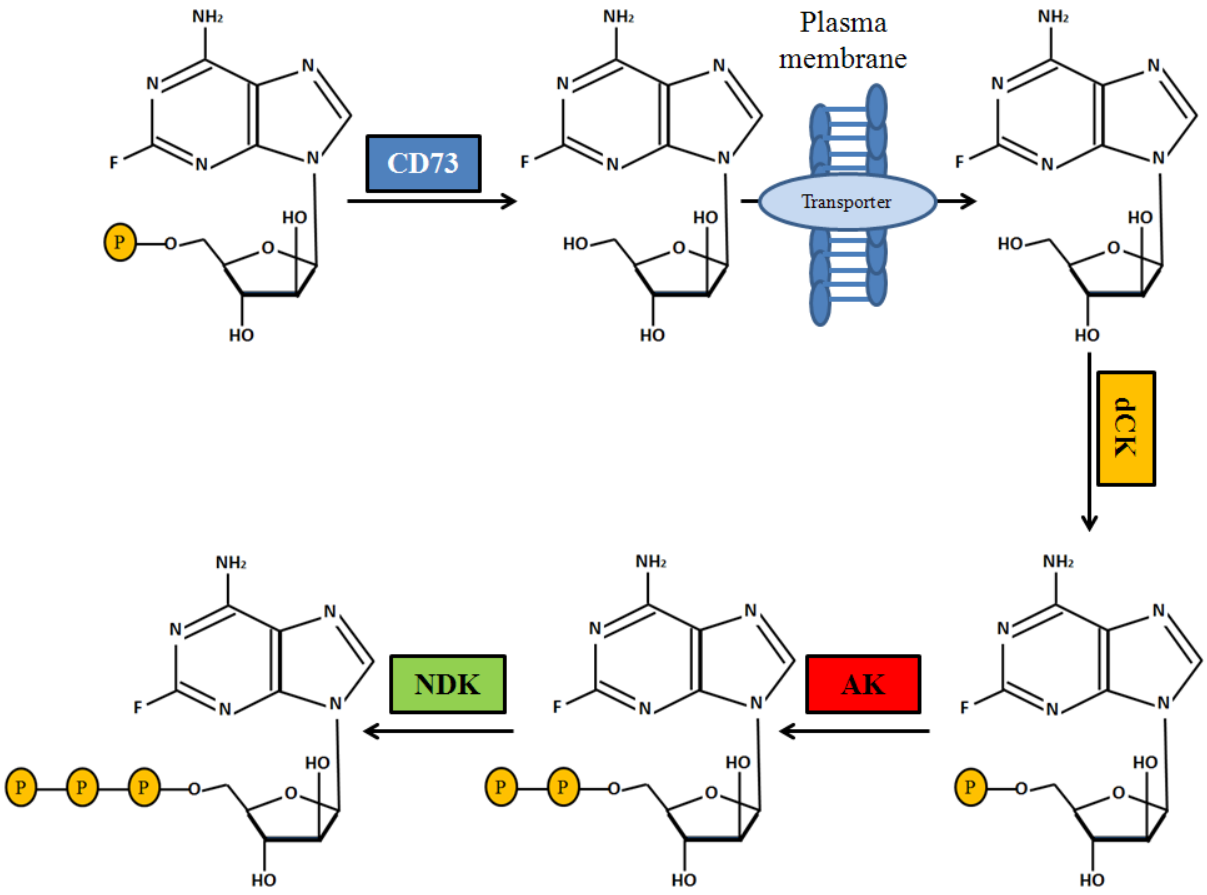

Figure 1.3 Schematic of Fludarabine uptake and metabolism by B-lymphocytes. The boxes represent the phosphatase CD73, deoxycytidine kinase (dCK), adenylate kinase (AK) and nucleoside diphosphate kinase (NDK). The circle in the plasma membrane represents nucleoside-specific membrane transporters.

1.2.2 Mechanisms of action

The principal mechanism of action of 2-FaraATP is inhibition of DNA synthesis [23, 24]. Specifically, the 2-FaraATP inhibits DNA polymerase by acting as an alternative substrate to deoxyadenosine 5'-triphosphate (dATP) and inhibits DNA primase by perturbing ribonucleoside triphosphates levels [25, 26]. 2-FaraATP also inhibits ribonucleotide reductase which results in lowering of cellular deoxynucloetide pools [27, 28]. 2-FaraAMP can also incorporate into the DNA and cause strand breaks due to the inability of DNA ligase I to join it to the adjacent DNA strand [29, 30].

2-FaraATP also inhibits RNA polymerase II and 2-FaraAMP is incorporated into mRNA resulting in premature termination of RNA transcripts resulting in inhibition of RNA and protein synthesis [31]. 2-FaraATP can induce cell death in quiescent cells without incorporation into DNA by activation of the intrinsic pathway from mitochondria, by the apoptotic cascade [32] Combinations of these effects lead to complete inactivation of DNA synthesis followed by initiation of apoptosis of cells [33, 34].

1.2.3 Therapy

Fludarabine was first established for treatment of relapsed or refractory CLL [35] and is now standard treatment for patients with CLL and indolent NHL [36]. Fludarabine is a first line therapy for CLL. A study published by Keating *et al.* involved the long term follow-up of a group of 174 patients with progressive or advanced CLL, treated with fludarabine [37]. Results from the study showed that fludarabine induced a complete response rate of 38% in these patients. Similarly, Hagenbeek *et al.* showed that patients with newly diagnosed low grade NHL who received fludarabine, achieved higher overall response and complete response compared with patients treated with the conventional CVP (cyclophosphamide, vincristine, and prednisone) therapy. They concluded that fludarabine is a highly active single agent agonist low grade NHL [38]. Other diseases that use fludarabine as mono-therapy include mantle cell lymphoma (MCL), Walddenström's macroglobulinemia (WM), hairy cell leukemia (HCL), MALT lymphoma and cutaneous T-cell lymphoma [39-41]. Fludarabine is also used in combination therapy most commonly with cyclophosphamide and rituximab (FCR) for relapsed CLL patients [42] and indolent NHL [43].

1.3 CELLULAR TUMOUR ANTIGEN P53

The tumour suppressor protein p53 is one of the most studied proteins in cancer research. As a transcription factor, p53 plays an essential role as the "guardian of the genome" [44] by regulating the expression of at least 361 genes [45] involved in cell cycle arrest, apoptosis and other functions in response to cellular stress signals. Loss of p53 function, through mutations or perturbations in the signalling pathways for p53, is a common feature of most human cancers [46].

1.3.1 History, structure and isoforms

p53 was inadvertently discovered in 1979, when studies of SV40-transformed cells showed that a 55-kDa protein co-precipitated with the large-T antigen. Mice inoculated with murine cells transformed by SV40 showed a strong immune reaction and produced antibodies against a nuclear protein known as Large T antigen. Immuno-precipitation of this large T antigen co-precipitated an associated protein of molecular weight 53 – 54 kDa [47-50]. This associated protein of cellular rather than viral origin was later called p53. The p53 gene was initially thought to be an oncogene and later proven to play the opposite role as a tumour suppressor; p53 has been the focus of thousands of research studies of cancer.

p53 is composed of 393 amino acids and has five major domains (Figure1.4) The N-terminal domain (amino acids 1-100) is required for the transcriptional activity of p53, it consists of two transactivation domains (TADs) and a proline-rich domain. At least one of the two TADs is necessary for transcriptional activity, and the first TAD is dispensable for apoptosis induction [51, 52]. It is also the binding site for the p53 inhibitor mdm2. The transactivation domains have 10 known phosphorylation sites that are S6, S9, S15, T18, S20, S33, S37, S46, T55 and T81. [53]. Amino acids 61 - 94 constitute the proline rich domain, that binds prolyl

isomerase PIN1 decreasing the affinity of p53 for the inhibitor MDM2 [54]. The proline rich domain has also been implicated in transcription-independent p53 functions [55]. The core DNA binding domain comprising amino acids 101-300 specifically binds to DNA consensus recognition elements in the promoters of target genes. It is in this domain that most p53 mutations are found in human tumours and most mutations in the DNA binding domain dramatically affected the transactivation efficiency of p53 in yeast assays. There are 4 known phosphorylated residues in the domain, S149, T150, T155 and S215. The C-terminal oligomerisation domain (OD) forms homo-tetramers. It contains a β-strand and α-helix, which associate with another p53 subunit across an interface containing anti-parallel β-sheet and an anti-parallel helix-helix, forming a dimer. The two dimers are held together by the large hydrophobic surface of each helix pair [56]. The native tetramer of p53 activates transcription whereas the monomer is transcriptionally inactive [57]. The last domain of p53, from amino acids 360 to 393, is the C-terminal regulatory domain that binds DNA non-specifically and may regulate specific DNA binding by the DBD [58, 59]. Residues phosphorylated in these domains include S313, S314, S315, S366, S371, T377, S378, T387 and S392.

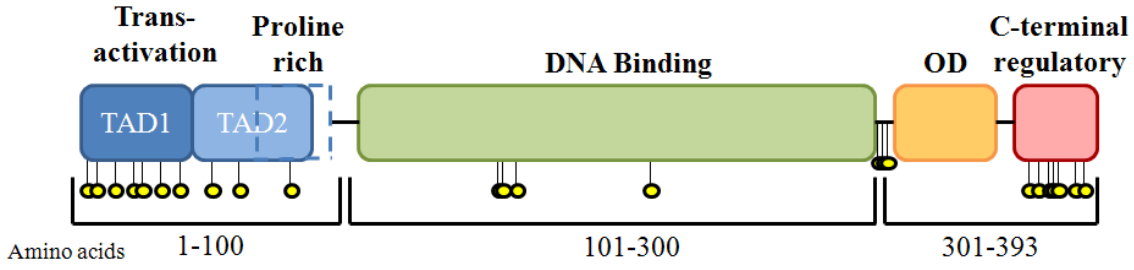

Figure 1.4 The major domains and sites of phosphorylation of p53. The transactivation domains (TAD1 and TAD2) are blue squares, the proline rich section is a clear square with dotted lines. The DNA binding, oligomerisation (OD) and the C-terminal regulatory domains are in green, orange and red squares, respectively.

In humans p53 is found in chromosome 17. There are nine natural isoforms of p53 generated by alternative transcription sites and splicing (Figure 1.5). Wild-type p53, p53β and p53γ are transcribed from promoter 1 and alternative splicing of intron 9 generates the p53β and p53γ isoforms. Δ40p53, Δ40p53β and Δ40p53γ transcribed from codon 40 and are alternatively spliced at intron 9, similar to the full length protein, to form the β and γ isoforms. Lastly, Δ133p53 Δ133p53β and Δ133p53γ are transcribed from codon 133 and undergo alternative splicing at intron 9 to generate the β and γ isoforms.

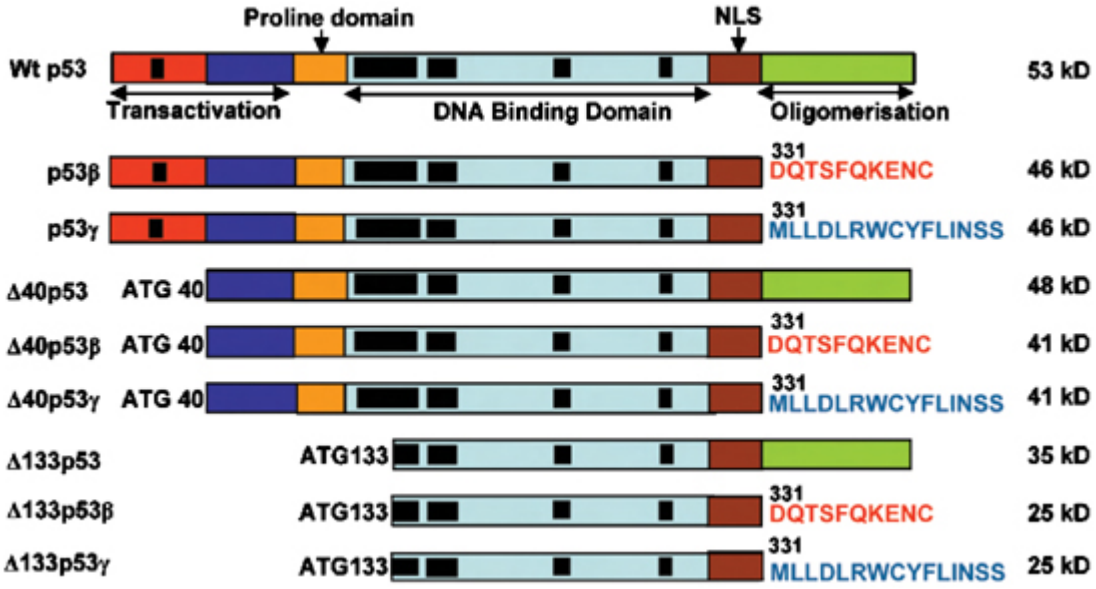

Figure 1.5 p53 protein isoforms generated from alternative splicing (α, β, γ) and alternative promoters [60]

1.3.2 Mechanism of action

In unstressed cells, p53 levels are minimal. Cellular stress stabilises p53 and allows it to accumulate resulting in events such as apoptosis, growth arrest and/or senescence [61, 62]. For example, DNA damage triggers the accumulation of signal mediators such as ATM and ATR kinases, and p14ARF (Figure 1.6). These mediators collectively lead to accumulation of p53 following phosphorylation, and p14ARF inhibits MDM2 that induces ubiquitination of

p53. The activated p53 tetramer can undergo further modifications such as acetylation [63, 64] and methylation [65]. p53 binds to the p53RE and triggers transcription of target genes. These genes vary according to the cell's requirement. For apoptosis, genes like Puma, Noxa, Bax and Fas are transcribed, whereas for cell cycle arrest p21, Waf1 and Snf proteins are required [66, 67].

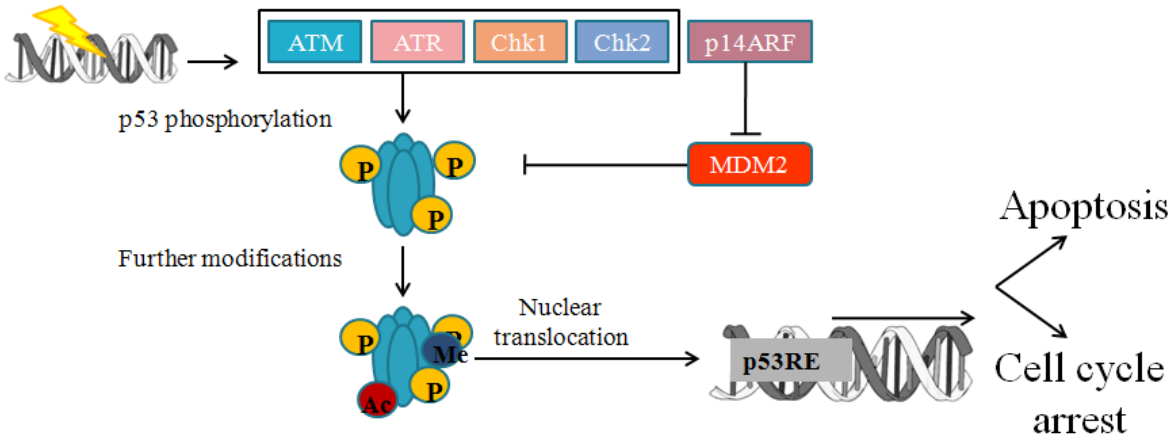

Figure 1.6 DNA damage induces apoptosis and cell cycle arrest following phosphorylation and accumulation of p53

1.3.3 Other p53 family proteins (p63 and p73)

The *p63* gene was discovered in 1997 as the last member of the p53 family [68]. The *p63* gene has a high degree of sequence homology to *p53* (Figure 1.7); however there are some differences between the two genes and their respective proteins. Human p63 has three alternatively spliced C-terminal isoforms (α, β, γ) and is transcribed from two different promoters. The promoter that is found upstream of exon 1 transcribes the transactivating isoforms (TAp63) and the promoter found in intron 3 transcribes the N-terminal truncated isoforms (ΔNp63). Taken with the C-terminal alternative splicing, *p63* has the potential to

express 6 different mRNAs encoding 6 p63 isoforms. The functional motifs of p63 are similar to p53 with one exception, the α-isoforms (both TAp63α and ΔNp63α) have an additional sterile alpha motif (SAM) implicated in protein-protein interactions associated with early developmental processes, a biological function unique to p63 [69]. The TAp63 isoforms are 'p53-like,' they can bind to DNA through p53 responsive elements (p53RE) and activate target genes to induce cell cycle arrest and apoptosis. They can also bind to the p63RE, similar to p53RE but only binds p63. The ΔNp63 isoforms can also bind to the p53RE but cannot induce transcription, thus exerting a dominant negative effect on transactivating p53 and p63. Therefore ΔNp63 isoforms hinder tumour suppressive functions and are thought to have oncogenic properties [68]. ΔNp63 isoforms also activate specific gene targets not induced by TAp63 isoforms and are abundantly expressed in progenitor cells of skin, breast and prostate where levels of TAp63 are barely detectable, indicating that ΔNp63 plays particular roles in differentiation [70].

Unlike p53, p63 mutations are not directly linked to cancer [71]. The role of p63 in cancer is difficult to define due to its contradictory activities as a tumour suppressor or an oncogene [72]. Mouse models have shown that some $p63^{+/-}$ mice develop cancer while others are not cancer prone, but may be subject to premature aging leading to senescence [73, 74]. Squamous cell carcinoma has ΔNp63 as the main isoform expressed, contradictory to most malignant lymphomas where TAp63 isoforms are expressed and ΔNp63 isoforms are not. In humans, the p63 gene is frequently amplified in squamous, lung and cervical cancers [75].

The *p73* gene was accidentally in 1997 discovered during a search for novel interleukins by Caput *et al. [76]* and found to have sequence homology with *p53*. The *p73* gene is located at human chromosome 1p36 and is frequently deleted in some human cancers, specifically

neuroblastomas, melanomas and breast cancers. Human *p73* have 15 exons, and similar to *p63*, the p73 gene can be transcribed from an alternative promoter in intron 3 generating the transactivating (TAp73) and amino terminal truncated (ΔNp73) isoforms. *p73* can also be alternatively spliced at the C-terminus to form 7 different isoforms (α, β, γ, δ, ε, ζ and η). Taken together, the *p73* gene expresses 35 mRNA variants, however only 14 have been described [77]. Structurally p73 is very similar to p63 (Figure 1.7) with homologous domains, in particular the DBD (~85% homology).

p73 does not have its own responsive element but can bind to p53RE to transcribe genes [78]. It induces p53-like responses (TAp73) in the cell as well as dominant negative responses (ΔNp73). In the developing mouse brain, the principal form of p73 is ΔNp73. The amino-truncated isoforms are required to counter p53-mediated neuronal death during sculpting of the developing mouse neuronal system [79-81]. TAp73 may also play important roles in the terminal differentiation program during nephron development in kidneys [82]. Studies using mouse models show that p73 null mice have striking defects such as hippocampal dysgenesis, hydrocephalus and suffer chronic infections and inflammation, with abnormalities in the pheromone sensory pathways [83].

The role of p73 in cancer is ambiguous. The *p73* gene is seldom found mutated in cancer but there is evidence of differential expression in different tumours. The functions of ΔNp73 are important for tumour survival as it inhibits the apoptotic effects of p53 [84]. Studies by Beitzinger *et al.* (2008) show that in pre-malignant stages, expression of TAp73 is triggered which helps increase sensitivity to chemotherapeutic agents and prevents anchorage-independent tumour growth, a hallmark of melanoma and ovarian cancers [85]. Studies in B-

CLL show expression of p73 gene variants was much higher in leukemic cells compared to controls [86].

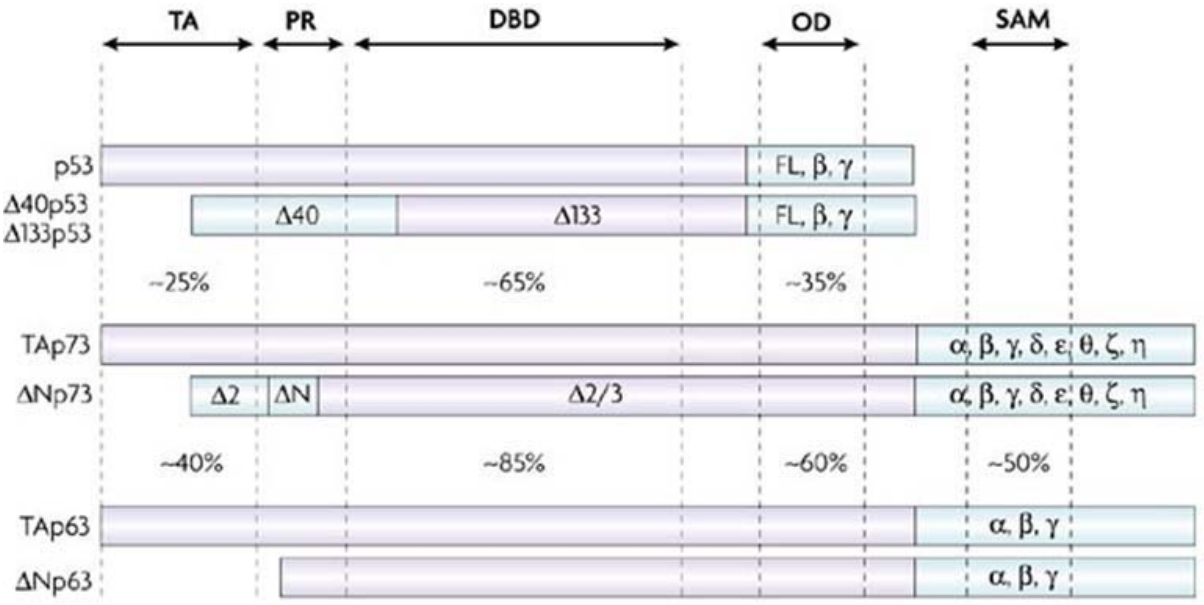

Figure 1.7 Homology between p53, p63 and p73. Functional domains include the transactivation domain (TA), proline-rich domain (PR), DNA binding domain (DBD), oligomerization domain (OD) and sterile alpha motif (SAM) [87].

Studies of cell biology over the years have curated an extensive knowledge of protein function, structure, localisation and modifications of multiple organisms in databases [88]. However a protein rarely acts individually. For a biological event to occur, a network of proteins collaborates to induce signalling cascades. Mapping the protein-to-protein interactions can provide a clearer picture of the molecular mechanisms involved with biological events. The complete map of a protein's interactions that can occur in a living organism is called the interactome [89]. For a protein like p53, the interactome can be complex as it is able to bind to DNA, RNA, and proteins (Figure 1.8) and is regulated by many macromolecules. Study of the p53 interactome will indicate the number of molecular and biological processes it's involved in.

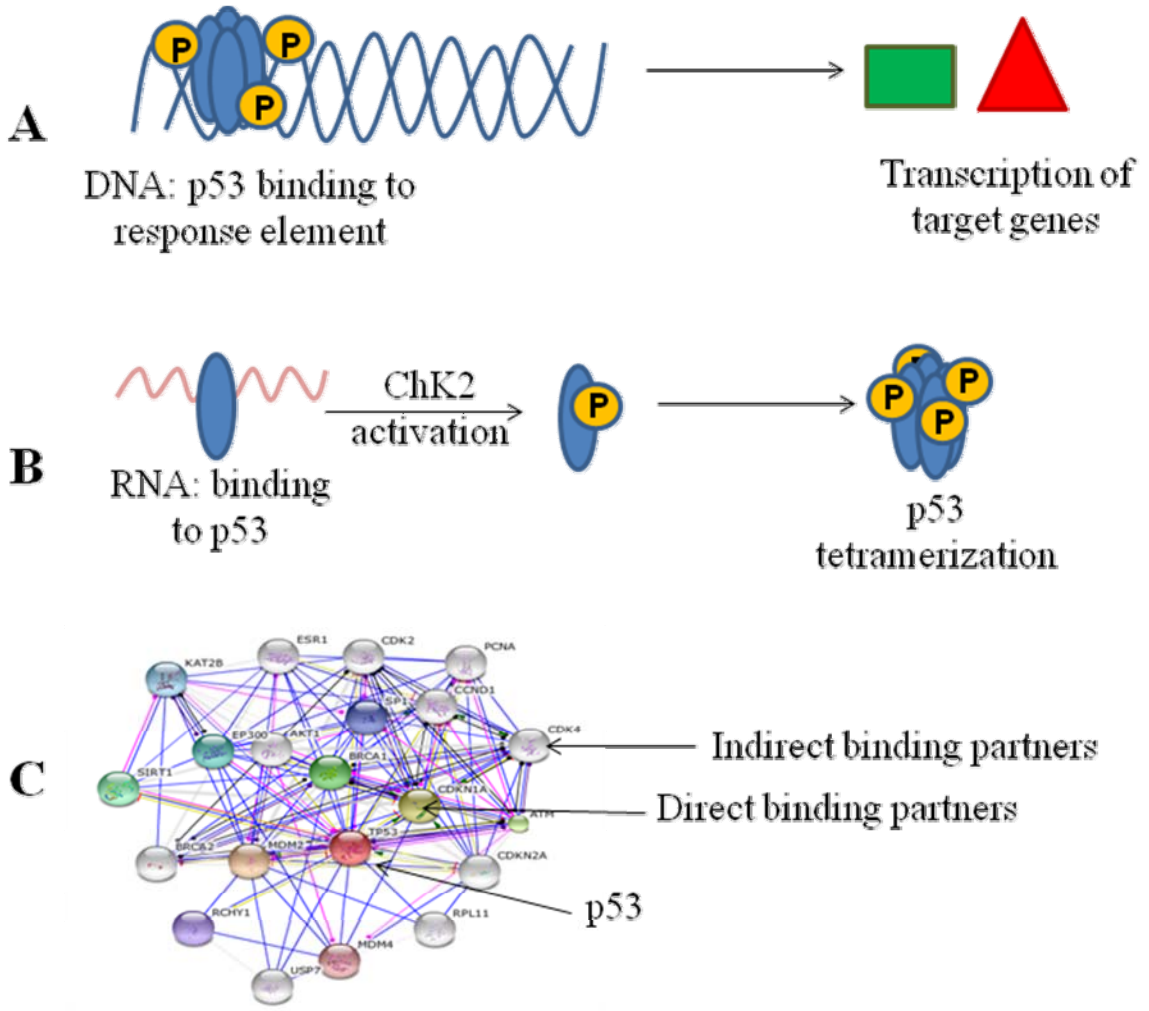

Figure 1.8 Components of the p53 interactome. (A) p53 binds to the p53RE of target genes and any other proteins binding to or near the p53RE may be detected in the interactome. (B) RNA may bind to p53 which aids in oligomerization [90], thus, other RNA binding proteins may form part of the interactome. (C) Proteins and protein complexes that directly bind to p53 as well as proteins that bind to p53 binding proteins (indirect) are a part of the interactome.

1.4 PRINCIPLES OF PROTEOMIC TECHNIQUES

The term ‘proteomics’ was coined in 1995 by Wilkins and co-workers in Australia [91]. Proteomics involves the identification, modification, quantification and localisation of a complete set of proteins in an organism or system. Factors that influence the success of a proteomics experiment include sample preparation, separation methods, data acquisition and analysis. There are more than 100,000 unique proteins within a typical human cell. Thus, enrichment techniques such as sub-cellular fractionation and as adsorption to TiO_2 for phosphorylation should be considered when designing studies. The two main approaches to proteomic analysis are ‘bottom-up’ and ‘top-down’ methods. Bottom-up (shotgun) analysis typically involves digestion of proteins using a specific protease (trypsin), and the resulting peptides are separated using liquid chromatography. The separated peptides are ionized and directly injected into a mass spectrometer, where the mass-to-charge (m/z) ratios of the molecular ions are determined. Peptide (precursor) ions are chosen on the basis of an abundance-guided heuristic and subjected to fragmentation. The mass of each precursor and fragment ions are then assigned by a database search tool to the best-matching peptide sequence in a database. Changes in protein abundance between samples can be quantified by directly comparing the ion abundance between subsequent mass spectrometric analyses (label-free quantification) or with stable isotope labelling. With all its advantage, there are also several drawbacks to the shotgun approach. The variability of the precursor selection means poor reproducibility between runs. Validation techniques such as western blot or flow cytometry are limited by availability of antibodies which limit hypothesis generation [92]. Recent advances with techniques such as selected reaction monitoring are being developed to combat this problem.

The top-down mass spectrometry involves the introduction of intact protein molecular ions generated by electrospray ionisation into the mass analyser and are subjected to gas-phase fragmentation. The two major advantages of the top-down strategy are the potential access to the complete protein sequence and the ability to locate and characterize post translational modifications. In addition, the time-consuming protein digestion required for bottom-up methods is eliminated. Top-down proteomics is a relatively young field compared to bottom-up proteomics, and has several limitations such as low sensitivity, as the technique does not favour intact proteins larger than ~50 kDa and underdeveloped bioinformatics.

1.4.1 Mass spectrometry

Mass spectrometry is an analytical technique that can provide both qualitative (structure) and quantitative (molecular mass or concentration) information on analyte molecules after their conversion to ions. The molecules of interest are introduced into the ionisation source of the mass spectrometer, where they are ionised to acquire positive or negative charges. The ions then travel through the mass analyser and arrive at different parts of the detector according to their mass/charge (m/z) ratio. After the ions make contact with the detector, useable signals are generated and recorded by a computer system. The computer displays the signals graphically as a mass spectrum showing the relative abundance of the signals according to their mass to charge (m/z) ratio [93]. Tandem mass spectrometry (MS/MS) enables identification of proteins by sequencing of their peptides. Peptides are individually selected from the mixture in the first mass analyser and dissociated by collision with an inert gas, such as argon or nitrogen. The resulting fragments are then separated in the second mass analyser, producing the tandem MS/MS spectrum [94]. Peptide sequences can be obtained by manual annotation of the MS/MS spectra and the parent protein identified by database searching.

1.4.1.1 Liquid chromatography

In proteomics, the use of liquid chromatography provides a high-speed, high-resolution and high-sensitivity separation of macromolecules. In addition, the unique features of chromatography enable the detection of low-abundance species and post-translational modified proteins [95]. In shotgun studies, liquid chromatography is used to fractionate peptides prior to mass spectrometry to achieve a greater depth of proteome coverage. This involves the separation of molecules in solution, based on their interactions with stationary and mobile phases [96, 97]. The 3 types of liquid chromatography used in this thesis are reverse phase (RP-LC), two dimensional (2D-LC) and gel based (GeLC).

Reverse phase liquid chromatography (RP-LC) separates proteins by their hydrophobicity. Polypeptides adsorb to the hydrophobic surface of the column matrix in a polar mobile phase. Decreasing the mobile phase polarity by adding more organic solvent reduces the hydrophobic interaction between the solute and the solid support resulting in desorption. The more hydrophobic the molecule the more time it will spend on the solid support and the higher the concentration of organic solvent that is required to promote desorption. Commonly used matrices in RP consist of small, spherical, porous silica beads with a hydrophobic surface such as C4, C8 or C18. The most popular mobile phase is the organic solvent, acetonitrile (ACN).

Two-dimensional (2D) separations involve fractionation of the sample based upon different properties [98], enabling resolution of complex samples such as cellular peptide digests. A typical 2D-LC separation couples strong cation exchange (SCX) with RP separation. The SCX separates the peptides by charge where a negatively-charged resin (stationary phase) binds positively charged analytes. All the peptides are positively charged by adjusting the pH to be lower than most peptide isoelectric points (pH 2-4). Increasing the salt concentration in

the mobile phase displaces peptides according to their charge due to competition for binding on the stationary phase. Buffers such as ammonium acetate and ammonium formate are generally used as competitive salts.

Gel based liquid chromatography (GeLC, slice and dice) is another form of 2D-LC. Here molecules are separated based on their molecular weight then fractionated by RP. Protein samples are first separated by SDS polyacrylamide gel electrophoresis (SDS-PAGE). The detergent SDS linearizes proteins and coats them with negative charge. Proteins are separated by their ability to migrate through the polyacrylamide gel. Equal portions of the acrylamide gel are sliced and then the peptides are generated by in-gel tryptic digestion. Each section is then further separated by RP.

1.4.1.2 Ionisation

Peptides must be ionised to proceed with mass spectrometry analysis. The two forms of ionisation are electrospray ionisation (ESI) and Matrix-Assisted Laser Desorption Ionisation (MALDI). ESI is primarily used with bottom-up approaches and is the method used in this thesis. For ESI, a micro-capillary is used under a high potential energy. As the liquid analyte emerges from the needle-tip of the capillary, a strong electric field causes charge separation between the ions, that is offset by surface tension resulting in formation of a Taylor cone and a jet of charged positive droplets at the capillary tip (Figure 1.9) [94]. Evaporation of these droplets brings the charges closer together, then increasing coulombic repulsion destabilises the droplets so they disperse into smaller droplets until gas-phase ions form [99].

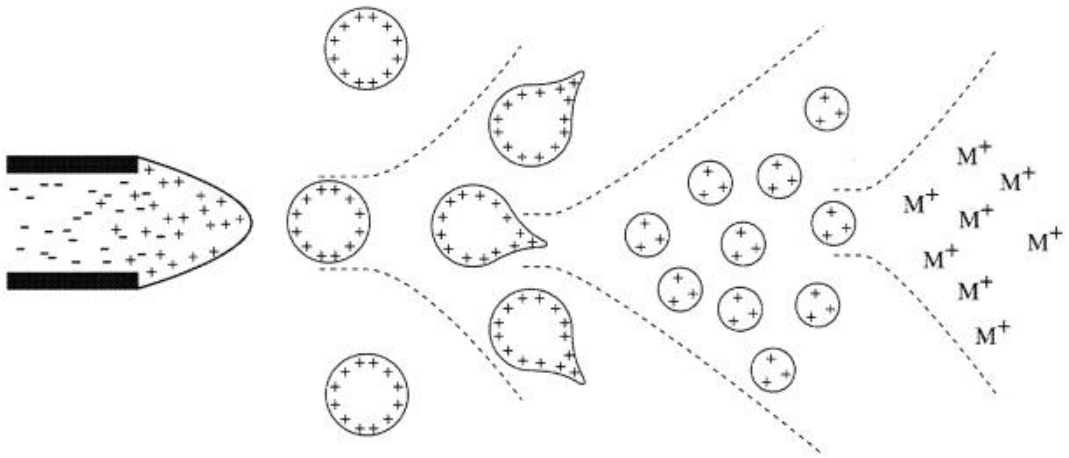

Figure 1.9 Mechanism of electrospray ionisation [100].

1.4.1.3 Fragmentation

The next step in the MS/MS process is the fragmentation of the precursor (parent) ions to form product (daughter) ions. Figure 1.10 depicts the various ion series a & x, b & y and c & z, that can be achieved through fragmentation. Fragments will only be detected if they carry at least one charge. If this charge is retained on the N terminal fragment, the ion is classed as either a, b or c. If the charge is retained on the C terminal, the ion type is either x, y or z. A subscript indicates the number of residues in the fragment. The most commonly used fragmentation is collision induced dissociation (CID). In this method, the parent ions are accelerated by an electric field to high kinetic energy and then allowed to collide with a neutral gas (helium, nitrogen or argon). This causes the fragmentation of the peptide backbone. CID largely generates a, b and y ions. In this thesis, trypsin was used to cleave C-terminal arginyl or lysyl residues of proteins [101]. Thus the predominant ion series observed is the y-ions. Fragmentation methodology can often vary depending on the type of mass analyser used. While CID can be used in most MS/MS experiments, it is useful to consider other methods when using ion trap instruments. For example, compared to traditional ion-

trap-based CID, a more recent type of fragmentation called higher-energy C-trap dissociation (HCD) provides detection of fragment ions at high resolution in the orbitrap mass analyser [102]. In HCD the ions pass through a C-trap and into the HCD cell, an added octopole collision cell, where dissociation takes place. The ions are then returned to the C-trap before injection into the orbitrap for mass analysis [103]. This form of analysis yields better data for post translational modification studies.

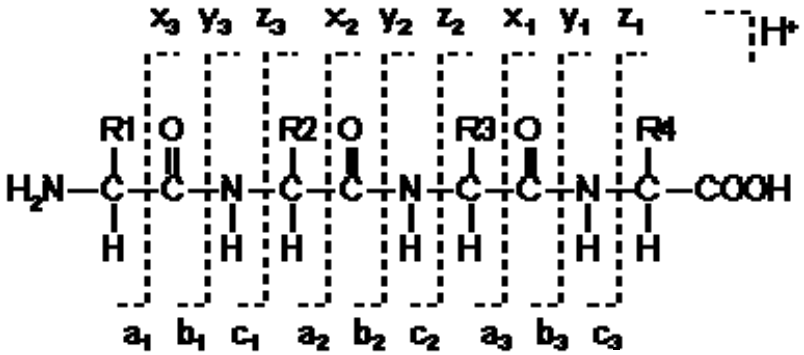

Figure 1.10 Peptide fragmentation and formation of two ion series [104].

1.4.1.4 TOF and TRAP mass analysers

Mass analysers store ions and separate them based on m/z ratios, which can be done in two ways, ion trap (TRAP) or time-of-flight (TOF). Ion trap mass analysers such as the orbitrap or ion cyclotron resonance (ICR), separate peptides based on m/z resonance, i.e., speed and distance of the cycling ion. Quadrupole TRAP setups measure m/z stability. In comparison, TOF instruments use the flight time required for the ion to reach the detector [105].

1.4.2 Phosphopeptide enrichment

Phosphopeptide enrichment uses the principle that phosphate groups in phosphorylated peptides have very low pKa values compared with other functional moieties in amino acids, so a negative charge is maintained even in an acidic environment. For efficient and selective capture of phosphorylated peptides, solid matrices with positive charges under acidic conditions are required, such as titanium dioxide (TiO_2) particles (Figure 1.11). However, the binding of non-phosphorylated peptides with multiple acidic residues, such as glutamic acid or aspartic acid, hinders the efficiency of enrichment and number of phosphopeptides identified via MS/MS [106]. Thus, TiO_2-based enrichments are improved by the use of 'non-phospho excluders' such as 2,5-dihydroxybenzoic acid, phthalic acid, and glycolic acid [107] although the physico-chemical mechanism is unclear. The adsorption of phosphate ions to TiO_2 forms a strong bidentate complex and is highly sensitive to the pH of the solution [108]. Minimal binding is seen at pH 11 where phosphopeptides are eluted from TiO_2. Lower pH values generate a gradient of binding strength enabling multiple fractionations of peptides from TiO_2 [109].

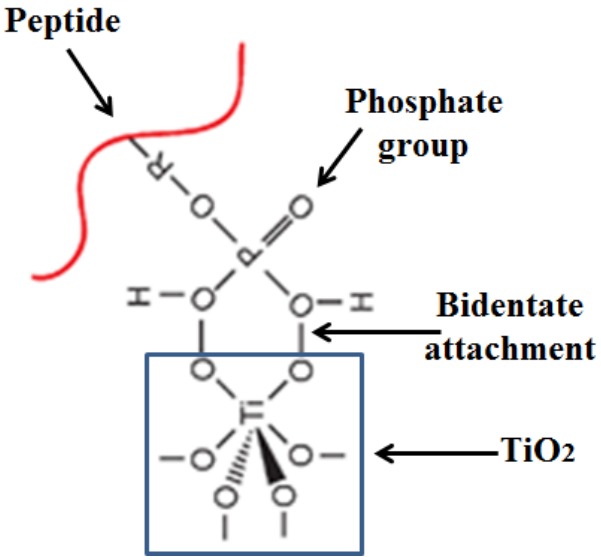

Figure 1.11 Binding of phosphorylated peptide to titanium dioxide (TiO_2). Adapted from Rogers *et al.* 2009 [110].

1.5 PRINCIPLES OF MOLECULAR TECHNIQUES

While the proteomics techniques discussed above are useful for discovery studies, molecular techniques are more useful for validation and targeted studies. Here a protein, gene or pathway of interest is selected, before experimental design. For example, when validating changes in surface antigens, flow cytometry is more useful compared to validating changes in intercellular molecular pathways, where RNA knockdown or q-PCR more suitable. Using molecular techniques to validate proteomic studies allows orthogonal analysis and greater confidence in data.

1.5.1 Immunoprecipitation and Western blotting

Both of these techniques use the affinity of antibodies (monoclonal or polyclonal) for their target proteins (antigens). Immunoprecipitation (IP) is a procedure in which an antigen is isolated by binding to a specific antibody attached to a sedimentable matrix. The source of antigen for immuno-precipitation can be unlabelled cells or tissues, radio-labelled cells, or *in vitro*-translated proteins [111]. Several type of immuno-precipitation can be achieved.

Normal IP involves using an antibody to isolate a particular protein out of a solution containing many proteins. Co-IP is immunoprecipitation of intact protein complexes using an antibody that targets a known protein (e.g., p53) that may be part of a complex of proteins. Targeting a known member of a complex may lead to the identification of new members. Chromatin immunoprecipitation (ChIP) is used to determine the location of DNA binding sites on the genome for a particular protein. DNA-binding proteins in cells can be cross-linked to the DNA which is then precipitated with the protein. ChIP is followed by DNA sequencing and PCR. This strategy can also be applied to RNA and RNA-binding proteins.

One of the major drawbacks of IP is non-specific binding of proteins to the antibody. It is important to use positive and negative controls in IP experiments with unrelated antibodies, or cell lines that that is null for target protein. Alternatively tagging the N or C terminal of the target protein and then pulling down the tag may be used to improve specificity; an example of this is the Strep-tagging of proteins described by Schmidt et al [112].

Western blots detect the relative abundance and isoforms of a protein. A complex protein mixture is separated by using 1D or 2D gel electrophoresis with transfer to polyvinylidene difluoride (PVDF) or nitrocellulose membrane, and incubation of the membrane with the antibody for the target protein. The protein is visualised and quantified using a secondary antibody coupled to an enzyme (e.g. horseradish peroxidase) that binds to the primary antibody followed by chemiluminescence using x-ray films or a scanner.

1.5.2 Quantitative PCR

qPCR or real-time PCR can measure the increase or decrease of a particular messenger RNA (mRNA) in a cell. This technique can be used to determine if an observed increase in protein is due to transcription or post- translational events. A typical analysis starts with the extraction and purification of cellular RNA. Reverse transcriptase PCR converts the RNA into single-stranded complementary DNA (cDNA). In qPCR, the amount of PCR product is measured at each heat cycle. Monitoring the reaction during exponential phase (Figure 1.12) enables determination of the initial amount of mRNA. The amount of DNA is measured after each PCR cycle using fluorescent markers (SYBER) incorporated into the PCR product. The threshold cycle (C_t) which is the cycle number at which the fluorescent signal of the reaction crosses the set threshold for change in fluorescent signal (Δ Rn) is used to calculate the initial

DNA copy number. The C_t value is inversely related to the amount of starting template (mRNA) thus the higher the C_t, the less of the target gene is transcribed. No template controls (no DNA) are used in PCR experiments to control for arbitrary products or fluorescent signals generated by the primers (Figure 1.12).

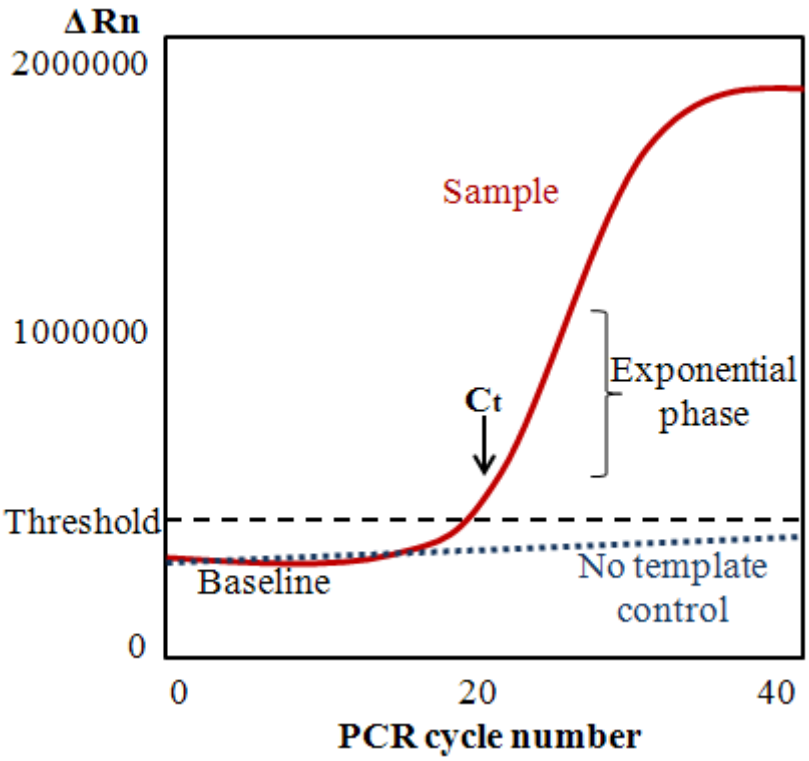

Figure 1.12 qPCR plot showing derivation of C_t and sample comparison to no template control. Δ Rn is an increment of fluorescent signal at each time point.

1.5.3 siRNA knock-down

Small interfering RNA (siRNA) knock-down uses the method of RNA Interference (RNAi), also a cell's natural mechanism of controlling gene expression. In RNAi response (e.g. after viral infection), siRNAs (21-23 nucleotides long) are snipped from longer dsRNA chains by an enzyme called Dicer. The anti-sense strand of the siRNA is used by an RNA-induced

silencing complex (RISC) to guide mRNA cleavage, so promoting mRNA degradation [113]. In RNAi-based knock-down, a double-stranded siRNA molecule is engineered to precisely match the protein-encoding nucleotide sequence of the target mRNA to be silenced. This engineered siRNA is then transfected into the cells by lipid based (Lipofectamine) fusion with the cell membrane, or by electroporation, forming pores in the cell membrane. After entering the cell, the siRNA uses this RNAi pathway. It associates with RISC and directs it to the target mRNA. The siRNA-associated RISC binds to the target mRNA through a base-pairing interaction and degrades it. Suppression of gene expression by RNAi is generally transient [114].

1.5.4 Flow cytometry

Flow cytometry uses the principles of light scattering, and excitation and emission of fluorochromes to measure the abundance of a particular cellular protein. Fluorescently labelled cells are hydro-dynamically focused in a sheath of fluid before excitation by a light source (laser). The emitted fluorescent light is detected at a longer wavelength and recorded. Flow cytometry is able to measure each cell individually. Detectors are aimed at the point where the narrow stream of cells passes through the light beam; the forward scatter (FSC) is in line with the light beam. The perpendicular detectors quantify side scatter (SSC), and fluorescence (Figure 1.13). FSC correlates with the cell size and SSC with granularity or internal complexity of the cell. Each cell passing through the beam scatters the light, and fluorescent antibodies attached to the cells may be excited to emit light at a longer wavelength. A fluorescent dye, conjugated to a monoclonal antibody, is used to determine the expression levels of surface CD antigens on each cell.

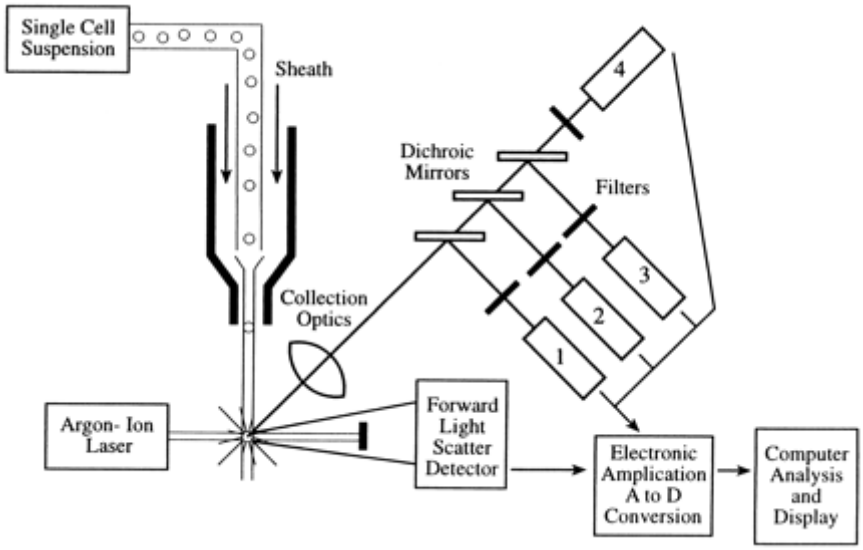

Figure 1.13 Schematic setup and components of a typical flow cytometer. A single cell suspension is hydro-dynamically focused with sheath fluid to intersect an argon-ion laser. Signals are collected by a forward angle light scatter detector, a side-scatter detector (1), and multiple fluorescence emission detectors (2–4). The signals are amplified and digitised for analysis and display on a computer [115].

1.6 AIMS

I. Elucidate the roles of the p53, p63 and p73 in the response of B-lymphoid cells to 2-FaraA. Using 1D and 2D Western blot analyses, look at changes in protein abundance and sub-cellular distribution in the human B-lymphoid cell lines Raji, IM9, MEC1 and U266 following treatment with the 2-FaraA. q-PCR will be used to measure mRNA levels for p53, p63 and p73 in all four cell lines. Similar experiments will be performed with clinical samples of CLL, to see if there is translation from the results with cell lines.

II. Qualitative study of p53 binding partners (interactome) using immuno-precipitation and mass spectrometry. This aim is in two parts (1) the study of the p53 interactome in the cell lines (Raji, IM9 and MEC1) with varying p53 mutational status. (2) the effects of 2-FaraA on the p53 interactome in the responsive (Raji and IM9) cell lines.

III. Quantitative study of protein phosphorylation in the p53 interactome using immuno-precipitation, isotopic labelling and mass spectrometry. p53 phosphorylation is a key event in the induction of apoptosis in B-lymphoid cancers. Phospho-proteomics will be utilised to assign increases or decreases in protein phosphorylation to identify phosphorylation cascades essential for the p53 network in response to 2-FaraA.

IV. Quantitative study of the effects of p53 siRNA knock-down on 2-FaraA treatment in Raji and IM9 cell lines, using isobaric labelling and mass spectrometry. Cancers that have mutant or null p53 are often resistant to DNA-damaging agents. Elucidation of the cellular response to 2-FaraA in Raji and IM9 cells with and without p53 may reveal p53-independent apoptotic pathways and/or mechanisms of chemo-resistance in B-lymphoid cancers.

CHAPTER TWO

Materials and Methods

2.1 CELL CULTURE SYSTEMS AND ASSAYS

2.1.1 Materials

The B-lymphoid cell lines Raji, IM9, MEC1 and U266 were obtained from the Deutsche Sammlung von Mikroorganismen und Zellkulturen GmbH (DSMZ), Braunschweig, Germany, and the American Type Culture Collection (ATCC), Manassas, VA, USA.

All other materials and reagents for this Chapter are listed in Appendix I.

2.1.2 Reconstitution, culture and storage of cell lines

Frozen cells were thawed rapidly in a 37°C water bath and resuspended in 10 mL of pre-warmed (37°C) RPMI growth medium. To remove DMSO, the cells were centrifuged (300 x *g*, 5 min, room temperature, Eppendorf 5810R). The cell pellet was resuspended in fresh RPMI growth medium to a final density of 3 x 10^5 cells/ mL.

The human cell lines were cultured in RPMI 1640 medium (HEPES modification) supplemented with 10% foetal calf serum and 50 μg/mL gentamicin in 25 cm^2, 75 cm^2, 175 cm^2 culture flasks or 24-well plate format, at 37°C in a non-humidified incubator (Heraeus, Hanau, Germany). All cell culture work was performed under sterile conditions using aseptic technique in a Class II biological safety cabinet (Westinghouse Pty. Ltd., Sydney, Australia). Cultures were passaged every 2-3 days to maintain cells in the exponential growth phase (10^5–10^6 cells/mL). Fresh cells were brought up from storage in liquid nitrogen at regular intervals (every 2-3 months) to replace older cultures.

To provide a stock of a certain cell line, cells were harvested (300 x *g*, 5 min, room temperature, Eppendorf 5810R) and resuspended in RPMI growth medium to a final

concentration of 10^7 cells/ mL. An equal volume of RPMI growth medium with 20% (v/v) DMSO was added drop-wise while swirling the cell suspension, resulting in a final cell density of 5 x 10^6 cells/mL and DMSO concentration of 10%. Cryovial aliquots of 1 mL were stored in a -80°C freezer overnight and then transferred into a liquid nitrogen Dewar container for long-term storage.

2.1.3 Isolation and primary culture of mononuclear cells from CLL patients

Blood was drawn from leukaemia patients (Symbion Pathology, North Ryde, Australia) with informed consent and approval of the Human Ethics Committee of the University of Sydney (reference number 99/07/07). Peripheral blood leukocytes were isolated from blood samples by density-gradient centrifugation using Ficoll-Histopaque (Sigma-Aldrich, 800 x g, 15 min, 4 ˚C). The layer of mononuclear cells was collected and washed with PBS. The leukocyte pellet was incubated in 155 mM NH_4Cl, 10 mM $KHCO_3$ and 0.1 mM EDTA for 5 min at 4˚C to lyse residual red blood cells. Purified leukocytes were washed in PBS, resuspended in RPMI medium supplemented with 50 μg/mL gentamycin and 10% (w/v) BSA to a final concentration of 2 x 10^5 cells/ml.

2.1.4 Cell density and viability

Cell density and viability were determined using the Trypan blue exclusion method. The cell sample (50 μL) was mixed with an equal volume of 0.4% Trypan blue solution in a microcentrifuge tube and then pipetted into the chamber of a Neubauer haemocytometer. Trypan blue stains DNA, but is not able to permeate the membrane of live cells, only dead cells are stained blue within a minute of exposure to the dye [315]. The number of viable and

dead cells within five squares was counted using a Nikon TMS microscope (Nikon, Kanagawa, Japan).

The following equations were used to calculate density and viability:

Density (cells/mL) = (total cells counted/number of squares) x dilution factor x 10^4

Cell viability (%) = (Viable cell density/ Total cells (viable + non-viable)) x 100

Alternatively the Countess ^{TM} automated cell counter system was used to determine cell viability and density using the manufacturer's protocol.

2.1.5 Treatment of cells with 2-FaraA and various inhibitors

Cells were grown to a density of 5 x 10^5 cells/ml and 2-FaraA (3 μM, Sigma, St. Louis, MO, USA) was added for the indicated times. Caspase activity was blocked using the pan-caspase inhibitor Z-VAD-FMK at 100 μM as previously described [116].

2.1.6 Sulforhodamine B (SRB) assay

Cell viability was determined for drug dose-response analyses using the Sulforhodamine B (SRB) assay that measures the total biomass by staining cellular proteins with Sulforhodamine B. The increase or decrease in the number of cells (total biomass) results in a concomitant change in the amount of dye incorporated by the cells in the culture. Briefly, 3x10^4 cells were seeded per well of a 96-well plate in a final volume of 100 μl of RPMI-1640 medium with the indicated concentrations of 2-FaraA (3 μM) and/or all *trans*-retinoic acid (1 μM) at 37^{o}C for the indicated times. Cells were fixed by incubating (1 h, 4^{o}C) in 10% (w/v) trichloroacetic acid. The supernatant was removed and cells were stained for 30 min with 0.4% sulforhodamine B dye. Wells were washed with 1% acetic acid to remove excess dye and the incorporated dye was solubilised with 10 mM Tris (base). Absorbance was measured

at 565 nm. Results are expressed relative to a vehicle-treated control well and are the means (+/- standard deviation) of three independent experiments.

2.1.7 Apoptosis kit (Annexin V and 7-AAD)

The proportion of apoptosis induced by drugs was determined using the Annexin V-PE Apoptosis Detection Kit I (BD Biosciences, San Diego, CA, USA). In cells undergoing apoptosis, phosphatidylserine (PS) is translocated from the inner to outer leaflet of the plasma membrane, exposing PS to the extracellular environment. Annexin V, a Ca^{2+}-dependent phospholipid-binding protein, binds with high affinity to the PS exposed on apoptotic cells. The Annexin V is conjugated to the fluorochrome phycoerythrin (PE).

Externalization of PS on cells during early apoptosis was quantified by Annexin V-PE binding, while the loss of cell membrane integrity on dead cells was detected by binding of 7-amino-actinomycin D (7-AAD) to DNA. The combination of Annexin V-PE and 7-AAD staining allows the detection of three states within a cell population:

- viable, non-apoptotic cells (7-AAD- and Annexin V-PE-negative);
- apoptotic cells (7-AAD-negative, Annexin V-PE positive);
- dead cells (7-AAD- and Annexin V-PE-positive).

The percentages of viable cells, apoptotic cells and dead cells were determined using the following protocol provided with the Annexin V-PE Apoptosis Detection Kit I. Cells were collected by centrifugation (450 x g, 5 min, room temperature, Sorvall® RT 6000D) washed twice with PBS and resuspended at a density of 10^6 cells/mL in binding buffer (10 mM HEPES pH 7.4, 140 mM NaCl, 2.5 mM $CaCl_2$). An aliquot of the suspension (50 µL; 0.5 x

10^5 cells) was transferred to a FACS tube and incubated with 2.5 µL of Annexin V-PE and 2.5 µL of 7-AAD for 15 min at room temperature in the dark. Cells were then resuspended in 450 µL of binding buffer and analysed with a FACScan flow cytometer (BD FACSCalibur, BD Biosciences, San Diego, CA, USA) using CellQuest™ Pro software, Version 5.2 (BD Biosciences, San Diego, CA, USA). The instrument detected 10,000 cells (events) per sample. Forward scatter (FSC) and side scatter (SSC) were detected using linear amplification. Annexin V-PE and 7-AAD fluorescence detection used logarithmic amplification (FL2 = 585/42 nm and FL3 = 650 nm long pass, respectively). Percentages of viable, apoptotic and dead cells were defined by their distribution in a fluorescence Annexin/7-AAD dot plot. Unstained cells, cells stained only with Annexin V-PE and cells stained only with 7-AAD were used as controls to set up laser compensation and fluorescence for the Annexin/7-AAD dot plot.

2.1.8 MTT Assay

Cell viability was determined for drug dose-response analyses using the 3-(4,5-dimethyl-2-thiazolyl)-2,5-diphenyl-2H-tetrazolium bromide (MTT) assay, where viable cells convert the yellow MTT reagent into blue formazan crystals.

Manufacturer's instructions were followed, briefly, $1x10^5$ cells were seeded per well of a 96-well plate in a final volume of 200 µl of RPMI-1640 medium with the indicated concentration of 2-FaraA at 37^oC for 48 h. For the final 4 h, 0.5 mg/ml MTT reagent was added. Cells were then spun down in the plate, the supernatant removed and the blue formazan crystals solubilised with 100 µl of dimethyl sulfoxide (DMSO). Absorbance was measured at 540 nm. Results are expressed relative to a vehicle-treated control well and are

the means (+/- standard deviation) of three independent experiments. IC_{50} calculations were performed using the BioDataFit software (http://www.changbioscience.com/stat/ec50.html).

2.1.9 Cell cycle analysis

Control and drug-treated cells were fixed and permeabilised in ice-cold 70% ethanol for 2 h at 20 °C. Cells were then pelleted (300 × *g*, 5 min, 4 °C) and stained in a solution containing 50 μg/mL propidium iodide, 0.1 mg/mL RNase A and 0.1% Triton-X-100 for 30 min at room temperature. The DNA content of the cells was analysed by flow cytometry (FACSCalibur, Becton Dickinson, Franklin Lakes, NJ) and the proportion of cells in each phase of the cell cycle was calculated using ModFit software (Verity Software House, Topsham, ME).

2.1.10 Intercellular staining for flow cytometry

Following treatment, cells were fixed in 1% paraformaldehyde for 30 min at 4C, centrifuged at 1400 rpm, washed in a PBS buffer containing 0.5% BSA, 0.1% saponin and 0.05% triton-X100 before being resuspended overnight in 100% methanol. Prior to staining, the cells were washed in the PBS/BSA buffer and incubated for 1 hour at room temperature with antibodies to either p21 or p27 (R&D Systems) at a concentration of 0.5 μg / 10^6 cells. The cells were then washed in PBS and incubated with a 1/100 dilution of a goat anti-mouse FITC-conjugated antibody for 15 minutes at room temperature. Cells were further washed in PBS and the expression of p21 and p27 was assessed using a FACS Calibur (Becton Dickinson) instrument and CellQuest Pro software.

2.2 ISOLATION OF SUB-CELLULAR FRACTIONS

2.2.1 Differential centrifugation

Cells (5×10^8, $n = 3$) were collected by centrifugation (450 *g*, 5 min, room temperature), washed twice in PBS, resuspended in 5 mL of lysis buffer (10 mM HEPES, pH 7.4, 10 mM KCl, 1.5 mM $MgCl_2$, 0.5 mM PMSF, 10 mM NaF, 1 mM Na_3VO_4, 0.2% (v/v) okadaic acid, 0.05% (v/v) NP-40), incubated on ice for 5 min and lysed with 10 gentle strokes using a Dounce glass homogenizer.

The cell suspension was vortexed for 30 s and centrifuged (800× *g*, 5 min, 4 °C) to remove crude nuclei and cellular debris. The supernatant was centrifuged (15,000× *g*, 30 min, 4 °C) to isolate crude mitochondria, followed by centrifugation (100,000× *g*, 60 min, 4 °C) to isolate the cytosolic proteome as the supernatant depleted of the microsomal fraction. Crude mitochondria were further purified by centrifugation on a two-step sucrose gradient. Mitochondria were resuspended in 5 mL isotonic buffer (10 mM Tris-HCl, pH 7.4, 0.25 M sucrose, 1 mM EDTA) and layered onto a 1.0/1.5 M sucrose step gradient (14 mL of 10 mM Tris-HCl, pH 7.4, 1.0 M sucrose, 1 mM EDTA over 20 mL of 10 mM Tris-HCl, pH 7.4, 1.5 M sucrose, 1 mM EDTA) and centrifuged with the brake off (87,000× *g*, 2 h, 4 °C).

The mitochondrial fraction sedimented at the 1.0/1.5 M sucrose interface and was carefully collected, diluted 2-fold in 50 mM Tris-HCl, pH 7.4, 150 mM NaCl, 1 mM EDTA, 0.5 mM PMSF and centrifuged (15 000× *g*, 20 min, 4 °C) to pellet mitochondria. The crude nuclear pellet was resuspended in 0.25 M sucrose, 10 mM $MgCl_2$, 20 mM Tris−HCl pH 7.4 and 1 mM DTT. To further purify the nuclei, the suspension was layered onto a two-step sucrose gradient (1.3 M sucrose, 6.25 mM $MgCl_2$, 20 mM Tris−HCl pH 7.4, 0.5 mM DTT above 2.3 M sucrose in 2.5 mM $MgCl_2$ and 20 mM Tris−HCl, pH 7.4), then centrifuged (5000× *g*, 45 min, 4 °C). The purified nuclear pellet was carefully resuspended in 10 mM HEPES pH 7.9,

10 mM KCl, 1.5 mM $MgCl_2$, 1 mM DTT and 0.5 mM PMSF and centrifuged again (1000× *g*, 5 min, 4 °C).

2.2.2 Protein solubilisation

The nuclear and mitochondrial pellets was solubilised in a 2DE compatible buffer (5 M urea, 2 M thiourea, 2% (w/v) CHAPS, 40 mM Tris–base, 65 mM DTT, 2% (w/v) sulfobetaine 3–10, 1% (v/v) Bio-Lyte 3–10 carrier ampholytes and 0.002% (w/v) bromophenol blue). To remove DNA from extracts of whole nuclei, Benzonase (200 U/mL) was added, the extract incubated at RT for 25 min and then centrifuged (20,000×g, 10 min, 25 °C) to remove insoluble material.

2.2.3 Protein quantification using 2D-Quant Kit (GE Healthcare)

Nuclear, cytosolic and mitochondrial proteins were purified using the ReadyPrep 2-D Cleanup Kit (Bio-Rad, Hercules, and CA). Samples for a standard curve were generated using the 2 mg/mL BSA standard solution provided with the kit (protein quantity range 0–50 µg). Tubes containing the samples (5 µL) were prepared in duplicate, and 500 µL of precipitant was added to both BSA standards and the samples. All tubes were then vortexed and incubated at RT for 2 min. After adding 500 µL of co-precipitant, the tubes were vortexed briefly again, and the precipitated protein pelleted by centrifugation (14,000 rpm, 10 min, RT). Supernatants were quickly decanted, and the tubes briefly centrifuged again to bring all remaining liquid to the bottom of the tube for removal. The precipitated protein was then resuspended in 100 µL copper solution and 400 µL MQ-water, before 1 mL of a 100: 1 solution of colour reagent A: B was added to all tubes. Samples, and standards, were incubated at RT for 15 min, before the absorbance at 480 nm was read on an UVVisible

spectrophotometer (SmartSpec^{TM} 3000, Bio-Rad Pty. Ltd. Hercules, CA, USA). MQ-water was used to zero the spectrophotometer. Protein concentrations of the unknown samples were then calculated from the equation obtained by linear regression to the BSA standard curve.

2.3 GEL ELECTROPHORESIS

2.3.1 1D electrophoresis

Proteins were separated with a Bio-Rad Mini- Protean III gel electrophoresis cell using a 5% polyacrylamide stacking gel (5% (w/v) acrylamide/bis, 125 mM Tris-HCl (pH 6.8), 0.1% (w/v) SDS, 0.05% (w/v) ammonium persulfate and 0.1% (v/v) TEMED) and a 12% polyacrylamide separating gel (12% (w/v) acrylamide/bis, 375 mM Tris-HCl (pH 8.8), 0.1% (w/v) SDS, 0.05% (w/v) APS and 0.1% (v/v) TEMED). Protein samples were resuspended in SDS-PAGE loading buffer (62.5 mM Tris-HCl (pH 6.8), 10% (v/v) glycerol, 5% (v/v) 2-mercaptoethanol, 2% (w/v) SDS and 0.02% (w/v) Bromophenol blue), heated at 95°C for 15 min and cooled on ice for 2 min prior to loading onto gels. Pre-stained molecular weight markers were loaded onto the first track. Electrophoresis was carried out at 120 V for approximately 90 min in running buffer (192 mM glycine, 0.1% (w/v) SDS, 24.8 mM Tris-HCl (pH 8.3)), until the dye front had run off the gel. Following electrophoresis, the gels were fixed for 1 h, stained in CCB-G250 (17% (w/v) ammonium sulphate, 3% (v/v) phosphoric acid, 0.1% (w/v) Coomassie G-250 and 34% (v/v) methanol) and de-stained overnight, or Western blotted.

2.3.2 2D electrophoresis

Samples were transferred onto 11 cm pH 4-7 pH linear gradient IPG gel strips for overnight passive in gel-rehydration. Isoelectric focusing was carried out in an IEF focussing cell (Bio-

Rad Pty. Ltd. Hercules, CA, USA) using a five-step program (2 h at 200 V, 2 h at 1000 V, 2 h at 3000 V, 42 KVh at 5000 V and 24 h at 100 V/hold) for a total of ~ 44 KVh. After focusing, the IPG strips were treated for 10 min in equilibration solution (6 M urea, 2% (w/v) SDS, 20% (v/v) glycerol, 5 mM TBP, 2.5% (v/v) 40% acrylamide, made up in 1 X Tris/HCl Gel Buffer for 2D SDS-PAGE, pH 8.8), then transferred onto an 11 cm second dimension Criterion XT Bis-Tris Gel, 4–12% acrylamide, sealed with 0.5% (w/v) agarose in 1 X MES buffer with a trace of Bromophenol blue. Second-dimension electrophoresis was run at 180 V until the Bromophenol blue dye front ran off the gel (~ 53 min) in a Criterion cell. The gels were fixed with 10% (v/v) methanol and 7% (v/v) acetic acid for 1 h, stained with Sypro Ruby overnight and washed in 10% (v/v) methanol and 7% (v/v) acetic acid for 2 h before visualisation using a Molecular Imager®FX (Bio-Rad Pty. Ltd. Hercules, CA, USA) or blotted directly onto Immobilon-P PVDF membranes.

2.3.3 Western blotting

The proteins from the gel were transferred onto the Immobilon-P PVDF membrane using the Criterion^{TM} Blotter (Bio-Rad Pty. Ltd. Hercules, CA, USA) for 45 min at 400 mA, at 4^{o}C.They were then washed 2 times with 0.1% TSBT (25 mM Tris-HCl (pH 7.5), 150 mM sodium chloride and 0.1% (v/v) Tween-20) for 10 min. The membranes were blocked with skim milk (Skim milk powder 5% (w/v) made up in 0.1% TBST) for 1 hour at RT or overnight at 4^{o}C on a rocker. The membranes were washed again with 0.1% TSBT for 10 min and then incubated at RT with primary antibody for 1 h (overnight for phospho-specific antibodies at 4 ^{o}C) on a rocker. The wash with 0.1% TSBT was repeated and the membrane was incubated with secondary antibody for 1 h at RT. The wash with 0.1% TSBT was repeated and the membrane was placed in PBS. The membranes were visualised with

AttoPhos® (Figure 2.1) and scanned using a Molecular Imager® FX Pro Plus (Bio-Rad Pty. Ltd. Hercules, CA, USA). When required, the membranes were stripped with 1% HCl. Three biological replicates were done for each antibody at each time point.

2.3.4 Estimation of protein phosphorylation from pI values

Western blot images were analysed using Adobe Photoshop CS3 vr 10.0.1 (Adobe Systems Inc, San Jose, CA, USA). A grid was placed over the gel image indicating 0.1 changes in pH. The pI values for isoforms of the protein were read from the grid starting with the most basic spot. A search was conducted on the PhosphoSitePlus website (www.phosphosite.org) and the 'Predict pI for various phosphorylation states' option was used to estimate the degree of phosphorylation of a protein from the pI value of the spot.

2.3.5 Protein dephosphorylation

Protein de-phosphorylation was conducted using calf intestinal alkaline phosphatase (CIP) according to the manufacturer's protocol. Briefly, solubilised proteins were precipitated from samples and reconstituted at 0.1 µg protein /µl in NEBuffer. CIP was added (5 U/µg of protein) to each sample, followed by incubation at 37 ^{o}C for 60 min.

2.4 QUANTITATIVE PCR

2.4.1 RNA extraction and quantification

Cell pellets were lysed in 1 mL TRI^{TM} Reagent Solution and centrifuged (20,000 x g, 20 min, 4 ^{o}C). The supernant was collected and incubated at room temperature for 5 min (dissociation of the nucleoprotein complex). Chloroform (200 µl) was added, the sample vortexed for 30 s

and allowed to stand at room temperature for 2 min and centrifuged (20,000 x g, 20 min, 4 ^{o}C). After separation of the sample into three distinct visible phases (RNA, DNA and protein), the top aqueous phase containing the RNA was retained and 500 µl of isopropanol was added and the sample was mixed by inversion and incubated at room temperature for 5 min. The sample was centrifuged (20,000 x g, 20 min, 4 ^{o}C) to precipitate the RNA. The supernatant was removed and the RNA pellet resuspended in 80% ethanol (1 ml), vortexed briefly and centrifuged (20,000 x g for 15 min, 4 ^{o}C). The supernatant was removed and the pellet resuspended in 20 µl TE buffer (pH 7.0). Quality of RNA was assessed by formaldehyde gel electrophoresis. Quantity of RNA was measured by the Nanodrop (ND-1000; NanoDrop Technologies Inc., Wilmington, DE, USA) at280 nm.

2.4.2 RNA quality assessment using formaldehyde gels

The RNA quantity and quality in the extracts were determined by spectrophotometry (Nanodrop) and with formaldehyde–agarose gels. Gels were prepared using 1.5% agarose, 40 mM MOPS and 6.6% v/v formaldehyde. RNA samples (1 µl) were mixed with the loading buffer (40 mM MOPS buffer pH 7.0, 2.2 M formaldehyde, 15.9 M formamide, 50% glycerol, 1 mM EDTA, 0.01% bromophenol blue, and 0.5% v/v Ethidium Bromide), heated at 65^{o}C for 5 min and immediately cooled on ice. Samples were then loaded onto formaldehyde–agarose gels, and run at 80 V for 40 min. Gels were visualised using Gel doc XR software (BioRad Laboratories, Hercules, CA, USA).

2.4.3 Reverse transcription

RNA was converted into cDNA using the SuperScript® VILO™ cDNA Synthesis Kit, (Invitrogen Life Technologies, Victoria, Australia) according to the manufacturer's protocol. Briefly, a reaction mixture of 200 ng RNA, 5x VILO^{TM} Reaction Mix (4 µl), 10 x SuperScript® Enzyme Mix (2 µl) was made up to 20 µl with DEPC–treated water and incubated at 25 ^{o}C for 10 min. The reaction mixture was further incubated for 60 min at 25 ^{o}C and terminated at 85 ^{o}C for 5 min. The resultant cDNA was diluted 1:1 and 1:8.

2.4.4 Real time PCR using SYBER green

Quantitative PCR (qPCR) was carried out in a final volume of 20 µl per reaction, containing 1 µl of cDNA, 10 µl of Fast SYBER Green Master Mix, 6 µl of H_2O and 1.5 µl of forward and 1.5 µl of reverse primers. A negative control (-PCR) was prepared with H_2O substituted for the cDNA. The PCR amplification was performed in a StepOne 7500 Fast Real-time PCR system (Applied Biosystems, Mulgrave, VIC, Australia). Amplification was carried out by heating the sample to 95°C for 30 s followed by repeating cycles of 95°C for 3 s, then 60°C for 30 s for a total of 40 cycles. The comparative Cycle Threshold (Ct) method was used for relative quantification of target gene expression normalized using a housekeeping gene encoding the 18S ribosomal RNA. Data were analysed using Microsoft Office Excel 2007.

2.5 DOTSCAN ANTIBODY MICROARRAY

2.5.1 Immunophenotyping of Raji and U266 cell lines and primary CLL cells

Purified mononuclear leukocytes or B-lymphocyte cell lines were washed and resuspended at a density of 1 x 10^7cells/mL in PBS. Optimally, 300 µL of the resuspended cells was used for each assay. The DotScan microarray was moistened with PBS and any excess liquid around the nitrocellulose film was carefully wiped off with Kimwipes tissues. Cell suspensions (300 µL) were incubated on the microarray in a humidified chamber at room temperature (20^{o}C). After 15 min, unbound cells were poured off and the microarray was gently washed with PBS (2 x10 s), and placed into the Array Fixative Solution (3.7% (w/v) formaldehyde in PBS) for at least 1 h, preferably overnight, to fix the cells to the antibodies of the microarray. The Fixative Solution was washed off with PBS and the microarray was scanned using a Medsaic DotReader^{TM} (Medsaic Pty. Ltd.). Dot intensities were quantified using DotScan software (Medsaic Pty. Ltd.) using 8-bit pixel greyness scale from 1-256. The arrays have alignment dots around the border consisting of a 1:1 mixture of CD44 and CD29 antibodies performing as positive controls for cell binding as well as immunoglobulin (IgG1, IgG2a, IgG2b, IgM and sIg) antibodies were used as isotype controls. Cell binding should not occur in non-antibody-dotted regions.

2.5.2 Statistical analysis

Numerical value of binding intensity (after intra-array normalisation) for each antibody was obtained from a csv file generated by the DotScan^{TM} software (Medsaic Pty. Ltd.). The values were normalised using mean-centered normalisation. The Log of the normalised values was used to conduct student 2-tailed, equal variance t-tests in Microsoft Excel (Microsoft Corp,

Redmond, WA USA). A p-value of <0.05 was required for significant differentially abundance.

2.6 IMMUNO-PRECIPITATION

2.6.1 Antigen pulldown

Cell lysates in RIPA buffer (10 mM Na_3HPO_4, 150 mM NaCl, 2 mM EDTA, 50 mM NaF, 1% Triton X, 1% Halt Phosphatase Inhibitor Cocktail, 1% protease inhibitor cocktail) were pre-cleared with 50 µL of Dynabeads. Dynabeads (50 µL) and 15 µg anti-p53 (DO1) were incubated in PBS-Tween (0.1 M PBS, 0.5% Tween 20, pH 7.3) 4^oC for 1 h with shaking. The tubes were placed on the magnet, the supernatant removed. 5 mM BS3 was added to cross-link the antibody–Dynabead complex for 30 min at room temperature, with shaking. The reaction was quenched by addition of 1 M Tris–HCl, pH 7.5 at room temperature for 15 min, shaking. The tubes were placed on a magnet and the antibody–Dynabead complex was washed three times using 1 ml of PBS-Tween. Protein lysate (300 µg) in 1,000 µL RIPA buffer was added to the antibody–Dynabead complex. The solution was incubated O/N at 4 ^OC with shaking. The tubes were placed on a magnet and the Dynabead complex was washed 3 X using 1 ml PBS-Tween.

2.6.2 Elution of antigen from Dynabeads

2.6.2.1 GeLC-MS based analysis

SDS-PAGE loading buffer (50 µl; 62.5 mM Tris-HCl (pH 6.8), 10% (v/v) glycerol, 5% (v/v) 2-mercaptoethanol, 2% (w/v) SDS and 0.02% (w/v) Bromophenol blue) was added to the beads with the antibody-antigen complex and heated at 95°C for 5 min. The samples were cooled on ice for 2 min before collecting the supernatant for subsequent analysis by SDS-PAGE.

2.6.2.2 Shotgun-MS analysis

The Dynabeads with the antibody-antigen complex were washed once with 400 µL of ice-cold 0.1 M TEAB. The beads were resuspended in 40 µL of Reduction Buffer (0.5M TEAB, 0.05% SDS, 0.0025M TCEP) and incubated at 85 ^{o}C for 5 min and 60 ^{o}C for 30 min respectively. Cysteine blocking reagent MMTS (5mM) was added, mixed and incubated at room temperature for 10 min. Trypsin (2 µg) was added and the samples were incubated overnight at 37 ^{o}C. Supernatant was collected and lyophilised.

2.7 GELC-MS

2.7.1 Trypsin in gel digestion

Lanes to be analysed were excised from SDS-PAGE gels using a razor blade and divided into 10 ~ 1 cm slices. Each slice was then further divided into ~ 1 mm^3 pieces. Each section was washed in water and completely destained using 100 mM ammonium bicarbonate in 50% acetonitrile. A reduction step was performed by addition of 100 µl 50 mM ammonium

bicarbonate pH 8.9 and 10 µl of 10 µM TCEP at 37 °C for 30 min. The proteins were alkylated by adding 100 µl 50 mM iodoacetamide and allowed to react in the dark at 20° C for 40 min. Gel sections were first washed in water, then acetonitrile, and finally dried by SpeedVac for 30 min. Digestion was carried out using 20 µg/ml sequencing grade modified trypsin in 50 mM ammonium bicarbonate. Sufficient trypsin solution was added to swell the gel pieces, which were kept at 4° C for 45 min and then incubated at 37° C overnight. Peptides were extracted from the gel pieces by vortexing 1 min and collecting the supernatant. Samples were lyophilised and resuspended in 0.1% formic acid prior to analysis on the mass spectrometer.

2.7.2 LC-MS/MS analysis with QSTAR Elite

Samples were analysed using an Agilent 1100 HPLC system interfaced with a QSTAR Elite mass spectrometer (AB SCIEX, 181 Foster City, CA, USA). The peptides were loaded onto the C18 trap column (ZORBAX 300SB-182 C18, 300 µm × 5 mm, 5 µm, Aligent) at 10 µL/min and washed for 7 min before switching the trap column in line with the C18 separation nano-column (ZORBAX 300SB C18, 3.5 µm, 150 x 0.1 mm, Agilent). The peptides were eluted directly into the ionization source of the mass spectrometer at 0.6 µL/min with the following gradient: 0 min, 5% solvent B (0.1% (v/v) formic acid in ACN); 8 min, 5% B; 10 min, 15% B; 90 min, 30% B; 105 min, 60% B; min, 5% B; 120 min, 5% B. Solvent A (0.1% (v/v) formic acid in water). The nano-LC-ESI-MS/MS system was set for data acquisition in the positive ion mode, with a selected range of 350–1750 m/z. Peptides with +2 to +4 charge states were selected for tandem mass spectrometry, and the time of summation of MS/MS events was 2 s. The three most abundantly charged peptides above a count threshold >30 were selected for MS/MS and dynamically excluded for 30 s with (50

ppm mass tolerance). The instrument was run in information dependent acquisition (IDA) mode using Analyst QS 2.0 software (AB SCIEX Inc., Foster City, CA, USA). Automatic collision energy and MS/MS accumulation modes were used in the advanced IDA settings.

2.7.3 Data analysis using ProteinPilot

GeLC-MS data were analysed using ProteinPilot 3.0 software (AB SCIEX), which uses the Paragon□□algorithm to perform protein identification. All MS/MS spectra were searched against a combined Swiss-Prot protein database, version uni_sprot_20070123. Parameters set in ProteinPilot 3.0 included (i) sample type, Identification, (ii) cysteine alkylation, Acryalmide, (iii) digestion, trypsin allowing two missed cleavages, (iv) species, *Homo sapiens*, (v) instrument, QSTAR Elite and (vi) special factors, Gel-based ID. The following processing options were used: bias correction, background correction, biological modifications and thorough identification search. A concatenated target-decoy database search strategy was also employed to estimate the rate of false positives. Only proteins identified with at least 95% confidence and unused ProtScore of >1.3 were reported. Microsoft Excel□□was used to combine data sets and select protein ID's that appear in all replicates and have more than two unique peptides.

2.8 PHOSPHO- PEPTIDE ENRICHMENT

2.8.1 Dimethyl labelling (reductive amination)

Peptides of the p53 interactome (Section 2.6.2.2) were dissolved in 40 µL TEAB (125 mM) 5 µL formaldehyde (1% v/v) was added, and then mixed with an Eppendorf Thermomixer (Eppendorf, Hamburg, Germany) for 5 min. $NaBH_3CN$ (light; 5 µL, 100 mM) or 100 mM

$NaBD_3CN$ (heavy) was added and the tubes were mixed for 15 min. To consume the excess formaldehyde, 1 µL of NH_4OH (25% v/v) was added and the tubes were vortexed, followed by addition of 1 µL formic acid (100% v/v). The digests were lyophilised and the samples were redissolved in TiO_2 loading buffer, and light and heavy were combined prior, to phospho-peptide enrichment. Figure 2.1 shows a schematic of how the mass shift in peptides is achieved for quantification.

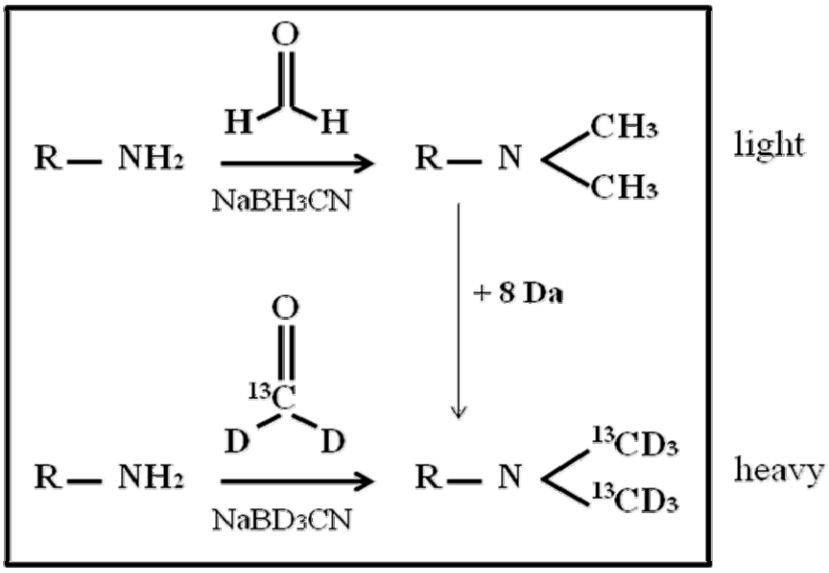

Figure 2.1 Labelling scheme of light and heavy stable isotope dimethyl labelling. Adapted from Boersema *et al*, 2008 [117].

2.8.2 TiO2 purification

Peptides were redissolved in TiO_2 loading buffer (80% ACN, 5% TFA, 1 M glycolic acid). The optimal ratio of TiO_2 beads (0.6 mg/100 µg) were added to the peptide mixture. The tubes were placed in an Eppendorf Thermomixer at 1400 rpm at room temperature for 10 min. After incubation, the sample was centrifuged briefly to pellet the beads. The solvent was removed carefully without disturbing the beads. A total of 100 µL of TiO_2 loading buffer was added to the beads, that were mixed and the contents transferred to a microcentrifuge tube.

This was centrifuged (1000 x g, 30 s, RT) to pellet the beads, and the solvent removed. The beads were washed first with 100 µL of washing buffer 1 (80% ACN, 1% TFA), mixed for 15 s, centrifuged (1000 x g, 30 s, RT) to pellet the beads, and the solvent was discarded. The beads were washed with 100 µL of washing buffer 2 (20% ACN, 0.1% TFA), mixed for 15 s, then centrifuged to pellet the beads, and the solvent was finally discarded. This final step was performed to remove peptides that bind to TiO_2 due to hydrophilic interactions. The TiO_2 beads were dried for 5 - 10 min in the vacuum centrifuge to remove all solvent. The TiO_2 beads were subsequently incubated with 100 µL of 1% NH_4OH, pH 11.3 for 10 min on a shaker. After incubation, the beads were pelleted and the supernatant was collected and acidified (0.1% formic acid) and subsequently desalted using Poros Oligo R3 RP microcolumns prior to LC–MS/MS**.**

2.8.3 LC-MS/MS analysis with VELOS Orbitrap

All of the titanium dioxide eluate or 5% of the titanium dioxide "flow through" was analysed by LC-MS/MS using a Dionex Ultimate 3000 HPLC and a Thermo Fisher Scientific Velos Orbitrap mass spectrometer. The sample was loaded onto a 300 µm inside diameter 5 mm long trap column packed with Acclaim PepMap100 C18, 5 µm, 100Å material (Dionex) at 5 ml/min and eluted through a 75 µm inside diameter 16 cm long C18 column (ReproSil-Pur 120 C18-AQ, 3 µm beads, Dr Maisch, Germany). The main part of the gradient was from 0% eluent B (90% acetonitrile, 0.1% formic acid and 9.9% water) to 40% eluent B in 105 min, to 65% eluent B in 10 min and to 100% eluent B in 3 min and held at 100% eluent B for 5 minutes. The outlet of the column was connected to a 10 µm i.d. uncoated SilicaTip (New Objective, USA) to electrospray the eluent into the mass spectrometer with 2.2 kV applied.

Other parameters were as follows: capillary temperature was 275 °C, the S-Lens radiofrequency level was 69%, peptide detection was between m/z 350-2000 at 60,000 resolution in the orbitrap, the top 8 peptides above 5,000 counts were selected for fragmentation, fragment ion detection was at 7,500 resolution in the orbitrap, predict ion injection time was enabled, charge state rejection was enabled (+1 rejected, >+4 not rejected), chromatography mode was enabled (expected FWHM = 14 s), dynamic exclusion was enabled (exclusion duration was 40 seconds), the FT first mass value was m/z 110, the isolation width was 2, the activations time was 0.1 ms and the normalized collision energy was set to 45.

2.8.4 Data analysis using Max Quant

The LC–MS/MS data were analysed using MaxQuant software (version 1.3.0.5, Max Planck Institute for Biochemistry, Martinsried, Germany). The algorithms used to assign protein identification, quantification and feature detection are described by Cox and Mann (2008) [118]. Analysis was conducted as described by the software user guide. Briefly, the RAW files generated by Thermo mass spectrometer were uploaded into MaxQuant. The following parameters were set (i) variable modifications: Oxidation (M), Acetyl (Protein N-term) and Phospho (STY) (ii) Type: Standard (iii) Labels: Light (DimethLys0, DimethNter0) and Heavy (DimethLys8, DimethNter8) (iv) Enzyme: Trypsin/P allowing two missed cleavages (v) fixed modifications: Carbamidomethyl (C). A reversed sequence database was used for false discovery rate analysis and the spectra were also scanned against a contaminants database. For quantification Oxidation (M) and Phospho (STY) modifications were included and only razor and unique peptides were used. For site quantification normalised ratio mode

was used. All MS/MS spectra were searched against a Uniprot database (human.fasta.gz) downloaded from:

ftp://ftp.uniprot.org/pub/databases/uniprot/current_release/knowledgebase/proteomes/.

2.9 SIRNA KNOCKDOWN WITH LIPOFECTAMINE

2.9.1 Knockdown with Lipofectamine RNAi MAX

Three siRNA duplexes for p53 were obtained from Invitrogen. Cells were transfected with siRNA duplexes at concentrations of 200 nM using 0.18% (v/v) Lipofectamine RNAiMAX (Invitrogen, Paisley, UK), according to the manufacturer's instructions. Briefly, using the 24-well plate format the siRNA and Lipofectamine complexes were incubated in 100 µL of serum-free OptiMEM media for 15 min. 1ml of 1 x 10^4 cells grown 24 h in complete RPMI media with 10% foetal calf serum minus antibiotics were added to wells. Plates were placed on an orbital shaker and gently mixed for 10 min at room temperature. Plates were incubated at 37 °C for 24 h, prior to western blotting for knockdown.

2.9.2 ITRAQ labelling and MS analysis

Figure 2.2 shows a flowchart of the iTRAQ labelling and analysis process. Protein samples were prepared from control and 2-FaraA-treated p53 wild-type and knock-down Raji and IM9 cells. Protein digestion and peptide labelling was performed according to manufacturer's protocol (AB Sciex, Foster City, CA, USA). Briefly, 20 µg proteins from each sample were resuspended in 0.5 M TEAB pH 8.5 and 0.1 % (w/v) SDS were reduced with 50 mM tris-(2-carboxyethyl) phosphine (TCEP) for 1 h at 60^{O}C. To block cysteine residues, samples were

incubated at room temperature for 10 min in 200 mM methyl methanethiosulfonate (MMTS). Protein digestion was performed by adding trypsin at a ratio of 1:100 (trypsin: protein) and the samples were incubated (37 ^{O}C, 16 h). Samples were dried in a vacuum centrifuge Concentrator 5301 (Eppendorf, Hamburg, Germany) and then resuspended in 7 µL 1M TEAB pH 8.5. The peptide samples labelled with iTRAQ tags according to Table 2.1. Briefly, the iTRAQ reagents were solubilised with 50 µL isopropanol and 20 µL of the resulting iTRAQ mix as added to the peptide samples ensuring a final organic concentration of at least 65% (v/v). The labelling reaction was incubated at room temperature for 2 h. Labelled samples with a set of iTRAQ tags (112-119, 121) were pooled together as one sample.

Table 2.1: iTRAQ labelling plan for samples

Sample	iTRAQ label
Raji control RNA control	113
Raji control RNA 2-FaraA	114
Raji knock-down Control	115
Raji knock-down 2-FaraA	116
IM9 control RNA Control	117
IM9 control RNA 2-FaraA	118
IM9 knock-down Control	119
IM9 knock-down 2-FaraA	121

Peptide samples were purified by strong cation-exchange (SCX) chromatography using the cartridge system (ICAT Accessories). All procedures were performed according to the manufacturer's instructions. Briefly, the peptide sample (40µg) was diluted to1 mL in cation exchange buffer-load solution 1 (10 mM KH_2PO_4 in 25% (v/v) acetonitrile (ACN), pH 3.0), ensuring the sample was between pH 2.5-3.3. The cartridge was washed first with 1 mL of cation exchange buffer-load solution 2 (10 mM KH_2PO_4 in 25% (v/v) ACN/1 M KCl at pH3.0), and 2 mL cation exchange buffer-load solution 1 to remove TCEP, SDS and excess

iTRAQ reagents. The peptides were eluted with 500 µL of cation exchanged buffer-eluate (10 mM KH_2PO_4in 25% (v/v) ACN/350 mM KCl, pH 3.0).

Eluted peptides were desalted and concentrated by hydrophilic-lipophilic-balanced (HLB) cartridges as per instructions. Briefly, the cartridge was conditioned with 1 mL 100% (v/v) methanol, followed by 100% (v/v) ACN and then 5% (v/v) ACN with 0.1% (v/v) formic acid. Before the sample load, the sample was diluted 5 times with 0.1% formic acid in water, then loaded and washed twice with 2 mL 5% (v/v) ACN with 0.1% (v/v) formic acid. The sample was eluted with 0.5 mL 50% ACN with 0.1% (v/v) formic acid, followed by 0.3 mL of 100% (v/v) ACN with 0.1% (v/v) formic acid.

The MS/MS analysis was carried out as described in section 2.7.2. In addition, a modified Enhance All mode Q2 transition setting was used, favouring low mass ions, therefore the iTRAQ reporter ions (113-119, 121) intensities were enhanced for quantification. Data analysis was conducted using ProteinPilot 3.0 software as described in section 2.7.3. Alternative parameters for iTRAQ analysis include (i) sample type: iTRAQ 8-Plex, (ii) cysteine alkylation, MMTS, (iii) digestion: trypsin, (iv) instrument: QSTAR ESI, (v) special factors: urea denaturation and (vi) species: *Homo sapiens*. The processing options were as following: quantitative, bias correction, background correction, biological modifications and thorough identification search. Relative peptide abundances were determined using the MS/MS scans of iTRAQ labelled peptides, where the ratios of peak areas of the iTRAQ reported ions reflect the relative abundances of peptides and hence the up-or down-regulation of the proteins associated with these peptides in different samples.

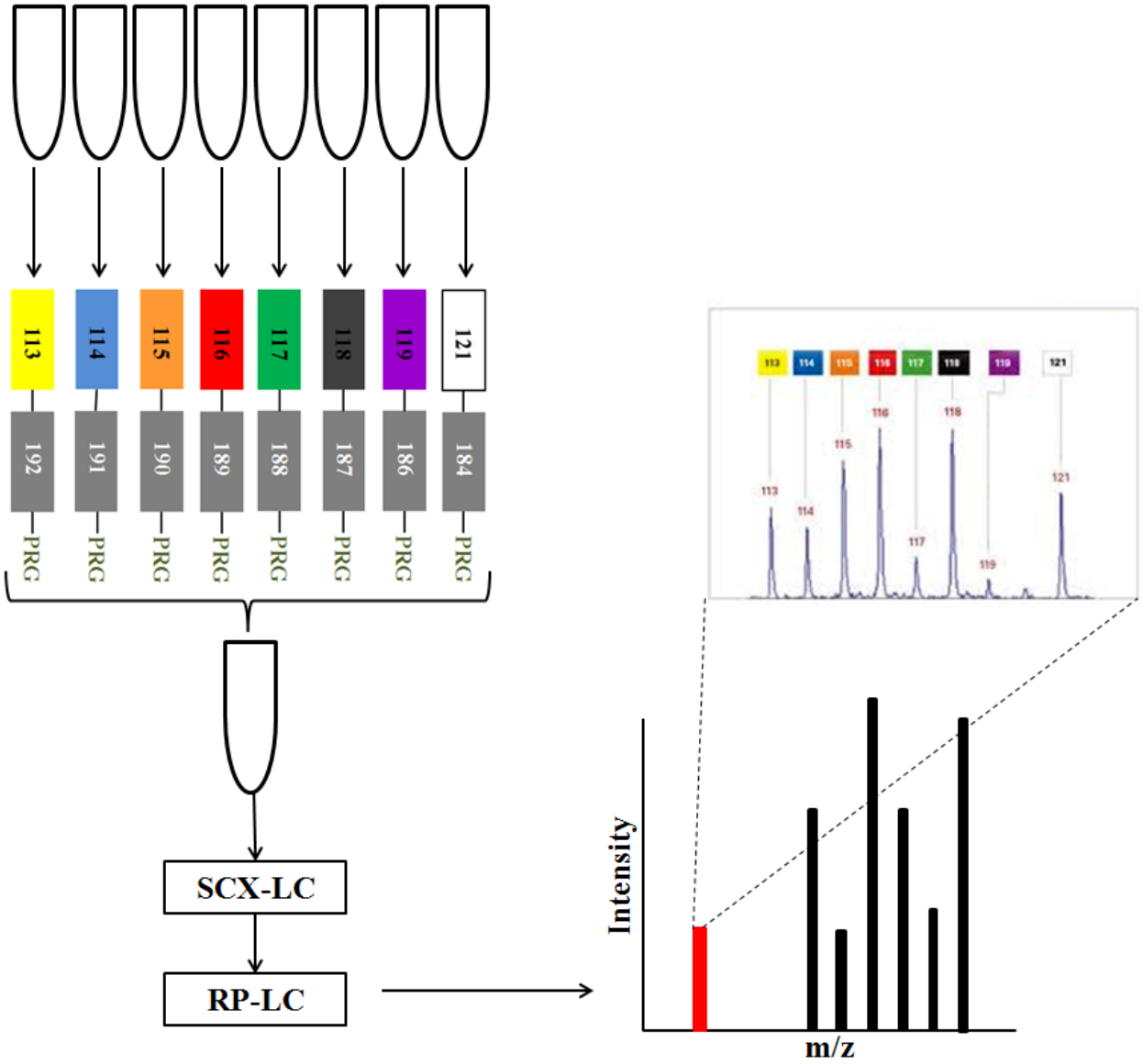

Figure 2.2 Flow-chart of iTRAQ labelling (8-plex) and LC-MS/MS analysis**.** Proteins were extracted from 8 samples and digested. Peptides were labelled with iTRAQ reagents and combined. The peptides were fractionated by SCX chromatography and analysed by RP-LC-MS. The fragmentation spectrum identifies the peptides and the spectrum inset shows the low-mass iTRAQ marker ions for peptide quantification

CHAPTER THREE

Fludarabine induced effects on p53 family proteins in B-lymphoid Raji, IM9, MEC1 and U266 cell lines

3.1 INTRODUCTION

DNA damage induced by 2-FaraA activates several protein kinases, including ATM, that which in turn trigger an accumulation of phosphorylated p53 and a p53-mediated gene expression response [119, 120] leading to cell cycle arrest and apoptosis. Wild-type p53 protein is short-lived and found at low levels in resting cells. In addition to its role as a transcription factor in the nucleus, p53 may also have an important pro-apoptotic role in mitochondria [121]. It is becoming increasingly apparent that p53 has multiple roles, targets and cellular locations.

The p53 family includes two other members, p63 and p73, with DNA binding domains homologous to p53. Both p63 and p73 have 2 major types of isoforms called TA and ΔN. The TAp63 and TAp73 isoforms have been described as 'p53-like', binding to DNA through p53, p63 and p73-responsive elements (RE) and activating target genes inducing cell cycle arrest and apoptosis [122]. The ΔNp63 and ΔNp73 isoforms also bind to p53RE but cannot induce transcription, thereby exerting a dominant negative effect on the activities of p53 and the TAp63 and TAp73 isoforms [123]. Despite the similarities in structure and function between p53, p63 and p73, mutations or deficiencies in p63 and p73 have not been linked with the development of spontaneous human cancers [71].

The Christopherson laboratory has previously reported that Raji cells treated with 2-FaraA (3 μM) accumulate multiple forms of nuclear, cytosolic and mitochondrial p53 with molecular weights of ~47, 43 and 40 kDa (Figure 3.1) and that the pattern of nuclear expression of p63 and p73 following treatment was similar to that of p53 [124-126].

To further elucidate the roles of the p53, p63 and p73 in the response of cells to 2-FaraA, we explored changes in their expression and sub-cellular distribution in the human B-lymphoid

cell lines Raji (Burkitt's lymphoma), IM9, MEC1 (chronic lymphocytic leukemia/prolymphocytic leukemia) and U266 (myeloma cells) following treatment with the purine analogue. This chapter aims to look at p63 and p73 isoforms in the cytosol and mitochondria of Raji cells and at the effects on mRNA levels of p53, p63 and p73 in all four cell lines. The observations with cell lines will be translated to clinical CLL samples.

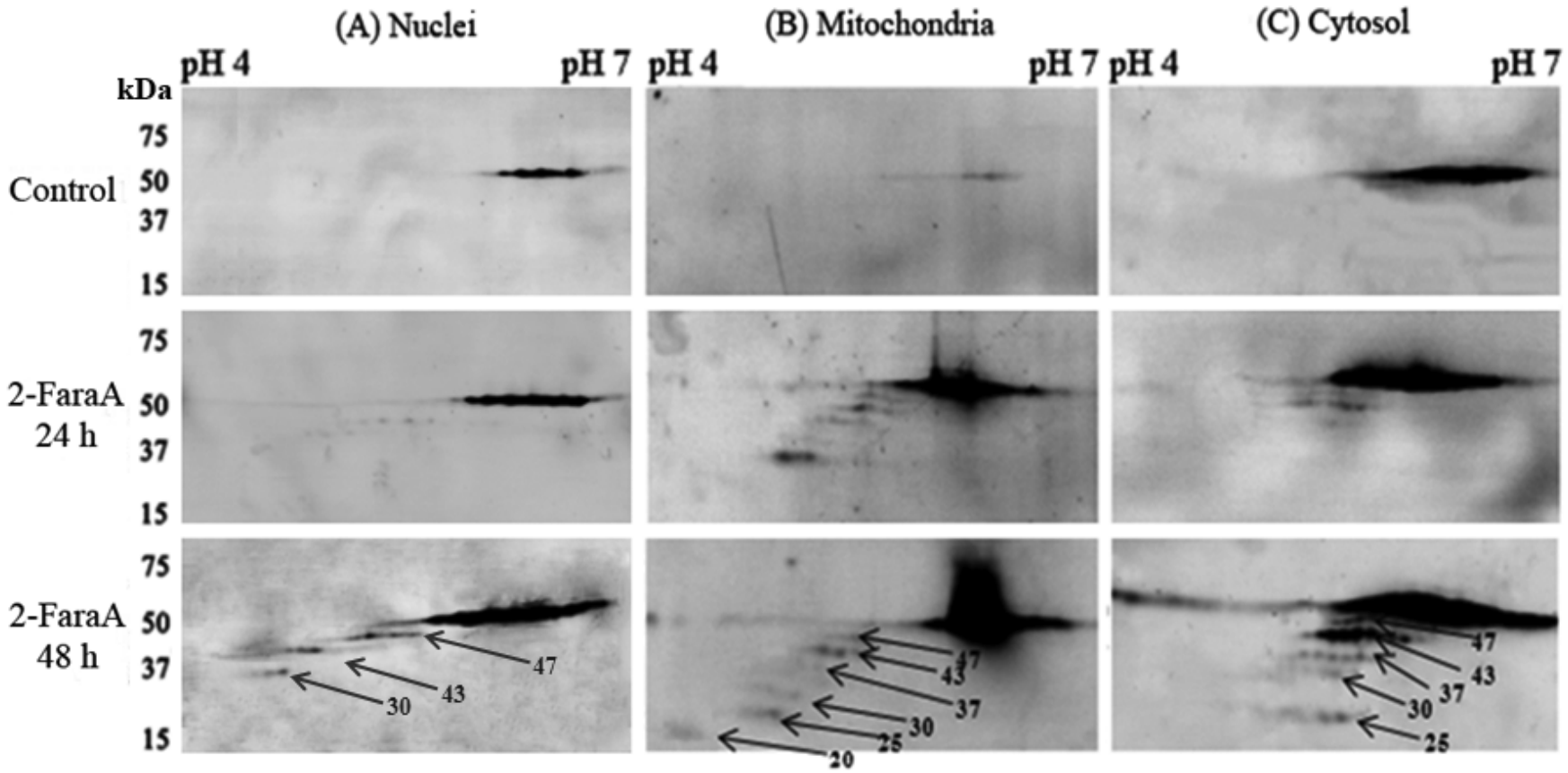

Figure 3.1 2D Western blots for p53 in sub-cellular fractions from Raji cells treated with 2-FaraA (3 µM, 24 h or 48 h). (A) nuclei, (B) mitochondria, (C) cytosol. Extracts (100 µg protein) were focused on an 11 cm pH 3-10 IPG strip and separated in the second dimension using 4-12% SDS-PAGE. Proteins were then transferred onto a PVDF membrane and Western blots were performed with the p53 antibody DO1.

3.2 METHODS

Raji, IM9, MEC1 and U266 cells were treated with 2-FaraA (3 μM for 24 h or 48 h). Cell viability was determined by MTT assay and apoptosis by flow cytometry. Nuclear, cytosolic and mitochondrial fractions were isolated as described in chapter 2. The resulting sub-cellular fractions were analysed by 1D SDS-PAGE or 2D gel electrophoresis followed by Western blotting using p53, p63, ΔNp63 and p73 specific monoclonal antibodies and actin and SDHA antibodies as loading controls. Western blots were quantified by Quantity One software. mRNA levels were quantified by reverse transcription PCR followed by Real-time quantitative PCR.

Blood samples from patients with B-CLL were collected with informed consent and under local ethical approval. All patients were diagnosed by criteria described by the international workshop on CLL (IWCLL). Peripheral blood mononuclear cells (PBMC) were isolated by Ficoll density centrifugation and stored in a viable state in FCS containing 10% DMSO in liquid nitrogen until required. All treatments were conducted in RPMI 1640 medium (HEPES modification) supplemented with 10% bovine serum albumin (BSA) and 50 μg/mL gentamicin in 24-well culture plates. Patient samples were selected based on ATM and p53 functionality, determined using the assay described by Best *et al*. [127]. Briefly, cryopreserved mononuclear cells from each case were thawed and exposed to 50 μM etoposide alone, or 50 μM etoposide plus 5 μM nutlin-3a and the expression of TP53 and p21 was detected using cell cycle analysis (section 2.1.9) and flowcytometry (section 2.1.10). Percentage increases in TP53 and p21 expression below 30 and 15% respectively defined dysfunctional cases. Those cases in which function was restored with the combination of

etoposide and nutlin-3a were classified as category 2 dysfunction, while failure to restore function was classified as category 1.

Previous studies have shown that categorisation of patient samples using this assay correlates well with the presence of mutations in the *ATM* or *TP53* genes and with the *in vitro* sensitivity of samples to 2-FaraA. Due to the limited availability of cells from each patient, sub-cellular fractionation was not possible and all experiments on patient cells were conducted on whole cell lysates.

In a pilot experiment, we also explored the effects of 2-FaraA on a CLL patient sample cultured in an *in vitro* model of the CLL tumour microenvironment. This was achieved by co-culture of the CLL cells with a feeder layer of mouse fibroblasts expressing the ligand to CD40 (referred to as CD40L cells). Viability of the CLL cells following treatment was determined by trypan blue exclusion on the Countess cell counter (Invitrogen). Changes in the immunophenotype of the CLL cells were evaluated by antibody microarray, while changes in protein expression were measured by 2D gel-based analysis.

3.3 RESULTS

3.3.1 Drug dose-responses and IC_{50} values for 2-FaraA

Figure 3.2 shows dose-response curves to 2-FaraA for the 4 human B-lymphoid cell lines, generated using the MTT assay. Results are expressed relative to vehicle-treated control cultures. As expected, the p53-wild type Raji and IM9 lines showed the greatest sensitivity to 2-FaraA following incubation for 48 h (Figure 3.2 A). Significant decreases in the number of viable Raji and IM9 cells were evident even at 1 µM 2-FaraA after 48 h. 2-FaraA (50 µM, 48 h) reduced the viability of Raji and IM9 cell cultures to <10%. In contrast, the *p53*-mutated MEC1 and U266 cell lines were relatively resistant to 2-FaraA; even following exposure to 200 µM 2-FaraA for 48 h, >50% of cells remained viable relative to controls. The IC_{50} values for 2-FaraA were as follows, Raji (2.6 µM), IM9 (11.7 µM), MEC1 (161 µM) and U266 (100 µM), calculated using the online tool BioDataFit (http://www.changbioscience.com/stat/ec50.html). Subsequent experiments exploring the effects of 2-FaraA on the expression of p53, p63 and p73 were conducted at 3 µM, as reports suggest that this represents the clinically achievable steady-state plasma level of 2-FaraA. Treatment with 2-FaraA (3 µM for 24 h) significantly decreased the viability of Raji and IM9 cells by 35 ±1.4 % and 8 ±1.4 % respectively In contrast, 3 µM 2-FaraA had no effect on the viability of either MEC1 or U266 cells (Figure 3.2B).

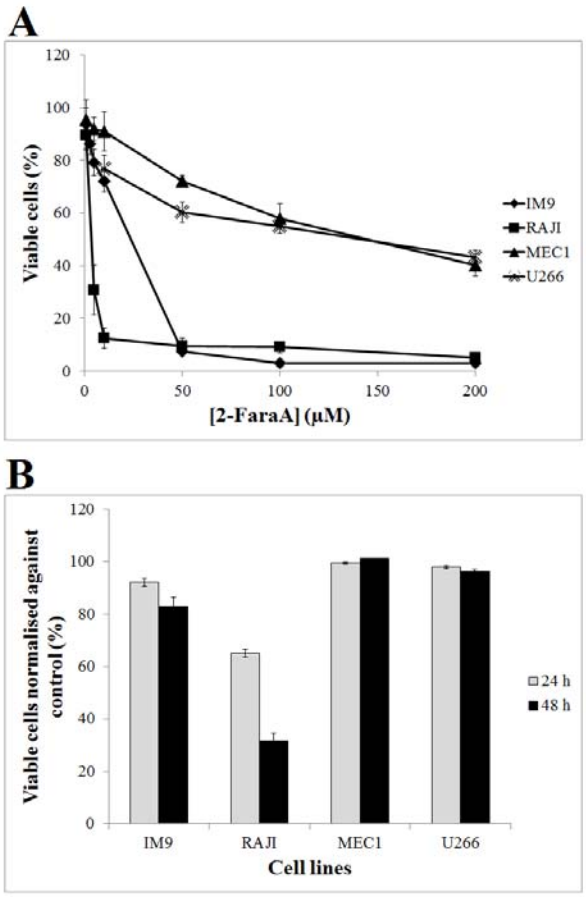

Figure 3.2 Effects of 2-FaraA on the viability of the 4 B-lymphoid cell lines. (A) Dose-response curves following 48 h with 2-FaraA, and (B) viability after 24 h or 48 h with 3 µM 2-FaraA**.** Viability was determined using the MTT assay, error bars indicate standard deviations (n=3).

3.3.2 p53, p63 and p73 sub-cellular distribution before and after 2-FaraA

Next, we examined the effect of 3 µM 2-FaraA on the expression and sub-cellular distribution of p53 (Fig 3.3.1), p63 (Fig 3.3.2) and p73 (Fig 3.3.3) in nuclear (A), mitochondrial (B) and cytosolic (C) extracts from the Raji, IM9, U266 and MEC1 cells. All results are expressed relative to expression of □-actin as a loading control.p53 protein was expressed at 53 kDa in Raji, IM9 and U266 cells and at ~47 kDa in MEC1 (Figure 3.3.1). Basal levels of p53 are higher in the Raji nucleus compared to the other cell lines and higher

in U266 and MEC1 mitochondria and cytosol. 2-FaraA induced a significant ($p < 0.05$) accumulation of p53 in the nuclear fraction of IM9 cells after 24 h, and in Raji and U266 by 48 h. In contrast, no p53 was evident in the nuclei of MEC1 cells before or after treatment (Figure 3.3.1A). In the mitochondrial fraction of Raji and IM9 cells, p53 expression was significantly ($p <0.05$) increased after 24 h 2-FaraA treatment (Figure 3.3.1B). However, no effect of 2-FaraA was apparent on the expression of p53 in the mitochondria of MEC1 or U266. Elevated levels of p53 in response to 2-FaraA in the cytosolic fraction were only observed in Raji and IM9 (Figure 3.3.1C).

p63 was detected in all 3 sub-cellular fractions of all 4 cell lines (Figure 3.3.2). In the nuclei (Fig 3.3.2 A), p63 was detected predominantly at ~120 kDa with an additional band of ~240 kDa in Raji cells. In the mitochondrial fractions, p63 was detected at 120 kDa in Raji and IM9 and at 63 kDa in MEC1 and U266. In the cytosol, p63 was found at 70 kDa in all 4 cell lines. Expression of p63 in the nuclei of Raji and IM9 cells increased significantly ($p < 0.05$) after 24 h 2-FaraA (3 μM), whereas in MEC1 and U266 cells, nuclear p63 was unchanged by the treatment (Fig 3.3.2A).

2-FaraA reduced p63 in the mitochondria of IM9 and MEC1 by 24 h. p63 levels in mitochondria were further decreased by 48 h in IM9, but returned to basal levels in MEC1. 2-FaraA had no effect on mitochondrial p63 in Raji or U266 cells. 2-FaraA reduced cytosolic p63 in IM9, but increased it in MEC1 and U266 cells. Raji cells showed no significant change in cytosolic p63 following 2-FaraA (Figure 3.3.2C). p73 was detected only in the nuclear fractions of the 4 cell lines (Figure 3.3.3 A). 2-FaraA induced an increase in nuclear p73 in all 4 lines, with the greatest increases observed in Raji and IM9. These observations are summarized in Table 3.1 below.

Table 3.1: Summary of the changes in p53 family after 2-FaraA treatment in the nuclei, mitochondria and Cytosol

	Nuclei		Mitochondria		Cytosol	
	Raji & IM9	U266 & MEC1	Raji & IM9	U266 & MEC1	Raji & IM9	U266 & MEC1
p53	↑	↑ U266	↑	-	↑	-
p63	↑	↓ MEC1	↓ IM9	↓ MEC1	↓ IM9	↑ MEC1
p73	↑	↑	-	-	-	-

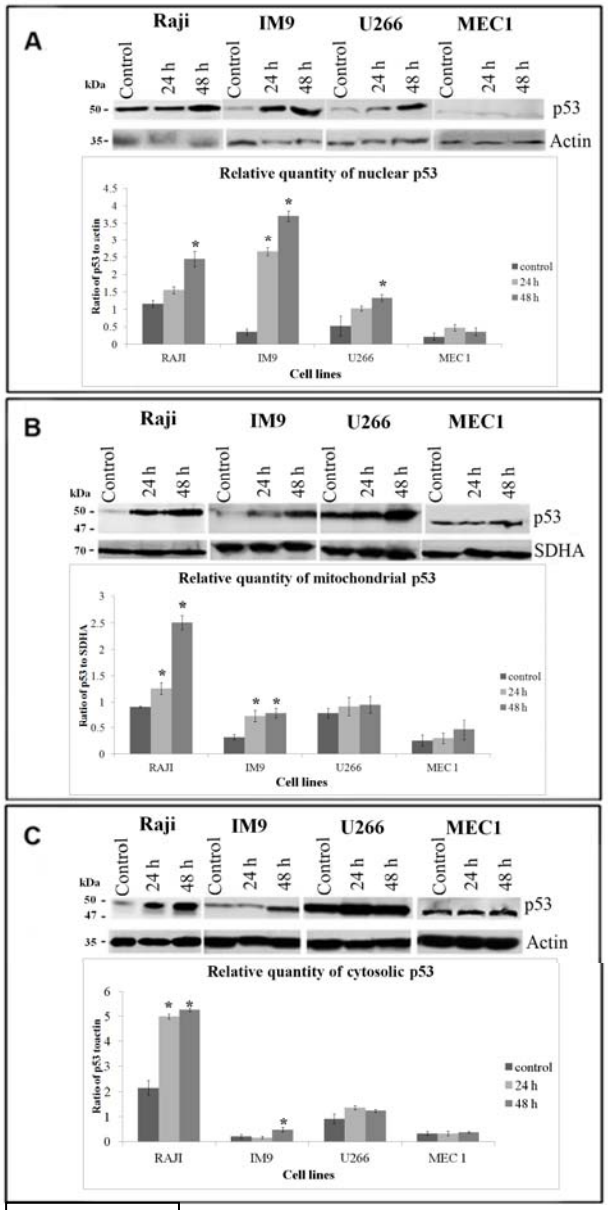

Figure 3.3

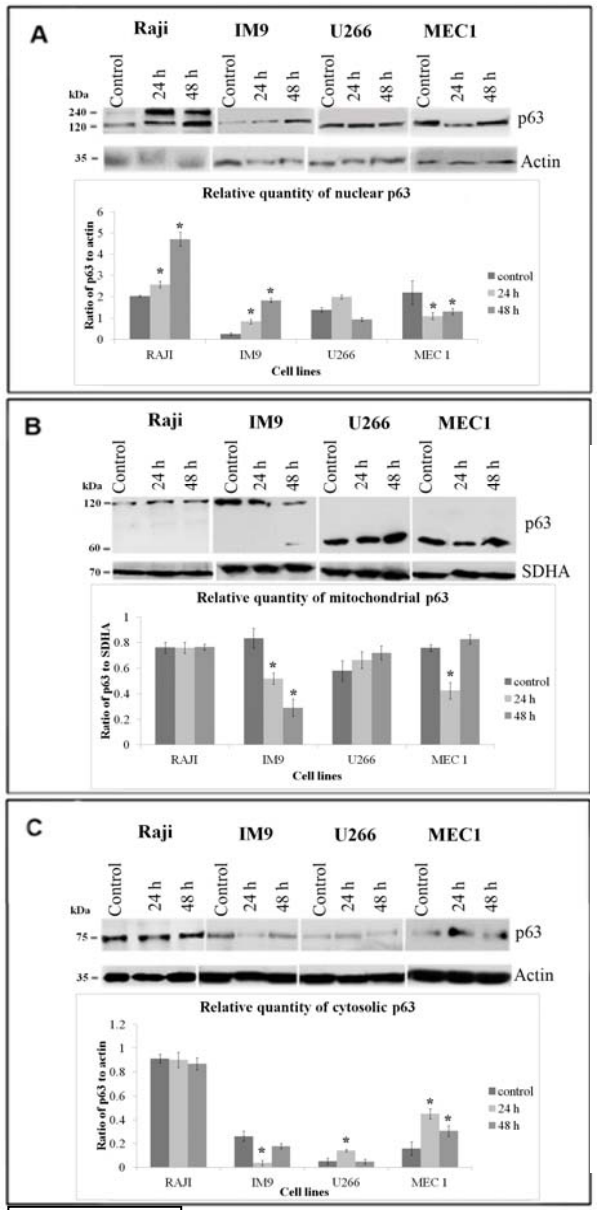

Figure 3.4

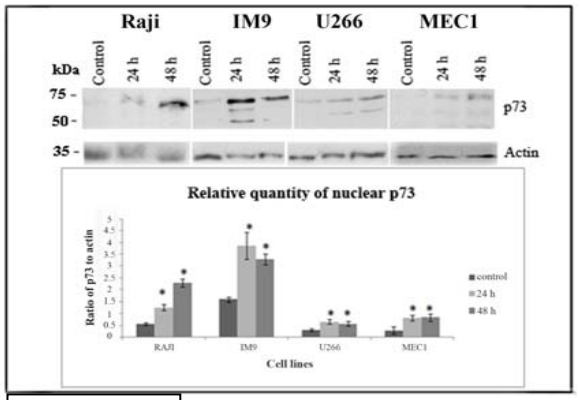

Figure 3.5

Figure 3.3-3.5 1D Western blots for p53 (**3.3**), p63 (**3.4**) and p73 **(3.5).** Panels (A) nuclear, (B) mitochondrial and (C) cytosolic fractions showing control, 2-FaraA 24 h treatment and 2-FaraA 48 h of B-lymphoid cell lines. Extracts (20 µg protein) were analysed by 1D SDS-PAGE in 12% gels and Western blots were performed for p53 (clones DO1 and Pab240). The PVDF membrane was then stripped and blotted with antibodies against actin (8 µg/mL, sc-8432 clone C-2) or succinate dehydrogenase complex subunit A (SDHA, 1 µg/mL, sc-59687 clone 2E3) as internal controls. Graphs of relative amounts of p53 in each fraction are shown. Significant changes ($p < 0.05$) are indicated by (*) relative to the control (n=3).

3.3.3 mRNA changes of p53, p63 and p73

To determine whether 2-FaraA regulates p53, p63 and p73 at the transcriptional level, we evaluated changes in the mRNA levels of the 3 proteins in the 4 cell lines following treatment. Figure 3.6 shows changes in mRNA levels for p53, p63 and p73 after 2-FaraA (3 μM, 24 h). p53 mRNA levels only increased in Raji cells (3.5-fold). In MEC1 and U266, p53 mRNA decreased 1.2-fold and 1.4-fold, respectively. No significant changes in p63 mRNA were observed for any of the cell lines. p73 mRNA increased in Raji and IM9 cells (3.8-fold and 2.5-fold, respectively), but no significant change were observed in MEC1 or U266 cells. Western blots for p53, p63 and p73 in whole cell lysates are provided in the APPENDIX II (Supplementary Figure SF3.1) for comparison of levels of mRNAs with proteins.

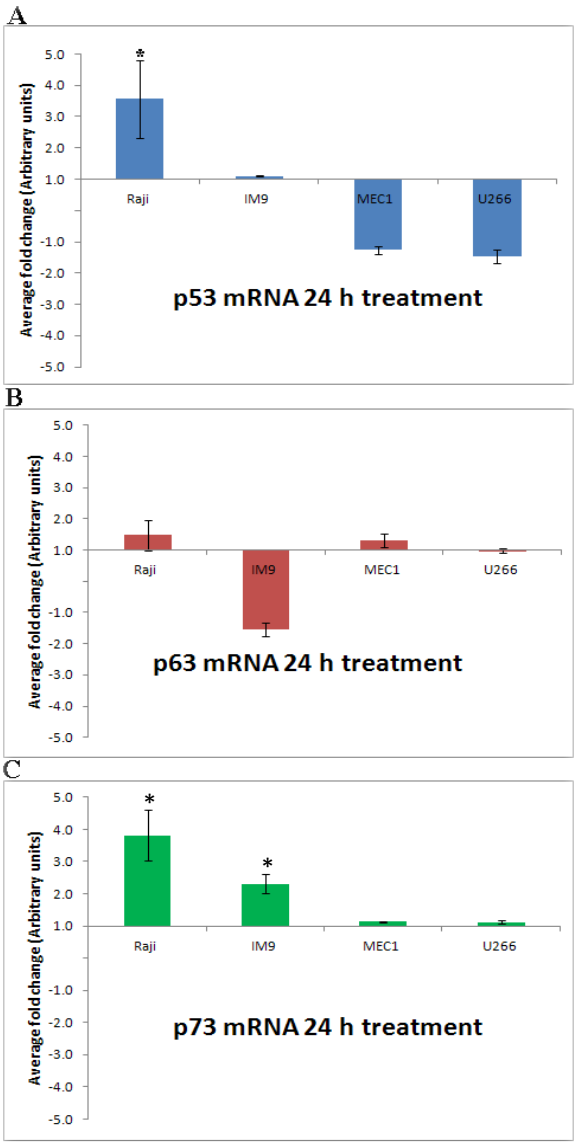

Figure 3.6 Fold-changes in mRNA levels in the 4 B-lymphoid cell lines after treatment with 2-FaraA (3 µM, 24 h). (A) p53, (B) p63, (C) p73, results are the means of two technical and three biological replicates. Significant changes (>2-fold) are indicated by (*).

3.3.4 Analysis of p63 isoforms and proteolytic derivatives in mitochondria and cytosol

In the Raji nuclear fraction, p63 and p73 have already been characterised [126], thus this chapter will only look at p63 in mitochondria and cytosol of Raji cells. Three isoforms of p63 at ~50 kDa were identified (pI 6.3 - 6.6) in mitochondria, (Figure 3.7B). 2-FaraA did not

affect the expression of these isoforms. In the cytosol, 3 isoforms of p63 at a higher molecular weight (~70 kDa, pI 6.2 - 6.4) were identified, and were again unaffected by 2-FaraA treatment (Figure 3.7C).

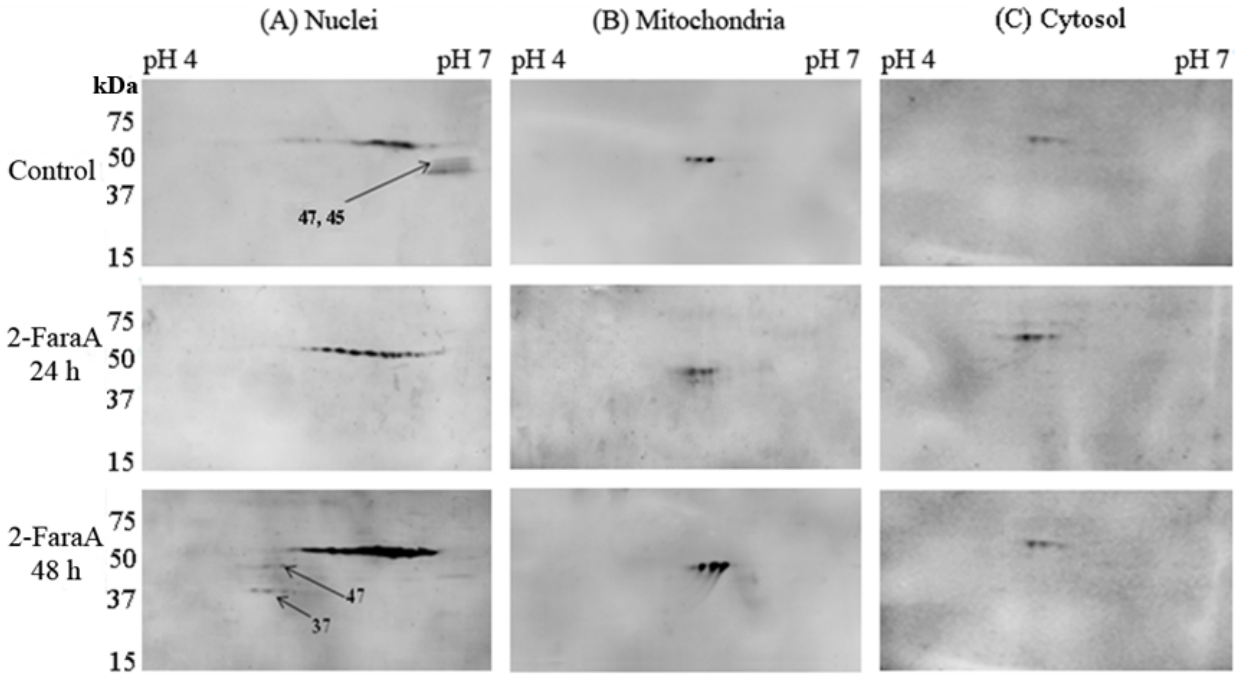

Figure 3.7 2D Western blots for p63 in sub-cellular fractions from Raji cells before and after treatment with 2-FaraA (3 μM, 24 h or 48 h). (A) nuclei (B) mitochondria (C) cytosol. Western blots were performed with the p63 antibody 4A4.

3.3.5 Translation of analysis to clinical CLL samples

Next, the levels of p53, p63 and p73 following 2-FaraA treatment was evaluated in CLL patient samples. Samples were selected on the basis of p53 functionality; 5 patients (1 to 5) were deemed to have functional p53 and 4 patients (6 to 9) to have dysfunctional p53, either as a consequence of inactivation of ATM or p53. Consistent with the functional categorisation, we observed an increase in p53 after 24 h of 2-FaraA (3 μM) in the p53 functional samples, and no change in p53 expression in the 4 p53 dysfunctional samples (Figure 3.8). In contrast, there was no distinct pattern of response for p63 and p73 that

correlated with the p53 functionality of the samples). Actin was used as internal control (Figures 3.8).

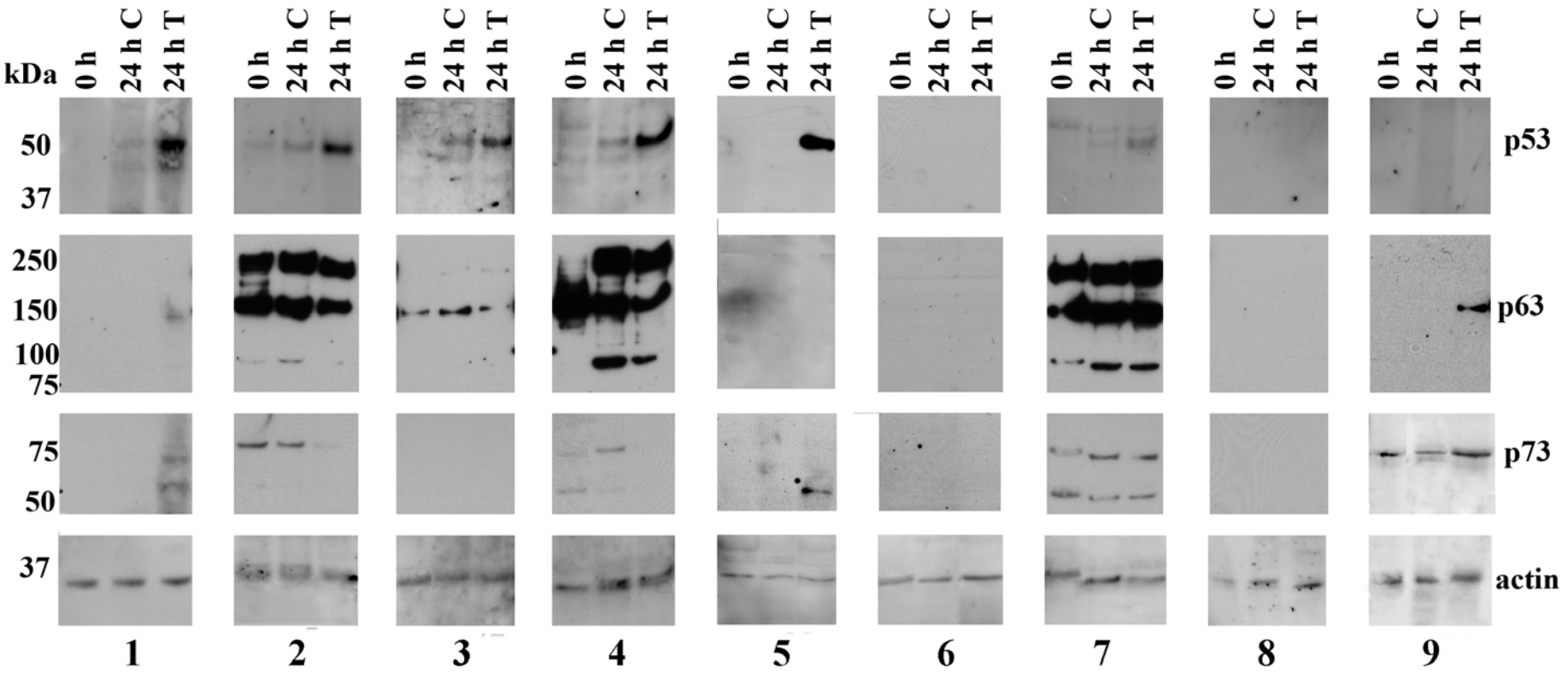

Figure 3.8 1D Western blots of p53, p63, p73 and actin of PBMC isolated from 9 CLL patient samples. Patients 1 to5 have functional p53, while 6 to 9 have dysfunctional p53. Actin is used as internal control.

3.3.6 Differential proteins that may contribute to resistance to 2-FaraA in CLL cells grown on fibroblast layer

The lymph nodes, and to a lesser extent the bone marrow, form important niche environments that support the survival and proliferation of CLL cells *in vivo*. A growing body of data highlights the importance of considering the contributions of these microenvironments in drug-effect studies. Several models of the CLL tumour microenvironment have been tested, including the method employed in this pilot study, that which involves the co-culture of CLL cells with a mouse fibroblast cell line expressing the ligand to CD40[128]

One patient CLL sample (Pt 10) was grown either in media or on a confluent layer of CD40L cells and treated with 3 μM 2-FaraA for 24 h (Table 3.2). Viability assays using trypan blue demonstrated that this dose of 2-FaraA had no effect on the growth or survival of the feeder layer. This patient deemed to be slowly progressive disease, ZAP70 and CD38+, but had responded well to treatment with fludarabine/cyclophosphamide/rituximab (FCR). These clinical and biological characteristics predict nodal and/or bone marrow involvement, making these cell forms appropriate for *in vitro* studies modelling the tumour microenvironment.

Table 3.2 details the viability of the patient cells following culture in media or on the feeder layer, with or without 2-FaraA. Following culture in media alone, 72% cells remained viable. 2-FaraA treatment of cells in media reduced the cell viability to 41% after 24 h. CLL cells cultured with the feeder layer were 95% viable in the control and 92% viable following 2-FaraA.

To investigate the effects of CD40L co-culture with the feeder layer and 2-FaraA treatment on the intracellular proteome, we used 2D gel electrophoresis and gel analysis using the PD Quest program. Four proteins were identified as up-regulated after co-culture with the feeder

layer and two were down-regulated. Due to low protein yield, it was only possible to identify the up-regulated proteins. The up-regulated proteins were Endoplasmin, Heat shock cognate 71 kDa protein, Lymphocyte-specific protein 1 and Protein SET (Figure 3.9 and Table 3.3).

Table 3.2: Cell viability of patient 10 by trypan blue staining followed by analysis with the Countess® Automated Cell Counter (Life Technologies)

Conditions	Viability after 24 h (%)
Control media	72
Test media	41
Control feeder	95
Test feeder	92

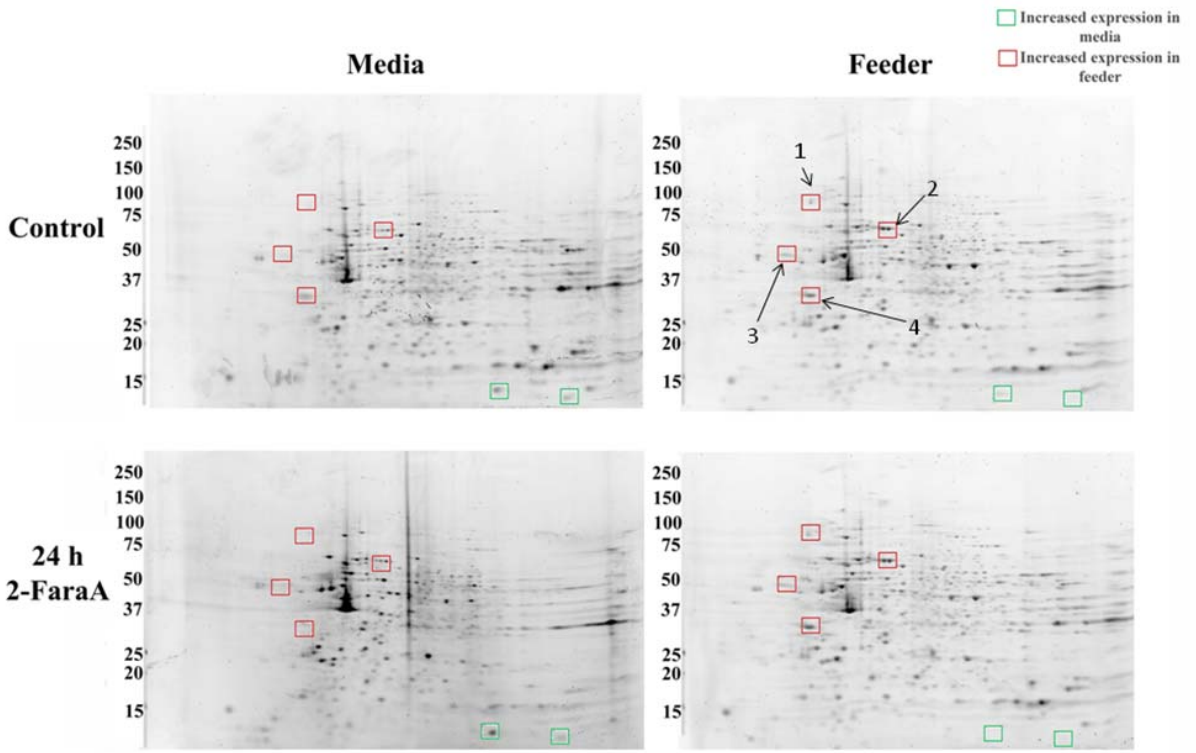

Figure 3.9 2D gel analysis of proteins up-regulated by co-culture with feeder CD40L cells.

Table 3.3: Identification of intracellular proteins up-regulated by CD40L co-culture in patient 10 by ESI-MS/MS

Spot number	Accession number	Protein	Gene	Mowse score	Unique peptide
1	P14625	Endoplasmin	HSP90B1	601	22
2	P11142	Heat shock cognate 71 kDa protein	HSPA8	270	7
3	P33241	Lymphocyte-specific protein 1	LSP1	169	7
4	Q01105	Protein SET	SET	124	4

3.3.7 Differential abundant surface antigens on primary CLL cell grown in medium and on a feeder layer treated with 2-FaraA

Results from section 3.3.6 established that growth on a feeder layer of fibroblasts alters the biochemistry of patient cells. We further investigated the effects of the feeder layer on CLL cells by profiling surface antigens using DotScan antibody microarrays in 4 patients (10, 11, 12 and 13). To determine statistical significance, the logarithm of the normalised raw vale was used for t-tests, tails (2, 2). A p-value of <0.05 and raw intensity values > 10 were considered differential. Table 3.4 summarises the antigens regulated under the various growth and treatment conditions. Comparing growth of cells in normal medium with growth on feeder layer, the antigens up-regulated with the feeder layer were CD23, CD54, CD80, CD262, CD264 and CD319. Antigens down-regulated were CD6, CD27, CD43, CD45, CD47, CD50, CD53 and CD185.

The surface profiles of cells growing in media compared with a feeder layer were treated with 3 μM 2-FaraA (24 h). In media 2-FaraA up-regulates CD24, CD262 and CD264, while CD39 was down-regulated. Treatment of cells on a feeder layer resulted in up-regulation of CD45 and CD222.

Table 3.4: Differentially abundant CD antigens on CLL cells from patients 10, 11, 12 and 13 levels on cell in growth media were compared with those on a feeder layer before and after 2-FaraA.

Antigen	B-cell Marker	Ratio	P-value	Function
Ratio in feeder layer compared to medium				
CD6	Yes	0.37	1.91E-03	Regulation of apoptosis in lymphocytes
CD23	Yes	2.53	3.39E-03	Roles in inflammation by release of TNF, IL-1, IL-6
CD27PH	No	0.27	4.23E-04	Activates NF-κB, SAPK, JNK kinases
CD43	No	0.21	1.61E-05	Promotes T-cell activation, proliferation, inducing IL-2
CD45	No	0.32	5.09E-04	Intrinsic cytoplasmic protein tyrosine phosphatase activity
CD47	No	0.55	2.03E-02	Mediate caspase independent cell death
CD50	Yes	0.50	1.63E-02	Primary immune response
CD53	No	0.39	6.92E-05	Decreased expression is found in activated and migrating leukocytes
CD54	No	4.18	7.33E-05	Inflammatory signalling
CD80	No	4.68	2.82E-03	Binding to CD28 on T cells for activation, or CD152 for T cell inhibition
CD185	No	0.51	8.96E-03	Migration & localisation of B-cells to primary and secondary follicles in lymphoid tissue
CD262	No	6.07	9.47E-06	Induced by p53, role in Caspase-8 related cell death

CD264	No	4.99	3.60E-02	Decoy receptor by competing for binding with other TRAIL receptors and inhibiting TRAIL induce apoptosis
CD319	Yes	8.01	7.50E-07	Expressed by activated b-cells, NK cell-mediated cytotoxity
Ratio for cells in medium after and before 2-FaraA				
CD24	No	2.78	4.19E-02	B-cell differentiation, adhesion and metastatic tumours
CD39	No	0.70	4.55E-02	Hydrolyses ATP and ADP which inhibits inflammatory response
CD262	No	2.52	3.25E-03	Induced by p53, role in Caspase-8 related cell death
CD264	No	1.80	8.67E-03	Decoy receptor by competing for binding with other TRAIL receptors and inhibiting TRAIL induce apoptosis
Ratio for cells on feeder layer after and before 2-FaraA				
CD45	Additional	1.81	2.61E-02	Intrinsic cytoplasmic protein tyrosine phosphatase activity
CD222	Other	2.87	4.54E-02	Internalizes a variety of extracellular ligands and directs them to lysosyme and sorts M6P-containing lysosomal enzymes

.

3.4 DISCUSSION

3.4.1 The p53 family response to 2-FaraA

Henrich and Christopherson (2008) showed that p53 accumulates in the nuclei of Raji cells treated with 2-FaraA (3 μM, 24 h) and that this accumulation preceded the onset of apoptosis. In the present study, we have extended these observations to the effects on cytosolic and mitochondrial p53 levels and to other members of the p53 family, namely p63 and p73, in 4 human B-lymphoid cell lines selected to represent cells with both wild-type and mutant *p53*, and sensitive or resistant to 2-FaraA. In response to a clinically relevant dose of 2-FaraA (3 μM), p53 accumulates in the mitochondria and nuclei of Raji and IM9 cells before apoptosis is apparent. In Raji cells, p53 accumulates in mitochondria earlier (24 h) than in nuclei (48 h), suggesting that prior to effects on transcription in nuclei, p53 may initiate apoptosis at mitochondria. p53 is known to induce apoptosis at mitochondria in response to stress signals including DNA damage and hypoxia [129, 130]. Accumulation of p53 at mitochondria occurs during p53-dependent apoptosis, but not during p53-independent apoptosis or p53-mediated cell cycle arrest [129]. Chipuk et al. demonstrated that p53 induces expression of Puma, that in turn frees cytoplasmic p53 from inhibitory interactions with the anti-apoptotic protein Bcl-xL. The 'free' p53 then induces homo-oligomerisation of Bax to form a pore in the mitochondrial outer membrane, resulting in apoptosis [131].

Our study suggests that translocation of p53 to nuclei may depend on the type of *p53* mutation. In MEC1 cells, the mutation has been reported to result in a protein with a truncated N-terminus [132], consistent with our observations of a lower molecular weight protein of ~47 kDa (Figure 3.3). The *p53* gene in U266 cells is reported to harbour a point mutation that does not affect its translocation to nuclei, but may prevent induction of genes

required for apoptosis. Our data suggest that p53 in nuclei and mitochondria are involved in 2-FaraA-induced apoptosis. Accumulation of p53 in Raji cells induced by 2-FaraA (3 μM, 48 h) may result from an increase in p53 mRNA levels (Figure 3.6A), and likely inhibition of p53 degradation. In contrast, the increase in p53 in IM9 cells in the absence of an increase in transcript levels (Figure 3.6A, Supplementary Figure SF3.1) suggests that accumulation of p53 in this line is likely due to reduced p53 protein degradation [133].

The transcription factors, p63 and p73, have significant sequence homology to p53 and overlapping functions, but are rarely mutated in cancers [122]. Recent studies indicate that the functions of these p53 family members depend on the status of all 3 proteins. For example, Flores et al. demonstrated that loss of p63 and p73 results in the failure of mouse E1A embryonic fibroblasts with functional p53 to undergo apoptosis in response to DNA damage [134]. In the present study, nuclear p63 was detected at higher than expected molecular weights of ~120 and 240 kDa (Figure 3.4A). Similarly in the mitochondrial fractions of Raji and IM9 cells, p63 was detected at ~120 kDa. This may be explained by the formation of dimers and tetramers of p63 complexed with DNA in the nuclear and mitochondrial fractions, but not in the cytosol. This hypothesis is further supported by the 2D western blot analysis of p63 in Raji cells. The 2DE compatible buffer (Section 2.2.2) contains benzonase which is breaks down DNA and RNA in the sample, and the higher molecular weight p63 can no longer be detected. Previous studies with nuclear extracts of HeLa cells have shown strong binding of homodimers of the thyroid hormone receptor alpha (TRα) to DNA in Western blots [135]. The high molecular weight forms of p63 were only found at the mitochondria of the 2-FaraA-responsive Raji and IM9 cells, and not the resistant MEC1 or U266 lines. These p63 complexes could contribute to the mechanisms of the cytotoxicity of

2-FaraA. 2-FaraA-induced apoptosis in Raji and IM9 cells with accumulation of transcription-activating TAp63 in nuclei (Figure 3.4) is consistent with previous studies with lymphoma and hepatocellular carcinoma cells where TAp63 was up-regulated by chemotherapeutic agent bleomycin [136]. It is important to note that the accumulation of p63 observed here is not due to increased gene expression since we observed no increase in mRNA levels (Figure 3.6B), but may be due to decreased degradation following p63 phosphorylation.

p63 is self-inhibitory, due to a transactivation inhibitory domain (TI) at the C-terminus of the Tap63α isoform that binds the transactivation domain within the N-terminus of an adjacent p63 molecule [137]. The p63 2D western blot analysis was only extended to Raji cells as it responds best to 2-FaraA treatment (Figure 3.2) and the changes observed in Raji p63 are more likely due to post-translational modifications, than changes in protein transcription (Figures 3.4 and 3.6)..Figure 3.7 shows that 2-FaraA treatment of Raji cells primarily affects p63 in nuclei; the smaller derivatives of p63 (~47 and 45 kDa, pI 6.5 - 6.8) found in untreated cells are the same size as the N-terminal truncated p63 (ΔNp63γ) isoform (~47–53 kDa) reported by Petitjean et al. (2008) [69]. However, Western blots with an antibody specific for ΔNp63 showed that these smaller p63 derivatives were not ΔNp63 isoforms, which eliminates the possibility of mRNA splice variants. The biological significance of the ~47 and ~45 kDa derivatives of p63 at 48 h (Figure 3.7A) is not clear, but it is possible that these derivatives are the result of proteolytic cleavage of TAp63α at the C-terminus, that removes the self-inhibitory element in the TAp63 molecule resulting in a TAp63 protein with enhanced transcriptional activity [137]. The acidic nature and lower molecular weights of these isoforms are consistent with loss of basic amino acid residues from the C-terminus. The low molecular weight derivatives of p63 (Figure 3.7A) could have a role in increasing the

sensitivity of cells to apoptosis. Sayan et al. found that p63 fragments localize in nuclei [137], a finding which is consistent with our data (Figure 3.4). There are limited reports describing the expression and role of p63 in mitochondria; Gressner et al. described the ability of TAp63α to induce expression of the CD95/FAS and BAX genes [138]. However, we observed no significant change in p63 in mitochondria after 2-FaraA treatment (Figure 3.7B).

The p63 isoforms observed in the cytoplasmic and mitochondrial fractions of Raji and IM9 cells (Figures 3.7B and C) have different molecular weights to those identified in nuclei. Cytosolic p63 of ~70 kDa may correspond with the 68 kDa splice variant TAp63β reported by Petitjean et al. The isoforms of ~50 kDa that accumulated in mitochondria are similar to the ΔNp63γ isoforms of 47–53 kDa described by Petitjean et al. It is interesting to note that the dimers and tetramers of p63 seen in 1D Western blots (Figure 3.4) are not seen in 2D Western blots (Figure 3.7), suggesting that the additional isoelectric focusing step in 2D gel analysis may dissociate such complexes.

The transcription factor, p73, accumulates in nuclei of Raji and IM9 cells after 2-FaraA (Figure 3.5). However, unlike p63, this accumulation may be due to increases in the levels of mRNA for p73 in Raji (4.0-fold) and IM9 (2.5-fold, Figure 3.6C). Zhu et al. showed that MCF7 breast cancer cells treated with camptothecin express the inactive p73α isoform [139]. The molecular weight of p73 here of ~70 kDa (Figure 3.5) is consistent with p73β that is transcriptionally active and pro-apoptotic [77, 122, 140]. Levrero et al. found that p73 accumulates in response to cisplatin and taxol in human colon cancer cells [122]. The present study is the first to report changes in p73 mRNA in response to 2-FaraA.

In 9 patient CLL samples, the pattern of response to 2-FaraA was less clear. The expression of p53 correlated well with our observations in the cell lines, however the same was not true for p63 and p73 (Figure 3.8). There may be several reasons for this, the most obvious being that p63 and p73 are dispensable, unlike p53, and do not play a role in 2-FaraA-induced apoptosis in CLL cells. However, we must consider that *in vitro* culture of CLL cells in media alone does not accurately mimic the *in vivo* conditions experienced by CLL cells. CLL cells undergo spontaneous apoptosis when cultured in media in the absence of any supportive factors such as cytokines or contact with stromal cells [141]. Under these conditions the roles of p63 and p73 may be masked by spontaneous apoptotic processes.

3.4.2 2-FaraA resistance of CLL cells grown in CD40L feeder layer

Our pilot study (Table 3.2) and those of others [142] suggest these effects can be overcome by modelling the CLL tumour microenvironment *in vitro*. Co-culture of the CLL patient cells with the CD40L feeder layer increased the viability of the CLL cells by 23%, that isolation of CLL cells from the tumour microenvironment causes the cells to undergo spontaneous apoptosis and/or necrosis. While reproducing the tumour microenvironment effectively increased cell viability to 95%, this also conferred resistance to 2-FaraA. Only a 3% loss in cell viability was observed following 2-FaraA treatment on the feeder layer compared with 31% in media alone (Table 3.2). This is an interesting observation, as records indicate that the patient had responded well to chemotherapy. Thus in the original microenvironment, chemotherapy had induced apoptosis in these CLL cells. So the resistance to treatment may be an artefact of the artificial culture microenvironment. Proteomic analysis of CLL patient cells yielded some interesting results (Figure 3.9 and Table 3.2). Endoplasmin (HSP90 beta) and HSP70 are molecular chaperones that are up-regulated in aggressive cancers and are

associated with metastasis [143]. Given the wide array of proteins that are stabilised by these molecular chaperones, their up-regulation may play a role in the survival of CLL cells on the feeder layer. The Lymphocyte-specific protein 1 (LSP1) is a human leukocyte marker, with no known role in cancer [144]. Nodal involvement in CLL is a clinical indication of aggressive/progressive disease and LSP1 may promote CLL cell survival and proliferation in the tumour microenvironment.

SET is an oncoprotein that inhibits the tumour suppressor protein phosphatase 2A (PP2A). Previous studies have linked increased levels of SET with CLL stage and disease progression. Accumulation of SET increases levels of phosphorylated Akt and PTEN and this pathway can contribute to cell survival [145]. However, our data suggest a role for SET in the survival of CLL cells in an *in vitro* model of the tumour microenvironment.

It should be noted that this pilot study only used one patient. This is due to the limitations of using clinical samples. Only patient ten yielded enough mononuclear cells to undergo the microenvironment studies with antibody microarray and 2DE. Unfortunately there was not sufficient protein extracts left to validate candidate proteins using western blotting or other orthogonal techniques. If possible future studies should focus on repeating the 2DE analysis with more patients.

Surface profiling [146] of 4 CLL samples with DotScan microarrays showed differences in the immunophenotype when cultured in media alone or on a feeder layer (Table 3.4 & Supplementary Figure SF3.2). CLL is a disease of accumulation; however recent evidence indicates that proliferation occurs in lymphocytes. CLL cells respond to stimuli provided by interactions with stromal cells and T-cells within specific micro- environmental niches. These interactions promote proliferation, up-regulate apoptosis-regulatory proteins and modulate the expression of chemokines and surface molecules. Regulation of CLL cell growth in

micro-environments is linked to antigen stimulation through the B-cell (antigen) receptor (BCR) on the surface of CLL cells. Inflammation is involved in the initiation and progression of several chronic lymphoid malignancies [147]. The observations in this pilot study correlate well with the biology of CLL. Comparison of cells in medium alone with growth on a fibroblast layer shows that the artificial stroma prevents cells from undergoing apoptosis/necrosis (Table 3.2).

CD23 and CD54 are up-regulated on CLL cells on the feeder layer and have reported roles in inflammation [148], known to aid CLL progression. Activation of T-cells and induction of an immune response may limit CLL survival. We have observed down-regulation of CD43, CD45, CD50 and CD53 involved with the immune response, and up-regulation of CD80 that may result in T-cell activation (binding to CD28) or inhibition (binding to CD152), the latter may aid cell survival.

There is also differential abundance of surface antigens involved in apoptosis. Down-regulation of CD6, CD27, and CD47 may prevent the cells from undergoing programmed cell death up-regulation of CD264 would inhibits TRAIL-induced apoptosis. A combination of these factors may determine cell survival on the feeder layer. Several pro-apoptotic factors such as CD262, CD319 are up-regulated which suggests an inclination for death; however these signals may be overridden by the multiple pro-survival signals.

A comparison of the effects of 2-FaraA on cellsin medium alone showed up-regulation of CD24 that enhance DNA-damage induced apoptosis by inducing NF-κB signalling in breast cancer [149]. There is also an increase in CD262 that induces p53-dependent apoptosis in response to DNA-damage [150]. Only two differentially abundant antigens were found after treatment on a feeder layer. CD45 was up-regulated, in contrast to its down-regulation for

untreated cells grown on a feeder layer compared to medium. CD222 is also up-regulated; CD45 and CD222 do not have known roles in apoptosis.

3.5 CONCLUSIONS

The data presented in this chapter demonstrate that the 2-FaraA-sensitive cell lines, Raji and IM9, accumulate p53 in their nuclei, mitochondria and cytosol. Raji cells accumulate p53 in mitochondria earlier than in the nucleus suggesting that initiation of apoptosis in these cells is dependent on the roles of p53 at mitochondria, prior to effects on gene expression in the nucleus. In Raji, accumulation of p53 is likely a result of increased p53 protein given the increased mRNA levels, and from inhibition of p53 degradation. 2-FaraA also induces phosphorylation and accumulation of lower molecular weight derivatives of p53, p63 and p73 in the nuclei of Raji cells that may have roles in inducing apoptosis. Several molecular weight and phosphorylated forms of p63 exist in the nuclear, mitochondrial and cytosolic fractions of Raji following 2-FaraA. 1D Western blots showed that mitochondrial p63 in the 2-FaraA-sensitive cell lines, Raji and IM9, exists as dimers and tetramers, while in the cell lines resistant to 2-FaraA (MEC1 and U266), p63 is found as a monomer. The data presented here provide further insight into the effects and mechanisms of action of 2-FaraA, and define patterns of response of the p53 family members in sub-cellular compartments of B-lymphoid cells. In addition, several surface antigens were differentially expressed in CLL cells grown on feeder layer that manipulate cellular apoptosis, inflammation and T-cell activation with parallel with increases in novel intracellular targets Protein SET and Lymphocyte-specific protein 1 that may contribute to CLL cell survival in the tumour microenvironment and to resistance of CLL cells to 2-FaraA based treatments.

CHAPTER FOUR

Qualitative analysis of p53 interactome in response to 2-FaraA and the effect of p53 mutational status

4.1 INTRODUCTION

As discussed in the preceding chapter, the treatment of Raji and IM9 cells with 2-FaraA induces apoptosis through a p53-dependent mechanism. Particularly, the treatment causes the appearance of phosphorylated isoforms and proteolytic derivatives of p53. Thus, an understanding of the interactions of the p53 protein with potential binding partners is very important in defining the mechanisms of sensitivity and resistance to 2-FaraA. In addition, it may provide insights into the candidates responsible for the generation of the p53 isoforms and derivatives seen in chapter 3.

The interactions of the p53 protein have been studied extensively, yet the versatility of p53 means that new interactions and functions are still being elucidated. Thus far, there are several p53 binding partners that are well known in the prevention and or induction of apoptosis. In resting cells, p53 is short-lived and found at low levels. This is largely due to the interaction of p53 with MDM2 which induces ubiquitination and subsequent proteosomal degradation of p53. Cellular stresses can result in DNA damage and accumulation of active forms of signal mediators such as ATM and ATR kinases at the sites of DNA damage. The activity of these kinases results in the accumulation of p53 through phosphorylation and p14ARF inhibition of MDM2 binding to p53. This chapter (1) describes the results of a qualitative study of the p53 interaction partners (interactome) in 3 cell lines with varying p53 mutational status and (2) investigates the p53 interacting proteins in Raji and IM9 cell lines after 2-FaraA treatment to better understand the mechanisms that regulate p53 expression and activity following drug treatment.

4.2 METHODS

Cell lines were cultured and treated with 2-FaraA (3 μM, 24 h) as described earlier (Chapter 2). Cells (5 x 10^8) were harvested, washed in phosphate buffered saline (PBS) and lysed with RIPA buffer (Chapter 2). p53 was precipitated from cell lysates using monoclonal antibody (clone DO1) coupled to Dynabead protein G. Western blotting was used to confirm successful p53 precipitation. There were 3 biological replicates for each cell line and treatment condition. Non-specific binding was detected by using a rabbit polyclonal antibody against CD3 and subjected to shotgun mass spectrometry analysis.

The samples were separated by SDS-PAGE followed by GeLC-MS analysis using the QSTAR Elite mass spectrometer. ProteinPilot 3.0 software (Paragon^{TM} algorithm) was used to search and assign protein ID followed by further analysis using Microsoft Excel®. Figure 4.1 shows a schematic of the procedure. Down-stream analysis was conducted using a combination of online software STRING (http://string-db.org/), BioMyn (http://www.biomyn.de/) and the Human Protein Reference Database (http://www.hprd.org/index_html).

p53 functionality was tested by measuring the expression of p21 and p27 using flowcytometry, as these two proteins are downstream targets of p53 modulated cell cycle arrest.

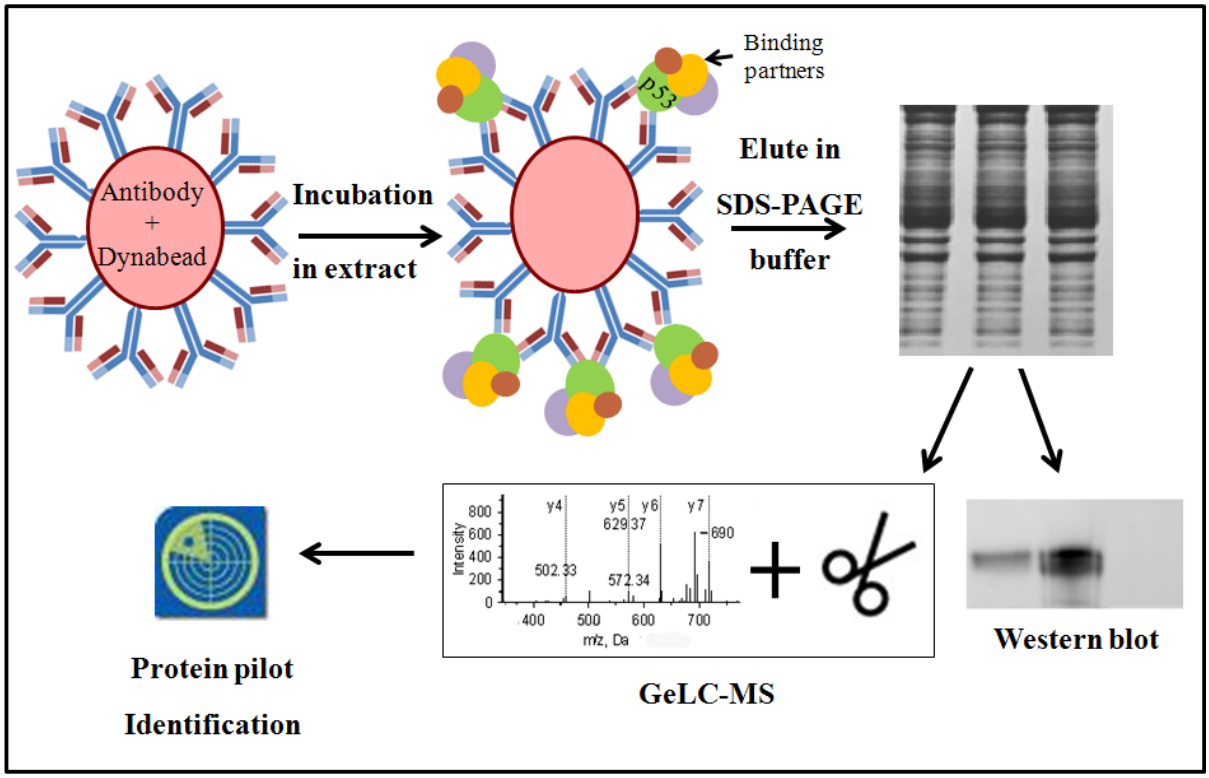

Figure 4.1 Schematic of the p53 pull-down workflow

4.3 RESULTS

4.3.1 Comparison of p53 interactome between cell lines with various p53 mutational status

In Raji, IM9 and MEC1 cells the number of interaction partners detected in all replicates with ≥2 unique peptides were 52, 80 and 73 respectively. In Raji and IM9 (functional p53), 27 common proteins were identified (Figure 4.2). The p53 precipitates from Raji and MEC1 shared only 5 proteins in common while IM9 and MEC1 shared only 2. There were no p53 interacting proteins common between all 3 cell lines. The Human Protein Reference Database (HPRD) assigned primary cellular localisation of p53 binding proteins (Figure 4.3A). In Raji cells, 62% of the p53 interaction proteins were primarily cytosolic. (including ribosome and endoplasmic recticulum), 21% were from the nucleus and 11% from the mitochondria. A similar pattern was observed in IM9 cells; 55% of the proteins identified were cytosolic , 35% nuclear and 7% mitochondrial. However, in MEC1 cells the pattern differed, with 81% of the proteins identified as cytosolic, 12% nuclear and 6% mitochondrial.

HPRD assigned biological processes for these p53 interactomes (Figure 4.3B) with some interesting trends. Firstly in the Raji and IM9 cell lines, 15% and 10% respectively of the p53 binding proteins identified are known regulators of cell growth/maintenance. However in MEC1, this percentage was higher at 32%. Secondly, in Raji and IM9 cell lines the percentage of the p53 interactome involved in energy production was 12% and 18%, respectively, while in MEC1 cells these proteins only represented 1% of the proteins precipitated. Proteins involved in nucleic acid metabolism are also higher in Raji (21%) and IM9 (28%) than in MEC1 (15%). All other functional groupings were represented equally between the 3 cell lines.

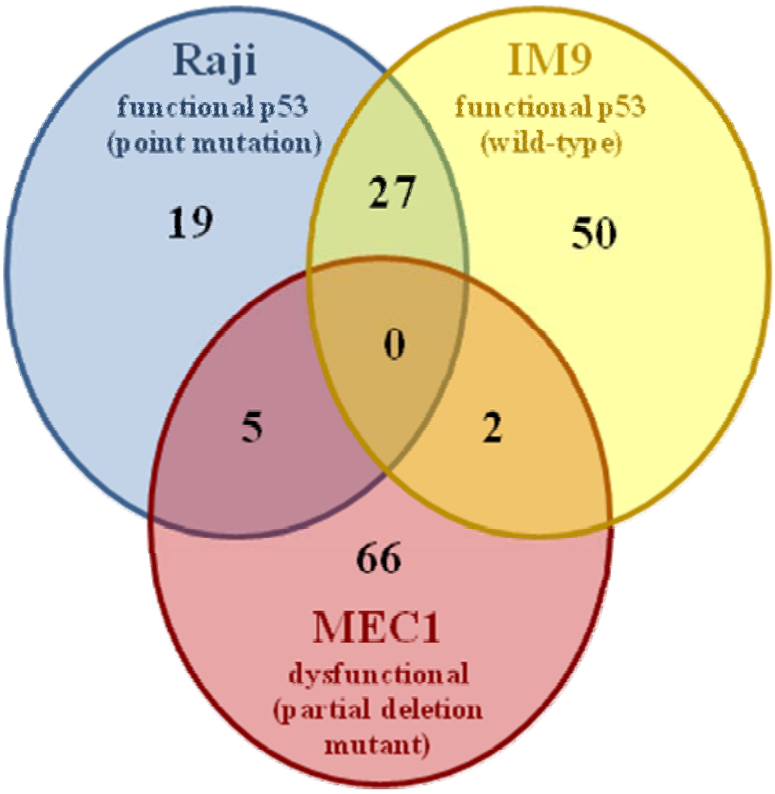

Figure 4.2 Venn diagram showing the numbers of p53 interaction partners that are common or distinct between the Raji, IM9 and MEC1 B-lymphoid cell lines.

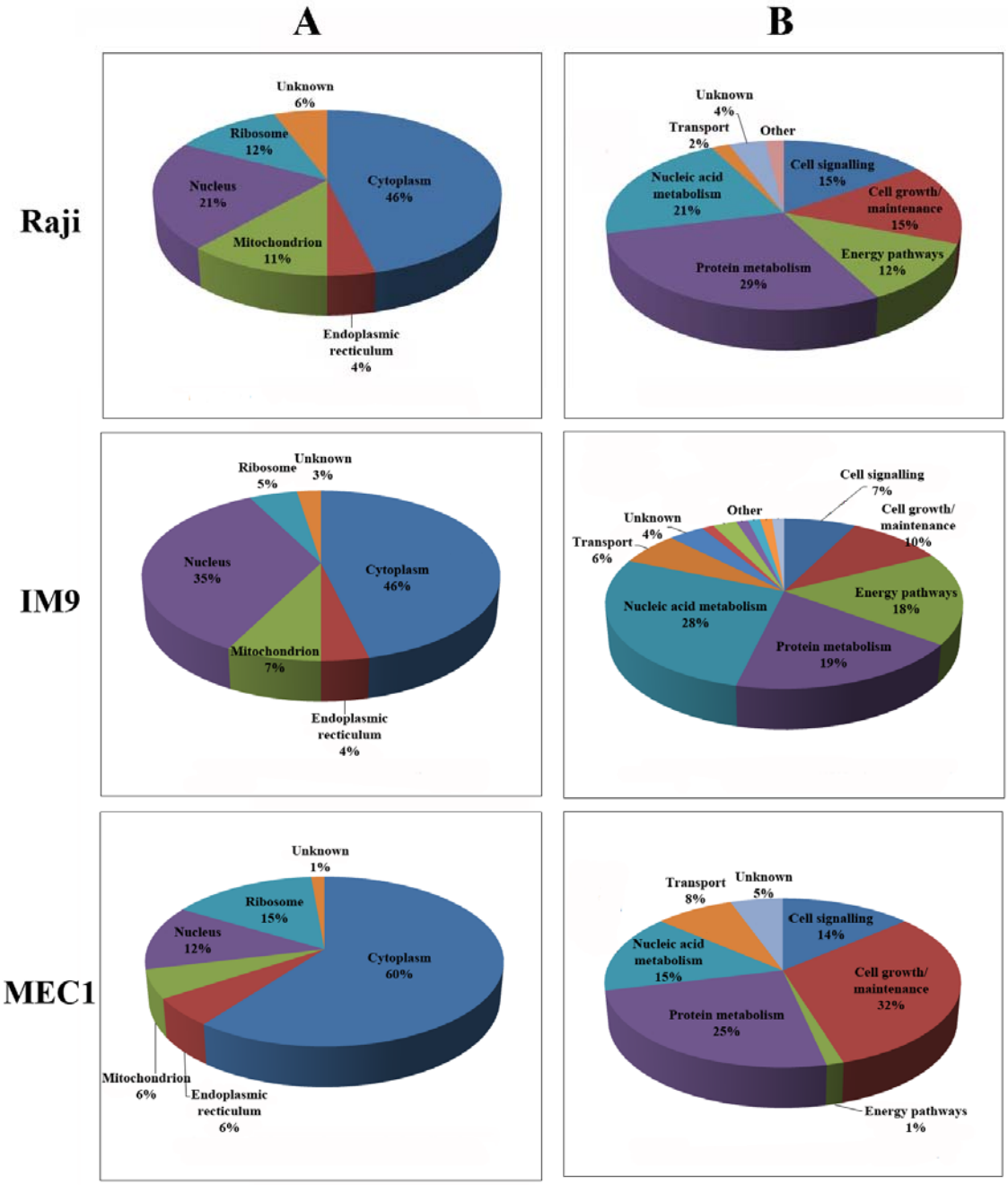

Figure 4.3 Pie charts of the p53 interactome in Raji, IM9 and MEC1 cells categorised by (A) cellular localisation and (B) biological function based on the Human Protein Reference Database.

4.3.2 p53 binding partners in Raji and IM9 cell lines after 2-FaraA treatment

4.3.2.1 2-FaraA-induced p53 binding proteins common to both Raji and IM9

Figure 4.4 shows a Venn diagram of the p53 interacting proteins found in control and 2-FaraA-treated Raji and IM9 cells. In control samples, there were 2 major cytosolic forms of the HSP90 protein, HSP90AA1, an inducible form, and HSP90AB1, a constitutive form. The other interaction partners of p53 identified under control conditions, all of which have been previously reported, are the ribosomal proteins L13, L13A, L23A, L14 and L26L1, DDX21, ATP5B, CLTC, LRPPRC, ERPS, PKM2, TAGLN2 and HNRNPA1L. Among the unreported partners are NUP210, NOL5 and CAD.

In the 2-FaraA-treated cells, DDX39, MCM5, HNRNPH1, HNRNPK, HNRNPM, PGD, EEF1A1 and RPL6 have all been reported as binding to p53. The novel partners identified were, MTHFD1, DYNC1H1, GRHPR, LOC92755, MYO18A, MYH11, and SRM.

Lastly among the p53 interaction partners that were common in both control and 2-FaraA-treated cells, GAPDH, TUMF, HSPD1, UBC, HYRC, PARP1, HNRNPU and SUPT16H have all been reported to bind to p53, whereas C1QBP, PHB2, TUBA4A, LDHA, MYH9, DARS, LMNB1, and LCP1 are novel p53 binding proteins.

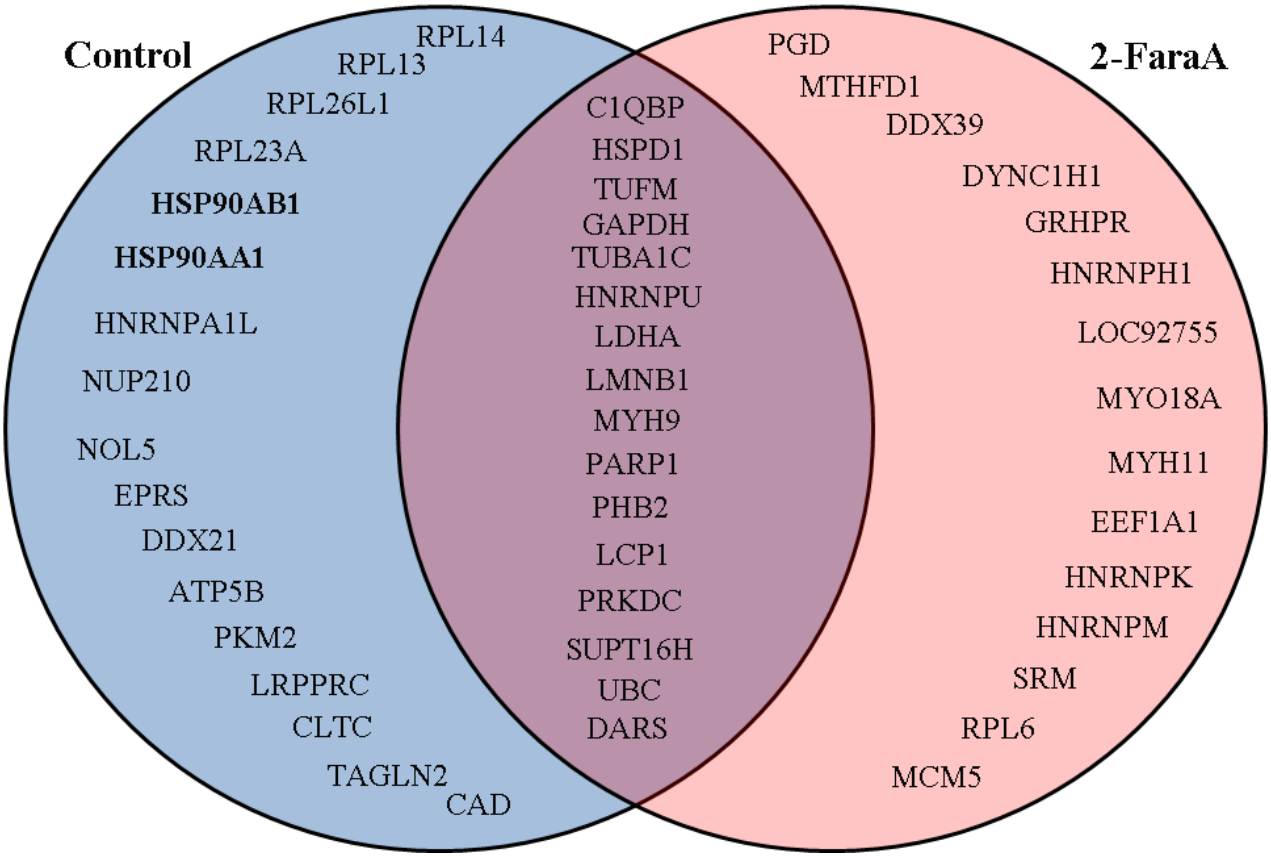

Figure 4.4 Venn diagram showing p53 interaction partners found in Control (Blue), 2-FaraA-treated (Red, 3μM, 24 h) in both Raji and IM9 cells. Proteins are represented by Gene names. Identifications that were found in both cell lines and in all replicates (n=3) with greater 2 or more unique peptides from MS/MS analysis are reported (Supplementary Table ST4.2, Appendix II).

4.3.2.2 p53 and HSP90 interactions

The interaction of p53 with HSP90 potentially represents a very important mechanism controlling p53 protein expression and function. To investigate the interaction of HSP90 with p53 further, HSP90 was immuno-precipitated in Raji, IM9 and MEC1 cells with and without 2-FaraA treatment (Figure 4.5). It is clear that HSP90 binds to p53 in all 3 cell lines before drug treatment and that 2-FaraA disrupts this interaction in Raji and IM9 but not MEC1 cells.

Flow cytometry analysis showed that inhibition of HSP90 with AUY-922 (Novartis) induced expression of p21 and p27 in Raji, IM9 and MEC1 cells, indicated by a right shift in the histogram peak (Figure 4.6). Figure 4.7 suggests that combining 2-FaraA and AUY922 has a greater effect on the distribution of cells within the cell cycle than either drug alone. The M1 region on each plot indicates the sub-G1 region that is indicative of apoptotic cells with fragmented DNA.

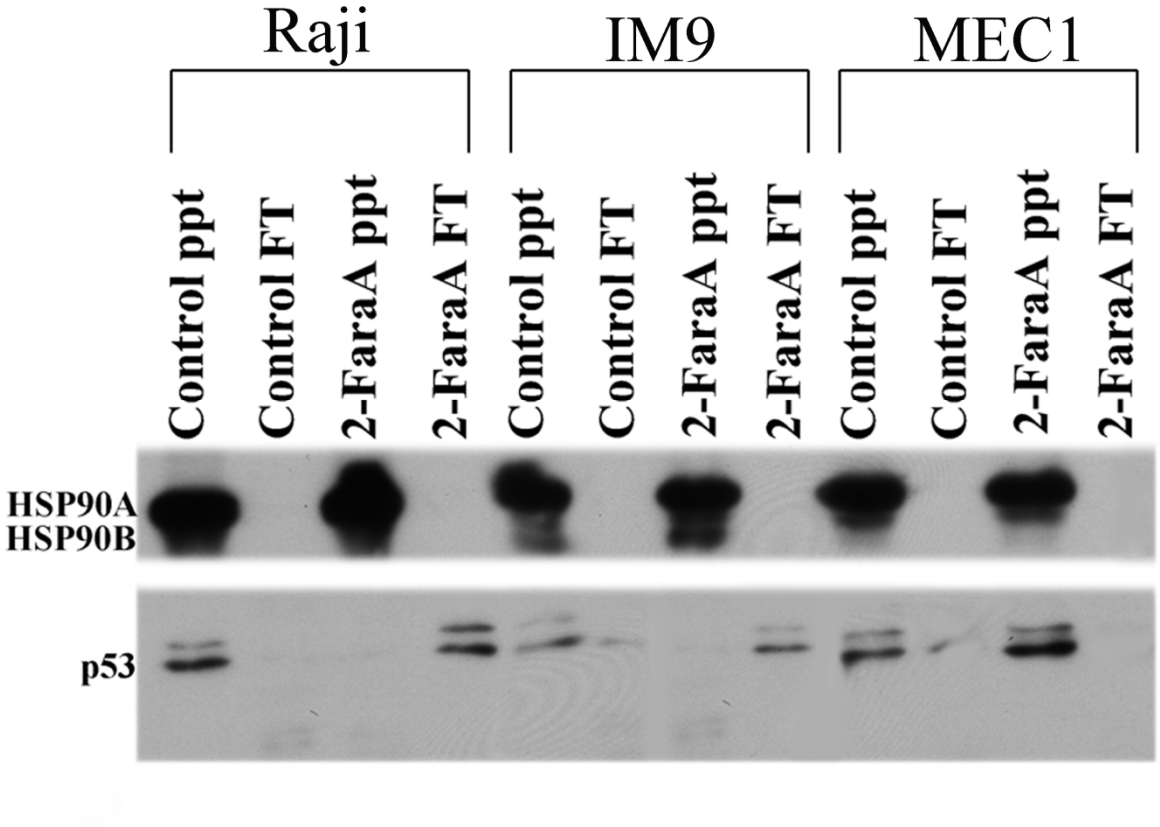

Figure 4.5 Western blots of HSP90 immuno-precipitates (ppt) and flow through (FT) from Raji, IM9 and MEC1 cells. Extracts (5 µg protein) were analysed by 1D SDS-PAGE in 12% gels, blotted and probed for p53 (clones DO1) and HSP90 (clone C45G5).

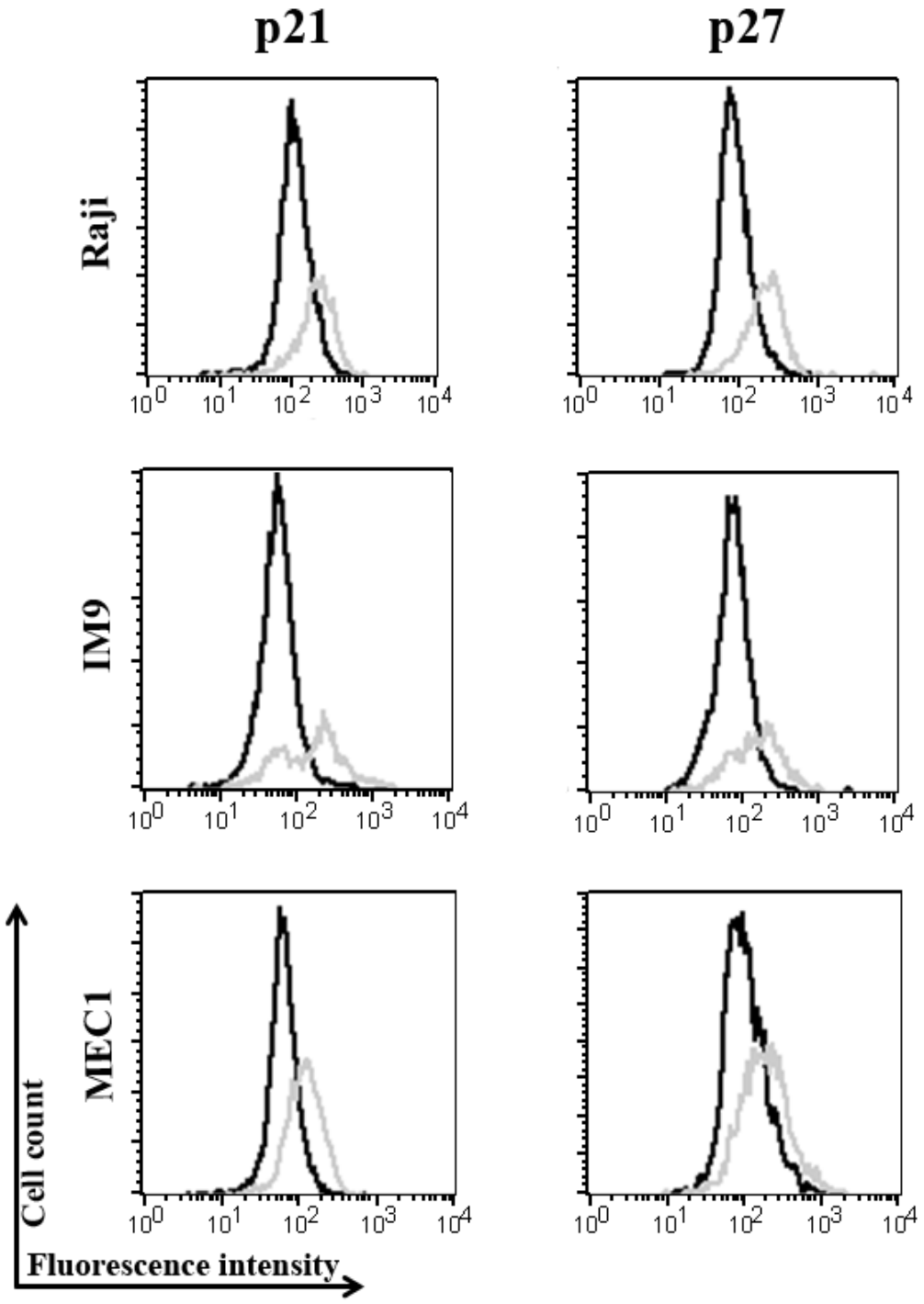

Figure 4.6 Flow cytometry analysis of p21 and p27 in Raji, IM9 and MEC1 cells in control (black outline) and treated (grey outline) with the HSP90 inhibitor AUY922 (Novartis, 20 nM, 48 h).

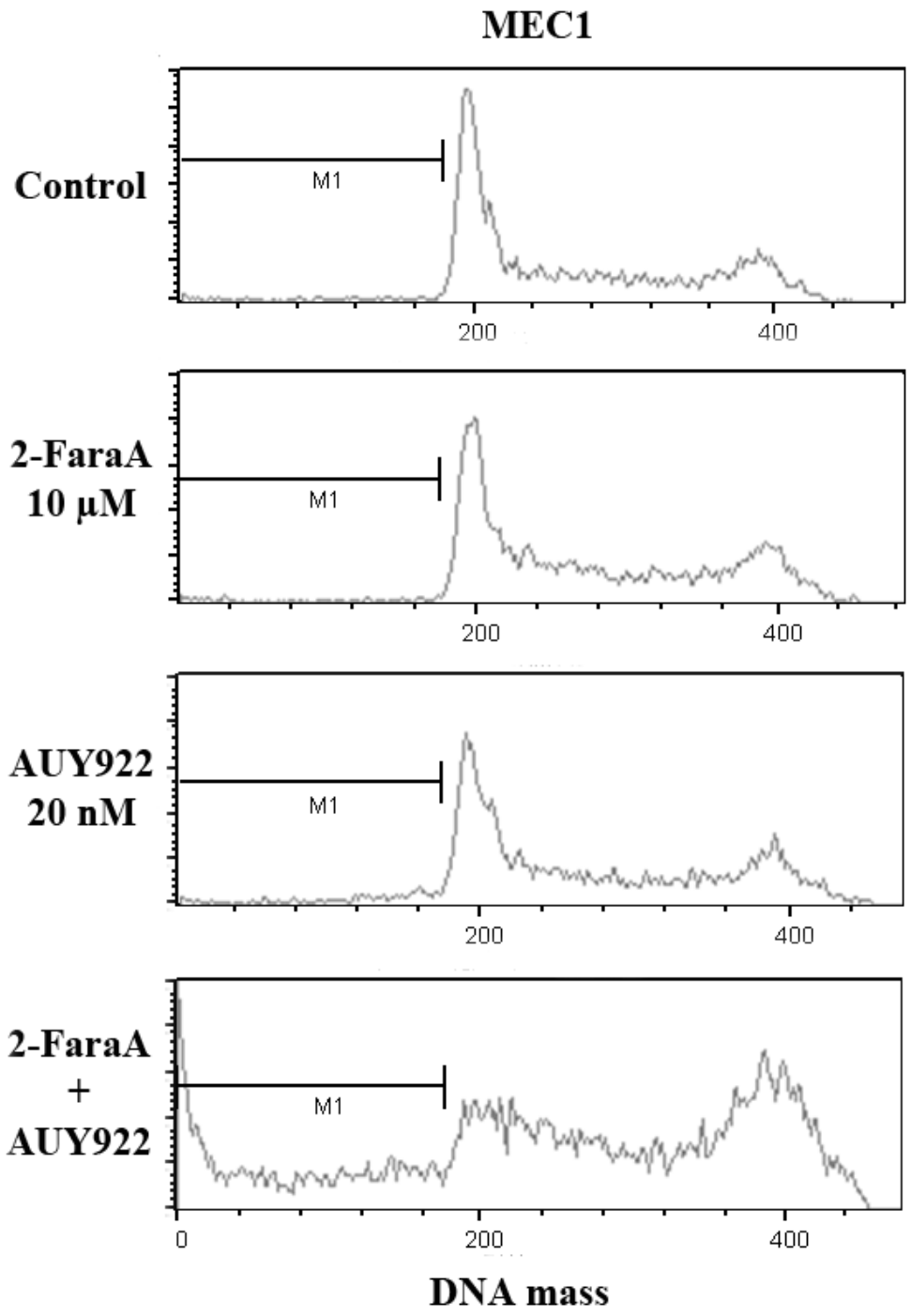

Figure 4.7 Cell cycle analysis of MEC1 cells with 2-FaraA, AUY992 or 2-FaraA+AUY992. The M1 region on each plot indicates the sub-G1 region that is indicative of the apoptotic cells with fragmented DNA.

4.3.3 Effect of 2-FaraA on the p53 interactome in Wild-type (IM9) cells

Treatment with 2-FaraA induced significant differences in the proteins bound to p53 in IM9 cells. Analysis with the online meta-search tool BioMyn categorised the interaction partners into a map of biological functions (Supplementary Figure SF4.1). The functional areas where 2-FaraA had the greatest effect are represented in Table 4.1

Table 4.1: Biomyn categorised functional groups of p53 interactome in IM9 cells

Number	Protein name	Entrez ID	Accession number	Control	Test	Other categories
Protein folding						
1	Heat shock protein HSP 90-beta	HS90B_HUMAN	P08238	YES	NO	
Nucleo-cytoplasmic transport/ protein targeting						
2	Stress-70 protein, mitochondrial	GRP75_HUMAN	P38646	NO	YES	
3	Importin subunit alpha-2	IMA2_HUMAN	P52292	NO	YES	
4	Spectrin beta chain	SPTB2_HUMAN	Q01082	NO	YES	Protein modification
5	Importin subunit beta-1	IMB1_HUMAN	Q14974	NO	YES	Cell death
Protein modification						
6	Interferon-induced, double-stranded RNA-activated protein kinase (PKR)	E2AK2_HUMAN	P19525	NO	YES	Cell death
7	Tyrosine-protein phosphatase non-receptor type 6 (SHPTP1)	PTN6_HUMAN	P29350	NO	YES	Cell death
8	Serine/threonine protein phosphatase 2A 65 kDa regulatory subunit A alpha isoform (PP2A)	2AAA_HUMAN	P30153	NO	YES	
9	Serine/threonine-protein phosphatase (PP-1A)	Q07161_HUMAN	Q07161	NO	YES	
10	Protein-tyrosine kinase 2-beta	FAK2_HUMAN	Q14289	NO	YES	Cell death

	(PYK2)					
11	Serine/threonine-protein kinase VRK1**(VRK1)**	VRK1_HUMAN	Q99986	NO	YES	
12	Ubiquitin carboxyl-terminal hydrolase isozyme L1	UCHL1_HUMAN	P09936	YES	NO	Cell death
13	Eukaryotic translation initiation factor 5A-1-like	IF5AL_HUMAN	Q6IS14	YES	NO	
14	Cullin-associated NEDD8-dissociated protein 1	CAND1_HUMAN	Q86VP6	YES	NO	
15	Protein-arginine deiminase type-1	PADI1_HUMAN	Q9ULC6	YES	NO	
16	26S proteasome non-ATPase regulatory subunit 13	PSD13_HUMAN	Q9UNM6	YES	NO	Cell death
Cell death						
17	Programmed cell death 6-interacting protein	PDC6I_HUMAN	Q8WUM4	YES	NO	
18	Cytoplasmic FMR1-interacting protein 2	CYFP2_HUMAN	Q96F07	YES	NO	
19	Pyruvate kinase isozymes M1/M2	KPYM_HUMAN	P14618	YES	NO	
20	Spectrin alpha chain	SPTA2_HUMAN	Q13813	NO	YES	

4.4 DISCUSSION

4.4.1 p53 interactome in cell lines with various p53 mutations

The comparison of the p53 interactome in the cell lines with their p53 mutational status showed striking trends. p53 is found in all sub-cellular compartments, this study was conducted using whole cell p53 precipitates, thus the HPRD assigned primary localisation of the interactome (Figure4.3A) was used to indicate the sub-cellular compartments from which the p53 binding partners originates. Interestingly, in IM9 and Raji the protein localisation is similar with ~50-60% cytosolic and ~20-30% nuclear but in MEC1, 81% of the interactome were cytosolic proteins while only 12% were nuclear. This observation is consistent with the results in Chapter 3 (Figure 3.3) where sub-cellular fractionation demonstrated that p53 mutation (truncation) prevented its translocation to the nucleus and therefore its association with nuclear proteins including certain transcription factors.

For Raji and IM9, 10-15% of the proteins identified in the p53 interactome have known functions in cell growth and maintenance, while in MEC1, proteins with these functions represent 32% of the interactome. Unlike Raji and IM9, MEC1 cells have a truncation mutation of p53 that confers growth and survival advantages, such as increased proliferation, evasion of apoptosis, and chemo-resistance [151, 152]. In the MEC1 but not Raji or IM9 lines, we identified DNA topoisomerase 2 beta as a p53 binding partner (Supplementary Table ST4.1, Appendix II). Topoisomerase 2 beta is the main target of topoisomerase 2-binding protein 1 (TOPBP1), and p53 and TOPBP1interactions are a hallmark of gain of function (GOF) mutations [153]. MEC1 mutant p53 may have a GOF that affects DNA repair through an interaction with TOPBP1 and may contribute toward the survival advantage and chemo-resistance of CLL cells harbouring this mutation of p53.

Comparison of the p53 interactomes showed a predominance of proteins with functions in cellular energy production and metabolism in the Raji and IM9 cell lines compared to MEC1. Many cancers have the Warburg effect that involves consumption of high amounts of glucose with less efficient production of ATP produced by the glycolytic pathway, even in the presence of oxygen. By contrast, normal cells preferentially use glycolysis and the mitochondrial tricarboxylic acid (TCA) cycle for the oxidative degradation of glucose and generation of ATP, resorting to glycolysis only under conditions of oxygen deprivation. Several studies show that by promoting oxidative phosphorylation, functional p53 might oppose the Warburg affect [154, 155]. It is interesting to note that in our study the two cell lines with normal p53, interactions of the p53 protein with proteins involved with energy pathways and metabolism were identified whereas in the p53 mutated MEC1 cell line no such interactions were observed.

4.4.2 Fludarabine induced effects on the p53 interactome in Raji and IM9 cells

In control cells, the p53 interactome included the ribosomal protein L13. Previous studies report that L13 plays an essential role in the progression of gastro-intestinal malignancies by suppressing activity of the p53 pathway, thus allowing tumorigenic growth in the presence of wild-type p53 [156]. We also identified the tri-functional protein CAD as binding to p53 in control cells; amplification of the *CAD* gene and over-expression of the CAD protein confers resistance to pyrimidine nucleotide biosynthesis inhibitor PALA. The process of gene amplification is facilitated by DNA strand breaks promoted by a deficiency in p53 [157, 158].

In response to 2-FaraA treatment, we observed dissociation of HSP90 from p53. HSP90 interactions with p53 have been reported previously; Walerych et al., showed that in human

fibroblasts HSP90 forms a complex with wild-type p53 partially unfolding it and preventing p53 regulation of p21 gene expression. Treatment with the HSP90 inhibitors geldanamycin or radicicol, promoted the transcriptional activities of p53 [159]. Our study shows for the first time that in the human B-cell lines Raji and IM9, treatment with 2-FaraA dissociates HSP90 from p53. This does not occur in p53-mutated MEC1, however treatment of MEC1 with the HSP90 inhibitor AUY922, results in increases of p21 and p27, known p53 targets. In addition, MEC1 cells do not respond to 2-FaraA or AUY922 individually but in combination of these two drugs causes cells to undergo apoptosis indicated by the higher proportion of cells with sub-G1 DNA content (Figure 4.7). Taken together, these data suggest HSP90 may negatively regulate the function of p53 in cells that respond to 2-FaraA (Raji and IM9) and in cells unresponsive to 2-FaraA (MEC1), HSP90 inhibition may restore sensitivity to DNA damaging agents in tumour cells with truncated forms of p53 releasing p53 from a mis-folded state.

4.4.3 Effects of 2-FaraA on the interactions of p53 in the IM9 cell line

Treatment with 2-FaraA induced significant changes in the proteins bound to p53 in IM9 cells. In response to 2-FaraA, several proteins involved in nucleo-cytoplasmic transport were found in the p53 interactome. These include Stress-70 protein (GRP75), Importin subunit alpha-2 (IMA2), Importin subunit beta-1 (IMB1) and Spectrin beta (SPTB2).

The Stress-70 protein (GRP75) is a known binding partner of p53. It binds to the cytoplasmic sequestering domain of p53. Studies by Wadhwa *et al*. show that GRP75 binds and retains p53 in the cytoplasm, suggesting that the binding inhibits p53 function by nuclear exclusion [160]. However recent studies demonstrate that p53 plays a different role in the cytoplasm, thus p53 cytoplasmic sequestering may aid cytoplasmic/mitochondrial apoptosis. The binding of GRP75 to p53 has not been reported in response to a DNA damaging agent such as 2-

FaraA and may play an important role in regulating apoptosis induced in the cytoplasm. Importin alpha is also implicated in p53 transport. Kim *et al.* show that importin alpha functions as a component of the nuclear localization signals receptor for p53 and mediates nuclear import of p53 [161]. The binding of importin alpha to p53 after 2-FaraA treatment and subsequent nuclear translocation of p53 may represent an important step in the induction of p53-dependent apoptosis in the nucleus.

It is interesting to note the interaction of spectrin/fodrin with p53 after 2-FaraA treatment. Studies have shown that during radiation and tumour necrosis factor-induced apoptosis, spectrin is cleaved by calpains and caspases to 150 kDa and 120 kDa fragments, respectively [162, 163]. However no reports to date have an interaction between full length spectrin, or its breakdown products, with p53.

Protein modification: Protein modification is an essential biological function crucial in many cellular pathways, including apoptosis. Proteins that interact with p53 after 2-FaraA treatment include kinases and phosphatases. Kinases include PKR, VRK1 and PYK2 and phosphatases include SHPTP1, PP-1A and PP2A.

All of the kinases have been reported to have interactions with p53. For example, interferon enhanced complex formation of PKR with wild-type p53 has been reported. In addition, phosphorylation of human p53 on serine392 is induced by activated PKR, stabilizing the p53 tetramer required for the action of p53 as a transcription factor [164]. This observation is consistent with previous findings showing that apoptosis induced by 2-FaraA increases p53 phosphorylation on serine 392 [165]. VRK1 is a nuclear kinase that has been reported to phosphorylate p53 at Thr18. This phosphorylation disrupts the p53-MDM2 interaction and stabilizes p53. In the absence of MDM2, VRK1 also stabilizes p53 through phosphorylation of MDMX and p300 [166].

The PYK2 kinase has a functional role that opposes VRK1. PYK2 is responsible for recruiting the ubiquitin ligase MDM2 to the nucleus, thereby regulating p53 activity by ubiquitination and proteosomal degradation [167]. This seemingly contradictory mechanism is typical as both pro- and anti- apoptotic mechanisms are induced by DNA damaging agents. Additionally, this may explain the presence of the lower molecular weight p53 derivatives observed in Chapter 3 when levels of p53 increase after 2-FaraA treatment.

Among the phosphatases, SHPTP1 does not directly interact with p53 but is a substrate of c-ab1; interaction of c-abl with p53 has been reported to play a role in the induction of JNK activity following DNA damage [168]. p53 and c-ab1 form a complex in response to DNA damage which induces cell cycle arrest [169]. Therefore, the observation in the current study that SHPTP1 interacts with p53 after 2-FaraA treatment may contribute to the 2-FaraA-induced cell cycle arrest observed in IM9 cells.

PP2A has been shown to mediate the dephosphorylation of p53 at Thr55 in response to DNA damage, thus reducing p53 stability, Bax expression and cell apoptosis [170]. Our observation that p53 interacts with PP2A following 2-FaraA treatment may be a pro-proliferative response. Lastly, PP1A has not been reported as interacting directly with p53, however it binds to BRCA1 [171] which interacts with p53 [172]. The BRCA1/2 pathway arbitrates DNA damage response pathways that mediate the repair of DNA double strand breaks. While this pathway has primarily been described in breast and ovarian cancers, it is also known to be suppressive of hematologic cancers [173].

Cell death: The previously discussed enzymes PKR, PYK2 and SHPTP1 that we have shown to interact with p53 after 2-FaraA treatment have described roles in cell death. Spectrin alpha (SPTA2) an isoform of the previously discussed SPTB2 also interacts with p53 after

treatment. Similar to the beta isoform, spectrin alpha is broken down by caspase-3 and calpains during apoptosis [174]. Its binding to p53 has not been reported.

4.5 CONCLUSION

Taken together, our analysis of the p53 interactome provides a snapshot of the cellular processes involving p53 and the effects of 2-FaraA on these interactions in B-lymphoid malignancies. Comparison of the p53 interactions in Raji, IM9 and MEC1 cells suggests that p53 in the MEC1 line interacts more closely with proteins involved in cell growth and cellular maintenance than in the Raji and IM9 lines. This could be attributed to a gain-of-function of the mutated p53 in this line, which may contribute to a survival advantage and the chemoresistance observed in Chapter 3 (Figure 3.2). We also observe that in p53 cell lines (Raji and IM9) the p53 interactome include several proteins involved in energy production and metabolism. Similar interactions were not identified in the MEC1 cells, suggesting that the functions of normal p53 may in the Raji and IM9 cells may include energy generation by the glycolytic pathway, described as the Warburg effect.

In the Raji and IM9 cell lines, HSP90 was identified as being bound to p53 in the untreated control samples but was shown to dissociate from p53 following 2-FaraA treatment. In contrast in MEC1, HSP90 remained bound to p53 even after 2-FaraA treatment. This suggests that HSP90 binding to p53 may play a role in regulating p53 activity and sensitivity to 2-FaraA treatment. This hypothesis is supported by evidence (Figure 4.6 and 4.7; Best *et al*., 2012) that suggests that inhibition of HSP90 restores sensitivity to 2-FaraA even in cell lines and CLL patient samples that are resistant to 2-FaraA as a single agent [175].

Further investigation of the effects of 2-FaraA on the p53 interactome in the p53 wild-type IM9 cell line, identified several proteins that bound to p53 following 2-FaraA treatment. These proteins (GRP75, IMA2, PKR, VRK1, PYK2, PP2A, SHPTP1 and SPTA2) have roles in biological functions such as nucleocytoplasmic transport, protein modification and cell

death. Several of these proteins include kinases and phosphatases that are known to function in regulating p53 phosphorylation and have crucial roles in the regulation of apoptosis.

In conclusion, the data presented within this chapter provide further insight into the effects of fludarabine on p53, extending the observations described in (Chapter 3 Figure 3.1). The identification of several previously undescribed p53 interactions indicates novel roles and mechanisms of p53 yet to be elucidated that may involve the sensitivity of B-lymphoid cells to 2-FaraA.

CHAPTER FIVE

Phosphorylation of the p53 interactome in B-lymphoid cancers treated with 2-FaraA

5.1 INTRODUCTION

Protein phosphorylation is a common post-translational modification (PTM) in living cells. Regulatory functions such as cell cycle control, receptor-mediated signal transduction, differentiation, proliferation, apoptosis, transformation, and metabolism [176] are all controlled by phosphorylation. Phosphopeptide enrichment increases sensitivity for low abundance proteins such as transcription factors that cannot otherwise be detected by mass spectrometers. Quantitative phospho-proteomics detects increases or decreases of phosphopeptides that are indicative of change in the protein abundance or a change in the phosphorylation status of particular amino acid residues. Parallel analysis by mass spectrometry of flow through of enrichment columns (unmodified peptides) often aids in distinguishing which of the aforementioned changes is occurring.

This chapter focuses on differentially abundant phosphopeptides in the p53 interactome with 2-FaraA treatment of the drug responsive B-lymphoid cell lines Raji and IM9.

5.2 METHODS

Cells lines were grown and treated with 2-FaraA (3 µM, 24 h) as described earlier (Chapter 2). Cells (5 x 10^8) were harvested, washed in phosphate buffered saline (PBS) and lysed in RIPA buffer (Chapter 2). p53 was precipitated from cell lysates using monoclonal antibody (clone DO1) coupled to protein G coated Dynabeads. Four biological replicates were prepared for each cell line and treatment condition. Western blotting was used to confirm successful precipitation of p53. The p53 interactome was digested from the beads and labelled using dimethyl labelling with sodium cyanoborohydride ($NaBH_3CN$) for light and sodium cyanoborodeuteride ($NaBD_3CN$) for heavy, followed by titanium dioxide enrichment and analysis by mass spectrometry (Orbitrap Velos). Max Quant software was used for protein identification, quantification. Statistical significance assigned by Microsoft Excel using student t-test (n=4) for each cell line and a fold change of ±1.5. This was determined by a screen of the phosphoproteome based literature where they deem a change of 1.5 to be a significant [177-180]. Up-stream and down-stream pathway analysis was conducted using Ingenuity Pathway Analysis.

5.3 RESULTS

5.3.1 Assessment of successful workflow

Prior to mass spectrometry, complete digestion of the p53 interactome was assessed by SDS-PAGE. Bands corresponding to proteins of the p53 interactome and the monoclonal antibody (DO1) (lane 2) were removed from the Dynabeads by tryptic digestion (lane 3) and appeared as a dark smear below 10 kDa in the digest supernatant in lane 4 (Figure 5.1). The efficiency of stable isotopic dimethyl labelling was assessed by inspection of the mass shifts (8 Da m/z) of the light (L) and heavy (H) peptide pair in the MS spectra (Figure 5.2).

Figure 5.2 shows phosphorylation of Histone H2A.x at serine 139 in the Raji p53 interactome. Unmodified peptide TSATVGPK had no change in relative abundance when comparing control (L) and treated (H) peaks, but phosphorylated peptide KATQAS*QEY increased in relative abundance after 2-FaraA. Phosphorylation at this residue was validated by flow cytometry using an antibody against γ-H2A.x conjugated to Alexa 488 fluorochrome. The formation of γ-H2A.x (H2A.x with phosphorylated serine 139) was quantified in Raji and IM9 cells after 24 h and 48 h with 2-FaraA (Figure 5.3). Results show the increase of γ-H2A.x in Raji cells after 24 h which persists at 48 h. In IM9 cells, there is no increase in γ-H2A.x until 48 h. These results were consistent with the data obtained by MS where 2-FaraA treatment for 24 h induced phosphorylation of H2a.x at serine 139 in Raji cells, but not in IM9 cells (Supplementary Tables 5.1 and 5.2).

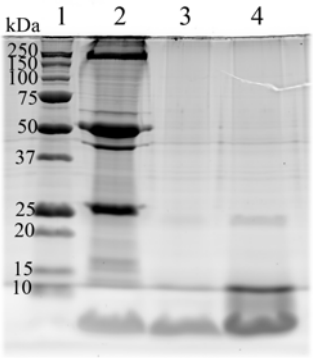

Figure 5.1 Sypro Ruby staining of p53 immuno-precipitated from Raji cells run on 15% SDS-PAGE, (1), molecular weight markers; (2), Dynabeads with p53 precipitate; (3), Dynabeads after on-bead-digestion with trypsin; (4), Supernatant from the beads after digestion.

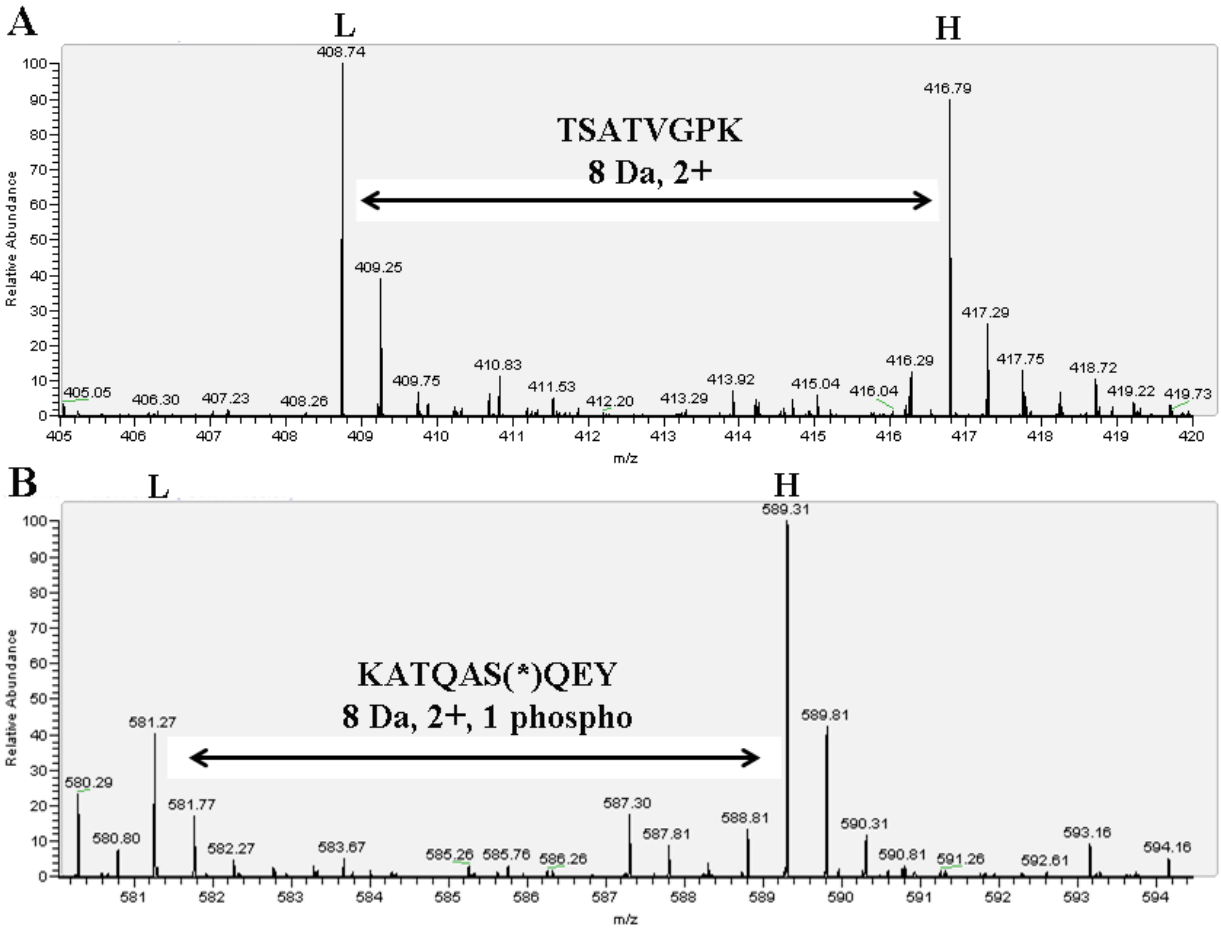

Figure 5.2 Quantitation of phosphorylation of Histone H2A.x in the p53 interactome of Raji cells. Spectra of 2 peptides of (A) unmodified and (B) phosphorylated (Ser139) following isotopic dimethyl labelling are shown. Peptides from vehicle control cells are indicated with (L), 2-FaraA treated cells (H).

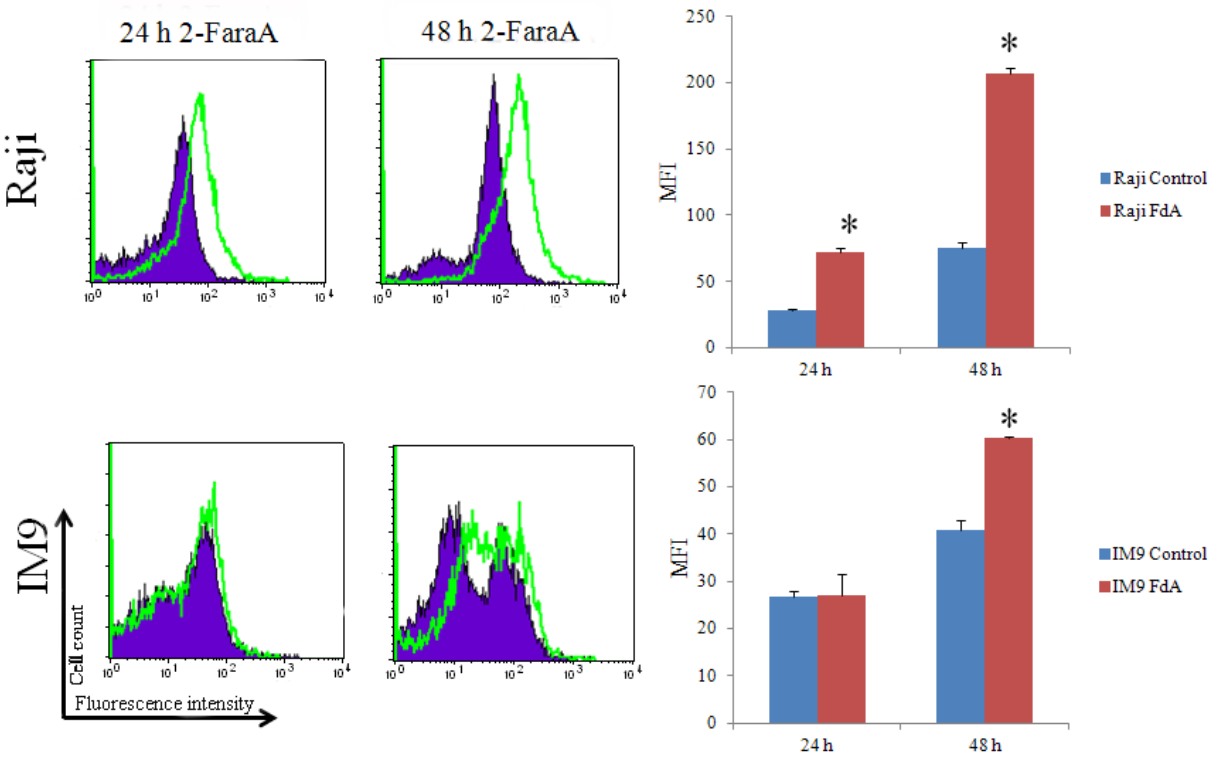

Figure 5.3 Phosphorylation of H2A.x to produce γ-H2A.x validated by flow cytometry using monoclonal antibody conjugated to Alexa 488 in Raji and IM9 cells treated with 2-FaraA (3 μM, 24 h, 48 h). The violet area represents untreated cells and the green outline 2-FaraA-treated cells. A shift in median fluorescence intensity (MFI) indicates an increase in γ-H2A.x. Graphs of relative amounts of γ-H2A.x in each cell line are shown on the right. Significant changes ($p < 0.05$) are indicated by (*) relative to the control (n=3).

5.3.2 Differential phosphorylation of p53 interactome after 24 h 2-FaraA treatment

In the IM9 p53 interactome a total of 301 phosphopeptides were detected, with 24 of these peptides showing increased phosphorylation and 75 peptides showed decreased phosphorylation after 2-FaraA treatment. In the Raji p53 interactome a total of 294 phosphopeptides were detected, with 15 peptides showing increased phosphorylation and 23 peptides showing decreased phosphorylation. Ingenuity Pathway Analysis (IPA) software was used to assign biological significance to differentially phosphorylated proteins in Raji and IM9 cell lines. The most significant biological pathways regulated were, RNA post transcriptional modifications, gene expression, cell cycle, cellular movement and haematological disease (Figure 5.4). Figure 5.5 shows the IPA of the differential phospho-proteome in Raji (A) and IM9 (B) cells. Consistent for both cell lines were pathways involved with the inhibition of Rnr (5.8S) ribosomal RNA.

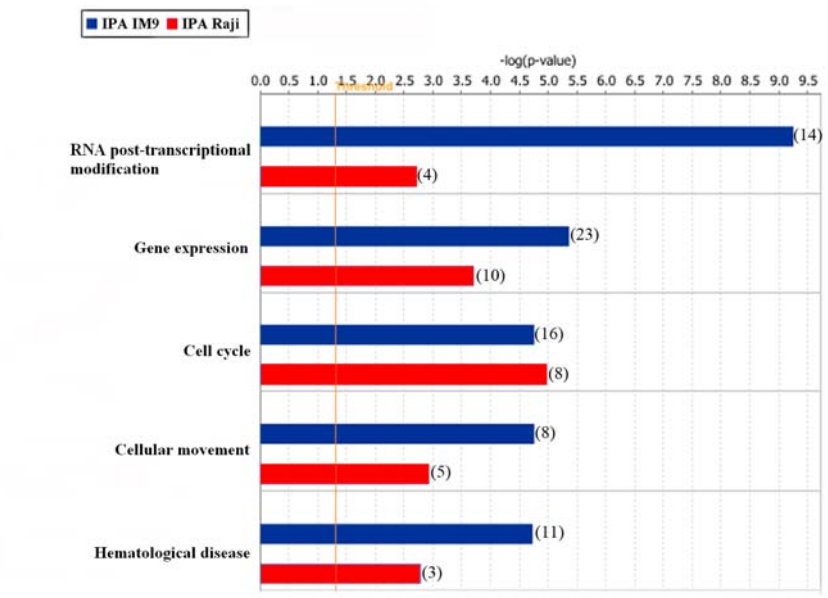

Figure 5.4 Biological pathway comparison for p53 interactome proteins that are differentially phosphorylated in Raji and IM9 cells after 2-FaraA. The significance threshold was set at –log (0.05). Pathways regulated by phosphorylation after 2-FaraA are shown as –log (*p*-value) > 1.3 (bars). The number of proteins detected that are involved in the pathway, are indicated in brackets.

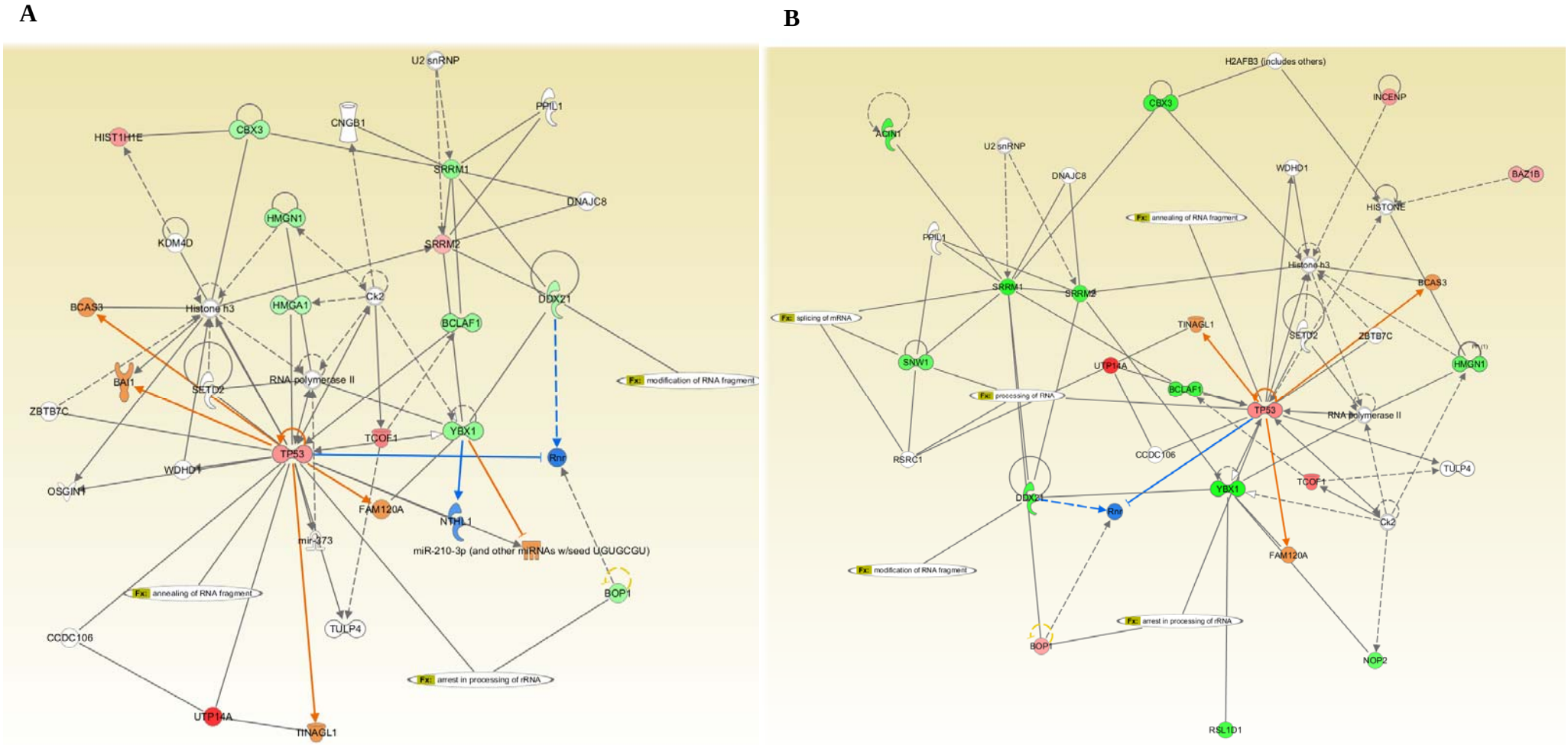

Figure 5.5 Ingenuity Pathway networks for the phospho-proteins common between (A) Raji (B) IM9. Proteins in red showed increased phosphopeptides and those in green decreased phosphopeptides in the p53 interactome. Proteins in orange are predicted to be activated and those in blue inhibited in function, based on the differential expression of proteins in the dataset.

5.3.3 Kinases and motif analysis

Table 5.1 summarises all the amino acid residues of proteins phosphorylated after 2-FaraA treatment of Raji and IM9 cells. The main predicted kinase families that contribute to the response to 2-FaraA include the CMGC kinases (ERK1, ERK2, CDK), AGC kinases (PKA, PKC, GRK1) and the Casein kinases (CK1, CK2). Analysis using Motif-x software revealed two phosphorylation motifs in common for the Raji and IM9 cell lines (Figure 5.6 A, B). The xxSPxx motif was from serine phosphorylated residues of CHD4, NCL, HIST1H1E, SRRM2, TCOF1 and TP53. The second motif SxxE was from serine phosphorylated residues of HSP90AB1, MCM2, TOP2A and NLC. A search using the online database PhosphoNetworks (http://www.phosphonetworks.org) revealed 3 kinases that have binding motifs analogous to those identified by Motif-x, in our study including MAPK8 (NCL), CDK7 (TP53) and CSNK2A1 (HSP90AB1) (Figure 5.6C).

Table 5.1 Proteins phosphorylated in the p53 interactome in Raji and IM9 cells after 2-FaraA (p-values and abundance ratios are in Supplementary Table 5.1 and 5.2).

Accession number	Protein name	Gene names	Sequence	Residues	Kinase substrate motif	Cell line
Q14839	Chromodomain-helicase-DNA-binding protein 4	CHD4	MSQPGSPSPK	S1535	ERK1, ERK2	Raji and IM9
P16104	Histone H2A.x	H2AFX	KATQASQEY	S140	ATM	Raji
P10412	Histone H1.4	HIST1H1E	KAPKSPAK	S187	ERK1, ERK2	Raji and IM9
			KASGPPVSELITK	S36	PKA,PKC	Raji
P17096	High mobility group protein HMG-I/HMG-Y	HMGA1	SSQPLASK	S8	GRK	Raji
P08238	Heat shock protein HSP 90-beta	HSP90AB1	IEDVGSDEEDDSGKDK	S254	CK2	Raji
P49736	DNA replication licensing factor MCM2	MCM2	GLLYDSDEEDEERPAR	S139	CK2	Raji
P19338	Nucleolin	NCL	VVVSPTKK	S67	MAPK8	Raji
P05388	60S acidic ribosomal protein P0	RPLP0	KEESEESDDDMGFGLFD	S304	CK2	Raji
Q9UQ35	Serine/arginine repetitive matrix protein 2	SRRM2	SATRPSPSPER	S351, S353	CK2	Raji
E9PHK9	Treacle protein	TCOF1	LGAGEGGEASVSPEKTSTTSK	S1376	ERK1, ERK2	Raji
P11388-4	DNA topoisomerase 2-alpha	TOP2A	KPSTSDDSDSNFEK	S1471, S1474	CK1, CK2	Raji
P04637	Cellular tumour antigen	TP53	ALPNNTSSSPQPK	S315	Aurora A	Raji and IM9

	p53					
Q9BVJ6	U3 small nucleolar RNA-associated protein 14 homolog A	UTP14A	SELSQDAEPAGSQETK	S445	DNA-PK, ATM	Raji and IM9
Q9UIG0	Tyrosine-protein kinase BAZ1B	BAZ1B	LAEDEGDSEPEAVGQSR	S1468	CK2	IM9
Q14137	Ribosome biogenesis protein BOP1	BOP1	IGDEYAEDSSDEEDIR	S126, S127	CK2	IM9
Q13112	Chromatin assembly factor 1 subunit B	CHAF1B	TQDPSSPGTTPPQAR	S429	GRK1	IM9
P07814	Glutamate-tRNA ligase	EPRS	EYIPGQPPLSQSSDSSPTR	S886	CDK1, 2, 4, 6	IM9
Q9NQS7	Inner centromere protein	INCENP	IAQVSPGPR	S263	ERK1, ERK2	IM9
P20700	Lamin-B1	LMNB1	TTIPEEEEEEEEAAGVVVEEELFHQQGTPR	T575	PKA,PKC	IM9
A8MXP9	Matrin-3	MATR3	RDSFDDRGPSLNPVLDYDHGSR	S188	PKA, PKC, CK2	IM9
P46013	Antigen KI-67	MKI67	AQSLVISPPAPSPR	S584	ERK1, ERK2	IM9
Q15154	Pericentriolar material 1 protein	PCM1	VTNDISPESSPGVGR	S65	ERK1, ERK2	IM9
Q9NTI5	Sister chromatid cohesion protein PDS5 homolog B	PDS5B	METVSNASSSSNPSSPGR	S116c	CK1, 2, 4, 6	IM9
P29590	Protein PML	PML	AVSPPHLDGPPSPR	S518, S527	ERK1, ERK2	IM9
			SSPEQPRPSTSK	S505	CK2	IM9

C9J3F9	Suppressor of SWI4 1 homolog	PPAN	LQDISELLATGAGLSESEAEPDGDHNITELPQAVAGR	S238, S240	CK2	IM9
Q5VTR2	E3 ubiquitin-protein ligase BRE1A	RNF20	VYGAGSSLYGGTITINARK	Y314	Src	IM9
Q9H7N4	Splicing factor, arginine/serine-rich 19	SCAF1	QRSPSPAPAPAPAAAAGPPTR	S498, S500	CK2	IM9
P18583-9	Protein SON	SON	SAASPVVSSMPER	S1769	ERK1, ERK2	IM9
			AALAPAKESPR	S906	PKA	IM9
E9PHK9	Treacle protein	TCOF1	EAASGTTPQK	T1270	CDK5	IM9
			TSQVGAASAPAKESPR	S381	PKA, PKC	IM9
Q9BVJ6	U3 small nucleolar RNA-associated protein 14	UTP14A	DYLLSESEDEGDNDGER	S29, S31	CK2	IM9

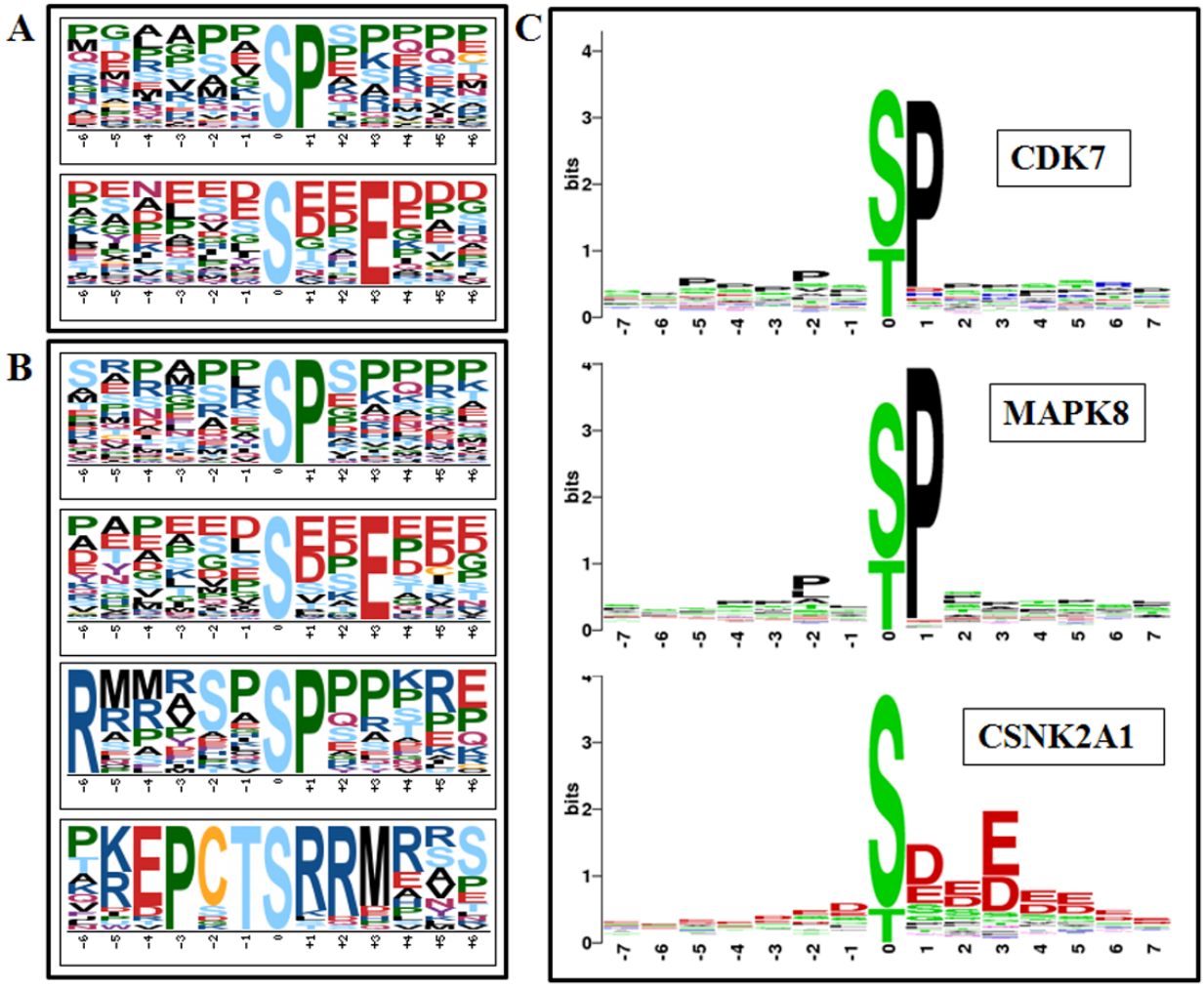

Figure 5.6 Motifs found in (A) Raji and (B) IM9 cells phosphorylated after 2-FaraA treatment identified using Motif-x software. (C) Binding motifs for kinases that are analogous to the motifs discovered by Motif-x.

5.3.4 Upstream molecule analysis of p53 interactome phosphorylation using IPA

In upstream molecule analysis significant proteins were determined by comparing Fisher's exact p-value and the number of associated proteins found in our study. The top 2 upstream molecules found to be regulated were a synthetic retinoic acid (CD437, 7.68×10^{-7}, 8) and the MYC protein (2.04×10^{-6}, 9). Figure 5.7 shows the p53 network incorporating these two upstream molecules and the differential proteins involved. Western blots of retinoic acid receptor alpha (RARα) were conducted

to determine whether RARs play a role in 2-FaraA-induced apoptosis. In Raji (2-FaraA responsive) RARα was up-regulated (2-fold) but not in MEC1 (2-FaraA resistant) cells (Supplementary Figure S5.2). Figure 5.8 shows histograms of Annexin V binding to externalised phosphatidyl serine (PS, apoptosis marker) in MEC1 and Raji cells treated with 2-FaraA (3 μM) and -*trans* retinoic acid (ATRA, 1 μM) alone and in combination. For MEC1 cells, the combination of ATRA and 2-FaraA induces apoptosis, in Raji ATRA does not alter the effect of 2-FaraA.

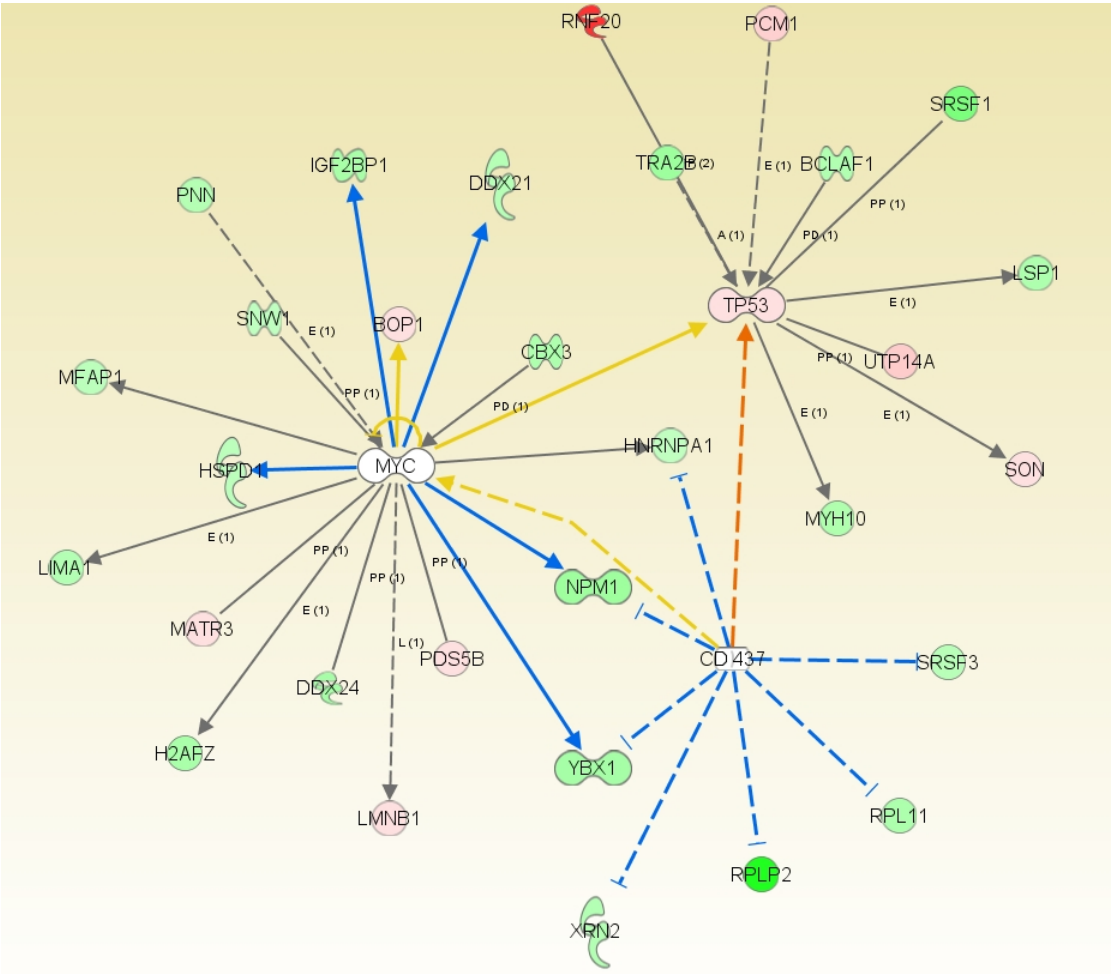

Figure 5.7 MYC and CD437 are the top 2 upstream molecules activated by changes in the p53 interactome induced by 2-FaraA. Proteins in red represent increase in phosphopeptides and green decrease in phosphopeptides in the p53 interactome.

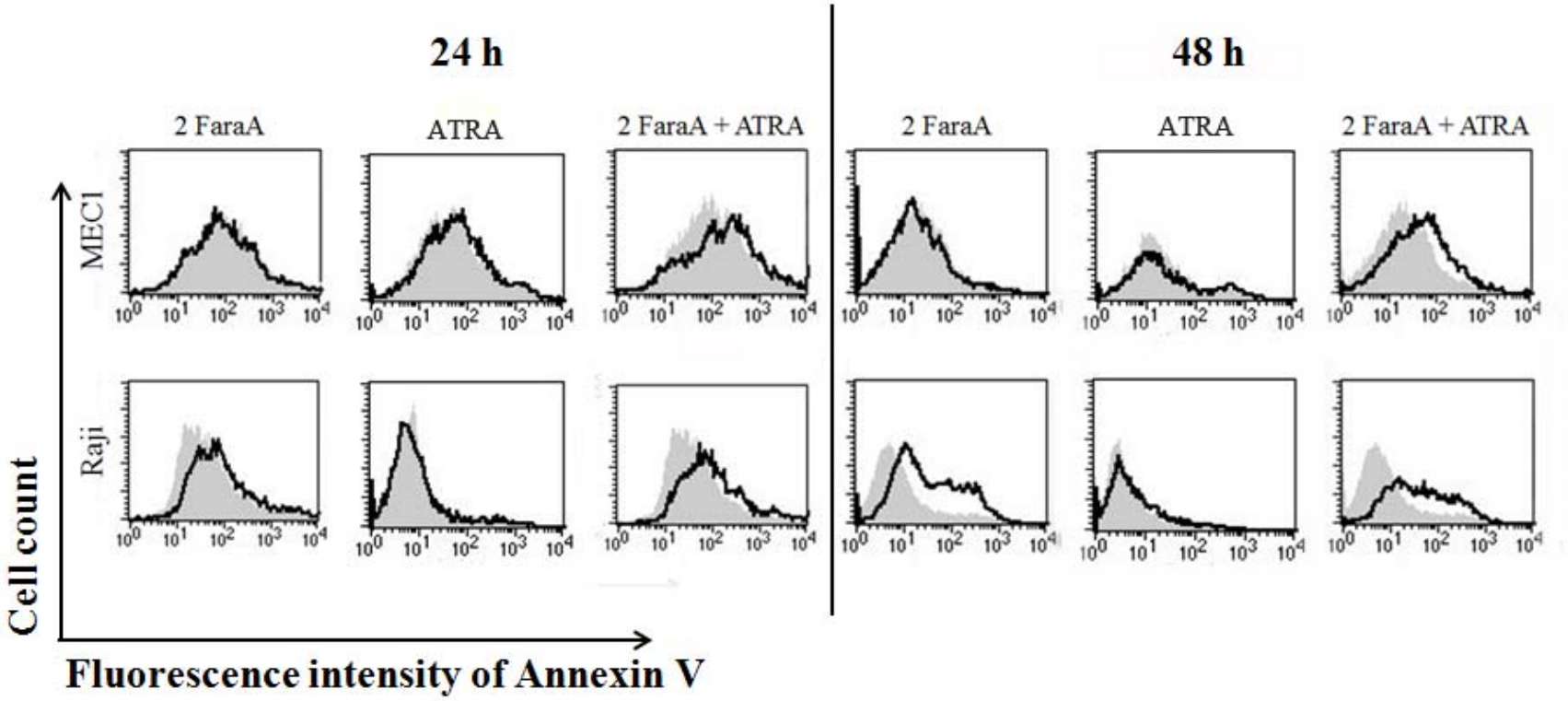

Figure 5.8 Apoptosis was determined by measuring the expression of Annexin V by MEC1 and Raji cells after treatment with 2-FaraA (3 μM) alone and combined with ATRA (1 μM). The grey area represents cells incubated with vehicle control; the black line represents cells incubated with 2-FaraA and/or ATRA. A shift in the median fluorescence intensity indicates an increase or decrease in Annexin V binding to PS.

5.4 DISCUSSION

5.4.1 DNA damage induces a protein phosphorylation signature

Identification of phosphopeptides in the p53 interactome high-lighted some interesting cellular functional nodes, including proteins involved in RNA modification and gene expression (Figure 5.4). This correlates well with transcriptional regulation by of p53 and the ability to bind to other transcription factors, as well as DNA and RNA. A comparison of our data with the literature showed several DNA damage phosphorylation signatures. Phosphorylation of H2AX at Serine 139 produces γH2AX that plays a key role in the DNA damage response (DDR) [181] and is required for the assembly of DNA repair proteins at sites containing damaged chromatin and activation of checkpoint proteins that arrest the cell cycle [182]. We observe the formation of γH2AX by mass spectrometry and flow cytometry (Figures 5.2, Figure 5.3 and Supplementary Table ST5.1). Bennetzen *et al.* identified proteins that were specifically phosphorylated in response to DNA damage in the nucleus. Several of the proteins listed overlap with our study. These include phosphorylation at NCL (S67), UTP14A (S445), CHAF1B (S429), MATR3 (S188), PPAN (S238) and dephosphorylation at BCLAF1 (S285), DDX21 (S71, S121), CCDC86 (S47), CTTN (T401, S405) and MATR3 (S9) [183]. Other protein identified, but with opposite responses were PDS5B (S1166), SCAF1 (S498, S500), and BCLAF1 (S496). Our study focused the on p53 interactome in multiple sub-cellular compartments, not exclusively nuclear p53.

Bracken *et al.* describes a novel SNARP complex composed of the proteins SNIP1, SNW1, THRAP3, BCLAF1 and PNN, required for production of mature cyclin D1 mRNA [184]. We found decreases in the phospho-proteins SNW1, THRAP3, BCLAF1 and PNN (Supplementary Table ST5.2) with decreases in cyclin D1 (Supplementary Figure SF5.4) after 2-FaraA. This indicates that dissociation and/or dephosphorylation of these proteins in

the p53 interactome could down-regulate the SNARP complex resulting in down-regulation of oncogenic Cyclin D1.

5.4.2 HSP90 phosphorylation and specific kinases

As discussed in Chapter 4, the dissociation of HSP90 from the p53 interactome after 2-FaraA treatment may play a crucial role in p53-induced apoptosis. However, the mechanism of the dissociation was unknown. In this chapter, we found phosphorylation of HSP90 at serine 254 (Table 5.1 and Supplementary Figure SF5.1). This phosphorylation of HSP90 has been shown to regulate apoptosome formation by modulating the affinity of HSP90 for apoptotic peptidase activating factor 1 (APAF1). In leukaemias, reduced phosphorylation of serine 254 strengthens the HSP90–APAF1 complex, abrogates cytochrome *c*-induced apoptosome assembly, and confers chemoresistance [185]. Accordingly, phosphorylation of HSP90 at Serine 254 here may reduce the affinity of HSP90-p53 binding resulting in release of p53 to induce apoptosis. Motif analysis programs indicate that casein kinase 2 alpha 1 (CSNK2a1) is primarily responsible for the HSP90 phosphorylation at Serine 254 (Table 5.1, Figure 5.6 C), activation of CSNK2a1 may enhance chemotherapeutic efficacy through by HSP90 phosphorylation and subsequent dissociation of p53 from HSP90. Site-specific mutagenesis studies of HSP90 may also be useful in determining the importance of this particular phosphorylation in 2-FaraA response.

5.4.3 Ribosome biogenesis and p53

Ribosome biogenesis is essential for cell survival. Defects in ribosome production cause p53 stabilization and induce p53-dependent inhibition of cell proliferation. A review by Donati *et*

al. describes the role of ribosomal proteins in this mechanism. Dysregulation of ribosome biogenesis results in release of RPL5, RPL11 and RPL23 as they are no longer required for ribosome construction. The ribosomal proteins bind to MDM2 and it dissociates from p53, with activation of p53 [186, 187]. Consistent with this theory, we show that after 2-FaraA treatment, RPL11 (Supplementary Table ST5.2) and RPL23 (Chapter 4, Figure 4.4) decrease in the p53 interactome, indicating their binding to MDM2 and disassociation from the interactome.

Secondly, we observe increases in the differential abundance of proteins involved with the production of rRNA such as DDX21, BOP1 and TP53 (Figure 5.5). The production of 5.8S rRNA is an essential step in ribosomal biogenesis [187] and is predicted to be inhibited by changes induced by 2-FaraA. Lastly, we observe the phosphorylation of Histone H1.4 at serine 187 that likely regulates transcription of ribosomal and steroid hormone-responsive genes [188] which may also regulate rRNA.

5.4.4 Retinoic acid

IPA upstream protein analysis indicates activation of the retinoic acid receptor (RAR) agonist CD437 (Figure 5.7). Sun *et al*. have shown that this synthetic retinoid induces apoptosis in a variety of cancer cells including human head and neck squamous cell carcinoma and lung cancer [189, 190]. Further these studies have demonstrated that cancer cells with wild-type p53 are more sensitive to CD437 than those with mutant p53, although CD437 can induce both p53-dependent and -independent apoptosis. We hypothesise the involvement of retinoic acid (RA) and receptors in the 2-FaraA induced apoptosis mechanism. To test this hypothesis, Western blotting of RARα was conducted in cells before and after 2-FaraA

(Supplementary Figure SF5.2). These results indicate that RARs and naturally occurring RA may have roles in 2-FaraA induced apoptosis. Ahmed *et al*. found that treatment of acute myeloid leukemia (AML) cell lines with a combination of 2-FaraA and all-*trans* RA (ATRA) induces greater apoptosis than 2-FaraA alone [191]. Other studies report that 1 μM ATRA induces p53–independent apoptosis in AML cells [192].

To observe the effects of RA in our laboratory the 2-FaraA responsive cell line Raji and the resistant cell line MEC1 were treated with increasing concentrations of ATRA (0-50 μM) for 24 h and 48 h (Supplementary Figure SF5.3). ATRA decreased proliferation of Raji and MEC1 cells after 48 h. Further, we found 1 μM ATRA induced apoptosis in MEC1 cells lines when treated in combination 2-FaraA after 48 h (Figure 5.8). In light of these findings we hypothesise that retinoic acid may increase chemo-sensitivity in p53 mutant cells. Future studies with both ATRA as well as the RAR agonist CD437 in combination with 2-FaraA in leukemic cell lines with p53 mutations as well as in primary CLL cells with fludarabine refractory disease should be conducted. Our study indicates that retinoic acid consumption or exposure may lead to better chemotherapeutic outcomes in patients with CLL.

5.5 CONCLUSIONS

Analysis of the p53 phospho-interactome revealed novel cellular responses to 2-FaraA. DNA-damage induced phosphorylation of H2A.x at serine 139 and residue specific phosphorylation of TP53, NCL and DDX21. We found de-phosphorylation of proteins of the SNARP complex with decreased cyclin D1; the p53 interactome could regulate this complex. Phosphorylation of HSP90 at serine 254 by CSNK2a1 may induce dissociation of the HSP90-p53 complex occurs after 2-FaraA treatment. Pathway analysis of the phospho-interactome indicated that 2-FaraA may dysregulate ribosome biogenesis, essential for cell survival. Upstream molecule analysis using IPA indicated retinoic acid receptors may play a role in 2-FaraA induced apoptosis; treatment with all *trans*-retinoic acid inhibits proliferation and induces apoptosis in 2-FaraA resistant MEC1 cells. The results indicate that ATRA may enhance the therapeutic effects of 2-FaraA.

CHAPTER SIX

Effects of siRNA knockdown of p53 on 2-FaraA induced apoptosis

6.1 INTRODUCTION

Previous chapters have demonstrated the responses of p53 and related proteins in 2-FaraA induced apoptosis in B-lymphoid cancers. This chapter will focus on the proteomic effects of p53 knockdown in 2-FaraA treated Raji and IM9 cell lines using quantitative iTRAQ labelling. Apoptosis in response to 2–FaraA and ATRA in p53 knock-down in Raji and MEC1 cells will be measured using the Annexin V-PE/7-AAD kit (BD Bioscience). This study could identify p53-independent mechanisms in 2-FaraA responsive cell lines, or mechanisms of drug resistance in p53 null cells.

6.2 METHODS

Raji, IM9 and MEC1 cells were grown in RPMI medium minus gentamycin. Cells were transiently transfected with p53 siRNA using Lipofectamine RNAiMax and incubated for 24 h. p53 knockdown was confirmed using Western blotting. The transfected cells were harvested and re-cultured in RPMI with gentamycin and treated with 2-FaraA (1 μM, 24 h). Proteins were extracted and analysed by 8-plex iTRAQ on a QSTAR Elite mass spectrometer. ProteinPilot 3.0 software (Paragon™ algorithm) was used to assign protein IDs and determine ratios for differential expression. Data were combined using Microsoft Excel® and proteins of interest were assigned biological pathways using Ingenuity Pathway Analysis software (IPA; Ingenuity® Systems, USA; www.ingenuity.com). Apoptosis was determined by measuring the externalisation of phosphatidyl serine using Annexin V-PE with analysis by flow cytometry.

6.3 RESULTS

6.3.1 Proteomic changes in response to 2-FaraA with p53 knockdown

The 2-FaraA-responsive cells (Raji and IM9) were transfected with small interfering RNA (siRNA) made by Life Technologies (Invitrogen) using a lipid-based transfection system. Figure 6.1A shows the mRNA sequence of p53, boxed areas are regions where the respective siRNAs bind to silence translation of the TP53 gene. After transfection, p53 knockdown was validated by Western blotting using p53 antibody (DO1, Figure 6.1B). In Raji and IM9 cells, RNA 2 and RNA 1, respectively, gave the most efficient p53 knock-down. These respective RNase were used to conduct transfections for the cell lines for subsequent proteomic analysis using ITRAQ. Cells transfected with scrambled RNA sequence was used for each cell line and treatment condition as a negative control. Table 6.1 summarises all the differentially abundant proteins that have opposite expressions (increase and decrease in abundance) when comparing p53 knockdown cells and control RNA cells. Proteins with increased abundance (fold-change >1.5) in knock-down cells and decreased abundance (fold-change <0.66) in control cells after 2-FaraA include PSMD12, ACTR2, BID, CORO7, COX2, HLA-DQB1, ICAM1, NGDN, KIAA0020, and YY1. Proteins decreased in knockdown cells but increased in control cells include RPS16, RPS9, DCTN2, EIF2A, EIF4E, FDPS**,** NAP1L1, PLIN3, PSMA2, SFPQ, UBE2K and EZR. IPA analysis of these differentially abundant proteins suggests several interesting mechanisms (Figure 6.2) such as the activation of the p38 MAPK pathway as well as an increase extracellular VEGF.

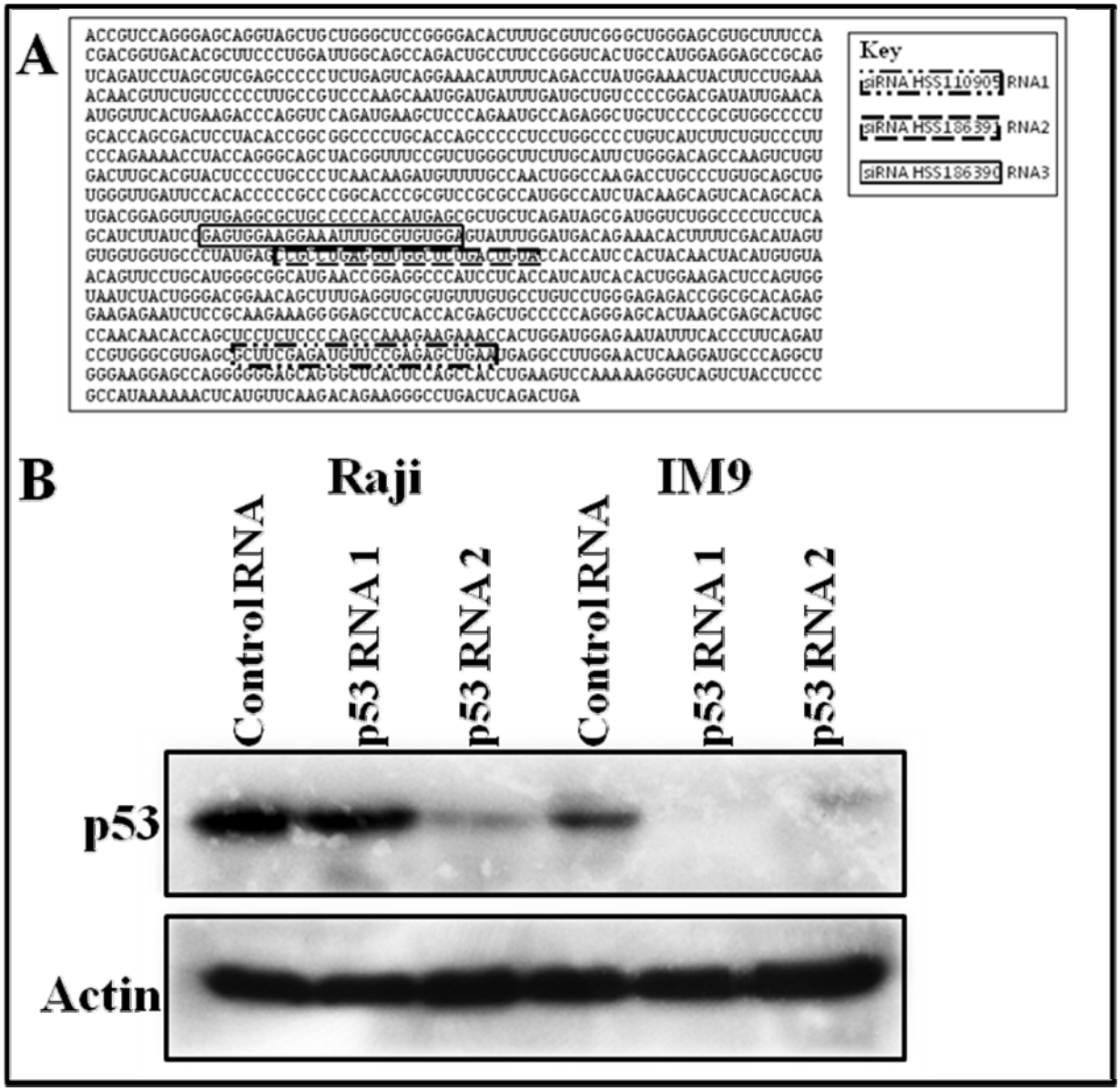

Figure 6.1 siRNA p53 knock-down (A) p53 RNA sequence for open reading frame coding region. The boxed regions show respective areas where the three different siRNA bind. (B) Western blots for p53 and actin (n=2), performed using p53 antibody (clone DO1). The PVDF membrane was then stripped and blotted with antibody against actin (clone C-2)

Table 6.1 Differentially abundant proteins in Raji and IM9 cell lines treated with 2-FaraA with and without p53 knockdown

Accession	Name	% coverage	Peptides (95%)	Fold-change (± 2-FaraA) *p53 knockdown*	Fold-change (± 2-FaraA) *Negative control*	p-value
O00232	26S proteasome non-ATPase regulatory subunit 12 **(PSMD12)**	16.5	4	3.76	0.36	0.167
P62249	40S ribosomal protein S16 **(RPS16)**	60.3	12	0.31	1.75	0.041
P46781	40S ribosomal protein S9 **(RPS9)**	54.1	14	0.23	2.42	0.012
F5H6T1	Actin-related protein 2 **(ACTR2)**	27.5	6	2.32	0.27	0.013
P55957	BH3-interacting domain death agonist **(BID)**	36.4	6	2.45	0.64	0.038
I3L416	Coronin-7 **(CORO7)**	10	4	2.28	1.45	0.017
P00403	Cytochrome c oxidase subunit 2 **(COX2)**	17.6	6	1.80	0.65	0.118
F8WAG8	Dynactin subunit 2 (**DCTN2)**	39.3	12	0.41	2.51	0.001
P05198	Eukaryotic translation initiation factor 2 **(EIF2A)**	24.8	5	0.24	1.99	0.016
D6RBW1	Eukaryotic translation initiation factor 4E **(EIF4E)**	12.2	2	0.28	2.39	0.004
E9PCI9	Farnesyl pyrophosphate synthase **(FDPS)**	16.2	3	0.40	5.39	0.001
Q5Y7D3	HLA class II antigen, DQ **(HLA-DQB1)**	29.9	8	4.07	0.48	0.011
P05362	Intercellular adhesion molecule 1 **(ICAM1)**	7.1	3	3.73	0.58	0.002
Q8NEJ9	Neuroguidin **(NGDN)**	29.2	4	8.40	0.41	0.082
P55209	Nucleosome assembly protein 1-like 1 **(NAP1L1)**	62.9	51	0.22	7.44	0.040
O60664	Perilipin-3 **(PLIN3)**	26.3	7	0.40	4.91	0.001
P25787	Proteasome subunit alpha type-2 **(PSMA2)**	31.2	11	0.16	3.30	0.000
Q15397	Pumilio domain-containing protein **(KIAA0020)**	4.9	2	2.40	0.49	0.026
P23246	Splicing factor, proline- and glutamine-rich **(SFPQ)**	45.8	38	0.39	2.48	0.017
P25490	Transcriptional repressor protein YY1 **(YY1)**	10.6	2	2.32	0.74	0.016
P61086	Ubiquitin-conjugating enzyme E2 K **(UBE2K)**	42	7	0.19	2.61	0.013
P15311	Ezrin **(EZR)**	61.6	40	0.30	1.80	0.006

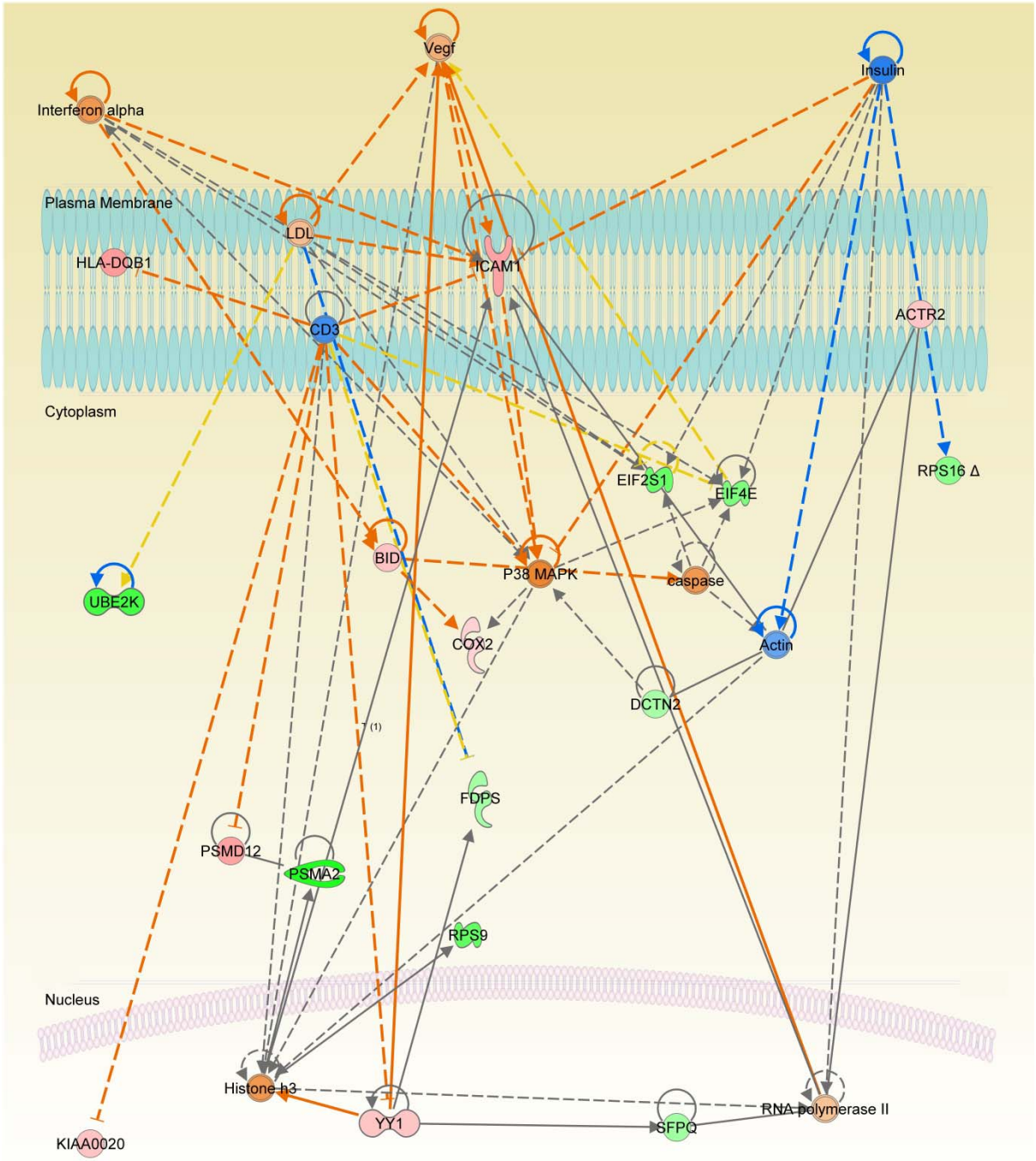

Figure 6.2 Ingenuity Pathway Analysis network of differentially abundant proteins induced after 2-FaraA treatment in p53 knock-down cells. Proteins in red represent increased abundance, and green a decrease in abundance in the p53 interactome. Molecules in orange are predicted to be activated and blue inhibited based on the differential abundance of proteins in the dataset and current knowledge.

6.3.2 p53 knockdown inhibits 2-FaraA and ATRA induced apoptosis

2-FaraA-responsive cells (Raji) and resistant cells (MEC1) were transfected with a negative control RNA sequence, or p53 siRNA 1 or 2, and treated with 2-FaraA (3 μM, 24 h) plus ATRA (1 μM, 24 h). The staining with Annexin V of cell lines with different drug treatments is shown in Figure 6.3. For MEC1, cells treated with control RNA, the combination of 2-FaraA + ATRA increased the exposure of phosphatidyl serine (PS) similar to Figure 5.8 in Chapter 5. In cells transfected with siRNA against p53, 2-FaraA + ATRA no longer induced an increase in Annexin V binding. For Raji cells with control RNA 2-FaraA + ATRA induced Annexin V binding. In p53 knock-down cells, neither drug had an effect.

Table 6.2 summarises the percentage of cells viable, apoptotic (Annexin V binding to PS) and dead (7-AAD binding to cellular DNA). In MEC1, only treatment with 2-FaraA + ATRA induced apoptosis. In cells with control RNA, cells with no treatment had a total of 5% apoptotic and 10% dead compared to the 7.3% apoptotic and 17% dead cells in 2-FaraA treated. In the p53 knock-down MEC1 cells, there was no increase of apoptosis when comparing treated to untreated samples. In Raji cells with control RNA, 2-FaraA treated cells were 12% apoptotic and 11% dead and 2-FaraA + ATRA treated cells were 9% apoptotic and 9.5% dead compared to control cells where only 2.5% were apoptotic and 3.3% were dead. After p53 knockdown the treatment was no longer effective.

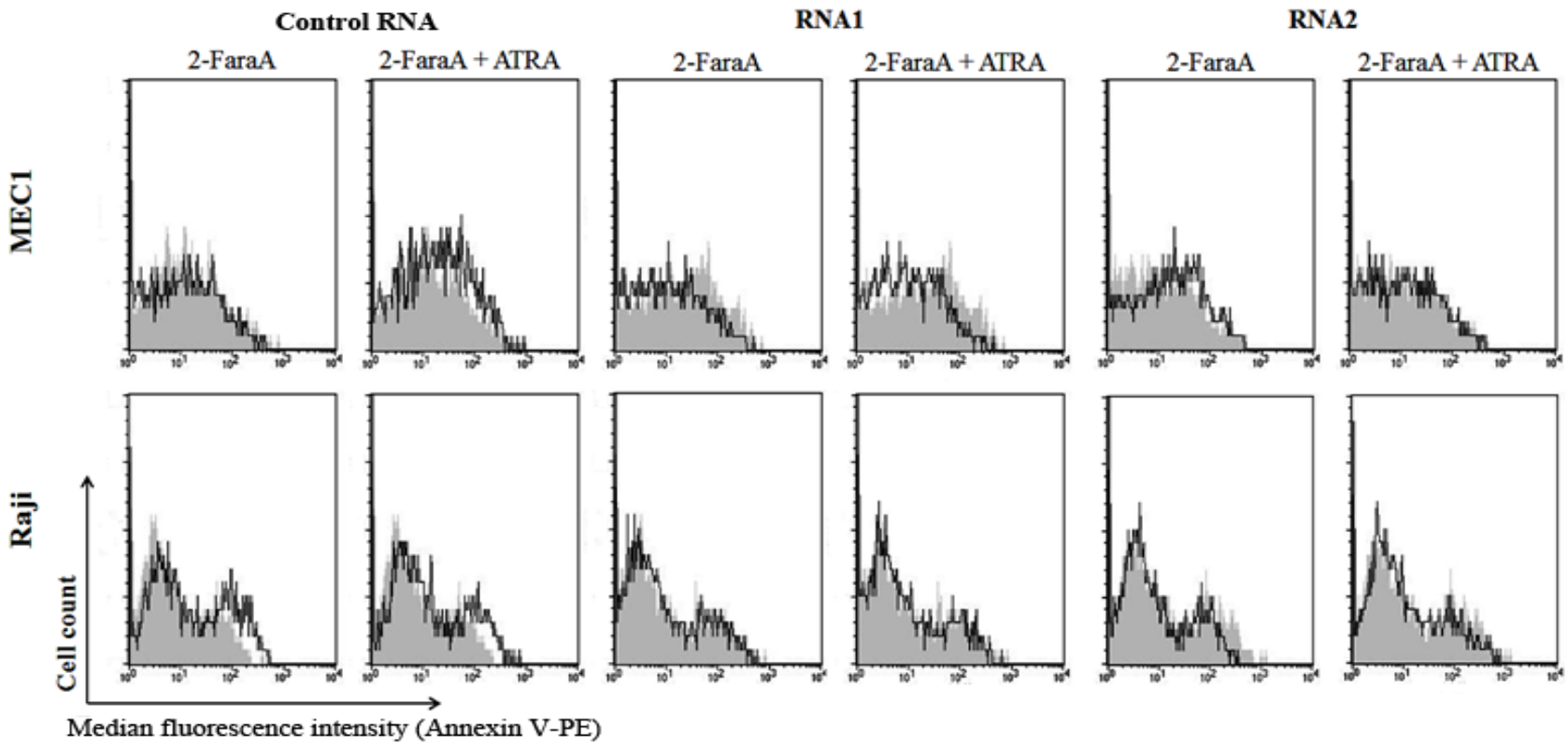

Figure 6.3 Effect of p53 knock-down on apoptosis induced in MEC1 and Raji cells by 2-FaraA ± ATRA. Apoptosis was determined by measuring the externalisation of phosphatidyl serine using Annexin V-PE. MEC1 and Raji cells were treated with 2-FaraA (3 µM, 24 h) ±ATRA (1 µM, 24 h). The grey area represents untreated cells; the black line represents cells incubated with 2-FaraA ±ATRA. A shift in the median fluorescence intensity indicates an increase in externalised phosphatidyl serine (apoptosis).

Table 6.2 Determination of percentage of viable, apoptotic and dead cells using the Annexin V-PE and 7-AAD kit

		Control RNA			**RNA 1**			**RNA 2**		
	(%)	Control	2-FaraA	2-FaraA +ATRA	Control	2-FaraA	2-FaraA +ATRA	Control	2-FaraA	2-FaraA +ATRA
MEC1	Viable	85.00	85	75	81	92	95	94	87	93
	Apoptotic	5.00	5.8	7.3	8	3.5	1.5	2	5	3
	Dead	10.00	9	17	11	4.3	3.5	4	8	4
Raji	Viable	94.00	77	81	87	87	86	80	86	86
	Apoptotic	2.50	12	9	6.8	6.4	7.7	12	5.7	8.1
	Dead	3.30	11	9.5	6	6	5.6	8	8.1	5.8

6.4 DISCUSSION

6.4.1 The role of YY1 in 2-FaraA response in p53 knocked-down Raji and IM9 cells

Expression of the transcription repressor Ying Yan 1 (YY1) increased 2.3-fold in cells with siRNA knock-down of p53. YY1 promotes formation of a p53 MDM2 complex inducing ubiquitination of p53 [193]. YY1 siRNA knockdown induces p53 and subsequent apoptosis in HeLa cells [194]. Our data show a complementary effect where knock-down of p53 increases YY1 protein levels and prevents apoptosis of B-cell lymphomas (Figures 6.3 and 6.4).

An increase in YY1 would increase in extracellular vascular endothelial growth factor (VEGF, Figure 6.2). VEGF mediates angiogenesis in tumours and is a target for cancer therapy. YY1 forms an active complex with hypoxia-inducible factor (HIF) 1α to activate VEGF gene expression [195]. The role of HIF1α in CLL survival is attributed to induction of VEGF [196]. CLL cells constitutively express HIF-1α under normoxia. HIF-1α is able to form an active complex with the transcriptional coactivator p300 and phosphorylated-STAT3 at the VEGF promoter and to recruit RNA polymerase II [197]. High VEGF levels elevate the tissue neovascularization in the marrow [198] and lymph nodes [199] of patients with CLL. Studies in non-Hodgkin's lymphoma showed that VEGF serum level is increased in active lymphomas [200]. In addition, VEGF increases expression of human ICAM1 mRNA in cultured HUVEC cells [201, 202] we have observed an increase of ICAM1 in B-cell lymphomas (Figure 6.2). Thus the increase in YY1 and predicted increase in VEGF may contribute to the chemo-resistance and cell survival in p53 knock-down cells.

6.4.2 Regulation of surface antigens on p53 knock-down cells may increase survival

ICAM1 (CD54) is up-regulated (3.7-fold, Table 6.1) in p53 knock-down (chemo-resistant) Raji and IM9 cells after 2-FaraA treatment. This effect is similar to the observations made in Chapter 3 (Table 3.4) where CLL cells grown on a feeder layer become 2-FaraA-resistant and up-regulate CD54 (4.2-fold). Thus the mechanism of chemo-resistance in both cases may be linked to increases in CD54. ICAM1 modulates cell–cell and cell–matrix adhesion and has roles in inflammation [203]. Studies with human endothelial cells show that ICAM-1 and VEGF synergise to promote production of each other [204] and metastatic potential [205]. For B-cell leukaemias, increased ICAM1 correlates with disease progression [206].

The observed increases in YY1, ICAM1, HLA-DQB1, KIAA0020 and PSMD12 would contribute to inhibition of CD3 activity (Figure 6.2). In T-lymphocytes, CD3 antibody increases transcription of the YY1 gene [207], increases ICAM1 [208, 209] and increased mRNAs of PSMD12, KIAA0020, HLA-DQB1 [210]. Tsoukas *et al*. show that in T-lymphocytes, inhibition of CD3 by binding to CD3 antibody induces proliferation of the cells in response to IL-2 [211]. Our study used B-lymphoid cell lines that may aberrantly express T-cell markers such as CD3 [212], although little is known about the biological significance. For these B-lymphoid cell lines, CD3 is predicted to be down-regulated after p53 knock-down (Figure 6.2) increasing cell viability in p53 knock-down cells (Figure 6.5). We hypothesise that down-regulation of CD3 on B-lymphomas after p53 knock-down would stimulate cell proliferation as for T-lymphomas. For the ITRAQ analysis the transfections were performed in 3 biological replicates for each cell line and treatment condition, however due to the extremely low yield of transfected cells, replicate cells from each condition had to be combined for the ITRAQ analysis. Thus there was only one technical replicate. This limitation should be considered when assessing the results. In addition, the candidates in this

study need to be further validated using techniques such as western blotting or flow cytometry, without which this discussion remains speculative in nature.

6.5 CONCLUSIONS

Comparison of the effects of 2-FaraA treatment of siRNA p53 knock-down and control RNA in Raji and IM9 cells showed a differentially regulated subset of proteins. We compiled a protein list with opposite effects between knockdown and control RNA, i.e. an increase in abundance in knock-down but decrease in abundance in control RNA cells. Proteins up-regulated in p53 knock-down cells included the p53 antagonist, transcription factor YY1 which may lead to an extracellular increase of VEGF contributing to increases cell survival after knock-down. The surface antigen ICAM1 (CD54) is also up-regulated and could modulate metastatic potential. The up-regulation of oncogenic transcription factor YY1 and the increase of adhesion molecule ICAM1 may change the biochemistry of the cells and allow them to become resistant to 2-FaraA-induced apoptosis in p53 knock-down cells.

CHAPTER SEVEN

Summary and Future Directions

7.1 PURPOSE OF THE STUDY

The tumour suppressor protein p53, is a transcription factor responsible for regulating the cell cycle and/or apoptosis in proliferating cells that may be subjected to a variety of stressful events, including DNA damage. Mutations of p53 occur in >50% of human tumours, *TP53* is the most frequently altered gene in cancers [213, 214]. p53 is not only the 'master watchman of the genome', but is also important for the response to many chemotherapeutic agents [215]. However, proteins rarely act alone and p53 is involved in multiple molecular events in various sub-cellular locations. Research into the p53 regulatory network provides a better understanding of the 'p53-centric' cellular responses to chemotherapy-induced DNA-damage in cancer. The overall purpose of this thesis was to contribute to our understanding of the treatment of B-lymphoid cancers by 1) looking at the response of p53 and the family proteins p63 and p73, after 2-FaraA induced DNA-damage, 2) compare the p53 interactome following DNA damage in cells with and without mutations in p53, 3) study the DNA-damage phosphorylation cascades in the p53 interactome and 4) analyse the effects of p53 knock-down on fludarabine-responsive cells. Detailed below are the novel p53-centric mechanisms and network events elucidated in this study that may be involved in 2-FaraA-induced DNA-damage in B-lymphoid cancers.

7.2 P53, P63, P73 RESPONSES TO 2-FARAA

Henrich and Christopherson (2008) showed that p53 accumulates in the nuclei of Raji cells treated with 2-FaraA (3 μM, 24 h), prior to apoptosis. As an extension of these observations, we demonstrate here that the 2-FaraA-sensitive cell lines, Raji and IM9, accumulate p53 in their nuclei, mitochondria and cytosol. p53 accumulates at the mitochondria of Raji earlier than in the nucleus suggesting that initiation of apoptosis in these cells may be dependent on

the roles of p53 at mitochondria, prior to effects on gene expression in the nucleus. In Raji cells, accumulation of p53 is attributed to increased *de novo* p53 protein expression with the concomitant increase in mRNA levels, and to inhibition of p53 degradation due to phosphorylation. 2-FaraA also induces phosphorylation and accumulation of lower molecular weight derivatives of p53, p63 and p73 in the nuclei of Raji cells that may have roles in inducing apoptosis. Several distinct molecular weight and phosphorylated forms of p63 exist in the nuclear, mitochondrial and cytosolic fractions of Raji following 2-FaraA treatment. 1D Western blots showed that mitochondrial p63 in the 2-FaraA-sensitive cell lines (Raji and IM9), exists as dimers and tetramers, while in the cell lines resistant to 2-FaraA (MEC1 and U266), p63 is found as a monomer. These data provide further insight into the effects and mechanisms of action of 2-FaraA, and define patterns of response of the p53 family members in sub-cellular compartments of B-lymphoid cancers.

7.3 INTERACTION OF HSP90 WITH P53

We used mass spectrometry and Western blotting to observe dissociation of HSP90 from p53 in response to 2-FaraA treatment (Figures 4.4 and 4.5). Interaction of HSP90 with p53 has been reported. Structural analysis has shown that the DNA-binding domain of p53 interacts with the middle and C-terminal domains of HSP90 [216, 217]. Walerych et al. showed that in human fibroblasts, HSP90 forms a complex with wild-type p53 partially unfolding it and preventing p53 regulation of p21 gene expression. Treatment with HSP90 inhibitors promoted the transcriptional activities of p53 [159]. Additionally, Lin et al. showed that treatment with the HSP90 inhibitor geldanamycin restored the functionality of mutated p53 [218]. Our study shows for the first time that in the human B-cell lines Raji and IM9, treatment with 2-FaraA dissociates HSP90 from p53. This does not occur in the p53-mutated

MEC1 cell line, however, treatment of MEC1 with the HSP90 inhibitor AUY922, did result in a significant increase in the expression of p21 and p27, known p53 targets. In addition, in MEC1 cells the combination of 2-FaraA with AUY922 was synergistic in inducing apoptosis (Figures 4.6 and 4.7). Taken together, these data suggest that HSP90 may negatively regulate the function of p53 in both 2-FaraA-responsive and resistant cells. HSP90 inhibition may restore sensitivity to DNA damaging agents in tumour cells with truncated forms of p53 releasing p53 from a misfolded state [218]. HSP90 and p53 undergo post-translational modifications that mediate their interactions with other binding partners. HSP90 and p53 are both phosphoproteins, containing several phospho-residues. Using a phospho-proteomic approach, we found phosphorylation of HSP90 at serine 254 (Table 5.1 and Supplementary Figure S5.1). This phosphorylation of HSP90 has been shown to modulate the affinity of HSP90 for apoptotic protease activating factor 1 (APAF1). In leukaemias, reduced phosphorylation of serine 254 of HSP90 strengthens the HSP90–APAF1 complex [185]. In the context of the current study, phosphorylation at HSP90 at serine 254 may reduce the availability of HSP90 to bind p53 resulting in release of p53 to induce apoptosis. Motif analysis programs indicate that casein kinase 2 alpha 1 (CSNK2a1) is primarily responsible for the HSP90 phosphorylation at Serine 254 (Table 5.1, Figure 5.6 C), suggesting that activation of CSNK2a1 may enhance chemotherapeutic efficacy.

7.4 RIBOSOME BIOGENESIS

Ribosome biogenesis is essential for cell survival. Defects in ribosome production result in p53 stabilization and induce p53-dependent inhibition of cell proliferation. Dysregulation of ribosome biogenesis results in release of RPL5, RPL11 and RPL23. These ribosomal proteins bind to MDM2 causing its dissociation from p53 [186, 187]. We show that 2-FaraA treatment

reduces the levels of RPL11 (Supplementary Table 5.2) and RPL23 (Chapter 4, Figure 4.4) present in the p53 interactome, that in turn is likely to decrease the level of Mdm2. In addition, we observed the differential phosphorylation of proteins involved with the production of rRNA (Figure 5.5). The production of 5.8S rRNA is an essential step in ribosomal biogenesis [187] and is predicted to be inhibited in our study. Lastly we observe the phosphorylation of Histone H1.4 at residue serine 187. Studies show that such phosphorylation regulates transcription of ribosomal and steroid hormone-responsive genes [188] that may also regulate rRNA. This is the first study to document the effects of 2-FaraA on ribosomal biogenesis in B-lymphoid cancer cell lines.

7.5 RETINOIC ACID INDUCED APOPTOSIS IN 2-FARAA RESISTANT CELLS

Upstream molecule analysis of post translational regulation, of a subset of proteins found in our phosphoproteomic study indicates the up-regulation of pathways involved in response to synthetic retinoic acid (CD473) treatment, after 2-FaraA treatment. As no synthetic retinoic acids were added to the cells, natural cellular retinoic acid (RA) and its receptors may underlie 2-FaraA-induced apoptosis. To test this hypothesis, Western blots of RARα were conducted on extracts from Raji and MEC1 cells before and after 2-FaraA (Supplementary Figure S5.2). These results indicate that RARs and naturally occurring RA may indeed have roles in 2-FaraA-induced apoptosis. Previously published studies support this hypothesis, demonstrating that for acute myeloid leukemia (AML) cells, treatment with 2-FaraA + all-*trans* RA (ATRA) induced more apoptosis than fludarabine alone, and suggested that ATRA may induce p53–independent apoptosis in AML cells [191, 192]. Co-administration of ATRA and 2-FaraA in our study showed that the combination does induce apoptosis in the p53 mutant MEC1 cell line while either drug as a single agent does not (Figure5.8).

7.6 SUMMARY OF OUTCOMES

This project revealed some interesting cellular mechanisms by which apoptosis may be induced in cells responsive to 2-FaraA (Raji and IM9). Figure 7.1 illustrates the p53-centric mechanisms in the cells after treatment. 2-FaraA is incorporated into DNA and induces strand breaks. This triggers the accumulation of kinases and phosphatases and other proteins involved in the regulation of transcription. Together they result in the accumulation and phosphorylation of p53, p63 and p73 in the nucleus that control the transcription of proteins required for apoptosis and cell cycle arrest. We demonstrated that kinase activation results in the phosphorylation of HSP90 in the cytosol that causes dissociation of HSP90-p53 complexes. Cytosolic p53 is then free to either translocate to the nucleus or mitochondria to induce apoptosis via MOMP or regulate energy metabolism. Kinase activation also phosphorylates H2AX, which is an essential step in the DNA repair process. Our data also showed de-phosphorylation of the SNARP complex in the cells following 2-FaraA-treatment, known to be responsible for cyclin D1 mRNA stability. The resulting decrease in cyclin D1 levels is likely to result in cell cycle arrest. We have also shown that 2-FaraA induced DNA damage induces the post-translational regulation (de/phosphorylation) of proteins involved in ribosomal biogenesis, leading to dysregulation of this process.

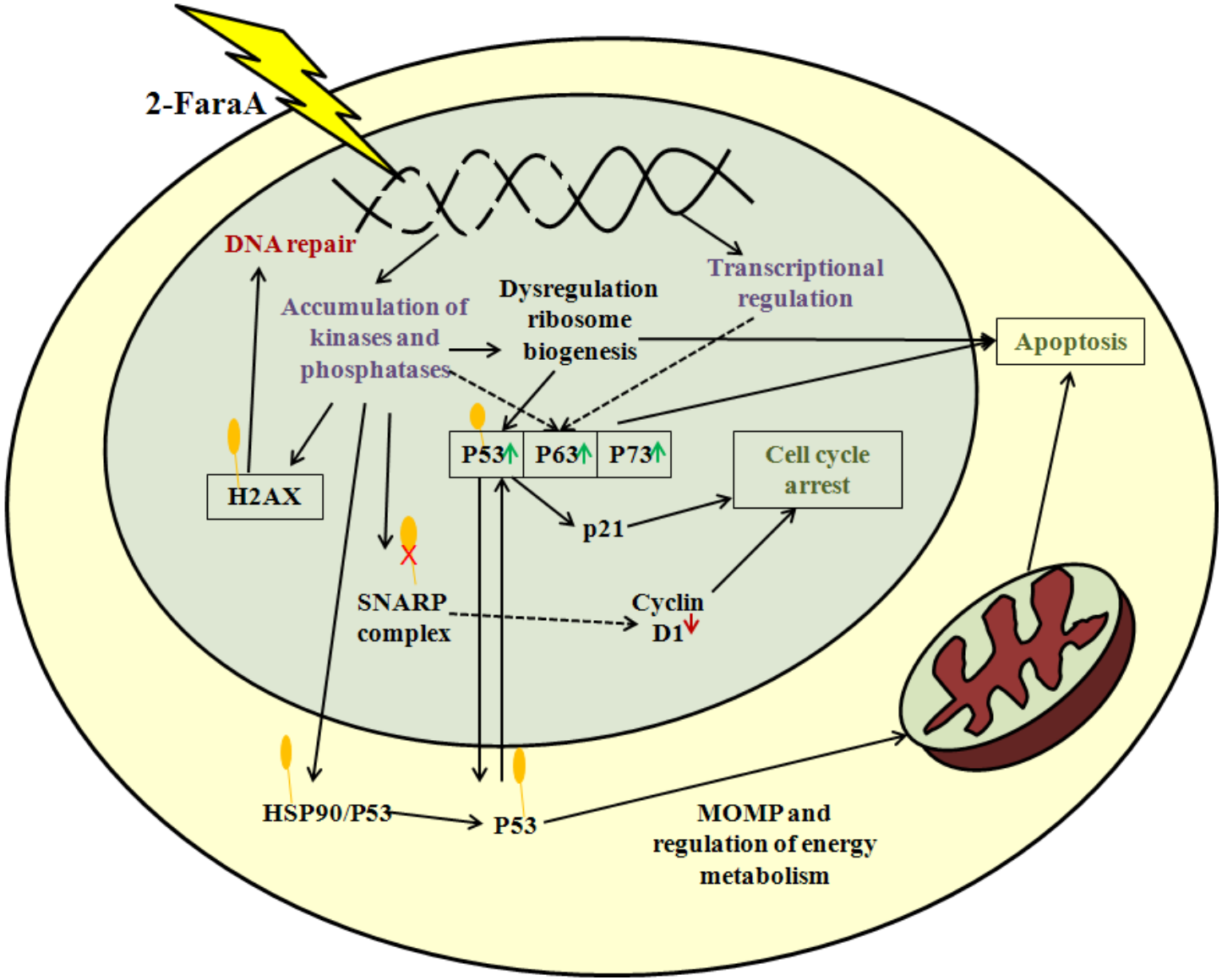

Figure 7.1 Schematic of the p53-centric mechanisms of 2-FaraA induced apoptosis. 2-FaraA is incorporated into DNA and induces strand breaks. This triggers the accumulation of kinases, phosphatases and proteins involved in the regulation of transcription. Resulting in accumulation and phosphorylation of p53, p63 and p73 in the nucleus of the cell and transcription of proteins required for apoptosis and cell cycle arrest. Phosphorylation of HSP90 in the cytosol causes dissociation of HSP90-p53 complexes. Cytosolic p53 may translocate to the nucleus or the mitochondria to induce apoptosis via MOMP or regulate energy metabolism. Phosphorylated H2AX, aids in the DNA repair process.

7.7 FUTURE DIRECTIONS

This thesis proposes novel p53-centric mechanisms that underlie 2-FaraA-induced apoptosis in B-lymphoid cancers. Protein phosphorylation plays a major role in this model. One approach to further validate the outcomes would be to inhibit the kinases identified using commercially available inhibitors or siRNA knockdown. Then using proteomic approaches, it might be possible to identify the impact of these kinases on the sensitivity of cells to 2-FaraA. One step further would be to determine the roles of specific sites of phosphorylation using site-specific mutagenesis to mutate these sites on a protein. For example, our data suggest that mutation of serine 254 in HSP90 would likely affect the response of Raji cells to 2-FaraA, as HSP90 could not be phosphorylated resulting in an inability to dissociate from p53.

ICAM1 (CD54), a plasma membrane protein, was significantly higher in 2-FaraA-resistant cells, following either p53 knockdown or co-culture of primary CLL cells with a CD40L feeder layer. Expression of this antigen may be a key marker for therapeutic outcome with 2-FaraA as it increases in cells that acquire 2-FaraA resistance. It would be interesting to investigate whether CD54 levels on B-CLL of patients correlated with resistance to 2-FaraA using a high-throughput flow cytometry assay. Further studies might determine whether blocking signalling through CD54, using a CD54 monoclonal antibody, enhances sensitivity to 2-FaraA.

Similarly, in p53 knockdown cells, there is an increase in the transcription factor YY1, a known proto-oncogene. In p53 mutant cells, it would be interesting to explore combination treatments that target the YY1 pathway such as the proteasome inhibitor NPI-0052 (salinosporamide A) [219], plus 2-FaraA.

p53 has been heavily researched in cancer studies since its discovery by Sir David Lane in 1979 [44] with over 67,000 published studies. In this thesis, we have contributed further novel data to add to p53 mechanisms with B-lymphoid cancers and 2-FaraA treatment. Further research may lead to advanced treatment strategies for patients suffering from B-lymphoid cancers.

APPENDIX I

List of Materials

MATERIALS	COMPANIES
2-Fluoroadenine-9-β-D-arabinofuranoside	Sigma-Aldrich (St. Louis, MO, USA)
2-Mercaptoethanol	Bio-Rad (Hercules, CA, USA)
3-[(3-cholamidopropyl)dimethylammonio]-1-propanesulfonate (CHAPS)	Sigma-Aldrich (St. Louis, MO, USA)
3-[N-Morpholine]propanesulfonic acid (MOPS)	Sigma-Aldrich (St. Louis, MO, USA)
4-(2-hydroxyethyl)-1-piperazineethanesulfonic acid (HEPES buffer)	Sigma-Aldrich (St. Louis, MO, USA)
Acrylamide/Bis solution, 40%, 37.5 1 (2.6% C)	Bio-Rad (Hercules, CA, USA)
Agarose biotech grade	Sigma-Aldrich (St. Louis, MO, USA)
all trans-RETINOIC ACID	Sigma-Aldrich (St. Louis, MO, USA)
Ammonium chloride (NH_4Cl)	Sigma-Aldrich (St. Louis, MO, USA)
Ammonium hydroxide solution (NH4OH)	Sigma-Aldrich (St. Louis, MO, USA)
Ammonium persulfate (APS)	Sigma-Aldrich (St. Louis, MO, USA)
Ammonium sulfate [(NH4)2SO4]	Sigma-Aldrich (St. Louis, MO, USA)
Benzonase	Sigma-Aldrich (St. Louis, MO, USA)
Bio-Lyte 3–10 carrier ampholytes	Bio-Rad (Hercules, CA, USA)
Bis[sulfosuccinimidyl] suberate (BS3)	Thermo Scientific (Rockford, IL USA)
Bovine serum albumin (BSA)	Sigma-Aldrich (St. Louis, MO, USA)
Bromophenol blue	Sigma-Aldrich (St. Louis, MO, USA)
Calcium chloride (CaCl2)	Ajax Finechem Pty Ltd (Auburn, NSW, Australia)
Calf intestinal alkaline phosphatase (CIP) Kit	New England Biolabs (Ipswich, MA, USA)
Caspase Inhibitor Z-VAD-FMK	Promega (Sydney, NSW, Australia)
Coomassie G-250	Sigma-Aldrich (St. Louis, MO, USA)
Countess ™ automated cell counter system	Invitrogen Life Technologies (Mulgrave, NSW, Australia)
Criterion XT Bis-Tris Gel	Bio-Rad (Hercules, CA, USA)
Diethyl pyrocarbonate (DEPC)	Sigma-Aldrich (St. Louis, MO, USA)
Dimethyl sulfoxide (DMSO)	Merck Pty Ltd (Kilsyth, VIC, Australia)
Diploma Instant Skim Milk Powder	Fonterra Foodservice (North Ryde,

	NSW, Australia)
Dithiothreitol (DTT)	Sigma-Aldrich (St. Louis, MO, USA)
Dithiothreitol (DTT)	Sigma-Aldrich (St. Louis, MO, USA)
DNAse, RNAse free cell culture flasks (25 cm^2, 75 cm^2 and 175 cm^2)	Greiner (Frickenhausen, Germany)
Dynabeads Protein G	Invitrogen Life Technologies (Mulgrave, NSW, Australia)
Ethanol	Ajax Finechem Pty Ltd (Auburn, NSW, Australia)
Ethidium Bromide (EtBr) 10mg/ml	Invitrogen Life Technologies (Mulgrave, NSW, Australia)
Ethylenediaminetetraacetic acid (EDTA)	Sigma-Aldrich (St. Louis, MO, USA)
Fast SYBER Green Master Mix	Applied Biosystems (Carlsbad, CA, USA)
Foetal Calf Serum (FCS)	Invitrogen Life Technologies (Mulgrave, NSW, Australia) JRH Biosciences inc.(Lenexa, USA)
Formaldehyde	Sigma-Aldrich (St. Louis, MO, USA)
Formamide	Sigma-Aldrich (St. Louis, MO, USA)
Forward and reverse primers	Sigma-Aldrich (St. Louis, MO, USA)
Gentamycin (50 mg/mL)	Invitrogen Life Technologies (Mulgrave, NSW, Australia)
Glycerol	Sigma-Aldrich (St. Louis, MO, USA)
Glycine	Sigma-Aldrich (St. Louis, MO, USA)
Glycolic acid	Sigma-Aldrich (St. Louis, MO, USA)
Halt Phosphatase Inhibitor Cocktail	Thermo Scientific (Rockford, IL USA)
Hydrochloric acid 32% (HCl)	Ajax Finechem Pty Ltd (Auburn, NSW, Australia)
Immobilon-P PVDF membrane	Millipore (Temecula, CA, USA)
Lipofectamine RNAiMAX	Invitrogen Life Technologies (Mulgrave, NSW, Australia)
Magnesium dichloride ($MgCl_2$)	Ajax Finechem Pty Ltd (Auburn, NSW,

Methanol	Australia) Ajax Finechem Pty Ltd (Auburn, NSW, Australia)
Mineral oil (biotechnology grade)	Sigma-Aldrich (St. Louis, MO, USA)
MMTS	Thermo Scientific (Rockford, IL USA)
N,N,N',N'-tetramethylethyl-ethylenediamine (TEMED)	Sigma-Aldrich (St. Louis, MO, USA)
Okadaic acid	Calbiochem (Darmstadt, Germany)
Opti-MEM® Reduced Serum Medium	Invitrogen Life Technologies (Mulgrave, NSW, Australia)
Pan-caspase inhibitor Z-VAD-FMK	BD Bioscience (San Jose, CA, USA)
Paraformaldehyde powder, 95%	Sigma-Aldrich (St. Louis, MO, USA)
Phenylmethylsufonyl fluoride (PMSF)	Sigma-Aldrich (St. Louis, MO, USA)
Phosphoric acid	Sigma-Aldrich (St. Louis, MO, USA)
Pierce Trypsin Protease, MS Grade	Thermo Scientific (Rockford, IL USA)
Potassium chloride (KCl)	Ajax Finechem Pty Ltd (Auburn, NSW, Australia)
Potassium hydrogen carbonate (KHCO3)	Ajax Finechem Pty Ltd (Auburn, NSW, Australia)
Precision Plus Protein™ Dual Color molecular weight standards	Bio-Rad (Hercules, CA, USA)
Precission Plus Protein™ unstained molecular weight standards	Bio-Rad (Hercules, CA, USA)
Propidium iodide	Sigma-Aldrich (St. Louis, MO, USA)
Protease inhibitor cocktail	Sigma-Aldrich (St. Louis, MO, USA)
ReadyStrip™ IPG Strips	Bio-Rad (Hercules, CA, USA)
RNase A	Invitrogen Life Technologies (Mulgrave, NSW, Australia)
RPMI-1640 medium HEPES modification	Sigma-Aldrich (St. Louis, MO, USA)
Saponin	Sigma-Aldrich (St. Louis, MO, USA)
Sodium cyanoborodeuteride (NaBD3CN)	Sigma-Aldrich (St. Louis, MO, USA)
Sodium cyanoborohydride (NaBH3CN)	Sigma-Aldrich (St. Louis, MO, USA)

Sodium dodecyl sulfate (SDS)	Sigma-Aldrich (St. Louis, MO, USA)
Sodium fluoride (NaF)	Sigma-Aldrich (St. Louis, MO, USA)
Sodium orthovanadate (Na_3VO_4)	Sigma-Aldrich (St. Louis, MO, USA)
Sucrose	Ajax Finechem Pty Ltd (Auburn, NSW, Australia)
Sulfobetaine 3–10	Sigma-Aldrich (St. Louis, MO, USA)
Surfact-Amps® NP-40	Sigma-Aldrich (St. Louis, MO, USA)
SYPRO®Ruby Protein Gel Stain	Invitrogen Life Technologies (Mulgrave, NSW, Australia)
Thiourea	Sigma-Aldrich (St. Louis, MO, USA)
Titansphere Titanium dioxide (TiO2) beads, (5µm)	GL Science Inc, Japan
Tributyl phosphine (TBP)	Sigma-Aldrich (St. Louis, MO, USA)
Triethyl Ammonium Bicarbonate (TEAB)	Sigma-Aldrich (St. Louis, MO, USA)
Tris (2-carboxyethyl) phosphine HCl (TCEP)	Sigma-Aldrich (St. Louis, MO, USA)
Tris-hydroxymethyl-methylamine (TRIS)	Ajax Finechem Pty Ltd (Auburn, NSW, Australia)
TRI™ Reagent Solution	Sigma-Aldrich (St. Louis, MO, USA)
Triton-X-100	Sigma-Aldrich (St. Louis, MO, USA)
Trypan Blue Solution (0.4%)	Sigma-Aldrich (St. Louis, MO, USA)
TWEEN® 20	Sigma-Aldrich (St. Louis, MO, USA)
Urea	Sigma-Aldrich (St. Louis, MO, USA)
XT MES Running Buffer	Bio-Rad (Hercules, CA, USA)

APPENDIX II

SUPPLEMENTARY DATA

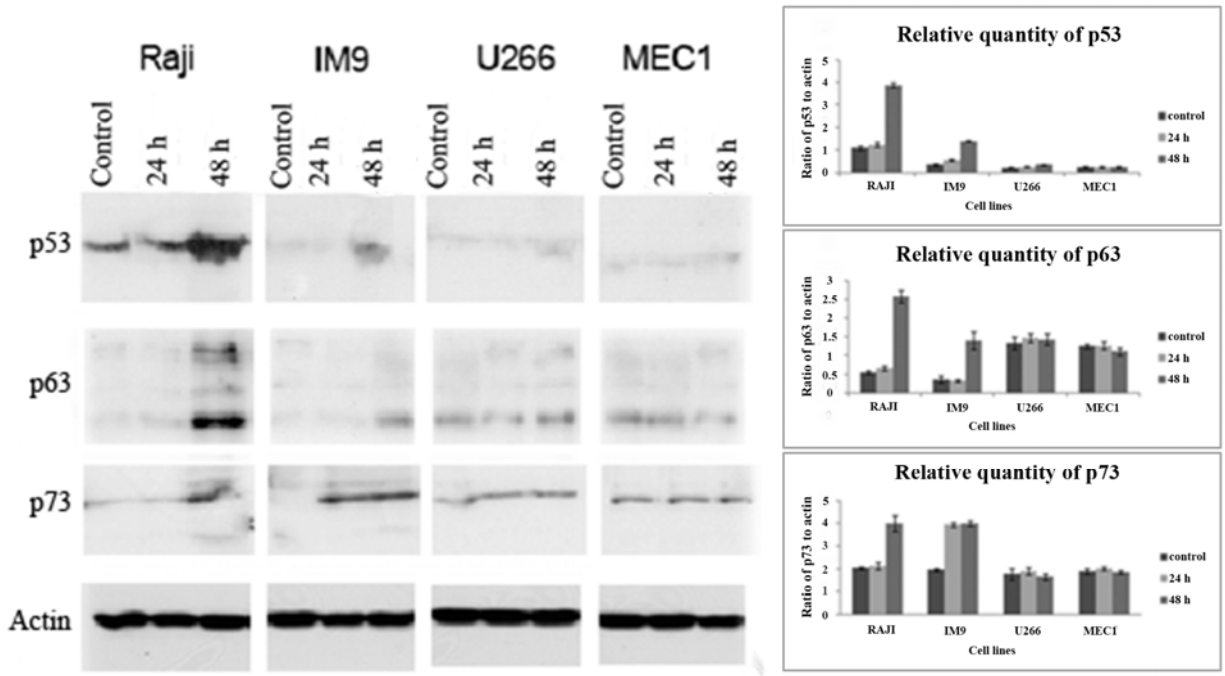

Supplementary Figure SF3.1 1D Western blots for p53 family members in whole lysates of different cell lines treated with 2-FaraA (3 μM). Cells were harvested and lysed in Laemmli buffer. Changes in protein levels can be compared with changes in mRNA levels in Figure 3.6.

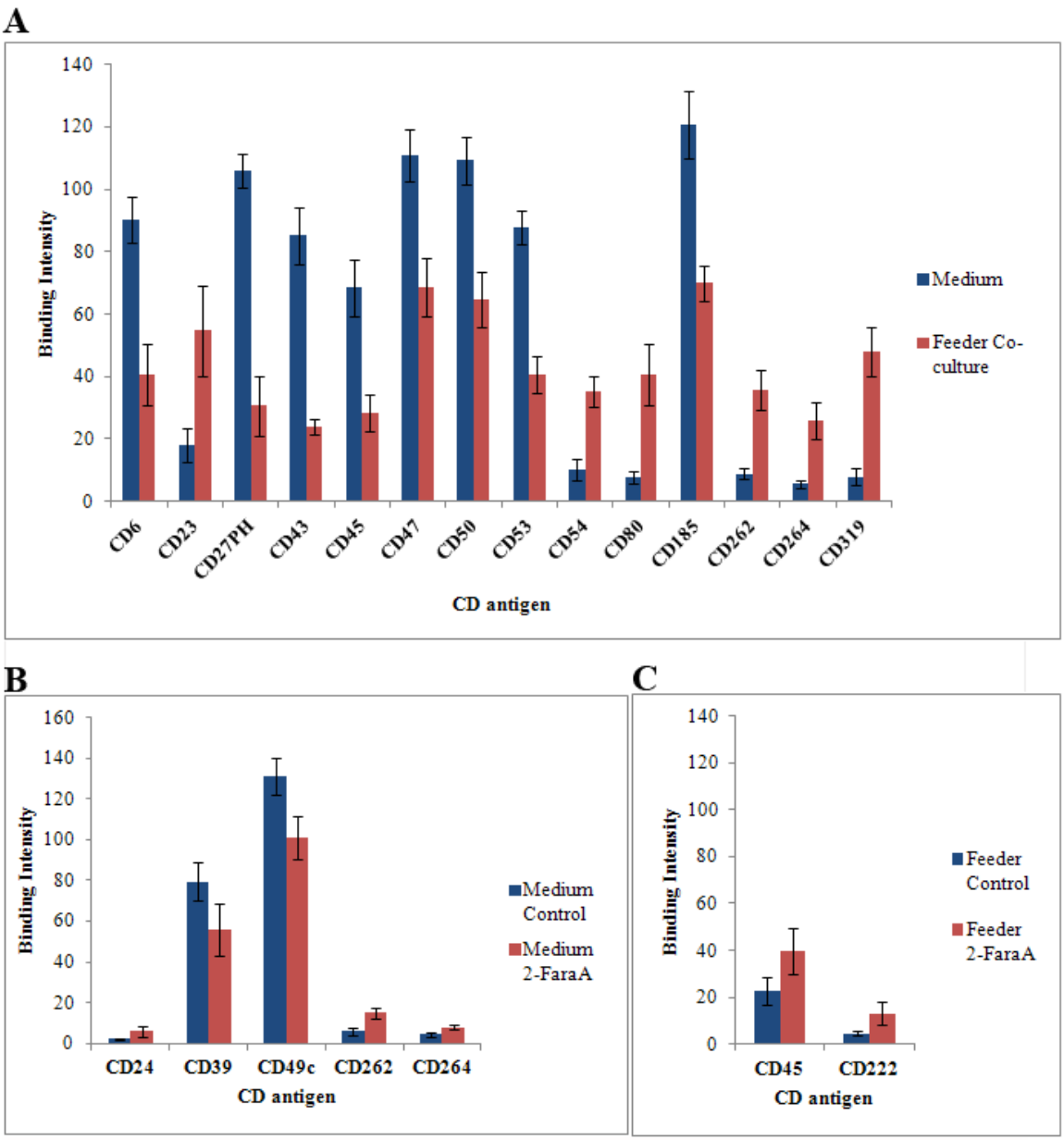

Supplementary Figure SF3.2 Differentially expressed antigens with p-value of < 0.05 in (A) media vs feeder co-culture, (B) media with 2-FaraA (C) feeder co-culture with 2-FaraA, after 24 h incubation. Standard error of mean (SEM) was used for error bars using 4 CLL samples and 2 technical replicates (n=8).

Supplementary Table ST4.1: List of p53 binding proteins identified in MEC1 (p53 truncated) cells

Uniprot ID	Name	Peptides (95%)	Sequence coverage (%)	Primary localisation	Biological processes
IPI:IPI00337387.3	Isoform 3 of Pre-mRNA-processing factor 40 homolog A	2	8.3	Nucleus	Nucleic acid metabolism
IPI:IPI00607818.2	MYH14 variant protein	28	31.1	Cytosol	Cell growth/maintenance
IPI:IPI00844172.1	Myosin	9	17.5	Cytosol	Cell growth/maintenance
IPI:IPI00873982.2	Myosin heavy chain 11	41	44.4	Cytosol	Cell growth/maintenance
HCD2	3-hydroxyacyl-CoA dehydrogenase type-2	2	18	Mitochondria	Metabolism ; Energy pathways
RS10	40S ribosomal protein S10	2	14.6	Ribosome	Protein metabolism
RS15A	40S ribosomal protein S15a	5	46.2	Ribosome	Protein metabolism
RLA1	60S acidic ribosomal protein P1	5	63.2	Ribosome	Protein metabolism
RL26	60S ribosomal protein L26	3	35.9	Ribosome	Protein metabolism
RL28	60S ribosomal protein L28	2	15.3	Ribosome	Protein metabolism
RL31	60S ribosomal protein L31	2	25.6	Ribosome	Protein metabolism
IPI:IPI00790339.1	ACTG1 22 kDa protein	99	61.6	Cytosol	Cell growth/maintenance
ACTC	Actin, alpha cardiac muscle 1	27	57.8	Cytosol	Cell growth/maintenance

ACTH	Actin, gamma-enteric	85	94.4	Cytosol	Cell growth/maintenance
IPI:IPI00470573.1	Actin-related protein 2 isoform a	6	22.6	Cytosol	Cell motility ; Cell growth/maintenance
ARF3	ADP-ribosylation factor 3	10	59.1	Cytosol	Cell signalling
ARF5	ADP-ribosylation factor 5	5	45.6	Cytosol	Cell signalling
A2MG	Alpha-2-macroglobulin	2	6.2	Cytosol	Protein Metabolism
APOA1	Apolipoprotein A-I	8	33.3	Cytosol	Transport
SYRC	Arginyl-tRNA synthetase, cytoplasmic	4	7.9	Cytosol	Protein metabolism
AKNA	AT-hook-containing transcription factor	2	10.4	Nucleus	Nucleic acid metabolism
A8K2X8	Chaperonin containing TCP1, subunit 5	4	17.4	Cytosol	Protein metabolism
CCD61	Coiled-coil domain-containing protein 61	2	11.2	Unknown	Unknown
COR1A	Coronin-1A	6	23.4	Cytosol	Cell growth/maintenance
MCM3	DNA replication licensing factor MCM3	2	7.9	Mitochondria	unknown
MCM5	DNA replication licensing factor MCM5	4	11.6	Nucleus	Nucleic acid metabolism
DREB	Drebrin	7	21	Cytosol	Cell growth/maintenance
EHD4	EH domain-containing protein 4	3	20.3	Cytosol	Cell signalling

FSCN1	Fascin	2	5.7	Cytosol	Cell growth/maintenance
GNAI2	Guanine nucleotide-binding protein G(i), alpha-2 subunit	2	6.2	Cytosol	Cell signalling
HSP71	Heat shock 70 kDa protein 1	4	31.5	Cytosol	Protein metabolism
Q86YQ1	Hemoglobin alpha-2	10	78	Cytosol	Transport
Q5T6W5	Heterogeneous nuclear ribonucleoprotein K	6	25.2	Nucleus	Nucleic acid metabolism
H2AZ	Histone H2A.Z	9	66.4	Nucleus	Nucleic acid metabolism
H2B1M	Histone H2B type 1-M	2	19.1	Nucleus	Nucleic acid metabolism
H31	Histone H3.1	2	43.4	Nucleus	Nucleic acid metabolism
MX1	Interferon-induced GTP-binding protein Mx1	4	15.1	Cytosol	Cell signalling
IPI:IPI00376005.2	Isoform 2 of Eukaryotic translation initiation factor 5A-1	2	25.5	Cytosol	Protein metabolism
IPI:IPI00220154.1	Isoform 3 of Myosin-Va	4	9.9	Cytosol	Cell growth/maintenance
IPI:IPI00828082.1	Isoform 4 of Myosin-XVIIIa	55	38.9	Endoplasmic recticulum	Cell growth/maintenance
KINH	Kinesin-1 heavy chain	2	8	Mitochondria	Cell growth/maintenance
IPI:IPI00425404.2	Kinesin-like protein KIF21A	8	15.9	Cytosol	Cell growth/maintenance
KIF2C	Kinesin-like protein KIF2C	2	5.5	Cytosol	Cell growth/maintenance
Q549N7	Mutant beta-globin	12	74.2	Cytosol	Transport

MYL6B	Myosin light chain 6B	9	66.4	Cytosol	Cell growth/maintenance
MRLC2	Myosin regulatory light chain MRLC2	37	79.7	Cytosol	Cell growth/maintenance
MRLC3	Myosin regulatory light chain MRLC3	41	80.1	Cytosol	Cell signalling
MYH11	Myosin-11	16	22.5	Cytosol	Cell growth/maintenance
MYO1C	Myosin-Ic	6	13.1	Cytosol	Cell growth/maintenance
MYO1D	Myosin-Id	16	21.6	Cytosol	Cell growth/maintenance
MYO1G	Myosin-Ig	12	18.6	Cytosol	Cell growth/maintenance
OFD1	Oral-facial-digital syndrome 1 protein	3	18.6	Nucleus	biological process unknown
PCM1	Pericentriolar material 1 protein	7	13.4	Centrosome	Cell growth/maintenance
PDIA1	Protein disulfide-isomerase	2	7.1	Cytosol	Protein metabolism
RB11B	Ras-related protein Rab-11B	2	17.9	Cytosol	Cell signalling
RAB14	Ras-related protein Rab-14	2	26.1	Cytosol	Cell signalling
RAB6A	Ras-related protein Rab-6A	2	29.8	Cytosol	Cell signalling
Q53G20	Ribosomal protein L14 variant	6	28	Ribosome	protein metabolism
Q59GK9	Ribosomal protein L21 variant	6	34.4	Ribosome	protein metabolism
Q6IPX5	Ribosomal protein S2	3	28.7	Ribosome	protein metabolism

IPI:IPI00793696.1	RPL24 19 kDa protein	4	45.2	Ribosome	Protein metabolism
IPI:IPI00872430.1	RPS8 25 kDa protein	5	33.6	Cytosol	Protein metabolism
A4QN19	SEC16A protein	26	26.2	Endoplasmic recticulum	Cell motility ; ER organization and biogenesis ; Protein transport
STAT1	Signal transducer and activator of transcription 1-alpha/beta	8	19.2	Cytosol	Nucleic acid metabolism
SON	SON protein	12	12.5	Cytosol	Nucleic acid metabolism
SMC2	Structural maintenance of chromosomes protein 2	2	11.5	Mitochondria	Biological processes unknown
IPI:IPI00414101.4	TOP2A Isoform 2 of DNA topoisomerase 2-alpha	6	12.3	Nucleus	Nucleic acid metabolism
IPI:IPI00217709.1	TOP2B Isoform Beta-1 of DNA topoisomerase 2-beta	5	18.9	Cytosol	Nucleic acid metabolism
SSRD	Translocon-associated protein subunit delta	2	13.9	Endoplasmic recticulum	Transport
TMOD1	Tropomodulin-1	6	35.7	Cytosol	Cell growth/maintenance
PTN6	Tyrosine-protein phosphatase non-receptor type 6	7	27.1	Cytosol	Cell signalling
Q3MIH3	Ubiquitin A-52 residue ribosomal protein fusion product 1	2	60.2	Ribosome	protein metabolism

Supplementary Table ST4.2: List of p53 binding proteins identified in Raji and IM9 cells following vehicle Control or 2-FaraA (3 μM, 24 h) and binding proteins unchanged following treatment.

Uniprot ID	Name	Peptides (95%)	Sequence coverage (%)	Primary localisation	Biological processes
Control (Raji and IM9)					
A8K3Q9	Ribosomal protein L14 (RPL14)	4	22.7	Ribosomes	Protein metabolism
ATPB	ATP synthase subunit beta, mitochondrial	6	30.4	Mitochondria	Energy pathways
HS90B	Heat shock protein HSP 90-beta	4	18.2	Cytosol	Cell signalling
IPI:IPI00382470.3	HSP90AA1 heat shock protein 90kDa alpha (cytosolic), class A member 1 isoform 1	20	33.6	Cytosol	Protein metabolism
IPI:IPI00793523.1	RPL23A Putative uncharacterized protein RPL23A	2	24.1	Cytosol	Nucleic acid metabolism
KPYM	Pyruvate kinase isozymes M1/M2	12	34.8	Cytosol	Energy pathways
PO210	Nuclear pore membrane glycoprotein 210	2	4.9	Nucleus	Transport
ROA1L	Heterogeneous nuclear ribonucleoprotein A1-like protein	3	21.3	Unknown	Nucleic acid metabolism
TAGL2	Transgelin-2	3	26.1	Unknown	Unknown
CLH1	Clathrin heavy chain 1	9	14.8	Cytosol	Cell growth/maintenance
DDX21	Nucleolar RNA helicase 2	4	19.2	Nucleolus	Energy pathways
LPPRC	Leucine-rich PPR motif-containing protein, mitochondrial	2	12	Nucleus	Nucleic acid metabolism
NOL5	Nucleolar protein 5	2	4.5	Nucleolus	Nucleic acid metabolism
PYR1	CAD protein	5	8.4	Cytosol	Energy pathways

RL13	60S ribosomal protein L13	2	19	Ribosomes	Protein metabolism
RL26L	60S ribosomal protein L26-like 1	2	29.7	Ribosomes	Unknown
SYEP	Bifunctional aminoacyl-tRNA synthetase	2	7.8	Cytosol	Protein metabolism
2-FaraA (Raji and IM9)					
6PGD	6-phosphogluconate dehydrogenase, decarboxylating	2	12.8	Cytosol	Energy pathways
C1TC	C-1-tetrahydrofolate synthase, Cytosolic	3	7.6	Cytosol	Energy pathways
DDX39	ATP-dependent RNA helicase DDX39	5	17.3	Nucleus	Nucleic acid metabolism
DYHC1	Cytosolic dynein 1 heavy chain 1	3	8.8	Cytosol	Energy pathways
GRHPR	Glyoxylate reductase/hydroxypyruvate reductase	2	11.6	Cytosol	Energy pathways
HNRH1	Heterogeneous nuclear ribonucleoprotein H	5	18.9	Nucleus	Nucleic acid metabolism
IPI:IPI00176692.7	32 kDa protein	2	19.9	Unknown	Unknown
IPI:IPI00848150.1	Tubulin beta1	10	57.6	Cytosol	Cell growth/maintenance
MY18A	Myosin-XVIIIa	2	16.5	Cytosol	Cell growth/maintenance
MYH11	Myosin-11	18	45.3	Cytosol	Cell growth/maintenance
Q53HR5	Elongation factor 1-alpha (Fragment)	6	28.8	Cytosol	Regulation of cell cycle
Q5T6W5	Heterogeneous nuclear ribonucleoprotein K	3	10.1	Nucleus	Nucleic acid metabolism
RL6	60S ribosomal protein L6	6	33.3	Nucleolus	Protein metabolism
SPEE	Spermidine synthase	2	10.6	Cytosol	Energy pathways
HNRPM	Heterogeneous nuclear ribonucleoprotein M	7	22.7	Nucleus	Nucleic acid metabolism

MCM5	DNA replication licensing factor MCM5	2	8.2	Nucleus	Nucleic acid metabolism
In BOTH Control and Treated (Raji and IM9)					
C1QBP	Complement component 1 Q subcomponent-binding protein, mitochondrial	2	11	Mitochondria	Immune response
CH60	60 kDa heat shock protein, mitochondrial	3	18.3	Cytosol	Protein folding, Apoptosis and Signal transduction
EFTU	Elongation factor Tu, mitochondrial	6	23.2	Mitochondria	Protein metabolism
G3P	Glyceraldehyde-3-phosphate dehydrogenase	11	55.5	Cytosol	Energy pathways
HNRPU	Heterogeneous nuclear ribonucleoprotein U	7	18	Nucleus	Nucleic acid metabolism
LDHA	L-lactate dehydrogenase A chain	4	23.8	Cytosol	Energy pathways
LMNB1	Lamin-B1 OS=Homo sapiens	2	3.9	Nucleus	Cell growth/maintenance
MYH9	Myosin-9 OS=Homo sapiens	86	54.1	Cytosol	Cell growth/maintenance
PARP1	Poly [ADP-ribose] polymerase 1	12	24.7	Nucleus	Protein metabolism
PHB2	Prohibitin-2	5	33.1	Nucleus	Nucleic acid metabolism
PLSL	Plastin-2	8	31.3	Cytosol	Cell signalling
PRKDC	DNA-dependent protein kinase catalytic subunit	23	17.3	Nucleus	Cell signalling
Q5UGI3	Ubiquitin C splice variant - Homo sapiens	4	71.9	Cytosol	Protein metabolism
SP16H	FACT complex subunit SPT16	8	24.5	Nucleus	Nucleic acid metabolism
SYDC	Aspartyl-tRNA synthetase, Cytosolic	2	21.4	Cytosol	Protein metabolism

TBA1C	Tubulin alpha-1C chain	12	40.1	Cytosol	Cell growth/maintenance

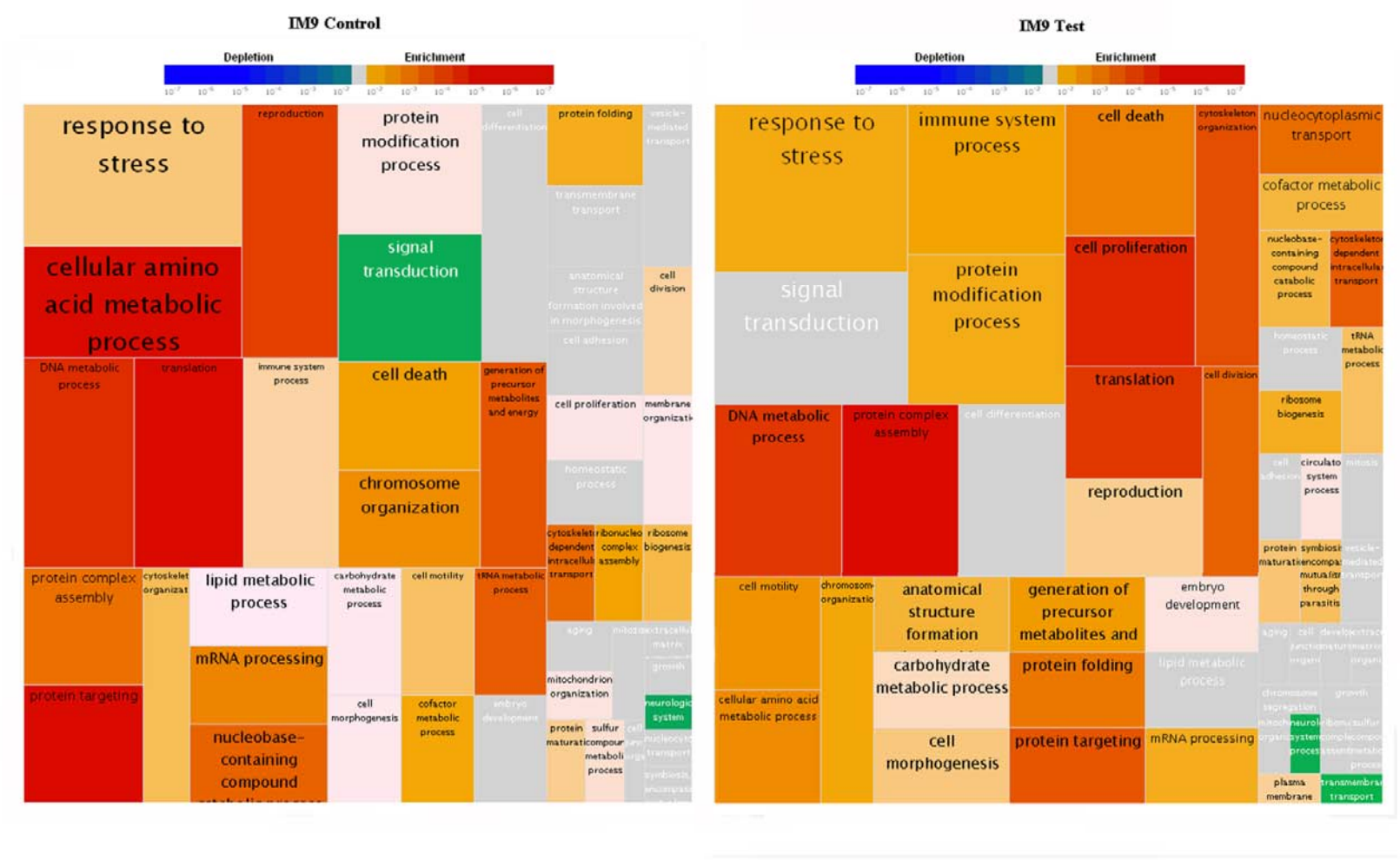

Supplementary Figure SF4.1 BioMyn generated map of biological functions in the p53 interactomes of IM9 in Control and 2-FaraA treated cells. The size of the boxes is an indication of the number of proteins in each category

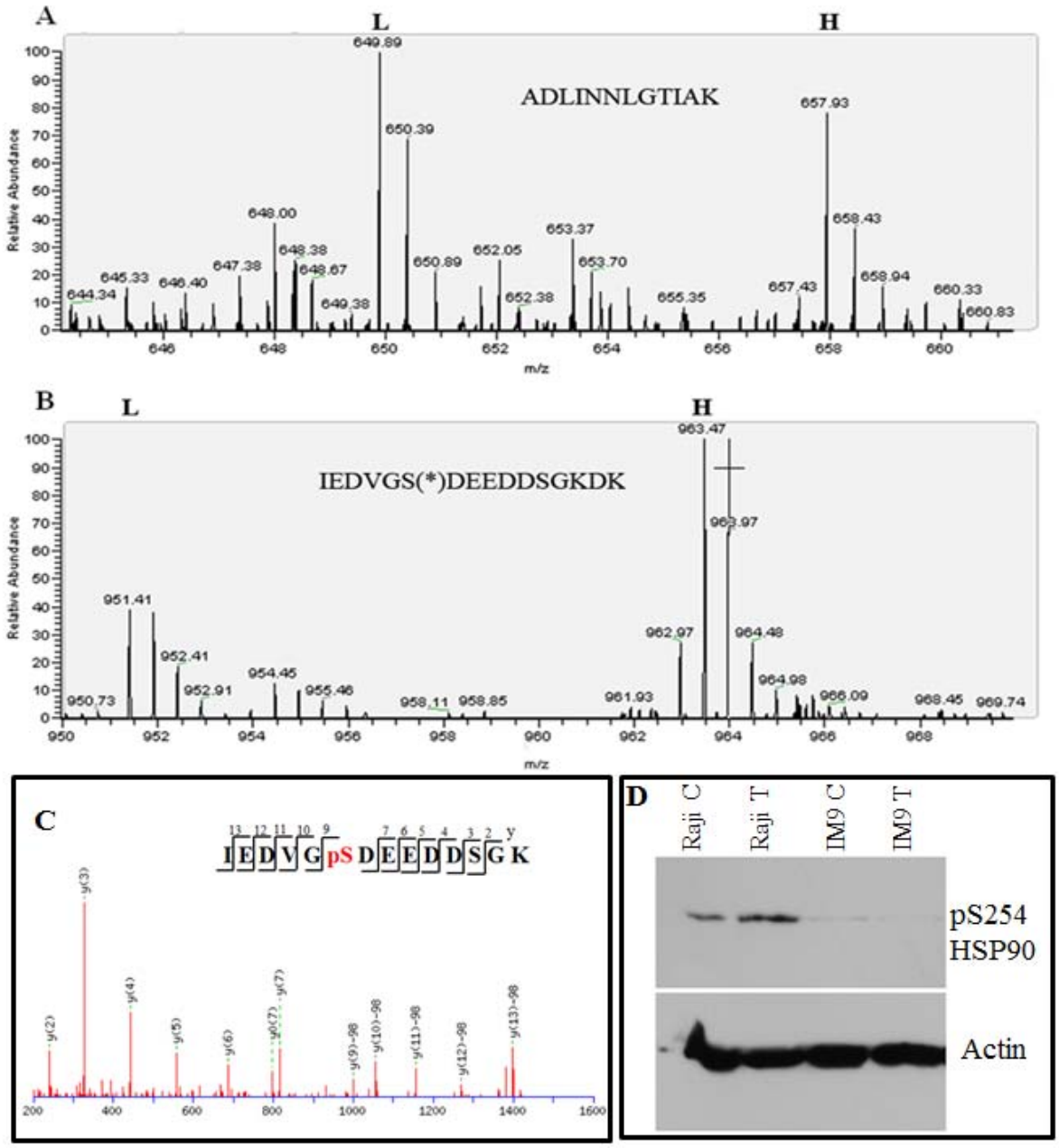

Supplementary Figure SF5.1 Spectra of 2 peptides of HSP90 (A) unmodified and (B) phosphorylated (ser254) using stable isotopic dimethyl labelling. Indicated are the light-labeled (L) peptides from vehicle control cells and the heavy-labeled (H) peptides from 2-FaraA treatment. (C) MS/MS ion spectra of phosphopeptide IEDVGSDEEDDSGK (D) western blots using antibody against phospho S254 of HSP90 and loading control actin after 2-FaraA treatment (24 h, 3 µM).

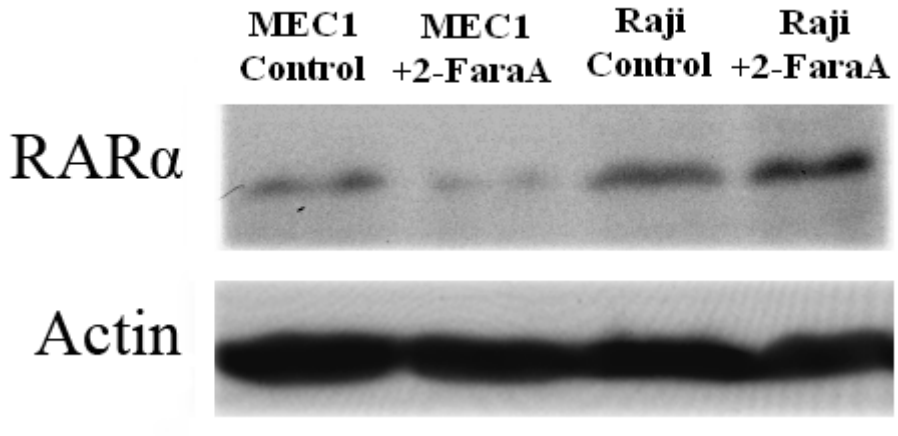

Supplementary Figure SF5.2 Western blots of RARα with loading control actin in MEC1 and Raji cells after 2-FaraA, 24 h.

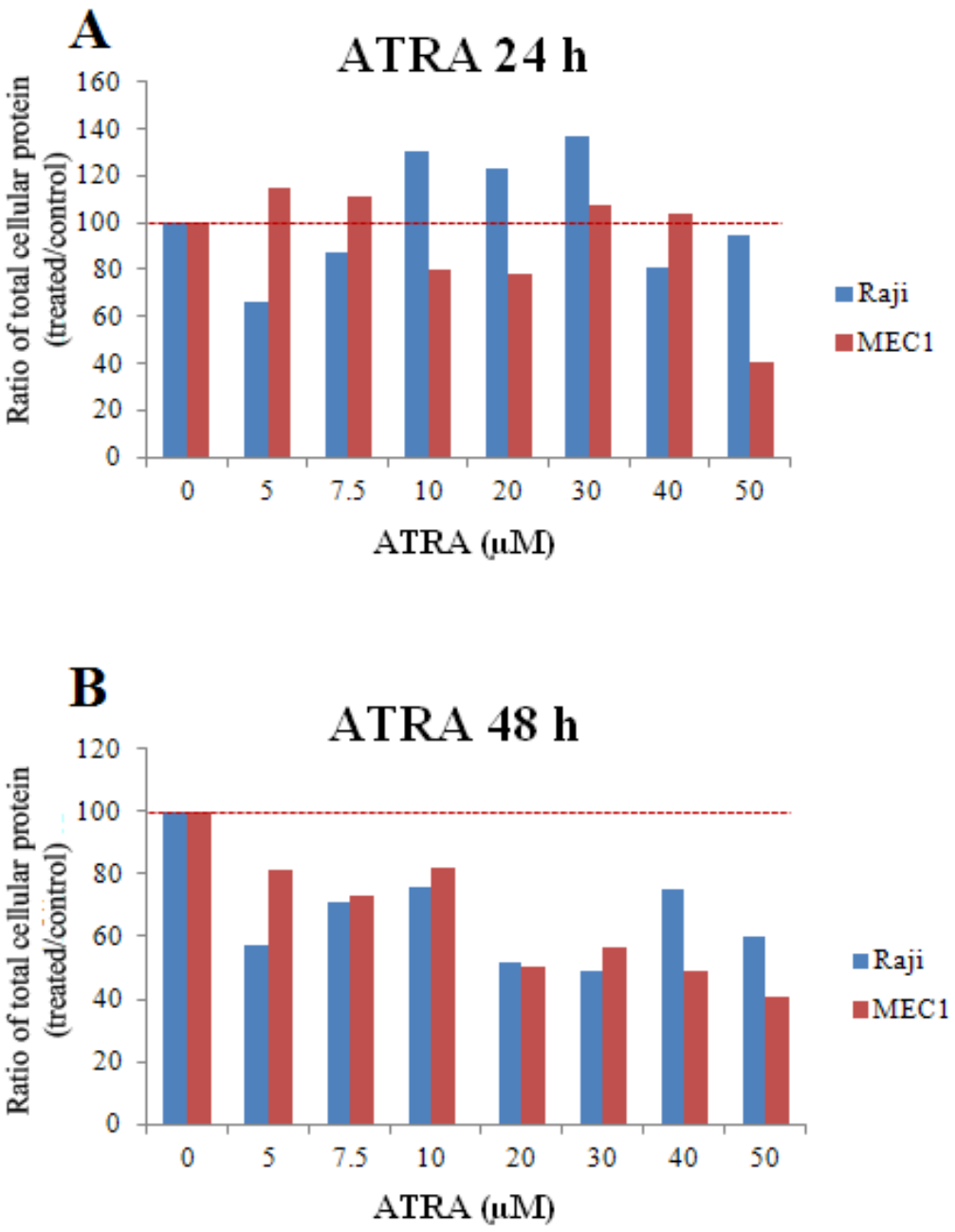

Supplementary Figure SF5.3 Sulforhodamine B Assay for Raji and MEC1 cells after (A) 24 h and (B) 48 h of treatment with all *trans*-retinoic acid. At 100% indicated by the dotted red line the number of cells in control and treated wells are equivalent indicating no effect.

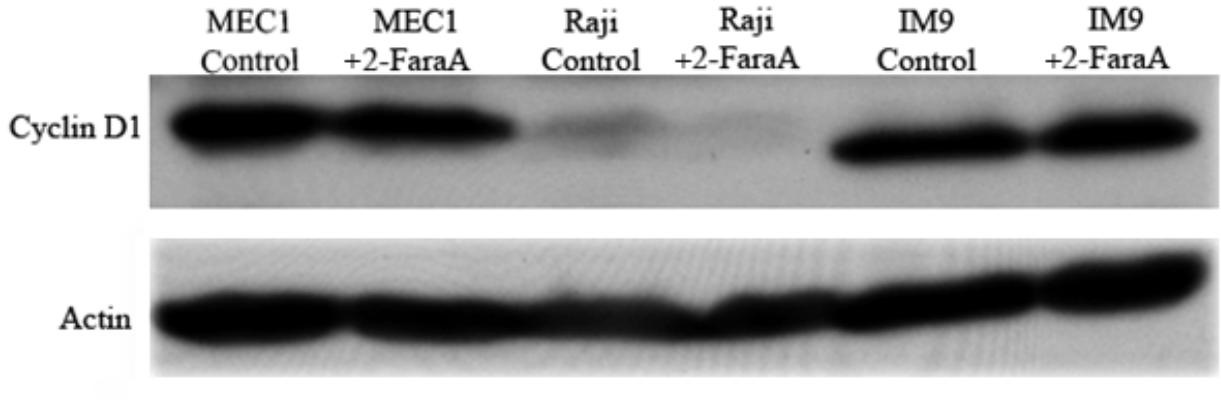

Supplementary Figure SF5.4 Western blots of Cyclin D1 after 2-FaraA treatment of MEC1, Raji and IM9 cells (24 h).

Supplementary Table ST5.1 2-FaraA induced differential phosphorylation of peptides in Raji cells after 24 h treatment

Accession	Protein Names	Gene Names	Sequence	Modification	Ratio H/L normalized	P-value
Q9NYF8	Bcl-2-associated transcription factor 1	BCLAF1	YSPSQNSPIHHIPSR	Phospho (STY)	0.53	0.0249
Q14137	Ribosome biogenesis protein BOP1	BOP1	IGDEYAEDSSDEEDIR	2 Phospho (STY)	0.57	0.0278
Q14137	Ribosome biogenesis protein BOP1	BOP1	SFIPSLVEK	Unmodified	1.03	0.6148
Q13185	Chromobox protein homolog 3	CBX3	RKSLSDSESDDSK	2 Phospho (STY)	0.64	0.0003
Q13185	Chromobox protein homolog 3	CBX3	KVEEAEPEEFVVEK	Unmodified	1.05	0.8329
Q9H6F5	Coiled-coil domain-containing protein 86	CCDC86	ALVEFESNPEETREPGSPPSVQR	Phospho (STY)	0.75	0.0235
Q9H6F5	Coiled-coil domain-containing protein 86	CCDC86	LQQGAGLESPQGQPEPGAASPQR	Phospho (STY)	0.55	0.0093

Q14839	Chromodomain-helicase-DNA-binding protein 4	CHD4	MSQPGSPSPK	Phospho (STY)	1.85	0.0259
Q14247	Src substrate cortactin	CTTN	TQTPPVSPAPQPTEER	2 Phospho (STY)	0.55	0.0230
Q9NR30	Nucleolar RNA helicase 2	DDX21	AEPSEVDMNSPK	Phospho (STY)	0.71	0.0188
Q9NR30	Nucleolar RNA helicase 2	DDX21	GVTFLFPIQAK	Unmodified	1.15	0.8663
Q9NR30	Nucleolar RNA helicase 2	DDX21	IGVPSATEIIK	Unmodified	1.09	0.8591
Q9NR30	Nucleolar RNA helicase 2	DDX21	EGAFSNFPISEETIK	Unmodified	1.09	0.5990
P16104	Histone H2A.x	H2AFX	KATQASQEY	Phospho (STY)	3.78	0.0420
P16104	Histone H2A.x	H2AFX	TSATVGPK	Unmodified	1.04	0.7849
P16401	Histone H1.5	HIST1H1B	ALAAGGYDVEK	Unmodified	2.81	0.0187
P16401	Histone H1.5	HIST1H1B	ALAAGGYDVEK	Unmodified	0.88	0.8353
P16401	Histone H1.5	HIST1H1B	ATGPPVSELITK	Unmodified	0.77	0.2516
P16401	Histone H1.5	HIST1H1B	KALAAGGYDVEK	Unmodified	1.25	0.9820
P16401	Histone H1.5	HIST1H1B	KATGPPVSELITK	Unmodified	0.88	0.8174
P16401	Histone H1.5	HIST1H1B	SETAPAETATPAPVEK	Unmodified	1.04	0.0341
P10412	Histone H1.4	HIST1H1E	KAPKSPAK	Phospho (STY)	NaN	0.0026
P10412	Histone H1.4	HIST1H1E	KASGPPVSELITK	Phospho (STY)	1.72	0.0398
P10412	Histone H1.4	HIST1H1E	SGVSLAALK	Unmodified	1.36	0.5363
P10412	Histone H1.4	HIST1H1E	SETAPAAPAAPAPAEK	Unmodified	0.99	0.5267
P10412	Histone H1.4	HIST1H1E	GTGASGSFK	Unmodified	2.45	0.8751
P68431	Histone H3.1	HIST1H3A	KSAPATGGVK	Phospho (STY)	0.27	0.0216

P68431	Histone H3.1	HIST1H3A	EIAQDFKTDLR	Unmodified	0.10	0.0213
P68431	Histone H3.1	HIST1H3A	EIAQDFK	Unmodified	0.82	0.4665
P68431	Histone H3.1	HIST1H3A	SAPATGGVK	Unmodified	0.57	0.2753
P68431	Histone H3.1	HIST1H3A	RVTIMPK	Unmodified	0.74	0.4548
P68431	Histone H3.1	HIST1H3A	STELLIR	Unmodified	0.97	0.7265
P68431	Histone H3.1	HIST1H3A	YRPGTVALR	Unmodified	0.83	0.6305
P62805	Histone H4	HIST1H4A	DAVTYTEHAK	Unmodified	3.30	0.0279
P62805	Histone H4	HIST1H4A	DNIQGITK	Unmodified	0.55	0.0097
P62805	Histone H4	HIST1H4A	TVTAMDVVYALKR	Oxidation (M)	0.67	0.0395
P62805	Histone H4	HIST1H4A	DNIQGITKPAIR	Unmodified	1.15	0.1936
P62805	Histone H4	HIST1H4A	VFLENVIR	Unmodified	2.83	0.7431
B4DR52	Histone H2B	HIST2H2BF	HAVSEGTK	Unmodified	6.51	0.0072
B4DR52	Histone H2B	HIST2H2BF	EIQTAVR	Unmodified	3.65	0.6028
B4DR52	Histone H2B	HIST2H2BF	LLLPGELAK	Unmodified	4.84	0.0951
B4DR52	Histone H2B	HIST2H2BF	IAGEASR	Unmodified	2.00	0.7612
P17096	High mobility group protein HMG-I/HMG-Y	HMGA1	SSQPLASK	Phospho (STY)	19.26	0.0066
P17096	High mobility group protein HMG-I/HMG-Y	HMGA1	EPSEVPTPK	Unmodified	0.84	0.2241
P17096	High mobility group protein HMG-I/HMG-Y	HMGA1	KQPPVSPGTALVGSQK	Unmodified	0.75	0.4337
A6NEL0	Non-histone chromosomal protein HMG-14	HMGN1	TEESPASDEAGEK	2 Phospho (STY)	0.58	0.0212
A6NEL0	Non-histone chromosomal protein	HMGN1	TEESPASDEAGEK	Unmodified	0.96	0.7263

	HMG-14					
Q1KMD3	Heterogeneous nuclear ribonucleoprotein U-like protein 2	HNRNPUL2	SKPAGSDGER	Phospho (STY)	0.60	0.0015
P08238	Heat shock protein HSP 90-beta	HSP90AB1	IEDVGSDEEDDSGKDK	Phospho (STY)	2.02	0.0442
P08238	Heat shock protein HSP 90-beta	HSP90AB1	ADLINNLGTIAK	Unmodified	1.29	0.9058
P08238	Heat shock protein HSP 90-beta	HSP90AB1	YIDQEELNK	Unmodified	1.26	0.5478
P08238	Heat shock protein HSP 90-beta	HSP90AB1	EGLELPEDEEEK	Unmodified	1.23	0.9829
P08238	Heat shock protein HSP 90-beta	HSP90AB1	GVVDSEDLPLNISR	Unmodified	1.33	0.7723
P08238	Heat shock protein HSP 90-beta	HSP90AB1	IDIIPNPQER	Unmodified	1.58	0.2931
P08238	Heat shock protein HSP 90-beta	HSP90AB1	SLVSVTK	Unmodified	1.93	0.3194
Q96ST2	Protein IWS1 homolog	IWS1	EAEDSDSDDNIKR	Phospho (STY)	0.62	0.0358
P49736	DNA replication licensing factor MCM2	MCM2	GLLYDSDEEDEERPAR	Phospho (STY)	1.76	0.0478
J3QRS3	Myosin regulatory light chain 12B;Myosin regulatory light polypeptide 9;Myosin regulatory light chain 12A	MYL12B	ATSNVFAMFDQSQIQEFK	Oxidation (M),Phospho (STY)	0.56	0.0079
J3QRS3	Myosin regulatory light chain 12B;Myosin regulatory light polypeptide 9;Myosin regulatory light chain 12A	MYL12B	EAFNMIDQNR	Oxidation (M)	0.74736	0.2912
P19338	Nucleolin	NCL	TLVLSNLSYSATEETLQEVFEK	Unmodified	2.04	0.0295

P19338	Nucleolin	NCL	VVVSPTKK	Phospho (STY)	1.71	0.0353
P19338	Nucleolin	NCL	ALELTGLK	Unmodified	1.13	0.7806
P19338	Nucleolin	NCL	ALVATPGK	Unmodified	1.18	0.9394
P19338	Nucleolin	NCL	GLSEDTTEETLK	Unmodified	1.31	0.6919
Q14978-2	Nucleolar and coiled-body phosphoprotein 1	NOLC1	GSPRPQAPK	Phospho (STY)	0.72	0.0056
Q14978-2	Nucleolar and coiled-body phosphoprotein 1	NOLC1	SPAVKPAAAPK	Unmodified	1.12	0.839097468
Q14978-2	Nucleolar and coiled-body phosphoprotein 1	NOLC1	VVPSDLYPLVLGFLR	Unmodified	0.90	0.1536
Q9H1E3	Nuclear ubiquitous casein and cyclin-dependent kinase substrate 1	NUCKS1	NSQEDSEDSEDKDVK	2 Phospho (STY)	0.54	0.0354
P38159	RNA-binding motif protein, X chromosome;RNA-binding motif protein, X chromosome, N-terminally processed	RBMX	GLPPSMER	Oxidation (M),Phospho (STY)	0.72	0.0452
P38159	RNA-binding motif protein, X chromosome;RNA-binding motif protein, X chromosome, N-terminally processed	RBMX	DVYLSPR	Phospho (STY)	0.67	0.0196
P38159	RNA-binding motif protein, X chromosome;RNA-binding motif protein, X chromosome, N-terminally processed	RBMX	LFIGGLNTETNEK	Unmodified	0.49	0.0245
P38159	RNA-binding motif protein, X chromosome;RNA-binding motif	RBMX	ALEAVFGK	Unmodified	0.55	0.2984

P38159	protein, X chromosome, N-terminally processed RNA-binding motif protein, X chromosome;RNA-binding motif protein, X chromosome, N-terminally processed	RBMX	RGPPPPPR	Unmodified	0.40	0.0696
P38159	RNA-binding motif protein, X chromosome;RNA-binding motif protein, X chromosome, N-terminally processed	RBMX	SAPSGPVR	Unmodified	1.12	0.9287
P38159	RNA-binding motif protein, X chromosome;RNA-binding motif protein, X chromosome, N-terminally processed	RBMX	VEQATKPSFESGR	Unmodified	0.93	0.9367
P05388	60S acidic ribosomal protein P0	RPLP0	KEESEESDDDMGFG LFD	Oxidation (M),Phospho (STY)	1.96	0.0478
Q9NW H9	SAFB-like transcription modulator	SLTM	DGQDAIAQSPEKESK	Phospho (STY)	0.71	0.0043
E9PCT 1	Serine/arginine repetitive matrix protein 1	SRRM1	HRPSPPATPPPK	2 Phospho (STY)	0.51	0.0086
E9PCT 1	Serine/arginine repetitive matrix protein 1	SRRM1	KAASPSPQSVR	2 Phospho (STY)	0.73	0.0430
E9PCT 1	Serine/arginine repetitive matrix protein 1	SRRM1	RASPSPPPKR	2 Phospho (STY)	0.75	0.0471
Q9UQ3 5	Serine/arginine repetitive matrix protein 2	SRRM2	SATRPSPSPER	2 Phospho (STY)	1.31	0.0403

E9PHK9	Treacle protein	TCOF1	LGAGEGGEASVSPEKTSTTSK	Phospho (STY)	2.13	0.0150
B0QYS7	Transcription factor EB	TFEB	VHGLPTTSPSGMNMAELAQQVVK	2 Oxidation (M),Phospho (STY)	0.71	0.0204
P11388-4	DNA topoisomerase 2-alpha	TOP2A	KPSTSDDSDSNFEK	2 Phospho (STY)	1.36	0.0479
P11388-4	DNA topoisomerase 2-alpha	TOP2A	TLAVSGLGVVGR	Unmodified	1.27	0.9386
P11388-4	DNA topoisomerase 2-alpha	TOP2A	IFDEILVNAADNK	Unmodified	1.33	0.8989
P04637	Cellular tumour antigen p53	TP53	ALPNNTSSSPQPK	Phospho (STY)	1.85	0.0460
Q9BVJ6	U3 small nucleolar RNA-associated protein 14 homolog A	UTP14A	SELSQDAEPAGSQETK	Phospho (STY)	3.49	0.0412
Q8IWA0	WD repeat-containing protein 75	WDR75	VQDTSNTGLGEDIIHQLSK	Phospho (STY)	0.25	0.0053
H0Y449	Nuclease-sensitive element-binding protein 1	YBX1	RPQYSNPPVQGEVMEGADNQGAGEQGR	Oxidation (M)	0.52	0.0012

Supplementary Table ST5.2 2-FaraA induced differential phosphorylation of peptides in IM9 cells after 24 h treatment

Accession	Protein Names	Gene Names	Sequence	Modifications	Ratio H/L normalized	P-value
Q9NY61	Protein AATF	AATF	YLVDGTKPNAGSEEISSEDDELVEEK	3 Phospho (STY)	0.53	0.0008
Q9UKV3	Apoptotic chromatin condensation inducer in the nucleus	ACIN1	SKSPSPPR	2 Phospho (STY)	0.56	0.0089

Q02040	A-kinase anchor protein 17A	AKAP17A	VVPEDGSPEKR	Phospho (STY)	0.61	0.0320
Q9UIG0	Tyrosine-protein kinase BAZ1B	BAZ1B	LAEDEGDSEPEAVGQSR	Phospho (STY)	1.39	0.0187
Q9NYF8	Bcl-2-associated transcription factor 1	BCLAF1	ETQSPEQVK	Phospho (STY)	0.66	0.0021
Q9NYF8	Bcl-2-associated transcription factor 1	BCLAF1	IDISPSTLR	Phospho (STY)	0.70	0.0002
Q9NYF8	Bcl-2-associated transcription factor 1	BCLAF1	YSPSQNSPIHHIPSR	2 Phospho (STY)	0.56	0.0013
Q14137	Ribosome biogenesis protein BOP1	BOP1	IGDEYAEDSSDEEDIR	2 Phospho (STY)	1.40	0.0266
Q9BX63	Fanconi anemia group J protein	BRIP1	PADEGVSEK	Unmodified	0.20	0.0034
Q13185	Chromobox protein homolog 3	CBX3	KSLSDSESDDSK	Phospho (STY)	0.54	0.0276
Q13112	Chromatin assembly factor 1 subunit B	CHAF1B	TQDPSSPGTTPPQAR	Phospho (STY)	1.42	0.0168
Q14839-2	Chromodomain-helicase-DNA-binding protein 4	CHD4	MSQPGSPSPK	Oxidation (M),Phospho (STY)	1.31	0.0484
Q9NR30	Nucleolar RNA helicase 2	DDX21	NEEPSEEEIDAPKPK	Phospho (STY)	0.60	0.0250
Q9NR30	Nucleolar RNA helicase 2	DDX21	NEEPSEEEIDAPKPK	Unmodified	0.61	0.0163
Q9NR30	Nucleolar RNA helicase 2	DDX21	EGAFSNFPISEETIK	Unmodified	0.89	0.0183
Q9NR30	Nucleolar RNA helicase 2	DDX21	APQVLVLAPTR	Unmodified	0.94	0.2255
Q9NR30	Nucleolar RNA helicase 2	DDX21	ELANQVSK	Unmodified	0.91	0.0563
Q9GZR7	ATP-dependent	DDX24	AQAVSEEEEEEEGKSSS	Phospho	0.49	0.0004

	RNA helicase DDX24		PK	(STY)		
Q5QJE6	Deoxynucleotidyl transferase terminal-interacting protein 2	DNTTIP2	VTPTKESYTEEIVSEAESHVSGISR	Phospho (STY)	0.68	0.0438
Q5QJE6	Deoxynucleotidyl transferase terminal-interacting protein 2	DNTTIP2	ASIQAASAESSGQK	Unmodified	0.81	0.2325
P07814	Bifunctional glutamate/proline--tRNA ligase;Glutamate--tRNA ligase;Proline--tRNA ligase	EPRS	EYIPGQPPLSQSSDSSPTR	Phospho (STY)	1.39	0.0352
Q92522	Histone H1x	H1FX	AGGSAALSPSK	Phospho (STY)	0.56	0.0277
Q6FI13	Histone H2A.x	H2AFX	HLQLAIR	Unmodified	0.48	0.0117
Q6FI13	Histone H2A.x	H2AFX	AGLQFPVGR	Unmodified	0.51	0.0002
Q6FI13	Histone H2A.x	H2AFX	TSATVGPK	Unmodified	1.07	0.2249
P0C0S5	Histone H2A.Z	H2AFZ	GDEELDSLIK	Unmodified	0.51	0.0002
P0C0S5	Histone H2A.Z	H2AFZ	ATIAGGGVIPHIHK	Unmodified	0.97	0.6709
P0C0S5	Histone H2A.Z	H2AFZ	GDEELDSLIK	Unmodified	0.88	0.2670
P14317	Hematopoietic lineage cell-specific protein	HCLS1	RSPEAPQPVIAMEEPAVPAPLPK	Oxidation (M),Phospho (STY)	0.65	0.0008
P14317	Hematopoietic lineage cell-specific protein	HCLS1	SAVGFNEMEAPTTAYK	Oxidation (M)	0.68	0.0004
P16401	Histone H1.5	HIST1H1B	ALAAGGYDVEK	Unmodified	0.34	0.0002
P16401	Histone H1.5	HIST1H1B	GTGASGSFK	Unmodified	0.50	0.0044
P16401	Histone H1.5	HIST1H1B	ALAAGGYDVEK	Unmodified	0.58	0.1595
P16401	Histone H1.5	HIST1H1B	KATGPPVSELITK	Unmodified	0.72	0.0637

P16401	Histone H1.5	HIST1 H1B	SETAPAETATPAPVEK	Unmodified	0.73	0.0259
P10412	HIST1H1C	Histone H1.2	KAPKSPAK	Phospho (STY)	NaN	0.0253
P10412	HIST1H1C	Histone H1.2	SGVSLAALK	Unmodified	0.52	0.0071
P10412	HIST1H1C	Histone H1.2	GTLVQTK	Unmodified	0.79	0.3350
P10412	HIST1H1C	Histone H1.2	ALAAAGYDVEK	Unmodified	0.81	0.0734
P10412	HIST1H1C	Histone H1.2	KALAAAGYDVEK	Unmodified	0.83	0.3271
P10412	HIST1H1C	Histone H1.2	GTGASGSFK	Unmodified	0.72	0.0827
P10412	HIST1H1C	Histone H1.2	ASGPPVSELITK	Unmodified	0.76	0.3217
P68431	HIST1H3A	Histone H3.1	KSAPATGGVK	Phospho (STY)	0.31	0.0080
P68431	HIST1H3A	Histone H3.1	STELLIR	Unmodified	0.59	0.0049
P68431	HIST1H3A	Histone H3.1	YRPGTVALREIR	Unmodified	0.83	0.0367
P68431	HIST1H3A	Histone H3.1	EIAQDFK	Unmodified	1.02	0.3093
P68431	HIST1H3A	Histone H3.1	KSAPATGGVK	Unmodified	0.43	0.0092
A6NEL0	Non-histone chromosomal protein HMG-14	HMGN 1	TEESPASDEAGEK	2 Phospho (STY)	0.69	0.0066
P09651	Heterogeneous nuclear ribonucleoprotein A1	HNRN PA1	SESPKEPEQLR	Phospho (STY)	0.70	0.0177
P09651	Heterogeneous nuclear ribonucleoprotein A1	HNRN PA1	EDSQRPGAHLTVK	Unmodified	0.64	0.1939
P10809	60 kDa heat shock protein, mitochondrial	HSPD1	ALMLQGVDLLADAVA VTMGPK	2 Oxidation (M)	0.65	0.0078
Q9NZI8	Insulin-like growth factor 2	IGF2B P1	QGSPVAAGAPAK	Phospho (STY)	0.50	0.0428

	mRNA-binding protein 1					
Q9NQS7	Inner centromere protein	INCENP	IAQVSPGPR	Phospho (STY)	1.61	0.0391
Q8N9T8	Protein KRI1 homolog	KRI1	QLPALDGSLMGPESPPAQEEEAPVSPHK	Oxidation (M),Phospho (STY)	0.63	0.0000
Q8N9T8	Protein KRI1 homolog	KRI1	YVDEENSDGETSNHR	Phospho (STY)	0.69	0.0003
Q9UHB6-4	LIM domain and actin-binding protein 1	LIMA1	ETPHSPGVEDAPIAK	Phospho (STY)	0.57	0.0086
Q9UHB6-4	LIM domain and actin-binding protein 1	LIMA1	SEVQQPVHPKPLSPDSR	Phospho (STY)	0.60	0.0023
P20700	Lamin-B1	LMNB1	TTIPEEEEEEEEAAGVVVEEELFHQQGTPR	Phospho (STY)	1.34	0.0405
P20700	Lamin-B1	LMNB1	ALYETELADAR	Unmodified	1.01	0.3870
P20700	Lamin-B1	LMNB1	DAALATALGDKK	Unmodified	1.16	0.1579
P20700	Lamin-B1	LMNB1	IQELEDLLAK	Unmodified	0.97	0.2752
P20700	Lamin-B1	LMNB1	LLEGEEER	Unmodified	1.29	0.2029
Q9Y608	Leucine-rich repeat flightless-interacting protein 2	LRRFIP2	RGSGDTSSLIDPDTSLSELR	Phospho (STY)	0.72	0.0004
E9PFP3	Lymphocyte-specific protein 1	LSP1	QASIELPSMAVASTK	Oxidation (M),Phospho (STY)	0.54	0.0072
E9PFP3	Lymphocyte-specific protein 1	LSP1	DIVAGDMSK	Unmodified	0.57	0.0160
E9PFP3	Lymphocyte-specific protein 1	LSP1	EGPGPEDTVQDNLGAAGAEEEQEEHQK	Unmodified	0.58	0.0018
E9PFP3	Lymphocyte-specific protein 1	LSP1	WETGEVQAQSAAK	Unmodified	0.73	0.0117
Q9BXY0	Protein MAK16 homolog	MAK16	ALEQQEAESDSSDTEEKDDDDDDEEDVGKR	2 Phospho (STY)	0.32	0.0000
Q9BXY0	Protein MAK16	MAK1	ALIAAQLDNAIEK	Unmodified	0.77	n/a

	homolog	6				
A8MXP9	Matrin-3	MATR3	RDSFDDRGPSLNPVLDYDHGSR	Phospho (STY)	1.68	0.0252
A8MXP9	Matrin-3	MATR3	SYSPDGKESPSDKK	2 Phospho (STY)	0.33	0.0020
P55081	Microfibrillar-associated protein 1	MFAP1	RPDYAPMESSDEEDEEFQFIK	Oxidation (M),2 Phospho (STY)	0.65	0.0003
P46013	Antigen KI-67	MKI67	AQSLVISPPAPSPR	Phospho (STY)	1.40	0.0014
P46013	Antigen KI-67	MKI67	AQALEDLAGFK	Unmodified	1.24	0.0095
O00566	U3 small nucleolar ribonucleoprotein protein MPP10	MPHOSPH10	SDLRKSPVFSDEDSDLDFDISK	3 Phospho (STY)	0.71	0.0034
O00566	U3 small nucleolar ribonucleoprotein protein MPP10	MPHOSPH10	TAEEENPEHVEIQK	Unmodified	1.10	0.2023
A5PL00	Myosin-binding protein C, cardiac-type	MYBPC3	VETTKDRSIFTVEGAEK	4 Phospho (STY)	0.59	0.0424
F8VTL3	Myosin-10	MYH10	QLHLEGASLELSDDDTESK	Phospho (STY)	0.55	0.0001
P35579	Myosin-9	MYH9	KGAGDGSDEEVDGKADGAEAK	Phospho (STY)	0.41	0.0250
P35579	Myosin-9	MYH9	DFSALESQLQDTQELLQEENR	Unmodified	0.81	0.0154
P35579	Myosin-9	MYH9	ELESQISELQEDLESER	Unmodified	0.59	0.0223
P35579	Myosin-9	MYH9	IAQLEEELEEEQGNTELINDR	Unmodified	0.75	0.0062
P35579	Myosin-9	MYH9	IMGIPEEEQMGLLR	Unmodified	0.46	0.0233
P35579	Myosin-9	MYH9	LQVELDNVTGLLSQSDSK	Unmodified	0.64	0.0390
Q3KQS4	Putative ribosomal RNA methyltransferase NOP2	NOP2	EAAAGIQWSEEETEDEEEEKEVTPESGPPK	2 Phospho (STY)	0.73	0.0120
Q3KQS4	Putative	NOP2	GTDTQTPAVLSPSK	Phospho	0.72	0.0105

	ribosomal RNA methyltransferase NOP2			(STY)		
Q3KQS4	Putative ribosomal RNA methyltransferase NOP2	NOP2	DLAQALINR	Unmodified	0.96	0.1978
Q3KQS4	Putative ribosomal RNA methyltransferase NOP2	NOP2	LVPTGLDFGQEGFTR	Unmodified	1.04	0.4784
P06748	Nucleophosmin	NPM1	DELHIVEAEAMNYEGSPIKVTLATLK	Oxidation (M),Phospho (STY)	0.46	0.0241
P06748	Nucleophosmin	NPM1	GPSSVEDIK	Unmodified	0.38	0.0493
P06748	Nucleophosmin	NPM1	LAADEDDDDDDEEDDDEDDDDDDFDDEEAEEKAPVKK	Unmodified	0.40	0.0017
P06748	Nucleophosmin	NPM1	LLSISGK	Unmodified	0.36	0.0006
P06748	Nucleophosmin	NPM1	MQASIEK	Unmodified	0.37	0.0263
P06748	Nucleophosmin	NPM1	MSVQPTVSLGGFEITPPVVLR	Unmodified	0.43	0.0049
P06748	Nucleophosmin	NPM1	TVSLGAGAK	Unmodified	0.40	0.0029
P06748	Nucleophosmin	NPM1	VDNDENEHQLSLR	Unmodified	0.41	0.2028
Q15154	Pericentriolar material 1 protein	PCM1	KDEETEESEYDSEHENSEPVTNIR	3 Phospho (STY)	0.56	0.0012
Q15154	Pericentriolar material 1 protein	PCM1	YMSQMSVPEQAELEK	2 Oxidation (M),Phospho (STY)	0.61	0.0012
Q15154	Pericentriolar material 1 protein	PCM1	VTNDISPESSPGVGR	Phospho (STY)	2.91	0.0048
Q9NTI5	Sister chromatid cohesion protein PDS5 homolog B	PDS5B	METVSNASSSSNPSSPGR	Oxidation (M),Phospho (STY)	1.41	0.0325
Q9P1Y6	PHD and RING finger domain-containing protein 1	PHRF1	VLSDSEDEEKDADVPGTSTR	2 Phospho (STY)	0.72	0.0006
P29590	Protein PML	PML	AVSPPHLDGPPSPR	2 Phospho (STY)	1.45	0.0179
P29590	Protein PML	PML	SSPEQPRPSTSK	Phospho (STY)	1.75	0.0490

Q9H307	Pinin	PNN	SLSPGKENVSALDMEK	Oxidation (M),Phospho (STY)	0.59	0.0010
Q9H307	Pinin	PNN	TLQEQLEK	Unmodified	0.73	0.2420
C9J3F9	Suppressor of SWI4 1 homolog	PPAN-P2RY11	LQDISELLATGAGLSESEAEPDGDHNITELPQAVAGR	2 Phospho (STY)	1.32	0.0472
O75475	PC4 and SFRS1-interacting protein	PSIP1	TGVTSTSDSEEEGDDQEGEK	2 Phospho (STY)	0.63	0.0009
Q13610	Periodic tryptophan protein 1 homolog	PWP1	EKLQEEGGGSDEEETGSPSEDGMQSAR	Oxidation (M),Phospho (STY)	0.75	0.0106
Q96I25	Splicing factor 45	RBM17	RPDPDSDEDEDYER	Phospho (STY)	0.62	0.0000
Q5VTR2	E3 ubiquitin-protein ligase BRE1A	RNF20	VYGAGSSLYGGTITINARK	4 Phospho (STY)	12.82	0.0437
Q15287	RNA-binding protein with serine-rich domain 1	RNPS1	RSPSPKPTK	2 Phospho (STY)	0.54	0.0166
P62913	60S ribosomal protein L11	RPL11	VLEQLTGQTPVFSKAR	Unmodified	0.53	0.0464
P62913	60S ribosomal protein L11	RPL11	YDGIILPGK	Unmodified	0.61	0.0016
P05387	60S acidic ribosomal protein P2;60S acidic ribosomal protein P1	RPLP2	KEESEESDDDMGFGLFD	Phospho (STY)	0.19	0.0053
O76021	Ribosomal L1 domain-containing protein 1	RSL1D1	AAESETPGKSPEK	Phospho (STY)	0.60	0.0050
O76021	Ribosomal L1 domain-containing	RSL1D1	EKSPSLGK	Phospho (STY)	0.56	0.0286

	protein 1					
O76021	Ribosomal L1 domain-containing protein 1	RSL1D1	DDVAPESGDTTVK	Unmodified	0.71	0.0277
O76021	Ribosomal L1 domain-containing protein 1	RSL1D1	LLPSLIGR	Unmodified	1.03	0.0165
Q5T802	Runt-related transcription factor 2	RUNX2	GGTMASNSLFSTVTPCQQNFFWDPSTSRR	Oxidation (M),4 Phospho (STY)	0.28	0.0022
Q9H7N4	Splicing factor, arginine/serine-rich 19	SCAF1	QRSPSPAPAPAPAAAAGPPTR	2 Phospho (STY)	1.70	0.0385
Q9NWH9	SAFB-like transcription modulator	SLTM	DGQDAIAQSPEKESK	Phospho (STY)	0.63	0.0028
Q9NWH9	SAFB-like transcription modulator	SLTM	ISSKSPGHMVILDQTK	Oxidation (M),Phospho (STY)	0.68	0.0040
G3V3A4	SNW domain-containing protein 1	SNW1	GPPSPPAPVMHSPSR	Oxidation (M),2 Phospho (STY)	0.69	0.0078
P18583-9	Protein SON	SON	SAASPVVSSMPER	Oxidation (M),Phospho (STY)	1.32	0.0231
Q01082	Spectrin beta chain, brain 1	SPTBN1	RPPSPEPSTK	Phospho (STY)	0.53	0.0010
E9PCT1	Serine/arginine repetitive matrix protein 1	SRRM1	AASPSPQSVR	2 Phospho (STY)	0.57	0.0000
E9PCT1	Serine/arginine repetitive matrix protein 1	SRRM1	ASPSPPPKR	2 Phospho (STY)	0.60	0.0000
E9PCT1	Serine/arginine repetitive matrix protein 1	SRRM1	EARSPQPNK	Phospho (STY)	0.55	0.0002
E9PCT1	Serine/arginine	SRRM	EKTPELPEPSVK	Phospho	0.50	0.0393

	repetitive matrix protein 1	1		(STY)		
E9PCT1	Serine/arginine repetitive matrix protein 1	SRRM 1	HRPSPPATPPPK	2 Phospho (STY)	0.58	0.0092
E9PCT1	Serine/arginine repetitive matrix protein 1	SRRM 1	RASPSPPPKR	2Phospho (STY)	0.61	0.0000
E9PCT1	Serine/arginine repetitive matrix protein 1	SRRM 1	RLSPSASPPR	2 Phospho (STY)	0.53	0.0115
E9PCT1	Serine/arginine repetitive matrix protein 1	SRRM 1	RRSPSPAPPPR	2 Phospho (STY)	0.65	0.0004
E9PCT1	Serine/arginine repetitive matrix protein 1	SRRM 1	RRSPSPPPTR	2 Phospho (STY)	0.72	0.0051
E9PCT1	Serine/arginine repetitive matrix protein 1	SRRM 1	RRTASPPPPPK	2 Phospho (STY)	0.48	0.0129
E9PCT1	Serine/arginine repetitive matrix protein 1	SRRM 1	RSPSPPPTR	2 Phospho (STY)	0.66	0.0021
E9PCT1	Serine/arginine repetitive matrix protein 1	SRRM 1	RVSHSPPPK	2 Phospho (STY)	0.50	0.0016
E9PCT1	Serine/arginine repetitive matrix protein 1	SRRM 1	RVSRTPEPK	2 Phospho (STY)	0.58	0.0012
E9PCT1	Serine/arginine repetitive matrix protein 1	SRRM 1	RYSPPIQR	Phospho (STY)	0.61	0.0188
E9PCT1	Serine/arginine repetitive matrix protein 1	SRRM 1	RYSPSPPPK	2 Phospho (STY)	0.53	0.0118
E9PCT1	Serine/arginine repetitive matrix protein 1	SRRM 1	SVSGSPEPAAK	Phospho (STY)	0.49	0.0004
E9PCT1	Serine/arginine repetitive matrix protein 1	SRRM 1	VSVSPGR	Phospho (STY)	0.56	0.0023
Q9UQ35	Serine/arginine repetitive matrix protein 2	SRRM 2	SATRPSPSPER	Phospho (STY)	0.57	0.0141
J3KTL2	Serine/arginine-rich splicing factor 1	SRSF1	VDGPRSPSYGR	2 Phospho (STY)	0.33	0.0004

P84103	Serine/arginine-rich splicing factor 3	SRSF3	ERSLSRER	2 Phospho (STY)	0.62	0.0087
Q16629	Serine/arginine-rich splicing factor 7	SRSF7	YFQSPSRSR	2 Phospho (STY)	0.40	0.0044
E9PHK9	Treacle protein	TCOF1	AALAPAKESPR	Phospho (STY)	1.80	0.0483
E9PHK9	Treacle protein	TCOF1	EAASGTTPQK	Phospho (STY)	1.49	0.0350
E9PHK9	Treacle protein	TCOF1	TSQVGAASAPAKESPR	Phospho (STY)	2.20	0.0293
E9PHK9	Treacle protein	TCOF1	TNVVTMPTAHPR	Unmodified	1.28	0.3602
E9PHK9	Treacle protein	TCOF1	VVTAAAQAK	Unmodified	0.75	0.5060
Q9Y2W1	Thyroid hormone receptor-associated protein 3	THRAP3	IDISPSTFR	Phospho (STY)	0.69	0.0003
P04637	Cellular tumour antigen p53	TP53	ALPNNTSSSPQPK	Phospho (STY)	1.87	0.0364
P62995	Transformer-2 protein homolog beta;Transformer-2 protein homolog alpha	TRA2B;TRA2A	RSPSPYYSR	2 Phospho (STY)	0.44	0.0113
Q9BVJ6	U3 small nucleolar RNA-associated protein 14 homolog A	UTP14A	DYLLSESEDEGDNDGER	2 Phospho (STY)	1.48	0.0128
Q9BVJ6	U3 small nucleolar RNA-associated protein 14 homolog A	UTP14A	SELSQDAEPAGSQETK	Phospho (STY)	3.18	0.0199
Q9Y5J1	U3 small nucleolar RNA-associated protein 18 homolog	UTP18	KTSSDDESEEDEDDLLQR	2 Phospho (STY)	0.58	0.0107
Q9Y5J1	U3 small nucleolar RNA-associated protein	UTP18	AGAGPGGPPQKPAPSSQR	Unmodified	0.93	0.3662

	18 homolog					
Q8IWA0	WD repeat-containing protein 75	WDR75	VQDTSNTGLGEDIIHQLSK	Phospho (STY)	0.74	0.0215
Q9H0D6	5-3 exoribonuclease 2	XRN2	KAEDSDSEPEPEDNVR	2 Phospho (STY)	0.58	0.0006
H0Y449	Nuclease-sensitive element-binding protein 1	YBX1	RPQYSNPPVQGEVMEGADNQGAGEQGR	Oxidation (M)	0.49	0.0104
J3QR07	YTH domain-containing protein 1	YTHDC1	AKSPTPDGSER	2 Phospho (STY)	0.59	0.0210

REFERENCES

1. Shaffer, A.L., A. Rosenwald, and L.M. Staudt, *Lymphoid malignancies: the dark side of B-cell differentiation.* Nature reviews. Immunology, 2002. **2**(12): p. 920-32.
2. Dalla-Favera, R., et al., *Translocation and rearrangements of the c-myc oncogene locus in human undifferentiated B-cell lymphomas.* Science, 1983. **219**(4587): p. 963-7.
3. Pasqualucci, L., et al., *Hypermutation of multiple proto-oncogenes in B-cell diffuse large-cell lymphomas.* Nature, 2001. **412**(6844): p. 341-6.
4. Hoang, A.T., et al., *A link between increased transforming activity of lymphoma-derived MYC mutant alleles, their defective regulation by p107, and altered phosphorylation of the c-Myc transactivation domain.* Molecular and Cellular Biology, 1995. **15**(8): p. 4031-42.
5. Levens, D., *Disentangling the MYC web.* Proceedings of the National Academy of Sciences of the United States of America, 2002. **99**(9): p. 5757-9.
6. Garrett, I.R., et al., *A murine model of human myeloma bone disease.* Bone, 1997. **20**(6): p. 515-20.
7. Bergsagel, P.L. and W.M. Kuehl, *Chromosome translocations in multiple myeloma.* Oncogene, 2001. **20**(40): p. 5611-22.
8. Pulvertaft, J.V., *Cytology of Burkitt's Tumour (African Lymphoma).* Lancet, 1964. **1**(7327): p. 238-40.
9. Vousden, K.H., T. Crook, and P.J. Farrell, *Biological activities of p53 mutants in Burkitt's lymphoma cells.* The Journal of general virology, 1993. **74 (Pt 5)**: p. 803-10.
10. Pellat-Deceunynk, C., et al., *Human myeloma cell lines as a tool for studying the biology of multiple myeloma: a reappraisal 18 years after.* Blood, 1995. **86**(10): p. 4001-2.
11. Fahey, J.L., D.N. Buell, and H.C. Sox, *Proliferation and differentiation of lymphoid cells: studies with human lymphoid cell lines and immunoglobulin synthesis.* Annals of the New York Academy of Sciences, 1971. **190**: p. 221-34.
12. Petitjean, A., et al., *Impact of mutant p53 functional properties on TP53 mutation patterns and tumour phenotype: lessons from recent developments in the IARC TP53 database.* Human mutation, 2007. **28**(6): p. 622-9.
13. Stacchini, A., et al., *MEC1 and MEC2: two new cell lines derived from B-chronic lymphocytic leukaemia in prolymphocytoid transformation.* Leukemia research, 1999. **23**(2): p. 127-36.
14. Zauli, G., et al., *Dasatinib plus Nutlin-3 shows synergistic antileukemic activity in both p53 wild-type and p53 mutated B chronic lymphocytic leukemias by inhibiting the Akt pathway.* Clinical cancer research : an official journal of the American Association for Cancer Research, 2011. **17**(4): p. 762-70.
15. Rowley, M., P. Liu, and B. Van Ness, *Heterogeneity in therapeutic response of genetically altered myeloma cell lines to interleukin 6, dexamethasone, doxorubicin, and melphalan.* Blood, 2000. **96**(9): p. 3175-80.
16. Gong, B. and A. Almasan, *Differential upregulation of p53-responsive genes by genotoxic stress in hematopoietic cells containing wild-type and mutant p53.* Gene expression, 1999. **8**(4): p. 197-206.
17. Montgomery, J.A. and K. Hewson, *Nucleosides of 2-fluoroadenine.* Journal of medicinal chemistry, 1969. **12**(3): p. 498-504.
18. Mackey, J.R., et al., *Quantitative analysis of nucleoside transporter and metabolism gene expression in chronic lymphocytic leukemia (CLL): identification of fludarabine-sensitive and -insensitive populations.* Blood, 2005. **105**(2): p. 767-74.
19. Pastor-Anglada, M., et al., *Nucleoside transporters in chronic lymphocytic leukaemia.* Leukemia : official journal of the Leukemia Society of America, Leukemia Research Fund, U.K, 2004. **18**(3): p. 385-93.
20. King, K.M., et al., *A comparison of the transportability, and its role in cytotoxicity, of clofarabine, cladribine, and fludarabine by recombinant human nucleoside transporters*

produced in three model expression systems. Molecular pharmacology, 2006. **69**(1): p. 346-53.
21. Molina-Arcas, M., et al., *Fludarabine uptake mechanisms in B-cell chronic lymphocytic leukemia.* Blood, 2003. **101**(6): p. 2328-34.
22. Van den Neste, E., et al., *Old and new insights into the mechanisms of action of two nucleoside analogs active in lymphoid malignancies: fludarabine and cladribine (review).* International journal of oncology, 2005. **27**(4): p. 1113-24.
23. Brockman, R.W., F.M. Schabel, Jr., and J.A. Montgomery, *Biologic activity of 9-beta-D-arabinofuranosyl-2-fluoroadenine, a metabolically stable analog of 9-beta-D-arabinofuranosyladenine.* Biochemical pharmacology, 1977. **26**(22): p. 2193-6.
24. Plunkett, W., et al., *Comparison of the toxicity and metabolism of 9-beta-D-arabinofuranosyl-2-fluoroadenine and 9-beta-D-arabinofuranosyladenine in human lymphoblastoid cells.* Cancer research, 1980. **40**(7): p. 2349-55.
25. Catapano, C.V., F.W. Perrino, and D.J. Fernandes, *Primer RNA chain termination induced by 9-beta-D-arabinofuranosyl-2-fluoroadenine 5'-triphosphate. A mechanism of DNA synthesis inhibition.* The Journal of biological chemistry, 1993. **268**(10): p. 7179-85.
26. Parker, W.B. and Y.C. Cheng, *Inhibition of DNA primase by nucleoside triphosphates and their arabinofuranosyl analogs.* Molecular pharmacology, 1987. **31**(2): p. 146-51.
27. Parker, W.B., et al., *Interaction of 2-halogenated dATP analogs (F, Cl, and Br) with human DNA polymerases, DNA primase, and ribonucleotide reductase.* Molecular pharmacology, 1988. **34**(4): p. 485-91.
28. Tseng, W.C., et al., *In vitro biological activity of 9-beta-D-arabinofuranosyl-2-fluoroadenine and the biochemical actions of its triphosphate on DNA polymerases and ribonucleotide reductase from HeLa cells.* Molecular pharmacology, 1982. **21**(2): p. 474-7.
29. Spriggs, D., et al., *Incorporation of 9-beta-D-arabinofuranosyl-2-fluoroadenine into HL-60 cellular RNA and DNA.* Biochemical pharmacology, 1986. **35**(2): p. 247-52.
30. Huang, P., S. Chubb, and W. Plunkett, *Termination of DNA synthesis by 9-beta-D-arabinofuranosyl-2-fluoroadenine. A mechanism for cytotoxicity.* The Journal of biological chemistry, 1990. **265**(27): p. 16617-25.
31. Huang, P. and W. Plunkett, *Action of 9-beta-D-arabinofuranosyl-2-fluoroadenine on RNA metabolism.* Molecular pharmacology, 1991. **39**(4): p. 449-55.
32. Robertson, L.E., et al., *Induction of apoptotic cell death in chronic lymphocytic leukemia by 2-chloro-2'-deoxyadenosine and 9-beta-D-arabinosyl-2-fluoroadenine.* Blood, 1993. **81**(1): p. 143-50.
33. Huang, P. and W. Plunkett, *Fludarabine- and gemcitabine-induced apoptosis: incorporation of analogs into DNA is a critical event.* Cancer chemotherapy and pharmacology, 1995. **36**(3): p. 181-8.
34. Huang, P., et al., *High molecular weight DNA fragmentation: a critical event in nucleoside analogue-induced apoptosis in leukemia cells.* Clinical cancer research : an official journal of the American Association for Cancer Research, 1995. **1**(9): p. 1005-13.
35. Grever, M.R., et al., *Fludarabine monophosphate: a potentially useful agent in chronic lymphocytic leukemia.* Nouvelle revue francaise d'hematologie, 1988. **30**(5-6): p. 457-9.
36. Johnson, S.A., *Nucleoside analogues in the treatment of haematological malignancies.* Expert opinion on pharmacotherapy, 2001. **2**(6): p. 929-43.
37. Keating, M.J., et al., *Long-term follow-up of patients with chronic lymphocytic leukemia (CLL) receiving fludarabine regimens as initial therapy.* Blood, 1998. **92**(4): p. 1165-71.
38. Hagenbeek, A., et al., *Phase III intergroup study of fludarabine phosphate compared with cyclophosphamide, vincristine, and prednisone chemotherapy in newly diagnosed patients with stage III and IV low-grade malignant Non-Hodgkin's lymphoma.* Journal of clinical oncology : official journal of the American Society of Clinical Oncology, 2006. **24**(10): p. 1590-6.
39. Foran, J.M., et al., *Multicenter phase II study of fludarabine phosphate for patients with newly diagnosed lymphoplasmacytoid lymphoma, Waldenstrom's macroglobulinemia, and*

mantle-cell lymphoma. Journal of clinical oncology : official journal of the American Society of Clinical Oncology, 1999. **17**(2): p. 546-53.
40. Leblond, V., et al., *Multicenter, randomized comparative trial of fludarabine and the combination of cyclophosphamide-doxorubicin-prednisone in 92 patients with Waldenstrom macroglobulinemia in first relapse or with primary refractory disease.* Blood, 2001. **98**(9): p. 2640-4.
41. Johnson, S.A., *Use of fludarabine in the treatment of mantle cell lymphoma, Waldenstrom's macroglobulinemia and other uncommon B- and T-cell lymphoid malignancies.* The hematology journal : the official journal of the European Haematology Association / EHA, 2004. **5 Suppl 1**: p. S50-61.
42. Badoux, X.C., et al., *Fludarabine, cyclophosphamide, and rituximab chemoimmunotherapy is highly effective treatment for relapsed patients with CLL.* Blood, 2011. **117**(11): p. 3016-24.
43. Tam, C.S., et al., *Fludarabine, cyclophosphamide, and rituximab for the treatment of patients with chronic lymphocytic leukemia or indolent non-Hodgkin lymphoma.* Cancer, 2006. **106**(11): p. 2412-20.
44. Lane, D.P., *Cancer. p53, guardian of the genome.* Nature, 1992. **358**(6381): p. 15-6.
45. Mirza, A., et al., *Global transcriptional program of p53 target genes during the process of apoptosis and cell cycle progression.* Oncogene, 2003. **22**(23): p. 3645-54.
46. Muller, P.A. and K.H. Vousden, *p53 mutations in cancer.* Nature cell biology, 2013. **15**(1): p. 2-8.
47. Chang, C., et al., *Identification and partial characterization of new antigens from simian virus 40-transformed mouse cells.* Journal of virology, 1979. **31**(2): p. 463-71.
48. Kress, M., et al., *Simian virus 40-transformed cells express new species of proteins precipitable by anti-simian virus 40 tumour serum.* Journal of virology, 1979. **31**(2): p. 472-83.
49. Lane, D.P. and L.V. Crawford, *T antigen is bound to a host protein in SV40-transformed cells.* Nature, 1979. **278**(5701): p. 261-3.
50. Linzer, D.I. and A.J. Levine, *Characterization of a 54K dalton cellular SV40 tumour antigen present in SV40-transformed cells and uninfected embryonal carcinoma cells.* Cell, 1979. **17**(1): p. 43-52.
51. Zhu, J., et al., *Definition of the p53 functional domains necessary for inducing apoptosis.* The Journal of biological chemistry, 2000. **275**(51): p. 39927-34.
52. Zhu, J., et al., *Identification of a novel p53 functional domain that is necessary for mediating apoptosis.* The Journal of biological chemistry, 1998. **273**(21): p. 13030-6.
53. Maclaine, N.J. and T.R. Hupp, *The regulation of p53 by phosphorylation: a model for how distinct signals integrate into the p53 pathway.* Aging, 2009. **1**(5): p. 490-502.
54. Toledo, F. and G.M. Wahl, *Regulating the p53 pathway: in vitro hypotheses, in vivo veritas.* Nature reviews. Cancer, 2006. **6**(12): p. 909-23.
55. Ruaro, E.M., et al., *A proline-rich motif in p53 is required for transactivation-independent growth arrest as induced by Gas1.* Proceedings of the National Academy of Sciences of the United States of America, 1997. **94**(9): p. 4675-80.
56. Jeffrey, P.D., S. Gorina, and N.P. Pavletich, *Crystal structure of the tetramerization domain of the p53 tumour suppressor at 1.7 angstroms.* Science, 1995. **267**(5203): p. 1498-502.
57. Kawaguchi, T., et al., *The relationship among p53 oligomer formation, structure and transcriptional activity using a comprehensive missense mutation library.* Oncogene, 2005. **24**(46): p. 6976-81.
58. McKinney, K., et al., *p53 linear diffusion along DNA requires its C terminus.* Molecular cell, 2004. **16**(3): p. 413-24.
59. Weinberg, R.L., et al., *Regulation of DNA binding of p53 by its C-terminal domain.* Journal of molecular biology, 2004. **342**(3): p. 801-11.
60. Murray-Zmijewski, F., D.P. Lane, and J.C. Bourdon, *p53/p63/p73 isoforms: an orchestra of isoforms to harmonise cell differentiation and response to stress.* Cell death and differentiation, 2006. **13**(6): p. 962-72.

61. Vogelstein, B., D. Lane, and A.J. Levine, *Surfing the p53 network.* Nature, 2000. **408**(6810): p. 307-10.
62. Moiseeva, O., et al., *DNA damage signaling and p53-dependent senescence after prolonged beta-interferon stimulation.* Molecular biology of the cell, 2006. **17**(4): p. 1583-92.
63. Sekaric, P., et al., *hAda3 regulates p14ARF-induced p53 acetylation and senescence.* Oncogene, 2007. **26**(43): p. 6261-8.
64. Gu, W. and R.G. Roeder, *Activation of p53 sequence-specific DNA binding by acetylation of the p53 C-terminal domain.* Cell, 1997. **90**(4): p. 595-606.
65. Chuikov, S., et al., *Regulation of p53 activity through lysine methylation.* Nature, 2004. **432**(7015): p. 353-60.
66. Tokino, T. and Y. Nakamura, *The role of p53-target genes in human cancer.* Critical reviews in oncology/hematology, 2000. **33**(1): p. 1-6.
67. Riley, T., et al., *Transcriptional control of human p53-regulated genes.* Nature reviews. Molecular cell biology, 2008. **9**(5): p. 402-12.
68. Yang, A., et al., *p63, a p53 homolog at 3q27-29, encodes multiple products with transactivating, death-inducing, and dominant-negative activities.* Mol Cell, 1998. **2**(3): p. 305-16.
69. Petitjean, A., et al., *Properties of the six isoforms of p63: p53-like regulation in response to genotoxic stress and cross talk with DeltaNp73.* Carcinogenesis, 2008. **29**(2): p. 273-81.
70. McKeon, F., *p63 and the epithelial stem cell: more than status quo?* Genes Dev, 2004. **18**(5): p. 465-9.
71. Keyes, W.M., et al., *p63 heterozygous mutant mice are not prone to spontaneous or chemically induced tumours.* Proc Natl Acad Sci U S A, 2006. **103**(22): p. 8435-40.
72. Alderton, G.K., *Tumour suppression: The burning issue of p63.* Nat Rev Cancer, 2010. **10**(12): p. 814-815.
73. Flores, E.R., et al., *Tumour predisposition in mice mutant for p63 and p73: evidence for broader tumour suppressor functions for the p53 family.* Cancer Cell, 2005. **7**(4): p. 363-73.
74. Keyes, W.M., et al., *p63 deficiency activates a program of cellular senescence and leads to accelerated aging.* Genes Dev, 2005. **19**(17): p. 1986-99.
75. Massion, P.P., et al., *Significance of p63 amplification and overexpression in lung cancer development and prognosis.* Cancer Res, 2003. **63**(21): p. 7113-21.
76. Caput, D., *[P73: a kin to the p52 tumour suppressor gene].* Bull Cancer, 1997. **84**(11): p. 1081-2.
77. Murray-Zmijewski, F., D.P. Lane, and J.C. Bourdon, *p53/p63/p73 isoforms: an orchestra of isoforms to harmonise cell differentiation and response to stress.* Cell Death Differ, 2006. **13**(6): p. 962-72.
78. Zheng, X. and X. Chen, *Aquaporin 3, a glycerol and water transporter, is regulated by p73 of the p53 family.* FEBS Lett, 2001. **489**(1): p. 4-7.
79. Meyer, G., et al., *Developmental roles of p73 in Cajal-Retzius cells and cortical patterning.* J Neurosci, 2004. **24**(44): p. 9878-87.
80. Pozniak, C.D., et al., *p73 is required for survival and maintenance of CNS neurons.* J Neurosci, 2002. **22**(22): p. 9800-9.
81. Pozniak, C.D., et al., *An anti-apoptotic role for the p53 family member, p73, during developmental neuron death.* Science, 2000. **289**(5477): p. 304-6.
82. Saifudeen, Z., et al., *Spatiotemporal switch from DeltaNp73 to TAp73 isoforms during nephrogenesis: impact on differentiation gene expression.* J Biol Chem, 2005. **280**(24): p. 23094-102.
83. Yang, A., et al., *p73-deficient mice have neurological, pheromonal and inflammatory defects but lack spontaneous tumours.* Nature, 2000. **404**(6773): p. 99-103.
84. Fillippovich, I., et al., *Transactivation-deficient p73alpha (p73Deltaexon2) inhibits apoptosis and competes with p53.* Oncogene, 2001. **20**(4): p. 514-22.
85. Beitzinger, M., et al., *p73 poses a barrier to malignant transformation by limiting anchorage-independent growth.* EMBO J, 2008. **27**(5): p. 792-803.

86. Leupin, N., et al., *P73 status in B-cell chronic lymphocytic leukaemia.* Leuk Lymphoma, 2004. **45**(6): p. 1205-7.
87. Stiewe, T., *The p53 family in differentiation and tumourigenesis.* Nat Rev Cancer, 2007. **7**(3): p. 165-8.
88. *The Universal Protein Resource (UniProt) in 2010.* Nucleic Acids Res, 2010. **38**(Database issue): p. D142-8.
89. Cusick, M.E., et al., *Interactome: gateway into systems biology.* Hum Mol Genet, 2005. **14 Spec No. 2**: p. R171-81.
90. Yoshida, Y., et al., *Binding of RNA to p53 regulates its oligomerization and DNA-binding activity.* Oncogene, 2004. **23**(25): p. 4371-9.
91. Wasinger, V.C., et al., *Progress with gene-product mapping of the Mollicutes: Mycoplasma genitalium.* Electrophoresis, 1995. **16**(7): p. 1090-4.
92. Picotti, P., B. Bodenmiller, and R. Aebersold, *Proteomics meets the scientific method.* Nat Methods, 2013. **10**(1): p. 24-7.
93. Ho, C.S., et al., *Electrospray ionisation mass spectrometry: principles and clinical applications.* Clin Biochem Rev, 2003. **24**(1): p. 3-12.
94. Mann, M., R.C. Hendrickson, and A. Pandey, *Analysis of proteins and proteomes by mass spectrometry.* Annu Rev Biochem, 2001. **70**: p. 437-73.
95. Shi, Y., et al., *The role of liquid chromatography in proteomics.* J Chromatogr A, 2004. **1053**(1-2): p. 27-36.
96. Issaq, H.J., et al., *Methods for fractionation, separation and profiling of proteins and peptides.* Electrophoresis, 2002. **23**(17): p. 3048-61.
97. McMurray, J., *Organic Chemistry*. 5th ed. 2000, California, USA: Brooks/Cole.
98. Giddings, J.C., *Two-dimensional separations: concept and promise.* Anal Chem, 1984. **56**(12): p. 1258A-1260A, 1262A, 1264A passim.
99. Wilm, M., *Principles of electrospray ionization.* Mol Cell Proteomics, 2011. **10**(7): p. M111 009407.
100. Ho, C.S., et al., *Electrospray ionisation mass spectrometry: principles and clinical applications.* The Clinical biochemist. Reviews / Australian Association of Clinical Biochemists, 2003. **24**(1): p. 3-12.
101. Olsen, J.V., S.E. Ong, and M. Mann, *Trypsin cleaves exclusively C-terminal to arginine and lysine residues.* Mol Cell Proteomics, 2004. **3**(6): p. 608-14.
102. Jedrychowski, M.P., et al., *Evaluation of HCD- and CID-type fragmentation within their respective detection platforms for murine phosphoproteomics.* Mol Cell Proteomics, 2011. **10**(12): p. M111 009910.
103. Olsen, J.V., et al., *Higher-energy C-trap dissociation for peptide modification analysis.* Nat Methods, 2007. **4**(9): p. 709-12.
104. *Peptide fragmentation*. 2013 [cited 2013 21 July]; Available from: http://www.matrixscience.com/help/fragmentation_help.html.
105. Yates, J.R., C.I. Ruse, and A. Nakorchevsky, *Proteomics by mass spectrometry: approaches, advances, and applications.* Annu Rev Biomed Eng, 2009. **11**: p. 49-79.
106. Park, S.S. and S. Maudsley, *Discontinuous pH gradient-mediated separation of TiO2-enriched phosphopeptides.* Anal Biochem, 2011. **409**(1): p. 81-8.
107. Jensen, S.S. and M.R. Larsen, *Evaluation of the impact of some experimental procedures on different phosphopeptide enrichment techniques.* Rapid Commun Mass Spectrom, 2007. **21**(22): p. 3635-45.
108. Connor, P.A., K.D. Dobson, and A.J. McQuillan, *Infrared Spectroscopy of the TiO2/Aqueous Solution Interface.* Langmuir, 1999. **15**(7): p. 2402-2408.
109. Connor, P.A. and A.J. McQuillan, *Phosphate Adsorption onto TiO2 from Aqueous Solutions: An in Situ Internal Reflection Infrared Spectroscopic Study.* Langmuir, 1999. **15**(8): p. 2916-2921.
110. Rogers, L.D. and L.J. Foster, *Phosphoproteomics--finally fulfilling the promise?* Mol Biosyst, 2009. **5**(10): p. 1122-9.

111. Bonifacino, J.S., E.C. Dell'Angelica, and T.A. Springer, *Immunoprecipitation*, in *Current Protocols in Molecular Biology*. 2001, John Wiley & Sons, Inc.
112. Schmidt, T.G. and A. Skerra, *The Strep-tag system for one-step purification and high-affinity detection or capturing of proteins.* Nature protocols, 2007. **2**(6): p. 1528-35.
113. Wilson, R.C. and J.A. Doudna, *Molecular mechanisms of RNA interference.* Annual review of biophysics, 2013. **42**: p. 217-39.
114. Yang, S., et al., *Specific double-stranded RNA interference in undifferentiated mouse embryonic stem cells.* Mol Cell Biol, 2001. **21**(22): p. 7807-16.
115. Brown, M. and C. Wittwer, *Flow cytometry: principles and clinical applications in hematology.* Clinical chemistry, 2000. **46**(8 Pt 2): p. 1221-9.
116. Arnoult, D., M. Karbowski, and R.J. Youle, *Caspase inhibition prevents the mitochondrial release of apoptosis-inducing factor.* Cell Death and Differentiation, 2003. **10**: p. 845–849.
117. Boersema, P.J., et al., *Triplex protein quantification based on stable isotope labeling by peptide dimethylation applied to cell and tissue lysates.* Proteomics, 2008. **8**(22): p. 4624-32.
118. Cox, J. and M. Mann, *MaxQuant enables high peptide identification rates, individualized p.p.b.-range mass accuracies and proteome-wide protein quantification.* Nat Biotech, 2008. **26**(12): p. 1367-1372.
119. Henrich, S., et al., *Fludarabine induces differential expression of proteins in human leukemia and lymphoma cells.* Nucleosides Nucleotides Nucleic Acids, 2008. **27**(6): p. 634-40.
120. Appella, E. and C.W. Anderson, *Post-translational modifications and activation of p53 by genotoxic stresses.* Eur J Biochem, 2001. **268**(10): p. 2764-72.
121. Mihara, M., et al., *p53 has a direct apoptogenic role at the mitochondria.* Molecular cell, 2003. **11**(3): p. 577-90.
122. Levrero, M., et al., *The p53/p63/p73 family of transcription factors: overlapping and distinct functions.* J Cell Sci, 2000. **113 (Pt 10)**: p. 1661-70.
123. M¨uller, M., et al., *One, two, three—p53, p63, p73 and chemosensitivity.* Drug Resistant Updates, 2006. **9**: p. 19.
124. Henrich, S. and R.I. Christopherson, *Multiple forms of nuclear p53 formed in human Raji and MEC1 cells treated with fludarabine.* Leukemia, 2008. **22**(3): p. 657-60.
125. Mactier, S., *EFFECTS OF PURINE ANALOGUES ON SUB-CELLULAR PROTEOMES OF B-LYMPHOID NEOPLASMS*, in *School of Molecular and Microbial Biosciences*2008, University of Sydney Camperdown. p. 276.
126. Almazi, J.G., *Multiple isoforms and proteolytic derivatives of p53 family proteins in Fludarabine treated lymphoma cells*, in *School of Molecular and Microbial Biosciences*2008, University of Sydney Camperdown p. 81.
127. Best, O.G., et al., *A novel functional assay using etoposide plus nutlin-3a detects and distinguishes between ATM and TP53 mutations in CLL.* Leukemia : official journal of the Leukemia Society of America, Leukemia Research Fund, U.K, 2008. **22**(7): p. 1456-9.
128. Dubovsky, J.A., et al., *Treatment of chronic lymphocytic leukemia with a hypomethylating agent induces expression of NXF2, an immunogenic cancer testis antigen.* Clinical cancer research : an official journal of the American Association for Cancer Research, 2009. **15**(10): p. 3406-15.
129. Marchenko, N.D., A. Zaika, and U.M. Moll, *Death signal-induced localization of p53 protein to mitochondria. A potential role in apoptotic signaling.* J Biol Chem, 2000. **275**(21): p. 16202-12.
130. Sansome, C., et al., *Hypoxia death stimulus induces translocation of p53 protein to mitochondria. Detection by immunofluorescence on whole cells.* FEBS Lett, 2001. **488**(3): p. 110-5.
131. Chipuk, J.E., et al., *PUMA couples the nuclear and cytoplasmic proapoptotic function of p53.* Science, 2005. **309**(5741): p. 1732-5.
132. Stacchini, A., et al., *MEC1 and MEC2: two new cell lines derived from B-chronic lymphocytic leukaemia in prolymphocytoid transformation.* Leuk Res, 1999. **23**(2): p. 127-36.

133. Moll, U.M. and O. Petrenko, *The MDM2-p53 interaction.* Molecular cancer research : MCR, 2003. **1**(14): p. 1001-8.
134. Flores, E.R., et al., *p63 and p73 are required for p53-dependent apoptosis in response to DNA damage.* Nature, 2002. **416**(6880): p. 560-4.
135. Demczuk, S., M. Harbers, and B. Vennstrom, *Identification and analysis of all components of a gel retardation assay by combination with immunoblotting.* Proceedings of the National Academy of Sciences of the United States of America, 1993. **90**(7): p. 2574-8.
136. Gressner, O., et al., *TAp63alpha induces apoptosis by activating signaling via death receptors and mitochondria.* EMBO J, 2005. **24**(13): p. 2458-71.
137. Sayan, B.S., et al., *Cleavage of the transactivation-inhibitory domain of p63 by caspases enhances apoptosis.* Proc Natl Acad Sci U S A, 2007. **104**(26): p. 10871-6.
138. Gressner, O., et al., *TAp63alpha induces apoptosis by activating signaling via death receptors and mitochondria.* EMBO 2005. **24**: p. 2458-2471.
139. Zhu, J., et al., *p73 cooperates with DNA damage agents to induce apoptosis in MCF7 cells in a p53-dependent manner.* Oncogene, 2001. **20**(30): p. 4050-4057.
140. Cabrera-Socorro, A., et al., *Comparative aspects of p73 and Reelin expression in Cajal-Retzius cells and the cortical hem in lizard, mouse and human.* Brain Research, 2007. **1132**: p. 59-70.
141. Friedberg, J.W., *CLL microenvironment: macro important.* Blood, 2011. **117**(2): p. 377-8.
142. Walsby, E., et al., *The Hsp90 inhibitor NVP-AUY922-AG inhibits NF-kappaB signaling, overcomes microenvironmental cytoprotection and is highly synergistic with fludarabine in primary CLL cells.* Oncotarget, 2012. **3**(5): p. 525-34.
143. Teng, Y., et al., *HSP90 and HSP70 proteins are essential for stabilization and activation of WASF3 metastasis-promoting protein.* The Journal of biological chemistry, 2012. **287**(13): p. 10051-9.
144. Pulford, K., et al., *Lymphocyte-specific protein 1: a specific marker of human leucocytes.* Immunology, 1999. **96**(2): p. 262-71.
145. Leopoldino, A.M., et al., *Accumulation of the SET protein in HEK293T cells and mild oxidative stress: cell survival or death signaling.* Molecular and cellular biochemistry, 2012. **363**(1-2): p. 65-74.
146. Belov, L., et al., *Screening microarrays of novel monoclonal antibodies for binding to T-, B- and myeloid leukaemia cells.* Journal of immunological methods, 2005. **305**(1): p. 10-9.
147. Caligaris-Cappio, F., *Inflammation, the microenvironment and chronic lymphocytic leukemia.* Haematologica, 2011. **96**(3): p. 353-5.
148. Zola, H., et al., *Leukocyte and Stromal Cell Molecules: The CD Markers* 2007, New Jersey: Wiley. 591.
149. Ju, J.H., et al., *CD24 enhances DNA damage-induced apoptosis by modulating NF-kappaB signaling in CD44-expressing breast cancer cells.* Carcinogenesis, 2011. **32**(10): p. 1474-83.
150. Wu, G.S., et al., *KILLER/DR5 is a DNA damage-inducible p53-regulated death receptor gene.* Nature genetics, 1997. **17**(2): p. 141-3.
151. Sigal, A. and V. Rotter, *Oncogenic mutations of the p53 tumour suppressor: the demons of the guardian of the genome.* Cancer research, 2000. **60**(24): p. 6788-93.
152. Brosh, R. and V. Rotter, *When mutants gain new powers: news from the mutant p53 field.* Nature reviews. Cancer, 2009. **9**(10): p. 701-13.
153. Liu, K., S. Ling, and W.C. Lin, *TopBP1 mediates mutant p53 gain of function through NF-Y and p63/p73.* Molecular and Cellular Biology, 2011. **31**(22): p. 4464-81.
154. Zawacka-Pankau, J., et al., *Inhibition of glycolytic enzymes mediated by pharmacologically activated p53: targeting Warburg effect to fight cancer.* The Journal of biological chemistry, 2011. **286**(48): p. 41600-15.
155. Corcoran, C.A., Y. Huang, and M.S. Sheikh, *The regulation of energy generating metabolic pathways by p53.* Cancer biology & therapy, 2006. **5**(12): p. 1610-3.
156. Sasaki, Y., et al., *Activation of the ribosomal protein L13 gene in human gastrointestinal cancer.* AACR Meeting Abstracts, 2006. **2006**(2): p. A22-.

157. Yin, Y., et al., *Wild-type p53 restores cell cycle control and inhibits gene amplification in cells with mutant p53 alleles.* Cell, 1992. **70**(6): p. 937-48.
158. Chernova, O.B., et al., *MYC abrogates p53-mediated cell cycle arrest in N-(phosphonacetyl)-L-aspartate-treated cells, permitting CAD gene amplification.* Molecular and Cellular Biology, 1998. **18**(1): p. 536-45.
159. Walerych, D., et al., *Hsp90 chaperones wild-type p53 tumour suppressor protein.* The Journal of biological chemistry, 2004. **279**(47): p. 48836-45.
160. Wadhwa, R., et al., *Hsp70 family member, mot-2/mthsp70/GRP75, binds to the cytoplasmic sequestration domain of the p53 protein.* Experimental cell research, 2002. **274**(2): p. 246-53.
161. Kim, I.S., et al., *Truncated form of importin alpha identified in breast cancer cell inhibits nuclear import of p53.* The Journal of biological chemistry, 2000. **275**(30): p. 23139-45.
162. Waterhouse, N.J., et al., *Calpain activation is upstream of caspases in radiation-induced apoptosis.* Cell death and differentiation, 1998. **5**(12): p. 1051-61.
163. Cryns, V.L., et al., *Specific cleavage of alpha-fodrin during Fas- and tumour necrosis factor-induced apoptosis is mediated by an interleukin-1beta-converting enzyme/Ced-3 protease distinct from the poly(ADP-ribose) polymerase protease.* The Journal of biological chemistry, 1996. **271**(49): p. 31277-82.
164. Cuddihy, A.R., et al., *The double-stranded RNA activated protein kinase PKR physically associates with the tumour suppressor p53 protein and phosphorylates human p53 on serine 392 in vitro.* Oncogene, 1999. **18**(17): p. 2690-702.
165. Almazi, J.G., et al., *Fludarabine nucleoside induces accumulations of p53, p63 and p73 in the nuclei of human B-lymphoid cell lines, with cytosolic and mitochondrial increases in p53.* Proteomics. Clinical applications, 2012. **6**(5-6): p. 279-90.
166. Vega, F.M., A. Sevilla, and P.A. Lazo, *p53 Stabilization and accumulation induced by human vaccinia-related kinase 1.* Molecular and Cellular Biology, 2004. **24**(23): p. 10366-80.
167. Lim, S.T., et al., *Pyk2 inhibition of p53 as an adaptive and intrinsic mechanism facilitating cell proliferation and survival.* The Journal of biological chemistry, 2010. **285**(3): p. 1743-53.
168. Yuan, Z.M., et al., *Regulation of DNA damage-induced apoptosis by the c-Abl tyrosine kinase.* Proceedings of the National Academy of Sciences of the United States of America, 1997. **94**(4): p. 1437-40.
169. Yuan, Z.M., et al., *Role for c-Abl tyrosine kinase in growth arrest response to DNA damage.* Nature, 1996. **382**(6588): p. 272-4.
170. Li, H.H., et al., *A specific PP2A regulatory subunit, B56gamma, mediates DNA damage-induced dephosphorylation of p53 at Thr55.* The EMBO journal, 2007. **26**(2): p. 402-11.
171. Liu, Y., et al., *Regulation of BRCA1 phosphorylation by interaction with protein phosphatase 1alpha.* Cancer research, 2002. **62**(22): p. 6357-61.
172. Ouchi, T., et al., *BRCA1 regulates p53-dependent gene expression.* Proceedings of the National Academy of Sciences of the United States of America, 1998. **95**(5): p. 2302-6.
173. Friedenson, B., *The BRCA1/2 pathway prevents hematologic cancers in addition to breast and ovarian cancers.* BMC cancer, 2007. **7**: p. 152.
174. CH, N.D., et al., - *Role of Tumour Suppressor Protein p53 in Apoptosis and Cancer Therapy.* 2011. - **0**(- 0): p. -.
175. Best, O.G., et al., *The Hsp90 inhibitor SNX-7081 synergizes with and restores sensitivity to fludarabine in chronic lymphocytic leukemia cells with lesions in the TP53 pathway: a potential treatment strategy for fludarabine refractory disease.* Leukemia & lymphoma, 2012. **53**(7): p. 1367-75.
176. Macek, B., M. Mann, and J.V. Olsen, *Global and site-specific quantitative phosphoproteomics: principles and applications.* Annual review of pharmacology and toxicology, 2009. **49**: p. 199-221.
177. Dos Santos, S.C., et al., *Quantitative- and phospho-proteomic analysis of the yeast response to the tyrosine kinase inhibitor imatinib to pharmacoproteomics-guided drug line extension.* OMICS, 2012. **16**(10): p. 537-51.

178. Chen, C., et al., *Comparative phosphoproteomics studies of macrophage response to bacterial virulence effectors.* J Proteomics, 2012. **77**: p. 251-61.
179. Xiao, K., et al., *Global phosphorylation analysis of beta-arrestin-mediated signaling downstream of a seven transmembrane receptor (7TMR).* Proc Natl Acad Sci U S A, 2010. **107**(34): p. 15299-304.
180. Zheng, J., et al., *Urinary proteomic and non-prefractionation quantitative phosphoproteomic analysis during pregnancy and non-pregnancy.* BMC Genomics, 2013. **14**: p. 777.
181. Rogakou, E.P., et al., *DNA double-stranded breaks induce histone H2AX phosphorylation on serine 139.* The Journal of biological chemistry, 1998. **273**(10): p. 5858-68.
182. Podhorecka, M., A. Skladanowski, and P. Bozko, *H2AX Phosphorylation: Its Role in DNA Damage Response and Cancer Therapy.* Journal of nucleic acids, 2010. **2010**.
183. Bennetzen, M.V., et al., *Site-specific phosphorylation dynamics of the nuclear proteome during the DNA damage response.* Molecular & cellular proteomics : MCP, 2010. **9**(6): p. 1314-23.
184. Bracken, C.P., et al., *Regulation of cyclin D1 RNA stability by SNIP1.* Cancer research, 2008. **68**(18): p. 7621-8.
185. Kurokawa, M., et al., *Inhibition of apoptosome formation by suppression of Hsp90beta phosphorylation in tyrosine kinase-induced leukemias.* Molecular and Cellular Biology, 2008. **28**(17): p. 5494-506.
186. Deisenroth, C. and Y. Zhang, *Ribosome biogenesis surveillance: probing the ribosomal protein-Mdm2-p53 pathway.* Oncogene, 2010. **29**(30): p. 4253-60.
187. Donati, G., L. Montanaro, and M. Derenzini, *Ribosome biogenesis and control of cell proliferation: p53 is not alone.* Cancer research, 2012. **72**(7): p. 1602-7.
188. Zheng, Y., et al., *Histone H1 phosphorylation is associated with transcription by RNA polymerases I and II.* The Journal of cell biology, 2010. **189**(3): p. 407-15.
189. Sun, S.Y., et al., *Dual mechanisms of action of the retinoid CD437: nuclear retinoic acid receptor-mediated suppression of squamous differentiation and receptor-independent induction of apoptosis in UMSCC22B human head and neck squamous cell carcinoma cells.* Molecular pharmacology, 2000. **58**(3): p. 508-14.
190. Sun, S.Y., et al., *The synthetic retinoid CD437 selectively induces apoptosis in human lung cancer cells while sparing normal human lung epithelial cells.* Cancer research, 2002. **62**(8): p. 2430-6.
191. Ahmed, N., et al., *Effect of all-trans retinoic acid on chemotherapy induced apoptosis and down-regulation of Bcl-2 in human myeloid leukaemia CD34 positive cells.* Leukemia research, 1999. **23**(8): p. 741-9.
192. Zheng, A., et al., *p53 pathway in apoptosis induced by all-trans-retinoic acid in acute myeloblastic leukaemia cells.* Acta haematologica, 2000. **103**(3): p. 135-43.
193. Sui, G., et al., *Yin Yang 1 is a negative regulator of p53.* Cell, 2004. **117**(7): p. 859-72.
194. He, G., et al., *YY1 is a novel potential therapeutic target for the treatment of HPV infection-induced cervical cancer by arsenic trioxide.* International journal of gynecological cancer : official journal of the International Gynecological Cancer Society, 2011. **21**(6): p. 1097-104.
195. de Nigris, F., et al., *CXCR4/YY1 inhibition impairs VEGF network and angiogenesis during malignancy.* Proceedings of the National Academy of Sciences of the United States of America, 2010. **107**(32): p. 14484-9.
196. Shachar, I., et al., *Regulation of CLL survival by hypoxia-inducible factor and its target genes.* FEBS letters, 2012. **586**(18): p. 2906-10.
197. Ghosh, A.K., et al., *Aberrant regulation of pVHL levels by microRNA promotes the HIF/VEGF axis in CLL B cells.* Blood, 2009. **113**(22): p. 5568-74.
198. Kini, A.R., N.E. Kay, and L.C. Peterson, *Increased bone marrow angiogenesis in B cell chronic lymphocytic leukemia.* Leukemia : official journal of the Leukemia Society of America, Leukemia Research Fund, U.K, 2000. **14**(8): p. 1414-8.
199. Chen, H., et al., *In vitro and in vivo production of vascular endothelial growth factor by chronic lymphocytic leukemia cells.* Blood, 2000. **96**(9): p. 3181-7.

200. Wrobel, T., et al., *[Vascular endothelial growth factor (VEGF) serum concentration in non-Hodgkin's lymphoma patients]*. Polskie Archiwum Medycyny Wewnetrznej, 2004. **112**(2): p. 919-23.
201. Z, R., A. H, and A. S, *Vascular endothelial growth factor up-regulates ICAM-1 expression via the phosphatidylinositol 3 OH-kinase/AKT/Nitric oxide pathway and modulates migration of brain microvascular endothelial cells.* The Journal of biological chemistry, 2000. **275**(27): p. 20770-4.
202. ME, G., et al., *Using gene expression profiling to identify the molecular basis of the synergistic actions of hepatocyte growth factor and vascular endothelial growth factor in human endothelial cells.* British journal of pharmacology, 2003. **140**(4): p. 595-610.
203. Dustin, M.L., et al., *Induction by IL 1 and interferon-gamma: tissue distribution, biochemistry, and function of a natural adherence molecule (ICAM-1).* Journal of immunology, 1986. **137**(1): p. 245-54.
204. Kim, I., et al., *Vascular endothelial growth factor expression of intercellular adhesion molecule 1 (ICAM-1), vascular cell adhesion molecule 1 (VCAM-1), and E-selectin through nuclear factor-kappa B activation in endothelial cells.* The Journal of biological chemistry, 2001. **276**(10): p. 7614-20.
205. Roland, C.L., et al., *ICAM-1 expression determines malignant potential of cancer.* Surgery, 2007. **141**(6): p. 705-7.
206. Molica, S., et al., *Expression on leukemic cells and serum circulating levels of intercellular adhesion molecule-1 (ICAM-1) in B-cell chronic lymphocytic leukemia: implications for prognosis.* Leukemia research, 1995. **19**(8): p. 573-80.
207. A, S., A. V, and M. A, *Nef triggers a transcriptional program in T cells imitating single-signal T cell activation and inducing HIV virulence mediators.* Immunity, 2001. **14**(6): p. 763-77.
208. R, S., et al., *Immunosuppressive activity of capsaicinoids: capsiate derived from sweet peppers inhibits NF-kappaB activation and is a potent antiinflammatory compound in vivo.* European journal of immunology, 2002. **32**(6): p. 1753-63.
209. PJ, B., et al., *CD40 ligand (CD154) triggers a short-term CD4(+) T cell activation response that results in secretion of immunomodulatory cytokines and apoptosis.* The Journal of experimental medicine, 2000. **191**(4): p. 651-60.
210. K, L., et al., *Augmentation in expression of activation-induced genes differentiates memory from naive CD4+ T cells and is a molecular mechanism for enhanced cellular response of memory CD4+ T cells.* Journal of immunology, 2001. **166**(12): p. 7335-44.
211. Tsoukas, C.D., et al., *Activation of resting T lymphocytes by anti-CD3 (T3) antibodies in the absence of monocytes.* Journal of immunology, 1985. **135**(3): p. 1719-23.
212. Wang, J., et al., *CD3-positive large B-cell lymphoma.* The American journal of surgical pathology, 2009. **33**(4): p. 505-12.
213. Harris, S.L. and A.J. Levine, *The p53 pathway: positive and negative feedback loops.* Oncogene, 2005. **24**(17): p. 2899-908.
214. Vousden, K.H. and X. Lu, *Live or let die: the cell's response to p53.* Nature reviews. Cancer, 2002. **2**(8): p. 594-604.
215. Mroz, E.A. and J.W. Rocco, *Functional p53 status as a biomarker for chemotherapy response in oral-cavity cancer.* Journal of clinical oncology : official journal of the American Society of Clinical Oncology, 2010. **28**(5): p. 715-7.
216. Hagn, F., et al., *Structural analysis of the interaction between Hsp90 and the tumour suppressor protein p53.* Nat Struct Mol Biol, 2011. **18**(10): p. 1086-1093.
217. Muller, L., et al., *Hsp90 regulates the activity of wild type p53 under physiological and elevated temperatures.* The Journal of biological chemistry, 2004. **279**(47): p. 48846-54.
218. Lin, K., et al., *Hsp90 inhibition has opposing effects on wild-type and mutant p53 and induces p21 expression and cytotoxicity irrespective of p53/ATM status in chronic lymphocytic leukaemia cells.* Oncogene, 2008. **27**(17): p. 2445-55.

219. Baritaki, S., et al., *Inhibition of Yin Yang 1-dependent repressor activity of DR5 transcription and expression by the novel proteasome inhibitor NPI-0052 contributes to its TRAIL-enhanced apoptosis in cancer cells.* Journal of immunology, 2008. **180**(9): p. 6199-210.